UNIVERSIDADE FEDERAL DO RIO GRANDE
ESCOLA DE QUÍMICA E ALIMENTOS PROGRAMA DE PÓS-GRADUAÇÃO EM ENGENHARIA E CIÊNCIA DE ALIMENTOS
UNIVERSITÉ CLERMONT AUVERGNE
ECOLE DOCTORALE DES SCIENCES DE LA VIE, SANTE, AGRONOMIE, ENVIRONNEMENT SCIENCES ET TECHNOLOGIES DE L'AGRICULTURE, DE L'ALIMENTATION ET DE L'ENVIRONNEMENT
INSTITUT PASCAL, UMR CNRS 6602 AXE GEPEB

EFFECT OF MAGNETIC FIELDS COMBINED WITH POLYMERIC NANOFIBERS IN MICROALGAE CULTIVATION AND THEIR BIOPRODUCTS

MATHEUS PEREIRA DE CARVALHO

Theses presented in partial fulfillment of the requirements for the degree of Doctoral of Philosophy in Food Science and Engineering / Agricultural, Food and Environmental Science and Technology.

PROF. DR. JORGE ALBERTO VIEIRA COSTA (Supervisor - FURG)
Universidade Federal do Rio Grande, Brazil
PROF. DR. CELINE LAROCHE (Supervisor - UCA)
Université Clermont Auvergne, France
PROF. DR. JÚLIO CESAR DE CARVALHO (Reviewer)
Universidade Federal do Paraná - Brazil
PROF. DR. VILÁSIA GUIMARÃES MARTINS (Examiner)
Universidade Federal do Rio Grande - Brazil
PROF. DR. PASCALE GILLON (Reviewer)
Nantes Université, France
PROF. DR. PIERRE FONTANILLE (UCA- Jury President/Examiner)
Université Clermont Auvergne, France

RIO GRANDE, RS
DEFENSE DATE: 04/09/2026

UNIVERSIDADE FEDERAL DO RIO GRANDE
ESCOLA DE QUÍMICA E ALIMENTOS PROGRAMA DE PÓS-GRADUAÇÃO EM ENGENHARIA E CIÊNCIA DE ALIMENTOS
UNIVERSITÉ CLERMONT AUVERGNE
ECOLE DOCTORALE DES SCIENCES DE LA VIE, SANTE, AGRONOMIE, ENVIRONNEMENT SCIENCES ET TECHNOLOGIES DE L'AGRICULTURE, DE L'ALIMENTATION ET DE L'ENVIRONNEMENT
INSTITUT PASCAL, UMR CNRS 6602 AXE GEPEB

EFFECT OF MAGNETIC FIELDS COMBINED WITH POLYMERIC NANOFIBERS IN MICROALGAE CULTIVATION AND THEIR BIOPRODUCTS

MATHEUS PEREIRA DE CARVALHO

Theses presented in partial fulfillment of the requirements for the degree of Doctoral of Philosophy in Food Science and Engineering / Agricultural, Food and Environmental Science and Technology.

PROF. DR. JORGE ALBERTO VIEIRA COSTA (Supervisor - FURG)
Universidade Federal do Rio Grande, Brazil
PROF. DR. CELINE LAROCHE (Supervisor - UCA)
Université Clermont Auvergne, France
PROF. DR. JÚLIO CESAR DE CARVALHO (Reviewer)
Universidade Federal do Paraná - Brazil
PROF. DR. VILÁSIA GUIMARÃES MARTINS (Examiner)
Universidade Federal do Rio Grande - Brazil
PROF. DR. PASCALE GILLON (Reviewer)
Nantes Université, France
PROF. DR. PIERRE FONTANILLE (UCA- Jury President/Examiner)
Université Clermont Auvergne, France

RIO GRANDE, RS
Defense date: 04/09/2026

C331e

Carvalho, Matheus Pereira de
Effect of magnetic fields combined with polymeric nanofibers in microalgae cultivation and their bioproducts / Matheus Pereira de Carvalho. – 2026.
210f.

Tese (Doutorado) – Universidade Federal do Rio Grande Programa de Pós-Graduação em Engenharia e Ciência de Alimentos, 2026.

Orientador: Dr. Jorge Alberto Vieira Costa
Coorientadora: Dra. Celine Laroche

1. Engenharia e Ciência de Alimentos. 2. *Porphyridium*. 3. *Limnospira*. 4. Exopolissacarídeos. 5. Pigmentos. 6. Polissacarídeos sulfatados. 7. campos magnéticos estáticos. 8. Nanofibras poliméricas. I. Costa, Jorge Alberto Vieira. II. Laroche, Celine. III. Título.

CDU 664

Catalogação na fonte: Bibliotecária Brenda Sequeira CRB10/1979

APROVAÇÃO

Tese defendida por Matheus Pereira de Carvalho, com orientação do Prof. Dr. Jorge Alberto Vieira Costa e coorientação da Profa. Dra. Céline Laroche, aprovada em 4 de setembro de 2026, pela Comissão Examinadora constituída pelos membros:

gov.br JORGE ALBERTO VIEIRA COSTA
Data: 02/10/2026 14:21:06-0300
Verifique em https://validar.iti.gov.br

Prof. Dr. Jorge Alberto Vieira Costa – FURG

Documento assinado digitalmente
gov.br JULIO CESAR DE CARVALHO
Data: 06/10/2026 19:36:47-0300
Verifique em https://validar.iti.gov.br

Prof. Dr. Júlio Cesar de Carvalho – UFPR

Pascale Gillon
Signé électroniquement par
Pascale Gillon
Le 07/10/2026 à 17:31

Profa. Dra. Pascale Gillon – NU - França

Signé électroniquement par
Pierre Fontanille
Le 16/10/2026 à 12:52

Prof. Dr. Pierre Fontanille – UCA - França

Documento assinado digitalmente
gov.br VILASIA GUIMARAES MARTINS
Data: 05/10/2026 09:18:39-0300
Verifique em https://validar.iti.gov.br

Profa. Dra. Vilásia Guimarães Martins – FURG

Laroche

Signé électroniquement par
Céline Laroche
Le 07/10/2026 à 17:02

Profa. Dra. Céline Laroche – UCA - França

“Science is always wrong. It never solves a problem without creating ten more."
- Bernard Shaw

ACKNOWLEDGEMENTS

À minha família, que sempre me apoiou em todas as minhas escolhas e que, desde cedo, despertou em mim o amor pelo saber e pela educação, base de tudo que construí até aqui.

Ao meu namorado, companheiro de todos os momentos, que me ouve com paciência, suporta meus sumiços e minhas chatices, e que, nos momentos em que eu mesmo duvidei, nunca deixou de acreditar em mim.

Aos meus amigos, os de perto e os de longe, que estiveram presentes nos altos e nos baixos, nas conquistas e nas crises, nos cafés que viraram horas de conversa, nas partidas de jogo que viraram madrugada e nas fofocas que aliviaram o peso dos dias difíceis. Vocês tornaram essa caminhada aturável e bem mais divertida, **VOCÊS SÃO INCRÍVEIS**.

Ao Prof. Dr. Jorge Alberto Vieira Costa, pela orientação dedicada, pela confiança depositada e pelas inúmeras oportunidades que me foram generosamente concedidas ao longo desta trajetória.

À Mme la professeure Céline Laroche, pour m'avoir accueilli à bras ouverts au sein de son groupe de recherche, pour sa disponibilité, son attention et pour m'avoir offert cette opportunité unique de bénéficier d'une cotutelle, qui a tant contribué à ma formation scientifique et personnelle.

Aos membros da banca, muito obrigado pela disponibilidade e contribuições ao trabalho.

Às equipes do LEB, MIBI e CEAS, pelo suporte técnico, pelo aprendizado compartilhado e pelo ambiente colaborativo que tornou possível a realização deste trabalho.

À Universidade Federal do Rio Grande (FURG) e à Université Clermont-Auvergne (UCA), pela estrutura, pelo ensino de qualidade e pelas oportunidades de desenvolvimento acadêmico proporcionadas. À CAPES, pelo apoio financeiro que viabilizou esta pesquisa.

A todos que, de alguma forma, contribuíram para esta jornada — o meu sincero e profundo

OBRIGADO/MERCI !!

TABLE LIST

CHAPTER III

Paper I - Production of biomass and biomolecules in *Limnospira indica* PCC 8005 cultivation under magnetic fields and polymeric nanofibers

Table 1 - Growth parameters of *Limnospira indica* PCC 8005 cultivated under the influence of SMF and nanofibers. SMF- Magnetic field 1h day-1; SMF + Nano – added nanofiber magnetic field; Nano – Added nanofibers; SMF +NanoMEA – Magnetic field and nanofiber produced with MEA; NanoMEA - Nanofiber addition produced with MEA. The results are expressed as mean (n=3) ± standard deviation. Different letters on the same line indicate a significant difference between p-values <0.05 (Tukey's test). 72

Table 2- Macronutrient composition of biomass *Limnospira* grown under SMF and nanofibers. SMF - Magnetic field 1h day^{-1}; SMF + Nano – added nanofiber magnetic field; Nano – Added nanofibers; SMF +NanoMEA – Magnetic field and nanofiber produced with MEA; NanoMEA - Nanofiber addition produced with MEA. The results are expressed as mean (n=3) ± standard deviation. Different letters on the same line *indica*te a significant difference between p-values <0.05 (Tukey's test). 75

Table 3 - Characterization of the EPS extracted from L. Indica biomass cultivated with nanofibers under the influence of SMF. SMF - Magnetic field 1h day^{-1}; SMF + Nano – added nanofiber magnetic field; Nano – Added nanofibers; SMF +NanoMEA – Magnetic field and nanofiber produced with MEA; NanoMEA - Nanofiber addition produced with MEA. The results are expressed as mean (n=3) ± standard deviation. Different letters on the same line indicate a significant difference between p-values <0.05 (Tukey's test). 81

Paper II - Production of β-phycoerythrin and exopolysaccharide in *Porphyridium purpureum* modulated via static magnetic fields and polymeric nanofibers.

Table 1 - Growth parameters and produced RPS of Porphyridium purpureum under the influence of SMF and nanofibers.CT- Control; M1- Magnetic field 1 h day^{-1}; MN – added nanofiber magnetic field; N – Added nanofibers; MNE – Magnetic field and nanofiber produced with MEA; NE- Nanofiber addition produced with MEA; M24 Magnetic field 24 h day^{-1}. The results are expressed as mean (n = 3) ± standard deviation. Different letters on the same line show a significant difference between treatments p-values < 0.05 (Tukey's test). 106

Table 2 - Main compounds of Porphyridium purpureum biomass.CT- Control; M1- Magnetic field 1 h day−1; MN – added nanofiber magnetic field; N – Added nanofibers; MNE – Magnetic field and nanofiber produced with MEA; NE- Nanofiber addition produced with MEA; M24 Magnetic field 24 h day−1. The results are expressed as mean (n = 3) ± standard deviation. Different letters on the same line show a significant difference between treatments, p-values < 0.05 (Tukey's test). 108

Table 3 - Biochemical composition of released/bound polysaccharide. CT- Control; M1- Magnetic field 1 h day^{-1}; MN – added nanofiber magnetic field; N – Added nanofibers; MNE – Magnetic field and nanofiber produced with MEA; NE- Nanofiber produced with MEA; M24 Magnetic field 24 h day^{-1}. The results are expressed as mean (n = 3) ± standard deviation. Different letters on the same column and EPS section show a significant difference between p-values < 0.05 (Tukey's test). 111

Paper III - Cultivation conditions drive divergent rheological behavior and hydrogel architecture in *Porphyridium purpureum* exopolysaccharides.

Table 1 - Zeta potential of the studied EPS. CT: control; M1- Magnetic field 1 h day^{-1}; M24 Magnetic field 24 h day^{-1}; MN – added nanofiber magnetic field. The results are expressed as mean

(n = 3) ± standard deviation. Different letters show a significant difference between samples *p*-values < 0.05 (Tukey's test). 142

FIGURE LIST

CHAPTER II

Figure 1 - Morphology of Limnospira fusiformis (A and C) and Arthrospira jenneri (B and D). Black arrows poit to the thickened cell wall. Whight arrows point to aerotope..... 36
Figure 2 - A The general schematic cell structure of red microalga genera Porphyridium . B Microphotographs of *P. purpureum* cells aggregate. 1 EPs, 2 nucleus, 3 Golgi, 4 cytosol, 5 mitochondrion, 6 intracellular polysaccharide, 7 chloroplast, 8 thylakoid, 9 pyrenoid, 10 phycobilisome, 11 vacuole, 12 plasmic membrane. Blue arrows *indica*tes extracellular space with exopolysaccharide. 39
Figure 3 - Chemical structure of chlorophyll α. 43
Figure 4 - Phycobilisome (PBS) structure model. 44
Figure 5 - Detailed protein structures of phycobiliproteins (allophycocyanin (APC), phycocyanin (PC), and phycoerythrin (PE), from subunits to hexamers..... 45
Figure 6 -Schematic representation of various types of physical and chemical crosslinking in hydrogels. 55

CHAPTER III

Paper I - Production of biomass and biomolecules in *Limnospira indica* PCC 8005 cultivation under magnetic fields and polymeric nanofibers
Figure 1 - Bioreactor diagram..... 66
Figure 2 -Growth curves and pH values of Limnospira indica PCC8005 cultures under magnetic field, nanofibers, and control treatments. 70
Figure 3 - Phycocyanin c and chlorophyll a concentration in L. indica biomass.SMF - Magnetic field 1h day^{-1}; SMF + Nano – added nanofiber magnetic field; Nano – Added nanofibers; SMF +NanoMEA – Magnetic field and nanofiber produced with MEA; NanoMEA - Nanofiber addition produced with MEA. The results are expressed as mean (n=3) ± standard deviation. Different letters on the same line indicate a significant difference between p-values <0.05 (Tukey's test)..... 78
Figure 4 - FT-IR spectrum of BPS extracted from L. indica biomass. SMF - Magnetic field 1h day^{-1}; SMF + Nano – added nanofiber magnetic field; Nano – Added nanofibers; SMF +NanoMEA – Magnetic field and nanofiber produced with MEA; NanoMEA - Nanofiber addition produced with MEA. The results are expressed as mean (n=3) ± standard deviation. Different letters on the same line indicate a significant difference between p-values <0.05 (Tukey's test)..... 84
Paper II - Production of β-phycoerythrin and exopolysaccharide in *Porphyridium purpureum* modulated via static magnetic fields and polymeric nanofibers.
Figure 1 - Used photobioreactor schematic for the proposed experiments. 99
Figure 2- Growth curves of Porphyridium purpureum under magnetic field, nanofibers, and control culture. 105
Figure 3 - Concentration of phycoerythrin (a), chlorophyll, and carotenoids (b) in produced P. purpureum biomass. CT- Control; M1- Magnetic field 1 h day^{-1}; MN – added nanofiber magnetic field; N – Added nanofibers; MNE – Magnetic field and nanofiber produced with MEA; NE- Nanofiber addition produced with MEA; M24 Magnetic field 24 h day^{-1}. The results are expressed as mean (n = 3) ± standard deviation. Different letters on different graphs represent a significant difference between treatments, p-values < 0.05 (Tukey's test)..... 109
Figure 3 - Monosaccharide profile composition of RPS and BPS in % molar ratios. CT- Control; M1- Magnetic field 1 h day^{-1}; MN – added nanofiber magnetic field; N – Added nanofibers; MNE

– Magnetic field and nanofiber produced with MEA; NE- Nanofiber produced with MEA; M24 Magnetic field 24 h day^{-1}. 112
Paper III - Cultivation conditions drive divergent rheological behavior and hydrogel architecture in *Porphyridium purpureum* exopolysaccharides.
Figure 1- FT-IR spectra of RPS and BPS produced by P. purpureum. CT: control; M1: magnetic field 1 h d^{-1}; M24: magnetic field 24 h d^{-1}; MN: magnetic field 1 h d^{-1} with nanofibers. 141
Figure 2 - TGA of RPS (A) and BPS (B). CT: control; M1: magnetic field 1 h d^{-1}; M24: magnetic field 24 h d^{-1}; MN: magnetic field 1 h d^{-1} with PAN nanofibers. 144
Figure 3-DSC curves of RPS (A) and BPS (B). CT: control; M1: magnetic field 1 h d^{-1}; M24: magnetic field 24 h d^{-1}; MN: magnetic field 1 h d^{-1} with nanofibers. 147
Figure 4- Flow curves of the studied polymeric solutions 1% m v^{-1}.CT: control; M1: magnetic field 1 h d^{-1}; M24: magnetic field 24 h d^{-1}; MN: magnetic field 1 h d^{-1} with nanofibers. 149
Figure 5 - Frequency sweeps of elastic and viscous moduli (A) and complex viscosity (|η*|), loss factor vs angular frequency (B) of the studied polymeric solutions 1% m v^{-1}. CT: control; M1: magnetic field 1 h d^{-1}; M24: magnetic field 24 h d^{-1}; MN: magnetic field 1 h d^{-1} with nanofibers. 152
Figure 6 - Hydrogels SEM images of RPS solution 1% (w v^{-1}) added of 0.3% (w v^{-1}) $Fe_2(SO_4)_3$. CT: control; M1: magnetic field 1 h d^{-1}; M24: magnetic field 24 h d^{-1}; MN: magnetic field 1 h d^{-1} with nanofibers. 158

CONTENTS

CHAPTER I 14
GENERAL ABSTRACT 15
RESUMO GERAL 16
RÉSUMÉ GÉNÉRAL 17
RÉSUMÉ ÉTENDU 18
1 INTRODUCTION 26
2 INTRODUÇÃO 29
3 OBJECTIVES 32
3.1 GENERAL OBJECTIVE 32
3.2 SPECIFIC OBJECTIVES 31

CHAPTER II 33
4 LITERATURE REVIEW 34
4.1 CYANOBACTERIA AND MICROALGAE 34
4.1.1 ***Limnospira, Arthrospira*** **and** ***Spirulina.*** 35
4.1.2 ***Porphyridium sp.*** 38
4.1.3 Photosynthesis and pigments in cyanobacteria/microalgae. 40
4.2 MICROALGAL AND CYANOBACTERIA CULTIVATION 45
4.2.1 Carbon dioxide in microalgae/cyanobacteria production 46
4.2.2 Magnetic fields in microalgal culture 48
4.3 MICROALGAE EXOPOLYSACCHARIDES EXTRACTION AND PURIFICATION 50
4.4 MICROALGAE POLYSACHARIDES 51
4.5 TECHNOLOGICAL PROPERTIES OF POLYSACCHARIDES 52
4.5.1 Technological properties of microalgal EPS. 56
4.6 SUSTAINABLE DEVELOPMENT OBJECTIVES 57

CHAPTER III 59
WORK OVERVIEW 60
PAPER I 61
ABSTRACT 62
1. INTRODUCTION 62

2. MATERIALS AND METHODS 64
2.1 MICROORGANISM INOCULUM 64
2.2 NANOFIBER PRODUCTION AND STATIC MAGNETIC FIELD APPLICATION 65
2.3 EXPERIMENT DESIGN 65
2.4 GROWTH KINETICS 66
2.5 BIOMASS CHARACTERIZATION 67
2.6 CELL WALL BOUND EXOPOLYSACCHARIDES (BPS) EXTRACTION AND CHARACTERIZATION 68
2.7 STATISTICAL ANALYSIS 69
3. RESULTS AND DISCUSSION 69
3.1 *Limnospira indica* GROWTH 69
3.2 BIOMASS CHARACTERIZATION 74
3.3 CHARACTERIZATION OF BOUND EXOPOLYSACCHARIDES (BPS) 80
4. CONCLUSION 85
REFERENCE 85
PAPER II 94
ABSTRACT 95
1. INTRODUCTION 95
2. MATERIALS AND METHODS 98
2.1 INOCULUM 98
2.2 EXPERIMENT DESIGN 98
2.3 GROWTH KINETICS 100
2.4 BIOMASS AND EPS HARVEST 101
2.5 BIOMASS CHARACTERIZATION 102
2.6 EPS BIOCHEMICAL CHARACTERIZATION 103
2.7 STATISTICAL ANALYSIS 104
3. RESULTS 104
3.1 *Porphyridium purpureum* GROWTH KINETICS 104
3.2 BIOMASS CHARACTERIZATION 107
3.3 EPS CHARACTERIZATION 110
4. DISCUSSION 113
4.1 *Porphyridium purpureum* GROWTH KINETICS AND EPS PRODUCTION 113
4.2 BIOMASS CHARACTERIZATION 116
4.3 EPS CHARACTERIZATION 120
5. CONCLUSION 122

REFERENCES 123
PAPER III 132
ABSTRACT 133
1. INTRODUCTION 134
2. MATERIALS AND METHODS 136
2.1 NANOFIBERS AND MAGNETIC FIELD 136
2.2 EXOPOLYSACCHARIDES PRODUCTION 136
2.3 FOURIER TRANSFORM INFRARED (FTIR) 137
2.4 DYNAMIC LIGHT SCATTERING (DLS) 137
2.5 THERMAL ANALYSIS TGA AND DSC 138
2.6 RHEOLOGY ASSAYS 138
2.7 HYDROGELS PREPARATION AND MORPHOLOGY 139
2.8 STATISTICAL ANALYSIS 139
3. RESULTS AND DISCUSSION 140
3.1 MOLECULAR CHARACTERISTICS OF EPS 140
3.1.1 Fourier Transform Infrared (FT-IR) of EPS produced by *P. Purpureum* 140
3.1.2 Zeta Potential of EPS produced by *P. purpureum* 141
3.2 EPS THERMAL ANALYSIS 143
3.2.1 Thermogravimetric analysis (TGA) 143
3.2.2 Differential Scanning Calorimetry (DSC) 146
3.3 RHEOLOGY ASSAYS 148
3.3.1 Apparent viscosity assay 148
3.3.2 Frequency sweep 150
3.4 HYDROGELS MORPHOLOGY 156
4. CONCLUSION 160
REFERENCE 162
CHAPTER IV 170
GENERAL CONCLUSION 171
CONCLUSÃO GERAL 173

CHAPTER V 175
GENERATED WASTE AND DESTINATION 176
SUGGESTIONS FOR FUTURE WORK 177

CHAPTER VI 179
REFERENCES 180
APPENDIX 206

CHAPTER I

GENERAL ABSTRACT

The cultivation of microalgae and cyanobacteria represents a promising strategy for the sustainable production of high-value-added compounds. These photosynthetic microorganisms metabolize CO_2 and can be cultivated in non-productive areas, contributing to carbon emission mitigation. A recurring challenge in bioprocess engineering is the metabolic trade-off between biomass productivity and secondary metabolite accumulation, since conventional stress-induction strategies (nutrient deprivation, light intensity adjustments) frequently increase metabolite yield at the expense of growth rate. This work investigated the effect of static magnetic fields (SMF) combined with polyacrylonitrile (PAN) polymeric nanofibers, with and without monoethanolamine (MEA) functionalization, as a dual intensification strategy in the cultivation of *Limnospira indica* PCC 8005 and *Porphyridium purpureum* CCAP 1380/1A, as well as in modulating their biopolymers, being divided into three studies. In the first study, *L. indica* cultures showed that SMF and PAN nanofibers exert distinct and partially antagonistic effects on cellular metabolism. The combined SMF+Nanofiber treatment provided the highest biomass yield (5.9 g L^{-1}, +28% versus control). SMF (1 h d^{-1}) mainly stimulated nitrogen metabolism, increasing protein content by 16%, c-phycocyanin by 36%, and chlorophyll a by 49%. Nanofiber-only treatments redirected metabolic flux toward carbon storage (+40% carbohydrates), with simultaneous suppression of pigment synthesis. Characterization of cell wall-bound polysaccharides (BPS) revealed that SMF+NanoMEA produced the highest uronic acid ratio (39.9%), while nanofibers alone gave the highest degree of sulfation (8.4%), highlighting the differentiated biotechnological potential of each fraction. In the second study, the temporal exposure pattern to SMF proved to be a critical variable in *P. purpureum* cultivation. Intermittent SMF (1 h d^{-1}) maximized biomass yield (+36%) and released polysaccharide production (+83%), while nanofibers induced a 196% increase in β-phycoerythrin content, along with significant increases in carotenoids. Exopolysaccharide (EPS) characterization revealed that the BPS fraction showed a higher sulfation ratio (15–21%) and lower uronic acid content (10–18%) compared to the its released fraction, demonstrating that physical stimuli modulate substitution patterns along the EPS polymer chain. The third study evaluated the rheological, thermal, and morphological properties of the EPS. Continuous SMF exposure (24 h d^{-1}) produced polymers forming a viscoelastic network comparable to xanthan gum (G′/G″ ratio of 3.21), while the combined SMF-nanofiber treatment generated hierarchical nanofibrillar hydrogels with biomimetic morphology of biomedical interest. All EPS exhibited an amorphous character, thermal stability up to 220–250 °C, and a zeta potential below −30 mV, confirming their colloidal stability and suitability for high value-added applications in the pharmaceutical, food, and biotechnology industries. Collectively, these results demonstrate that the deliberate selection of SMF regimes and functionalized nanofibers allows microalgal metabolism to be steered and the structural properties of biopolymers to be pre-designed, without genetic modification or chemical induction, positioning this approach as a sustainable strategy for biomolecule production from microalgal sources.

Keywords: *Porphyridium*, *Limnospira*, exopolysaccharides, pigments, sulfated polysaccharides, static magnetic fields.

RESUMO GERAL

O cultivo de microalgas e cianobactérias representa uma estratégia promissora para a produção sustentável de compostos de alto valor agregado (CAVA). Esses microrganismos metabolizam CO_2 e podem ser cultivados em áreas não produtivas, contribuindo para a mitigação das emissões de carbono. Um desafio recorrente na engenharia de bioprocessos é o compromisso entre a produtividade em biomassa e o acúmulo de metabólitos secundários, já que as estratégias convencionais de indução de estresse (privação de nutrientes, ajustes na intensidade luminosa) frequentemente aumentam a produção de CAVA em detrimento do crescimento. Estratégias não convencionais, como campos magnéticos que agem no sistema como um todo e nanofibras poliméricas, focadas na retenção de CO_2, surgem como alternativa às convencionais. Este trabalho investigou o efeito de campos magnéticos estáticos (CMF) combinados com nanofibras poliméricas de poliacrilonitrila (PAN), com e sem monoetanolamina (MEA), como estratégia dual de intensificação no cultivo e CAVA em *Limnospira indica* PCC 8005 e *Porphyridium purpureum* CCAP 1380/1A, sendo dividido em três partes. Na primeira parte, as culturas de *L. indica* mostraram que os CMF e as nanofibras exercem efeitos distintos e parcialmente antagônicos. O tratamento combinado CMF+Nanofibra forneceu o maior rendimento em biomassa (5,9 g L^{-1}, +28% em relação ao controle). Os SMF (1 h d^{-1}) estimularam o metabolismo do nitrogênio, aumentando as proteínas em 16%, a c-ficocianina em 36% e a clorofila a em 49%. As nanofibras isoladamente redirecionaram o fluxo metabólico para o armazenamento de carbono (+40% de carboidratos), com supressão da síntese pigmentar. A caracterização dos polissacarídeos ligados à parede celular (PSL) revelou que CMF+NanoMEA produziu o maior teor de ácido urônico (39,9%), enquanto as nanofibras isoladas resultaram no maior grau de sulfatação (8,4%), destacando o potencial diferenciado de cada fração. No segundo estudo, o esquema temporal de exposição aos SMF mostrou-se uma variável crítica para *P. purpureum*. Os CMF intermitentes (1 h d^{-1}) maximizaram a biomassa (+36%) e os polissacarídeos liberados (+83%), enquanto as nanofibras induziram um aumento de 196% no teor de ficoeritrina, além de elevações significativas em carotenoides. A fração ligada à parede celular dos EPS apresentou maior grau de sulfatação (15–21%) e menor teor de ácido urônico (10–18%) que a fração liberada, mostrando que os estímulos físicos modulam os padrões de substituição da cadeia polimérica. O terceiro estudo avaliou as propriedades reológicas, térmicas e morfológicas dos EPS. A exposição contínua aos CMF(24 h d^{-1}) produziu polímeros formando uma rede viscoelástica comparável à goma xantana ($G'/G'' = 3,21$), enquanto o tratamento combinado CMF-nanofibra gerou hidrogéis nanofibrilares hierárquicos com morfologia biomimética de interesse biomédico. Todos os EPS apresentaram caráter amorfo, estabilidade térmica até 220–250 °C e potencial Zeta inferior a −30 mV, confirmando sua estabilidade coloidal e adequação para aplicações farmacêuticas, alimentícias e biotecnológicas. Coletivamente, esses resultados demonstram que a seleção deliberada de regimes de CMF e nanofibras funcionalizadas permite direcionar o metabolismo microalgal e pré-projetar as propriedades estruturais dos biopolímeros, sem modificação genética nem indução química, posicionando essa abordagem como estratégia sustentável para a produção de biomoléculas a partir de fontes microalgais.

Palavras-chave: *Porphyridium*, *Limnospira*, exopolissacarídeos, pigmentos, polissacarídeos sulfatados, campos magnéticos estáticos, nanofibras poliméricas.

RÉSUMÉ GÉNÉRAL

La culture de microalgues et de cyanobactéries représente une stratégie prometteuse pour la production durable de composés à haute valeur ajoutée. Ces microorganismes photosynthétiques métabolisent le CO2 et sont cultivables dans des zones non productives, contribuant à l'atténuation des émissions de carbone. Un défi récurrent en génie des bioprocédés est le compromis entre productivité en biomasse et accumulation de métabolites secondaires, les stratégies conventionnelles d'induction de stress (privation de nutriments, ajustements de l'intensité lumineuse) augmentant souvent le rendement en métabolites au détriment de la croissance. Ce travail a investigué l'effet de champs magnétiques statiques (SMF) combinés à des nanofibres polymériques de polyacrylonitrile (PAN), avec et sans fonctionnalisation par la monoéthanolamine (MEA), comme stratégie duale d'intensification dans la culture de Limnospira indica PCC 8005 et Porphyridium purpureum CCAP 1380/1A, ainsi que dans la modulation de leurs biopolymères. Dans la première étude, les cultures de L. indica ont montré que les SMF et les nanofibres exercent des effets distincts et partiellement antagonistes. Le traitement combiné SMF+Nanofibre a fourni le rendement en biomasse le plus élevé (5,9 g L^{-1}, +28% vs contrôle). Les SMF (1 h j^{-1}) ont stimulé le métabolisme de l'azote, augmentant les protéines de 16%, la c-phycocyanine de 36% et la chlorophylle a de 49%. Les nanofibres seules ont redirigé le flux métabolique vers le stockage du carbone (+40% de glucides), avec suppression de la synthèse pigmentaire. La caractérisation des polysaccharides pariétaux (BPS) a révélé que SMF+NanoMEA a produit le ratio d'acide uronique le plus élevé (39,9%), tandis que les nanofibres seules ont donné le plus haut degré de sulfatation (8,4%), soulignant le potentiel différencié de chaque fraction. Dans la deuxième étude, le schéma temporel d'exposition aux SMF s'est révélé critique pour P. purpureum. Les SMF intermittents (1 h j^{-1}) ont maximisé la biomasse (+36%) et les polysaccharides libérés (+83%), tandis que les nanofibres ont induit une augmentation de 196% de la β-phycoérythrine, ainsi que des hausses significatives en caroténoïdes. La fraction BPS des EPS a présenté un ratio de sulfatation plus élevé (15–21%) et un taux d'acide uronique plus faible (10–18%) que la fraction RPS, montrant que les stimuli physiques modulent les schémas de substitution de la chaîne polymérique. La troisième étude a évalué les propriétés rhéologiques, thermiques et morphologiques des EPS. L'exposition continue aux SMF (24 h j^{-1}) a produit des polymères formant un réseau viscoélastique comparable à la gomme xanthane ($G'/G'' = 3,21$), tandis que le traitement combiné SMF-nanofibre a généré des hydrogels nanofibrillaires hiérarchiques à morphologie biomimétique d'intérêt biomédical. Tous les EPS ont présenté un caractère amorphe, une stabilité thermique jusqu'à 220–250 °C et un potentiel zêta inférieur à −30 mV, confirmant leur stabilité colloïdale et leur adéquation à des applications pharmaceutiques, alimentaires et biotechnologiques. Collectivement, ces résultats démontrent que la sélection délibérée de régimes de SMF et de nanofibres fonctionnalisées permet d'orienter le métabolisme microalgal et de pré-concevoir les propriétés structurales des biopolymères, sans modification génétique ni induction chimique, positionnant cette approche comme stratégie durable pour la production de biomolécules à partir de sources microalgales.

Mots-clés : *Porphyridium*, *Limnospira*, exopolysaccharides, pigments, polysaccharides sulfatés, champs magnétiques statiques.

RÉSUMÉ ÉTENDU

Chapitre I — Introduction, contexte et objectifs

La demande mondiale croissante de composés bioactifs produits de manière durable a positionné les microalgues et les cyanobactéries comme des plateformes de production stratégiques. Ces microorganismes photosynthétiques offrent une combinaison unique d'avantages : ils fixent le CO_2 atmosphérique en matière organique, prospèrent dans des zones non arables et accumulent des molécules à haute valeur commerciale, notamment des protéines, des pigments, des acides gras polyinsaturés et des exopolysaccharides (EPS). Parmi les espèces les plus étudiées,

Limnospira indica PCC 8005 — une cyanobactérie filamenteuse étroitement apparentée à *Arthrospira (Spirulina)* — est largement exploitée pour sa teneur élevée en protéines et ses pigments phycobiliprotéiques. *Porphyridium purpureum*, une microalga rouge unicellulaire, se distingue particulièrement par sa production d'EPS sulfatés et de β-phycoérythrine, des composés à bioactivité démontrée et présentant un intérêt commercial dans les secteurs pharmaceutique, alimentaire et cosmétique.

Un défi persistant en ingénierie des bioprocédés microalgaux est le compromis métabolique entre la productivité en biomasse et l'accumulation de métabolites secondaires à haute valeur ajoutée. Les stratégies de stress conventionnelles — privation de nutriments, modulation de la lumière, stress osmotique — tendent à améliorer les rendements en métabolites spécifiques au détriment de la croissance. Cette thèse explore deux stimuli physiques : les champs magnétiques statiques (CMS) et les nanofibres polymériques de polyacrylonitrile (PAN), avec et sans fonctionnalisation à la monoéthanolamine (MEA), comme stratégie duale pour optimiser simultanément la biomasse et la production de métabolites.

Les CMS agissent sur les systèmes biologiques par induction magnétique, effets magnéto-mécaniques et mécanisme des paires radicalaires, avec des effets documentés sur l'activité enzymatique, la perméabilité membranaire et l'efficacité photosynthétique. Les nanofibres de PAN fonctionnent comme adsorbants physiques de CO_2 grâce à leur rapport surface/volume élevé, tandis que les nanofibres fonctionnalisées au MEA introduisent un mécanisme de chimisorption via la formation de carbamate, doublant théoriquement la rétention et la disponibilité du CO_2 dans le milieu de culture. La combinaison de ces stimuli a été supposée permettre de découpler le

compromis habituel biomasse/métabolites en ciblant indépendamment différentes voies métaboliques.

La thèse est structurée autour de trois objectifs principaux : (1) évaluer l'effet des CMS et des nanofibres sur le rendement en biomasse et la composition moléculaire de *L. indica* PCC 8005 ; (2) évaluer ces mêmes stimuli dans la culture de *P. purpureum* en se concentrant sur la production de pigments et d'EPS ; et (3) caractériser les propriétés rhéologiques, thermiques et morphologiques des EPS de *P. purpureum* en fonction du traitement de culture appliqué.

Chapitre II — Revue de littérature

La revue de littérature synthétise l'état actuel des connaissances dans cinq domaines thématiques sous-jacents aux travaux expérimentaux. Les cyanobactéries et les microalgues sont présentées comme les modèles biologiques de l'étude, avec une attention particulière à la taxonomie et à la biologie de culture de *Limnospira/Arthrospira* et de *Porphyridium* sp. L'appareil photosynthétique, les voies de fixation du carbone et la biosynthèse des phycobiliprotéines — phycocyanine et phycoérythrine — sont décrits dans le contexte de la plasticité métabolique sous stress environnemental.

La revue aborde ensuite les systèmes de culture microalgale, en couvrant le rôle de la disponibilité en CO_2 et sa régulation, ainsi que les effets documentés des champs magnétiques statiques sur la physiologie microalgale selon les espèces et les régimes d'exposition. Les réponses diverses et fréquemment non linéaires des microorganismes aux CMS — allant de stimulatrices à inhibitrices selon l'intensité du champ, la durée et l'espèce — soulignent l'importance d'une investigation expérimentale ciblée pour chaque système biologique.

La biochimie des EPS et les méthodologies d'extraction sont examinées en profondeur, couvrant les différences structurelles entre les polysaccharides libérés (RPS) et les polysaccharides liés à la paroi cellulaire (BPS), la signification du degré de sulfatation et de la teneur en acide uronique comme marqueurs de bioactivité et de fonction rhéologique, ainsi que les propriétés technologiques des polysaccharides microalgaux en tant qu'épaississants, émulsifiants, gélifiants et agents bioactifs. Enfin, le chapitre examine le cadre des Objectifs de Développement Durable (ODD) contextualisant la recherche, notamment l'ODD 2 (faim zéro), l'ODD 3 (bonne santé), l'ODD 9 (industrie et innovation) et l'ODD 13 (action climatique), positionnant la biotechnologie microalgale comme contributeur à la bioéconomie.

Chapitre III — Résultats expérimentaux

Le Chapitre III constitue le cœur scientifique de la thèse et est organisé en trois articles scientifiques. Chaque article aborde une étape distincte du programme expérimental, couvrant deux espèces de microalgues et progressant de la caractérisation de la culture et de la biomasse jusqu'à la physicochimie avancée des polymères.

Article I *— Production de biomasse et de biomolécules chez Limnospira indica PCC 8005 sous CMS et nanofibres polymériques*

La première étude a investigué les effets combinés et individuels des CMS (11 ± 2 mT, 1 h j^{-1}) et des nanofibres de PAN (0,1 mg mL^{-1}), non fonctionnalisées (Nano) et fonctionnalisées au MEA (NanoMEA), sur la cinétique de croissance, la composition macromoléculaire de la biomasse, la teneur en pigments photosynthétiques et le profil des exopolysaccharides liés à la paroi cellulaire (BPS) de *Limnospira indica* PCC 8005.

Croissance et rendement en biomasse. Tous les traitements avec CMS ont produit des concentrations en biomasse finale supérieures au contrôle. La biomasse finale la plus élevée (Xfinal) a été atteinte par le traitement CMS+Nano à 5,87 ± 0,06 g L^{-1}, représentant une augmentation de 28 % par rapport au contrôle (4,6 ± 0,1 g L^{-1}). La productivité maximale (Pmax) était significativement plus élevée dans les traitements CMS et CMS+Nano (0,395 et 0,434 mg L^{-1} j^{-1}, respectivement), confirmant le CMS comme facteur principal de stimulation de la croissance. Le pH plus bas observé dans les traitements contenant du CMS a été attribué à l'effet Hall stabilisant la couche limite gaz-liquide et améliorant la solubilité du CO_2, tandis que les nanofibres réduisaient le pH par adsorption physique et rétention du CO_2.

Composition de la biomasse. La composition macromoléculaire de la biomasse récoltée a révélé une divergence métabolique claire entre les traitements CMS et nanofibres. Les cultures exposées aux CMS ont dirigé le flux de carbone préférentiellement vers l'assimilation de l'azote et la synthèse protéique, atteignant une teneur maximale en protéines de 65,5 ± 1,4 % (pp^{-1}) — une augmentation de 16 % par rapport au contrôle (55,2 ± 1,8 %). En revanche, les traitements nanofibres seules ont atteint la teneur en glucides la plus élevée (39,6 ± 0,98 % pp^{-1}), une augmentation de 40 % par rapport aux traitements CMS, cohérente avec l'hypothèse que l'augmentation de la disponibilité en CO_2 favorise le stockage du carbone via le cycle de Calvin-Benson-Bassham. La teneur en lipides n'a pas été significativement affectée par les traitements, variant entre 6,1 et 8,1 % (pp^{-1}).

Pigments photosynthétiques. Les CMS ont exercé un effet positif prononcé sur la synthèse des pigments. Le traitement CMS a produit la concentration la plus élevée en c-phycocyanine (PC) à 75,2 ± 0,1 mg g^{-1} (augmentation de 36 % par rapport au contrôle à 55 ± 1,2 mg g^{-1}) et la teneur en chlorophylle a la plus élevée à 13,7 ± 0,2 mg g^{-1} (augmentation de 49 %). En revanche, les traitements nanofibres seules ont provoqué une réduction significative de la synthèse de PC (−103 % par rapport au contrôle), révélant une compétition métabolique entre le stockage des glucides et la biosynthèse des phycobiliprotéines. L'effet stimulateur des CMS sur la PC et la chlorophylle a a été mécanistiquement lié à l'influence des champs magnétiques sur les cofacteurs paramagnétiques (Fe^{2+}, Mg^{2+}) impliqués dans la voie de biosynthèse des tétrapyrroles.

Exopolysaccharides liés (BPS). Les BPS extraits de la biomasse de *L. indica* ont été identifiés comme des hétéropolymères acides et sulfatés. Les sucres neutres totaux constituaient la fraction dominante dans tous les traitements (56–69 % de la masse BPS). Le traitement CMS+NanoMEA a produit le ratio d'acide uronique le plus élevé (39,9 ± 2,49 %), indiquant un polymère plus fonctionnalisé avec des propriétés potentielles de formation de gel. Les essais nanofibres seules ont donné le degré de sulfatation le plus élevé (8,4 ± 0,15 %), l'*indica*teur fonctionnel le plus pertinent pour les applications EPS bioactives. Ces résultats ont établi que les stimuli physiques exercent non seulement des effets quantitatifs sur la productivité en biomasse, mais aussi des effets modulateurs qualitatifs sur la composition des biopolymères extracellulaires.

Article II *— Production de β-phycoérythrine et d'EPS chez Porphyridium purpureum modulée par les CMS et les nanofibres*

La deuxième étude a étendu le cadre du double stimulus à *Porphyridium purpureum* CCAP 1380/1A et a introduit une variable expérimentale supplémentaire : le régime temporel d'exposition aux CMS. Sept conditions expérimentales ont été évaluées : Contrôle (CT), CMS intermittent à 1 h j^{-1} (M1), CMS continu à 24 h j^{-1} (M24), nanofibres simples (N), CMS intermittent combiné à des nanofibres simples (MN), nanofibres MEA seules (NE) et CMS intermittent combiné à des nanofibres MEA (MNE).

Cinétique de croissance et production de RPS. L'effet des CMS sur la croissance de *P. purpureum* dépendait de façon critique de la durée d'exposition. Le CMS intermittent (M1) a produit la biomasse maximale (Xmax = 5,59 ± 0,42 g L^{-1}), soit une augmentation de 36 % par rapport au contrôle (4,12 ± 0,34 g L^{-1}), et la concentration en polysaccharides libérés la plus élevée (0,66 ± 0,11 g L^{-1}, augmentation de 83 % par rapport au contrôle). En revanche, le CMS continu

(M24) s'est révélé inhibiteur, réduisant la biomasse de 45 % à 2,27 ± 0,1 g L^{-1}. Cette relation dose-réponse a mis en évidence la nature non linéaire des effets biologiques des CMS : à des intensités et durées appropriées, les CMS stimulent l'activité enzymatique, améliorent la perméabilité membranaire et favorisent la photosynthèse ; lors d'expositions prolongées, ils génèrent des espèces réactives de l'oxygène excessives et perturbent les centres enzymatiques paramagnétiques.

Composition de la biomasse et pigments. La composition macromoléculaire de la biomasse de *P. purpureum* était dominée par les glucides dans tous les traitements, allant de 40,1 % (M1) à 52,4 % (M24). Le résultat pigmentaire le plus remarquable a été l'augmentation spectaculaire de la β-phycoérythrine (B-PE) dans les cultures traitées aux nanofibres. Le traitement NE (nanofibres MEA seules) a atteint une teneur en B-PE de 41,3 ± 3,22 mg gps^{-1}, soit une augmentation de 196 % par rapport au contrôle (13,9 ± 0,95 mg gps^{-1}). La teneur en caroténoïdes a augmenté dans tous les traitements (d'environ 100 à 342 %), avec NE produisant à nouveau la concentration en caroténoïdes la plus élevée. Ces résultats suggèrent que l'augmentation de la disponibilité en CO_2 médiée par les nanofibres favorise le flux glycolytique et l'approvisionnement en précurseurs d'acides aminés pour la biosynthèse de la phycoérythrine.

Caractérisation des EPS. Les profils biochimiques des RPS et BPS ont été analysés pour les sucres totaux, les protéines, les sucres neutres, l'acide uronique et la teneur en sulfate. La pureté des RPS était systématiquement plus élevée (60–92 %) que celle des BPS (40–52 %). La condition MNE a produit le ratio d'acide uronique le plus élevé dans les RPS (28 %), tandis que M24 a donné la sulfatation RPS la plus élevée (16,9 %). Pour les BPS, tous les traitements ont montré un ratio de sulfatation plus élevé (15–21 %) par rapport aux RPS, avec M1 présentant simultanément un sulfate élevé (19 %) et un acide uronique élevé (18 %) — un profil biochimique *indica*tif d'un fort potentiel bioactif. Le profilage des monosaccharides a confirmé un squelette hétéropolymérique conservé dominé par le xylose, le galactose et le glucose.

Article III *— Propriétés rhéologiques et structurelles des EPS de P. purpureum modulées par les CMS et les nanofibres*

La troisième étude s'est concentrée exclusivement sur la caractérisation physicochimique des fractions EPS produites par *P. purpureum* dans quatre conditions de culture : CT, M1, M24 et MN. La batterie analytique comprenait la spectroscopie FTIR, la diffusion dynamique de la lumière (DLS/potentiel zêta), l'analyse thermogravimétrique (ATG), la calorimétrie différentielle à balayage (DSC), la rhéologie oscillatoire et en régime permanent, et la microscopie électronique à

balayage (MEB) des hydrogels ioniques au Fe^{3+}. Cet article représente l'investigation en science des matériaux la plus approfondie de la thèse, établissant le lien entre les modifications moléculaires des EPS induites par la culture et leurs propriétés fonctionnelles en tant que biopolymères.

FTIR et stabilité colloïdale. Les spectres FTIR de toutes les fractions RPS et BPS ont confirmé les caractéristiques structurelles des hétéropolymères acides sulfatés. Tous les échantillons ont présenté des valeurs de potentiel zêta inférieures à −30 mV (plage : −44,4 à −68,3 mV), confirmant une forte stabilité colloïdale électrostatique dans toutes les conditions et fractions. Les effets des traitements sur le potentiel zêta étaient dépendants de la fraction : les CMS ont augmenté la charge négative des RPS (M1 atteignant −65,2 mV contre CT à −44,4 mV), tandis que pour les BPS, le traitement nanofibre combiné (MN) a montré la charge négative la plus élevée (−68,3 mV). Ce profil de stabilité est directement comparable à celui de l'alginate et de la pectine, positionnant les EPS de *P. purpureum* comme candidats pour l'encapsulation, la stabilisation des émulsions et les applications d'administration de médicaments mucoadhésifs.

Propriétés rhéologiques. Les courbes d'écoulement en régime permanent ont confirmé un comportement non newtonien et pseudoplastique (rhéofluidifiant) pour tous les échantillons de RPS, avec une viscosité apparente diminuant continûment de 1 à 100 s^{-1}. L'ajustement à la loi de puissance a donné des indices de comportement d'écoulement (n) allant de 0,079 (CT) à 0,286 (M1), tous inférieurs à 1,0. Le résultat le plus significatif a été la performance viscoélastique supérieure du traitement M24 : l'exposition continue aux CMS a produit un réseau EPS avec $G' = 17{,}10$ Pa à 1 rad s^{-1} et un rapport G'/G'' de 3,21, approchant 66 % du module élastique de la gomme xanthane ($G' = 25{,}89$ Pa ; $G'/G'' = 4{,}25$). La viscosité complexe de M24 (88,92 Pa·s à 0,1 rad s^{-1}) s'étendait sur près de trois ordres de grandeur, pleinement comparable à la plage dynamique de la gomme xanthane. Le traitement MN a produit le réseau le plus faible ($G' = 4{,}43$ Pa ; $G'/G'' = 1{,}94$), indiquant que la co-exposition aux nanofibres ne synergise pas avec les CMS pour l'assemblage du réseau EPS.

L'interprétation mécanistique proposée est que l'exposition continue au champ magnétique favorise un réseau polymère plus organisé à travers une ramification accrue, des associations inter-chaînes plus fortes (liaisons hydrogène, interactions électrostatiques) ou une proportion plus élevée de conformations hélicoïdales ordonnées. La nature cumulative et dépendante du temps de la réponse cellulaire aux CMS explique pourquoi M24 surpasse M1 rhéologiquement, malgré la

supériorité de M1 pour le rendement en biomasse — les deux régimes optimisent différents résultats métaboliques et ne peuvent pas être simultanément maximisés dans une seule condition de culture.

Propriétés thermiques. L'analyse ATG a révélé un profil de dégradation thermique caractéristique en trois étapes pour tous les EPS : perte d'humidité en dessous de 120 °C (environ 8 %, s'élevant à 22 % pour les RPS M24, indiquant une capacité de liaison à l'eau plus élevée) ; clivage primaire des liaisons glycosidiques entre 220 et 400 °C (perte de masse d'environ 53–58 %) ; et formation progressive de char au-dessus de 400 °C. L'apparition de l'événement de dégradation primaire au-dessus de 220 °C pour tous les échantillons confirme une stabilité thermique compatible avec les traitements industriels à basse température. Le caractère amorphe de toutes les fractions, confirmé par l'absence de pics de fusion cristallins nets en DSC, est avantageux pour le coulage de films, l'encapsulation et la formulation d'hydrogels.

Morphologie des hydrogels. Les hydrogels ioniques réticulés au Fe^{3+} de RPS et BPS ont été analysés par MEB après lyophilisation. Cette analyse a révélé que les conditions de culture exercent une influence substantielle sur l'architecture du réseau. Les RPS CT et M1 ont formé des réseaux macroporeux uniformes en forme de feuillets avec des diamètres de pores d'environ 10–11 µm. Les RPS M24 ont produit une structure hybride fibrillaire-laminaire distinctive. De façon la plus remarquable, les RPS MN ont produit un maillage nanofibriillaire hiérarchique avec des pores en nid d'abeilles (12,15 ± 2,3 µm) ressemblant étroitement à l'architecture de la matrice extracellulaire native — une découverte d'intérêt direct pour les applications de biomatériaux, notamment les pansements de plaies, les vecteurs de délivrance de médicaments et les constructs d'ingénierie tissulaire. Ces résultats démontrent que l'organisation tridimensionnelle de l'hydrogel résultant peut être pré-conçue par la sélection délibérée du stimulus de culture, sans aucune modification chimique des EPS.

Chapitre IV — Conclusions générales

Les résultats collectifs de cette thèse établissent que les champs magnétiques statiques et les nanofibres de PAN fonctionnalisées au MEA sont des outils non chimiques efficaces pour moduler le métabolisme microalgal et modifier les propriétés structurelles et fonctionnelles des biopolymères résultants. Les deux stimuli engagent des voies métaboliques largement indépendantes : pour *L. indica*, les CMS ciblent principalement le métabolisme de l'azote et améliorent la synthèse des pigments via la modulation du photosystème tout en augmentant les

ratios de croissance, tandis que pour *P. purpureum*, ils augmentent la production de RPS et la croissance. Les nanofibres, quant à elles, redirigent le flux de carbone vers les pigments (phycobiliprotéines et caroténoïdes) pour *P. purpureum* et vers les glucides pour *L. indica* grâce à une biodisponibilité accrue du CO_2. Leur combinaison produit des effets additifs sur le rendement en biomasse chez *L. indica* (CMS+Nano : +28 %), mais des interactions complexes chez *P. purpureum* qui dépendent à la fois du type de stimulus et du régime temporel d'exposition.

La thèse démontre en outre que l'environnement de culture peut être utilisé comme paramètre de conception moléculaire. Par la sélection et la combinaison de régimes de CMS et de nanofibres fonctionnalisées, il est possible de produire des EPS avec différents profils biochimiques — des polymères bioactifs hautement sulfatés aux réseaux viscoélastiques supérieurs approchant la gomme xanthane en termes de résistance du gel — sans modification génétique ni post-traitement chimique. Cette approche de conception de bioprocédés basée sur des stimuli physiques se positionne comme une stratégie viable et durable pour la production sur mesure de biomolécules microalgales à des fins nutraceutiques, pharmaceutiques et biomédicales.

Chapitre V — Perspectives futures

Les directions de recherche futures identifiées comprennent : la caractérisation de la masse moléculaire par SEC-MALS des fractions EPS pour lier mécanistiquement l'architecture des polymères au comportement rhéologique ; le criblage in vitro de la bioactivité (antivirale, antioxydante, anti-inflammatoire) des fractions EPS sulfatées ; la rhéométrie oscillatoire des hydrogels ioniques au Fe^{3+} pour la comparaison quantitative de la résistance des réseaux ; des études de culture à l'échelle pilote pour évaluer la viabilité économique et les performances des CMS/nanofibres à des volumes plus importants ; et l'évaluation in vitro de la biocompatibilité des hydrogels RPS MN pour des applications d'ingénierie tissulaire. En outre, une investigation plus poussée de l'intensité des CMS variables et du temps d'application permettrait de définir des fenêtres optimales pour chaque résultat métabolique. Une stratégie de stimuli séquentiels adaptés à l'état physiologique de la culture présente également un intérêt particulier.

Mots-clés : *Porphyridium*, *Limnospira*, exopolysaccharides, pigments, polysaccharides sulfatés, champs magnétiques statiques, nanofibres polymériques.

1 INTRODUCTION

The growing interest in sustainably produced, natural foods with functional appeal for improving quality of life, health, and well-being has sparked a demand for the development of new products and ingredients (Caetano *et al.*, 2022). This trend motivates industry and researchers to investigate traditional raw materials to enhance their functionality or to find alternatives that are healthier, more sustainable, and economically viable (Gohara-Beirigo *et al.*, 2022).

Microalgae/cyanobacteria fit perfectly within this description, as oxygenic photosynthetic microorganisms that metabolize CO_2 to produce organic matter and O_2, as well as being cultivated in non-productive areas. Their biomass contains commercially valuable molecules such as essential amino acids, polyunsaturated fatty acids, carbohydrates, and natural pigments(Aly; Rizk; Shams, 2023). Microalgae/cyanobacteria may be used for countless purposes, ranging from food production to biofuel generation. Additionally, some species have a high production of exopolysaccharides (EPS) with both biological and technological potential, making them valuable for the chemical, pharmaceutical, and food industries (Aly; Rizk; Shams, 2023; Ferreira *et al.*, 2021).

Microalgae EPS have interesting mechanical and biochemical properties, making them potential texture modifiers, emulsifiers, antivirals, antibacterials, and antioxidants. EPS are found as released polysaccharides (RPS) in the media and bound polysaccharides (BPS) attached to the cell wall (Pierre *et al.*, 2019). These polymers act as a gelatinous coating on the cell surface, serving important functions in the protection and acclimation of the microalga. The protection provided by these biopolymers is related to their composition and structure. Sulfated EPS are recognized for their antiviral, antibacterial, and antioxidant activities (Costa *et al.*, 2021; Naveed *et al.*, 2019).

Another group of high-value molecules present in microalgae biomass are pigments, which are primarily divided into three main categories: chlorophylls, carotenoids, and phycobiliproteins. Microalgal pigments hold significant economic potential due to their applications in food pharmaceutical and biotechnological productions, e.g. price of phycocyanin varies from $0.13 to $15.00 per mg depending on its purity (Mao *et al.*, 2024). Microalgae pigments are widely used as natural colorants in the food, cosmetic, and biotech industries due to their bright and stable colors. Phycobiliproteins such as phycocyanin and phycoerythrin can be used as food pigments, dietary

supplements, emulsifiers, gel, and toxin detectors (Mao *et al.*, 2024). Whereas, carotenoids, such as astaxanthin and beta-carotene, have gained prominence in the nutraceutical and aquaculture sectors for their antioxidant properties and their role in enhancing the pigmentation of farmed fish and crustaceans (Lafarga *et al.*, 2020; Yu, Z. *et al.*, 2024).

The production of high-value compounds requires significant energy expenditure from the microalga and is produced in greater concentrations when the microorganism is under stress. Utilizing this response as a strategy to enhance the production of metabolites is widely explored, with specific considerations for each microalgal lineage (Delattre *et al.*, 2016; Esqueda; Gardarin; Laroche, 2022; Laroche, 2022; Villay *et al.*, 2013). The application of stress in microalgal cultivation may be achieved by physical means (light intensity, magnetic fields, salinity, etc.), chemical (nutrient deprivation, CO_2 application, heavy metals, etc.), and biological (symbiosis, hormones, etc.). When managed effectively, these stressors may promote an increase in the production of EPS (Laroche, 2022), pigments, proteins, and other high value compounds (Deamici *et al.*, 2022a; Leal *et al.*, 2026; Li *et al.*, 2022).

Scaling microalgae production to industrial levels is often constrained by productivity challenges. Conventional methods for enhancing high-value molecule synthesis, such as nitrogen or phosphorus deprivation, tend to reduce overall biomass yields (Maizatul *et al.*, 2021). Therefore, developing approaches that simultaneously maintain biomass productivity while boosting high-value molecule production is essential. In this context, Static Magnetic Fields (SMF) have gained attention as a viable strategy, offering an accessible, non-toxic, and cost-effective means to optimize microalgal cultivation (Deamici *et al.*, 2022a). This physical stimulus influences biological systems through magnetic induction, magneto-mechanical effects, and the radical pair mechanism, with the potential to regulate DNA transcription, enzymatic activity, metabolic pathways, photosynthetic processes, and oxidative status (Deamici *et al.*, 2019; Font *et al.*, 2023; Santos *et al.*, 2022). However, microalgal responses to SMF are highly variable and depend on factors including field source, intensity, exposure duration, and the specific microorganism involved, underscoring the necessity for targeted investigations into SMF effects across different microalgal species (Font *et al.*, 2023; Santos *et al.*, 2022).

Optimizing CO_2 availability in microalgae cultivation systems to avoid the lost of this nutrient to the atmosphere is crucial. Chemical absorbents, particularly alkanolamines such as monoethanolamine (MEA) and diethanolamine (DEA), are well-established for enhancing CO_2

retention in liquid media through carbamate formation (Daneshvar *et al.*, 2022; Rosa; Morais; Costa, 2018; Rosa *et al.*, 2016). Also, polymeric nanofibers offer an additional strategy to increase inorganic carbon bioavailability; their high surface area to volume ratio enables them to function as effective physical adsorbents of CO_2 in microalgal culture systems (Vaz *et al.*, 2019; Vaz; Costa; Morais, 2020). Notably, nanofiber production permits compositional customization, making it feasible to produce polymeric nanofibers functionalized with MEA. These nanofibers theoretically have a double-retention mechanism: the nanofiber matrix provides a dense network of physical adsorption sites, while the functionalized MEA enables localized chemisorption, increasing CO_2 availability for microalgal cultivation (Cardias; Morais; Costa, 2024)

This work explores the impact of integrating static magnetic fields and functionalized nanofibers as a dual-stimuli strategy to optimize the growth and metabolite productivity of *Limnospira indica* PCC8005 and *Porphyridium purpureum* CCAP 1380/1A.

2 INTRODUÇÃO

O crescente interesse por alimentos naturais produzidos de forma sustentável, com apelo funcional para melhorar a qualidade de vida, a saúde e o bem-estar, tem impulsionado a demanda pelo desenvolvimento de novos produtos e ingredientes (Caetano *et al.*, 2022). Essa tendência motiva setores de pesquisa a investigar o aprimoramento de matérias-primas tradicionais ou alternativas mais saudáveis, sustentáveis e economicamente viáveis (Gohara-Beirigo *et al.*, 2022).

As microalgas/cianobactérias se enquadram perfeitamente nessa descrição, sendo microrganismos fotossintéticos que metabolizam CO_2 produzindo matéria orgânica e O_2, são ainda cultivados em áreas não produtivas. Sua biomassa contém moléculas de alto valor comercial, como aminoácidos essenciais, ácidos graxos poli-insaturados, carboidratos e pigmentos naturais (Aly; Rizk; Shams, 2023). As microalgas/cianobactérias podem ser utilizadas para inúmeras finalidades, que vão desde a produção de alimentos até a geração de biocombustíveis. Além disso, algumas espécies apresentam elevada produção de exopolissacarídeos (EPS) com potencial tanto biológico quanto tecnológico, tornando-as valiosas para as indústrias química, farmacêutica e alimentícia (Aly; Rizk; Shams, 2023; Ferreira *et al.*, 2021).

Os EPS microalgais possuem propriedades mecânicas e bioquímicas interessantes, tornando-os potenciais modificadores de textura, emulsificantes, antivirais, antibacterianos e antioxidantes. Os EPS são encontrados como polissacarídeos liberados (RPS) no meio de cultura e polissacarídeos estruturais ligados (BPS) à parede celular do microrganismo (Pierre *et al.*, 2019) (Pierre et al., 2019). Esses polímeros atuam como um revestimento gelatinoso na superfície celular, desempenhando funções importantes na proteção e aclimatação da microalga. A proteção conferida por esses biopolímeros está relacionada à sua composição e estrutura. Os EPS sulfatados são reconhecidos por suas atividades antivirais, antibacterianas e antioxidantes (Costa *et al.*, 2021; Naveed *et al.*, 2019).

Outro grupo de moléculas de alto valor presente na biomassa de microalgas são os pigmentos, divididos principalmente em três categorias: clorofilas, carotenoides e ficobiliproteínas. Os pigmentos microalgais possuem significativo potencial econômico devido às suas aplicações nas produções alimentícia, farmacêutica e biotecnológica, por exemplo, o preço da ficocianina varia de US$ 0,13 a US$ 15,00 por mg dependendo de sua pureza (Mao *et al.*, 2024). Os pigmentos de microalgas são utilizados como corantes naturais nas indústrias alimentícia, cosmética e

biotecnológica devido às suas cores vivas e estáveis. Assim, ficobiliproteínas, como a ficocianina e a ficoeritrina, podem ser empregadas como pigmentos alimentares, suplementos dietéticos, emulsificantes, géis e detectores de toxinas (Mao *et al.*, 2024). Já os carotenoides, como a astaxantina e o beta-caroteno, ganharam destaque nos setores de nutracêuticos e aquicultura por suas propriedades antioxidantes e seu papel no aprimoramento da pigmentação de peixes e crustáceos de criação (Lafarga *et al.*, 2020; Yu, Z. *et al.*, 2024).

A produção de compostos de interesse requer alto gasto energético da microalga e ocorre em maiores concentrações quando o microrganismo está sob estresse. Utilizar essa resposta como estratégia para potencializar a produção de compostos de alto valor agregado é amplamente explorada, e cada linhagem microalgal responde de maneira especifica a seu metabolismo (Delattre *et al.*, 2016; Esqueda; Gardarin; Laroche, 2022; Laroche, 2022; Villay *et al.*, 2013) . A aplicação de estresse no cultivo de microalgas pode ser realizada por meios físicos (intensidade luminosa, campos magnéticos, salinidade, etc.), químicos (privação de nutrientes, aplicação de CO_2, metais pesados, etc.) e biológicos (simbiose, hormônios, etc.). Quando manejados de forma eficaz, esses estressores podem promover um aumento na produção de EPS (Laroche, 2022), pigmentos, proteínas e outros compostos de alto valor (Deamici; Morais; *et al.*, 2022; Leal *et al.*, 2026; Li, C. *et al.*, 2022).

Escalar a produção de microalgas a nível industrial é frequentemente limitado por desafios de produtividade. Os métodos convencionais para aumentar a síntese de moléculas de alto valor, como a privação de nitrogênio ou fósforo, tendem a reduzir os rendimentos globais de biomassa (Maizatul *et al.*, 2021). Portanto, o desenvolvimento de abordagens que mantenham simultaneamente a produtividade da biomassa enquanto aumentam a produção de moléculas de alto valor é essencial. Nesse contexto, os Campos Magnéticos Estáticos (CMF) têm ganhado atenção como uma estratégia viável, oferecendo um meio acessível, não tóxico e economicamente eficiente para otimizar o cultivo de microalgas (Deamici *et al.*, 2022a). Este estímulo físico influencia os sistemas biológicos por meio de indução magnética, efeitos magnetomecânicos e agindo em pares radicais, com potencial para regular transcrição do DNA, atividade enzimática, vias metabólicas, processos fotossintéticos e estado oxidativo (Deamici *et al.*, 2019; Font *et al.*, 2023; Santos *et al.*, 2022). Entretanto, as respostas das microalgas aos CME são altamente variáveis e dependem de fatores como a fonte do campo, intensidade, duração da exposição e o microrganismo específico envolvido, ressaltando a necessidade de investigações direcionadas

sobre os efeitos dos CME em diferentes espécies de microalgas (Font *et al.*, 2023; Santos *et al.*, 2022).

A otimização da disponibilidade de CO_2 nos sistemas de cultivo de microalgas, para evitar a perda desse nutriente para a atmosfera, é fundamental. Absorventes químicos, particularmente alcanolaminas como a monoetanolamina (MEA) e a dietanolamina (DEA), são bem estabelecidos para melhorar a retenção de CO_2 em meios líquidos por meio da formação de carbamato (Daneshvar *et al.*, 2022; Rosa; Morais; Costa, 2018; Rosa *et al.*, 2016). Além disso, as nanofibras poliméricas oferecem uma estratégia adicional para aumentar a biodisponibilidade de carbono inorgânico; sua elevada relação superfície/volume as permite funcionar como eficientes adsorventes físicos de CO_2 em sistemas de cultivo de microalgas systems (Vaz *et al.*, 2019; Vaz; Costa; Morais, 2020). Notavelmente, a produção de nanofibras permite a personalização composicional, tornando viável a produção de nanofibras poliméricas funcionalizadas com MEA. Essas nanofibras possuem teoricamente um mecanismo de dupla retenção: a matriz da nanofibra fornece uma densa rede de sítios de adsorção física, enquanto a MEA funcionalizada possibilita a quimissorção localizada, aumentando a disponibilidade de CO_2 para o cultivo de microalgas (Cardias; Morais; Costa, 2024).

Este trabalho explora o impacto da integração de campos magnéticos estáticos e nanofibras funcionalizadas como uma estratégia de duplo estímulo para otimizar o crescimento e a produtividade de metabólitos de *Limnospira indica* PCC 8005 e *Porphyridium purpureum* CCAP 1380/1A.

3 OBJECTIVES

3.1 GENERAL OBJECTIVE

Study the effect of magnetic fields combined with nanofibers in the cultivation of *Limnospira indica* PCC8005 and *Porphyridium purpureum* CCAP 1380/1A.

3.2 SPECIFIC OBJECTIVES

- Investigate the individual and joint relationships of magnetic fields and nanofibers in the cultivation of *Limnospira indica* PCC8005 and *Porphyridium purpureum* CCAP 1380/1A ;
- Extract and purify the EPS from cultivation supernatant and biomass;
- Characterize the produced EPS according to their composition and structure;
- Evaluate *Porphyridium purpureum* CCAP 1380/1A RPS rheology and EPS hydrogel morphology;
- Mesure main compounds of the biomass produced.

CHAPTER II

4 LITERATURE REVIEW

4.1 CYANOBACTERIA AND MICROALGAE

Microalgae and cyanobacteria are unicellular or multicellular phototrophic organisms that perform photosynthesis, efficiently using light, water, and carbon dioxide (CO_2) to produce organic matter. (1) Cyanobacteria, or Cyanophyta, are prokaryotic organisms with a blue-green color, and (2) eukaryotic microalgae, are divided into different phyla based on their pigments and cellular structures. Among the most relevant eukaryotic groups are Rhodophyta (red algae), Chlorophyta and Charophyta (green algae), and Ochrophyta, Haptophyta, and Miozoa (golden and brown algae). Each group has distinct pigmentation and metabolic characteristics that influence their ecological roles and industrial applications (Rossi; Philippis, 2016).

Among the commercially utilized photosynthetic microorganisms (PM), *Spirulina* (Cyanobacteria) and *Chlorella* (Chlorophyta) stand out as the most common strains added to food products. This is due to their high content of proteins, vitamins, minerals, and antioxidants, making them popular in human diets and nutritional supplements (Benavente-Valdés *et al.*, 2021; Gaignard *et al.*, 2019). Recently, the industrial production of *Porphyridium* has been intensified due to its production of exopolysaccharides and pigments, specifically phycobiliproteins, both of which hold high market value in the cosmetics and pharmaceutical industries (Bayu *et al.*, 2023).

The use of these PM as a food source has been documented for thousands of years among peoples in Africa, North America, and Asia. In the 1950s, microalgae gained popularity as they were recognized as a promising source of protein (Benavente-Valdés *et al.*, 2021). When added to food, microalgal biomass adds nutritional value to the product. Microalgae are rich in proteins (essential amino acids and peptides), polyunsaturated fatty acids, carbohydrates, vitamins, minerals, and bioactive compounds such as antioxidants and anti-inflammatories (Chen, C. *et al.*, 2022). Those characteristics make these PM an excellent ingredient for the production of functional foods (Levasseur; Perré; Pozzobon, 2020).

In addition to biomass, during cultivation microalgae release extracellular polymeric biocompounds, some species more than others, these polymers are formed mainly by sugars, and proteins which can have substitution of functional groups such as sulphates, and methyl groups. As these polymers are mostly chains of sugars and mainly found outside/part of the cell wall they are

denominated exopolysaccharides (EPS), and act as a defense mechanism of the microalgae (Laroche, 2022).

Microalgae and cyanobacteria from all genera produce EPS, which vary in composition, quantity, and rheological properties. However, thousands of these PM species remain unexplored in terms of the production and characterization of their EPS (Laroche, 2022). These biomolecules exhibit biological activities, such as antimicrobial, antitumor, and antiviral properties, and also have technological potential as thickeners and gelling agents (Costa *et al.*, 2021; Wang, W. N. *et al.*, 2021; Zhang, J. *et al.*, 2019).

4.1.1 *Limnospira, Arthrospira* and *Spirulina.*

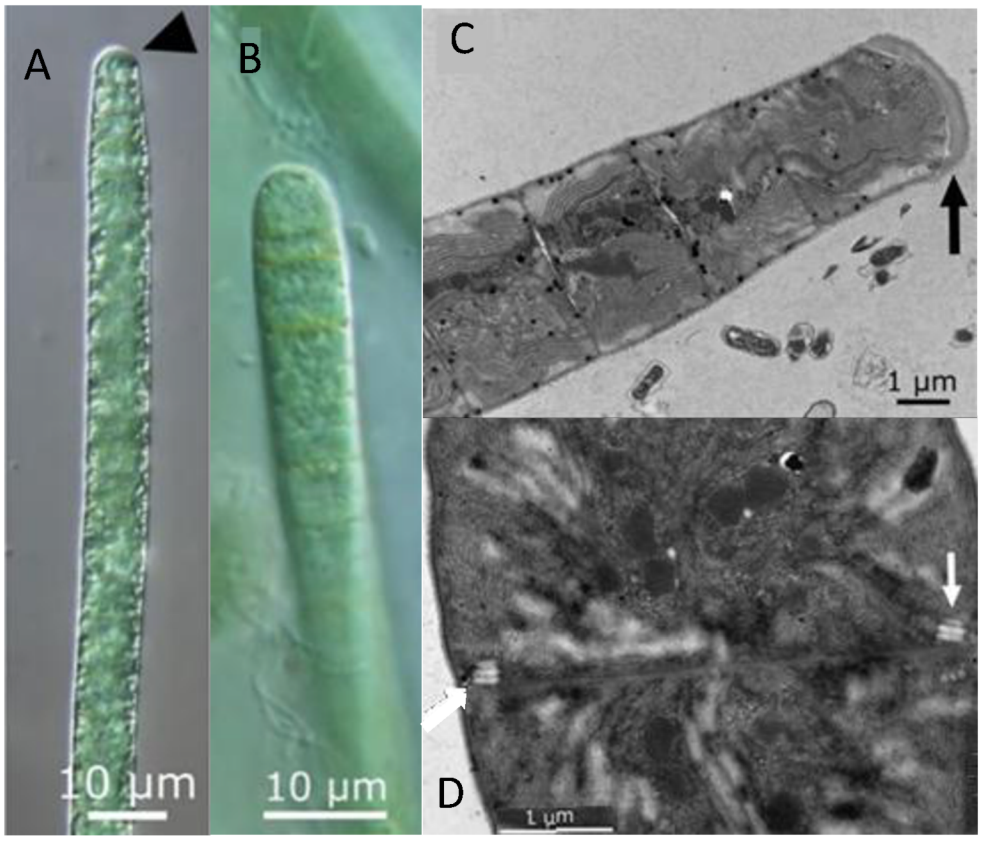
Limnospira, *Arthrospira,* and *Spirulina* are cyanobacteria, autotrophic blue-green, filamentous multicellular prokaryotic microorganisms that grow naturally in alkaline lakes exposed to the sun and high temperatures. They are prokaryotes, so they do not have membranous organelles, formed by cylindrical cells aligned in spirals or lines (Wan; Wu; Kuča, 2016). Cyanobacteria are the only group of photosynthetic bacteria that have oxygen metabolism, producing oxygen as a waste product of photosynthesis (Blankenship, 2021). Cyanobacteria that have helical tricomes are divided into *Spirulina*, *Halospirulina,* and *Arthrospira*: of which *Arthrospira* is the most produced as a food supplement and additive, being promoted under the name "Spirulina" due to marketing and historical reasons (Nowicka-Krawczyk; Mühlsteinová; Hauer, 2019).

The genus *Liminospira* (Figure 1A and C) has been proposed to characterize variances within the genus *Arthrospira* (Figuere 1B and D) being differentiated by its disorganized distribution of intracellular thylakoids and enlarged cell wall in apical cells, which can be seen in Figure A and C *indica*ted by the black arrows. Whereas *Arthrospira* are characterized by radially-arranger thylakoids and facultative gas vesicles forming aerotopes (white arrows in Figure 1D). Another common characteristic of *Liminospira* is its affinity for alkaline media, which facilitates its production by the food industry, due to the minimization of contamination (Nowicka-Krawczyk; Mühlsteinová; Hauer, 2019).

The biomass of *Spirulina* is regarded as safe for consumption and is considered an ingredient in the production of functional foods, due to its nutritional profile and bioactive

compounds, such as exopolysaccharides, peptides, and polyunsaturated fatty acids (Ai *et al.*, 2023; Lafarga *et al.*, 2021, 2020).

Figure 1 - Morphology of *Limnospira fusiformis* (A and C) and *Arthrospira jenneri* (B and D). Black arrows poit to the thickened cell wall. Whight arrows point to aerotope.



Source**:** Nowicka-Krawczyk; Mühlsteinová; Hauer (2019).

These cyanobacteria are primarily cultivated for human and animal consumption due to its high concentration of macronutrients. The average protein content in *Spirulina* is 43.1%, followed by lipids (11.7%), carbohydrates (21.8%), and ash (8.12%) in its proximate composition (Finkel *et al.*, 2016). The composition of the biomass is directly related to the cultivation conditions, as well as the availability of nutrients and environmental stress factors.(Lafarga *et al.*, 2020). Colla et al. (2020) report a concentration of 60-70% of proteins in Spirulina (*Arthrospira*) grown in Zarrouk medium at 35 ºC, supplemented with 1.875 g L^{-1} of sodium nitrate.

Protein formation in cyanobacteria is primarily attributed to nitrogen (N) assimilation. This nutrient can be present in the medium in both inorganic forms (ammonium and nitrates) and organic forms (urea and amino acids). Once absorbed, nitrogen is enzymatically converted to ammonium

within the cytoplasm, where it is incorporated into carbon skeletons to facilitate the synthesis of proteins (Berges; Mulholland, 2008; Muro-Pastor; Reyes; Florencio, 2005). Besides proteins function as enzymes, there is their structural role. In cyanobacteria (*Limnospira*, *Arthrospira,* and *Spirulina*), they are the building blocks for phycobilinprotein (phycocyanin), responsible for these cyanobacteria's natural blue color, which can be used in the food, pharmaceutical, and biotech industry, varying from $0.13 to $15.00 per mg if food or pharmaceutical grade, respectively (Mao *et al.*, 2024).

In *Limnospira/Arthrospira* (industrial "Spirulina"), carbohydrate formation begins with CO_2 fixation by the Calvin–Benson–Bassham cycle, producing triose phosphates that feed into glycolysis and the oxidative pentose phosphate (OPP) pathway (Blankenship, 2021). These central routes interconvert glyceraldehyde-3-phosphate, fructose-6-phosphate, and glucose-6-phosphate, which are then converted to glucose-1-phosphate as the precursor for storage and structural carbohydrates. Genome-scale models of *Arthrospira platensis* explicitly include these reactions as the core of its central carbon metabolism (Blankenship, 2021; Kanehisa *et al.*, 2025).

The main assimilation product is glycogen: glucose-1-phosphate is converted to ADP-glucose by ADP-glucose pyrophosphorylase (GlgC), elongated into α-1,4-glucan chains by glycogen synthase (GlgA), and branched by GlgB (Kanehisa *et al.*, 2025). Under nitrogen and SO_4^{2-} stress, *A. platensis* C1 can accumulate up to 70% of its dry weight as glycogen, with glucose accounting for over 80% of total monosaccharides, *indica*ting that photosynthate and even recycled protein carbon are redirected into this storage polymer (Blankenship, 2021; Klanchui *et al.*, 2018). Glycogen is then mobilized via glycogen phosphorylase and debranching enzymes back to glucose-1-phosphate, which feeds the OPP pathway to support photosynthesis start-up and energy balance during dark–light transitions (Blankenship, 2021; Kanehisa *et al.*, 2025).

Polymerized sugars in the form of exopolysaccharides (EPS) also have structural and stress-protective functions in cyanobacteria, including *Limnospira/Arthrospira* and Spirulina. These polymers occur as capsular layers and sheaths closely associated with the cell envelope and as released EPS forming the extracellular polymeric matrix; in both cases, they create a hydrated, viscoelastic barrier that stabilizes the microenvironment, promotes adhesion and biofilm formation, and buffers cells from fluctuations in moisture, light, salinity, and nutrient availability as well as protects against toxins and biohazards (Li, Z. *et al.*, 2022; Phélippé *et al.*, 2019). EPS produced by these cyanobacteria are complex heteropolymers that are directly influenced by the cultivation

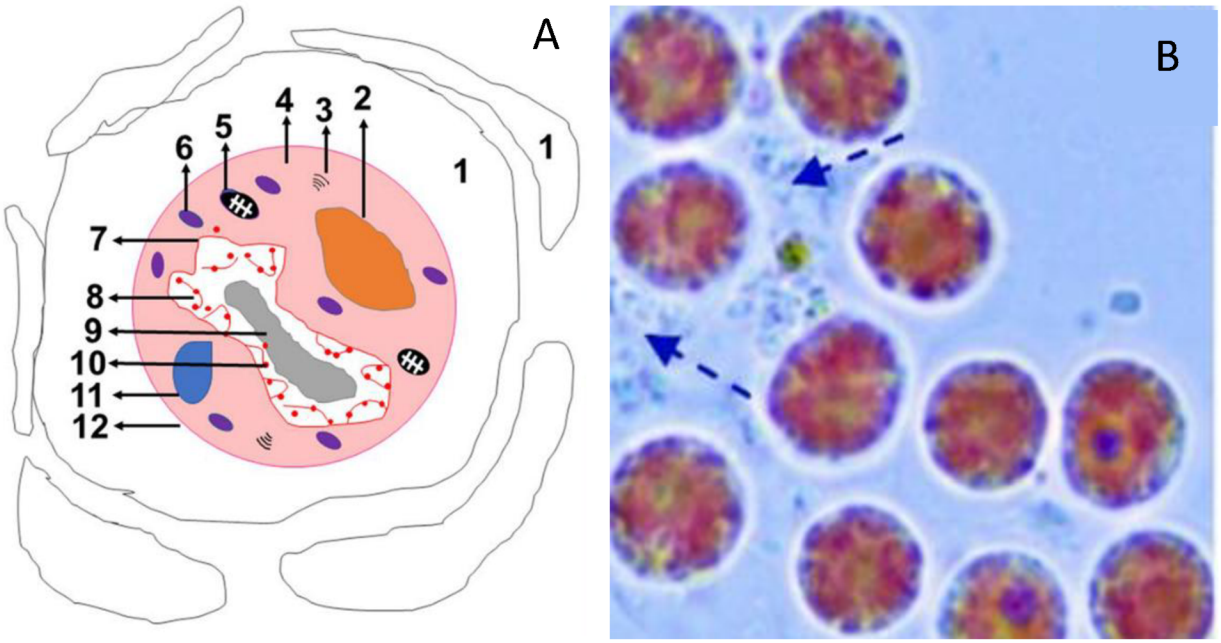
conditions (Phélippé *et al.*, 2019). Changes in nutrient availability, such as nitrogen and light (El Baz KF, 2014; Panyakampol *et al.*, 2016) as well as environmental factors like osmotic stress, high temperature, and nutrient deprivation, modify both the composition and quantity of these exopolymers (Lee; Chen; Peng, 2012; Panyakampol *et al.*, 2016).

"*Spirulina*" is one of the most widely cultivated cyanobacteria worldwide, with estimated global annual production at roughly 10,000–12,000 t of dry biomass. China dominates this output, reported in scientific articles as responsible for about 70–80% of world production, followed by more limited but still significant production in the United States, Taiwan, Thailand, and India. A total of ~0.102 million tons of "*Spirulina*" within the broader 36.5 million tons of global all algae production in 2022 (Hosseini; Bounnit; Saadaoui, 2026).

4.1.2 *Porphyridium sp.*

Red microalgae of the genus *Porphyridium* (Figure 2A and B) comprise four species: *P. purpureum* (including *P. cruentum* and *P. marinum*), *P. aerugineum*, *P. sordidum*, and *P. wittrockii*. These microalgae are characterized by spherical cells approximately 6 μm in diameter, with a nuclear membrane covered by ribosomes (Figure 2A). They can aggregate into cellular clusters through the production of gelatinous polysaccharides, which act as a physical barrier, encapsulating the cells and complementing the cell wall, which lacks a microfibrillar layer (Figure 2B). This layer of exopolysaccharides (EPS) is thin during the logarithmic growth phase but becomes thicker during the stationary phase, at which point it is also released into the surrounding medium, increasing its viscosity (Bayu *et al.*, 2023; Borovkov *et al.*, 2026).

Figure 2 – (A) The general schematic cell structure of red microalga genera Porphyridium . (B) Microphotographs of *P. purpureum* cells aggregate. 1 EPs, 2 nucleus, 3 Golgi, 4 cytosol, 5 mitochondrion, 6 intracellular polysaccharide, 7 chloroplast, 8 thylakoid, 9 pyrenoid, 10 phycobilisome, 11 vacuole, 12 plasmic membrane. Blue arrows *indica*tes extracellular space with exopolysaccharide.



Source**:** Bayu *et al.*, (2023), Borovkov *et al.* (2026)

P. purpureum is the most extensively studied species within its genus and is also the most widely produced at a commercial scale. Its commercial potential arises from its ability to thrive in adverse conditions, alongside its carbohydrate content (ranging from 23% to 52%), protein content (15% to 47%), and production of sulfated exopolysaccharides (EPS) and phycobiliproteins (pigments). The latter, in particular, holds significant value in the pharmaceutical industry. Although *P. purpureum* is not a major lipid producer, it does contain long-chain polyunsaturated fatty acids, especially arachidonic acid (ARA, C20:4, ω-6) and eicosapentaenoic acid (EPA, C20:5, ω-3), both of which are known for their bioactive properties (Bayu *et al.*, 2023).

The carbohydrates found in the cultivation of *Porphyridium* are classified into floridean starch and exopolysaccharides (EPS). The former is a polymer of D-glucopyranose linked by α-(1 → 4) glycosidic bonds, which are present in the cytosol. In contrast, EPS can be found either attached to the plasma membrane or released into the culture medium (Simon-Bercovitch; Bar-Zvi;

Arad, 1999). The formation of EPS in *Porphyridium purpureum* occurs primarily as a result of metabolic reprogramming triggered by abiotic stress, specifically progressive nitrogen deprivation. As nitrate availability declines, cells downregulate growth and energy-intensive processes and redirect carbon flux toward polysaccharide synthesis and secretion. At the metabolic level, this shift involves dynamic regulation of central carbon pathways, particularly glycolysis, gluconeogenesis, and the pentose phosphate pathway, which maintain energy and redox balance while generating the hexose and pentose intermediates required as polysaccharide precursors. These intermediates feed directly into nucleotide-sugar biosynthesis pathways, with early nitrogen limitation triggering coordinated upregulation of the enzymes responsible for producing activated sugar donors, including UDP-glucose, UDP-glucuronic acid, UDP-xylose, GDP-mannose, and GDP-galactose (Guerreiro *et al.*, 2026; Simon-Bercovitch; Bar-Zvi; Arad, 1999).

With the necessary building blocks available, polymerization of the EPS backbone is carried out by carbohydrate-active enzymes (CAZymes), a specific group of proteins whose expression is selectively upregulated under nitrogen stress. Among these, glycosyltransferases (GTs), particularly families GT4, GT8, and GT77, catalyze the formation of glycosidic bonds that link individual sugar units into complex polysaccharide chains. Parallel, the cell upregulates pathways associated with glycan assembly and glycoprotein synthesis, which mediate post-polymerization modifications essential for completing cell wall biosynthesis and facilitating the release of mature polysaccharides into the extracellular medium (Guerreiro *et al.*, 2026)..

The final structure of the secreted EPS reflects this highly coordinated enzymatic control. It consists of neutral sugars (glucose, galactose, xylose), acidic sugars (galacturonic and glucuronic acids), and sulfate groups. This compositional regularity underscores the precision of the underlying biosynthetic machinery and provides a biochemical basis for the characteristic physicochemical properties of *P. purpureum* EPS, including its anionic character, high water-binding capacity, and rheological functionality (Geresh *et al.*, 2009; Guerreiro *et al.*, 2026; Keidan *et al.*, 2006).

4.1.3 Photosynthesis and pigments in cyanobacteria/microalgae.

Photosynthesis is a biological process that uses light energy as a trigger, initiating a series of physical and biochemical reactions responsible for generating the necessary energy to sustain and propagate the organism's cellular metabolism. During the light phase, the captured energy is used to produce ATP and NADPH, which drive the dark phase, where carbon dioxide is fixed through the Calvin cycle. This process results in the production of glyceraldehyde-3-phosphate (G3P), a crucial intermediate for the synthesis of carbohydrates such as glucose and starch, as well as the formation of precursors for proteins and lipids (Blankenship, 2021). Thus, photosynthesis not only provides immediate energy but also generates the building blocks needed for the synthesis of essential biomolecules. In addition, photosynthesis is the primary biological mechanism for capturing inorganic carbon globally, with much of this process carried out by macro- and microalgae. The latter mediates approximately 50% of the planet's oxygenic photosynthesis (Hoque *et al.*, 2025).

Blankenship (2021) divided photosynthesis into four main phases: (1) light absorption and energy transfer by antenna systems, (2) primary electron transfer at reaction centers, (3) generation of electrochemical gradients for ATP synthesis, and (4) production and export of stable compounds.

Light absorption: Photosynthesis begins with the absorption of photons by pigments in the antenna system, such as chlorophylls, carotenoids, and bilins, pigments associated with proteins in specific arrangements. The excitation of electrons in these pigments creates a high-energy state that is transferred to the reaction centers. Pigments at the periphery of the antenna system absorb shorter wavelengths, while core pigments absorb longer wavelengths, facilitating energy transfer (Blankenship, 2021; Lokstein; Renger; Götze, 2021).

Electron transfer: In the reaction centers, pigment-protein complexes located in the photosynthetic membranes, light energy is converted into chemical energy. Cofactors like quinones and iron-sulfur centers, associated with hydrophobic polypeptides, participate in electron transfer. The energy is directed to pigment dimers, which reach a higher excited state. The system is highly optimized, with the photochemical quantum yield, the ratio of products formed per photon absorbed, in most cases close to 1.0 (Blankenship, 2021; Poluektov; Utschig, 2021).

Generation of electrochemical gradients for ATP synthesis: The electron transfer is coupled with proton transport across the membrane, creating an electrochemical potential gradient, known as the proton-motive force. This gradient drives ATP synthesis, the main energy molecule of the

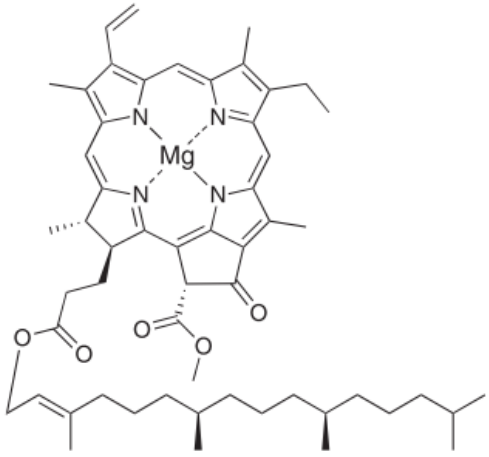
cell. Proton-motive force is also generated as protons are transported through the membrane to the thylakoid lumen. In oxygen-releasing photosynthetic organisms, Photosystems I and II work together. Photosystem II extracts electrons from water, releasing molecular oxygen, while Photosystem I uses a second light energy-induced mechanism to reduce NADP+ into NADPH, a key reducing agent for the final phase of photosynthesis (Blankenship, 2021).

Synthesis and export of stable products: In the final phase, NADPH and ATP are used in the Calvin-Benson cycle to reduce carbon dioxide into sugars. This cycle is divided into three stages: (a) carboxylation, which fixes CO_2 and generates 3-phosphoglyceric acid (PGA); (b) reduction, using ATP and NADPH to convert PGA into triose phosphate; and (c) regeneration, where trioses are converted into ribulose 5-phosphate, restarting the cycle. Phosphorylated sugars are then exported from the chloroplast to fuel various cellular functions, such as carbohydrates, lipids, and proteins synthesis (Chen *et al.*, 2022).

Photosynthesis relies on a diverse array of pigments, with chlorophyll playing a pivotal role due to its functional significance. Among the various types of chlorophyll, chlorophyll α (Figure 1) stands out as the primary light-harvesting pigment. The molecular structure of chlorophyll is characterized by a central magnesium (Mg) atom coordinated with four nitrogen atoms, which are integral components of a tetrapyrrole ring system. This tetrapyrrole structure is derived from pyrrole, a heterocyclic organic compound comprising a five-membered ring with four carbon atoms and one nitrogen atom. The unique tetrapyrrole configuration is a defining feature of all chlorophyll molecules, enabling their efficient light-absorption properties (Tamiaki; Kichishima, 2024).

Chlorophyll α (Figure 3) also has a fifth ring attached to its central structure and a long phytol hydrocarbon tail, which plays a crucial role in anchoring the molecule within the thylakoid membranes of the chloroplast. This tail ensures that chlorophyll remains firmly positioned within the photosynthetic complexes, facilitating efficient light absorption and maximizing energy transfer (Blankenship, 2021; Tamiaki; Kichishima, 2024).

Figure 3 - Chemical structure of chlorophyll α.



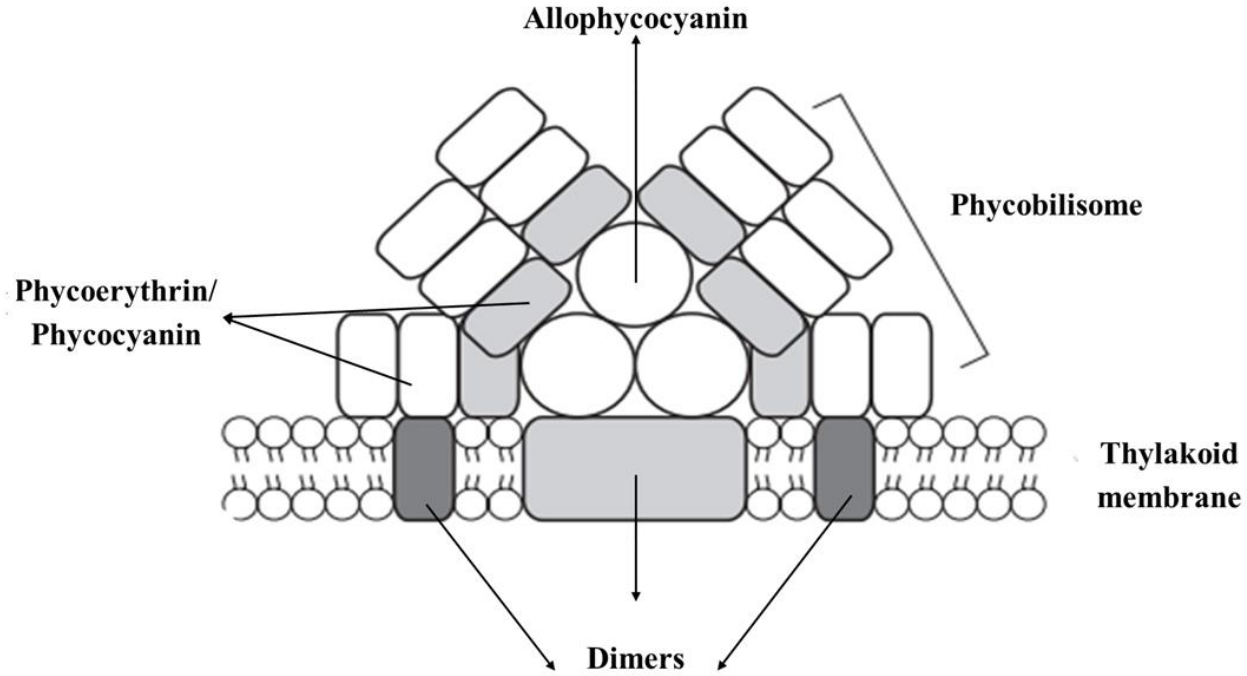
Source: Blankenship (2021)

Carotenoids are essential accessory pigments present in most photosynthetic antenna complexes. They assist in light harvesting by absorbing wavelengths between 400 and 500 nm, which gives them their characteristic yellow to orange coloration. After absorbing light, carotenoids transfer the captured energy to chlorophyll molecules, thereby complementing the process of light energy capture (Aly; Rizk; Shams, 2023; Blankenship, 2014; Oliveira *et al.*, 2022).

In addition to their role in light harvesting, carotenoids play a crucial role in photoprotection. They help protect photosynthetic cells from the formation of singlet oxygen, a reactive form of oxygen that can damage cellular structures. In the xanthophyll cycle, a specific mechanism of photoprotection, carotenoids dissipate excess absorbed energy under intense light conditions by converting it to heat. This process prevents plants and other photosynthetic organisms from experiencing oxidative damage due to the overexcitation of photosynthetic pigments (Blankenship, 2014; Nguyen *et al.*, 2024).

Bilin pigments are linear, open-chain tetrapyrroles that play an essential role in light harvesting in photosynthetic organisms. They are located in the phycobilisomes (PBS) (Figure 4), specialized structures that capture light at wavelengths between 450 nm and 650 nm. This absorption range is particularly advantageous, as it complements light harvesting where chlorophyll exhibits lower efficiency, thereby enabling a broader absorption spectrum (Blankenship, 2014; Ma *et al.*, 2020).

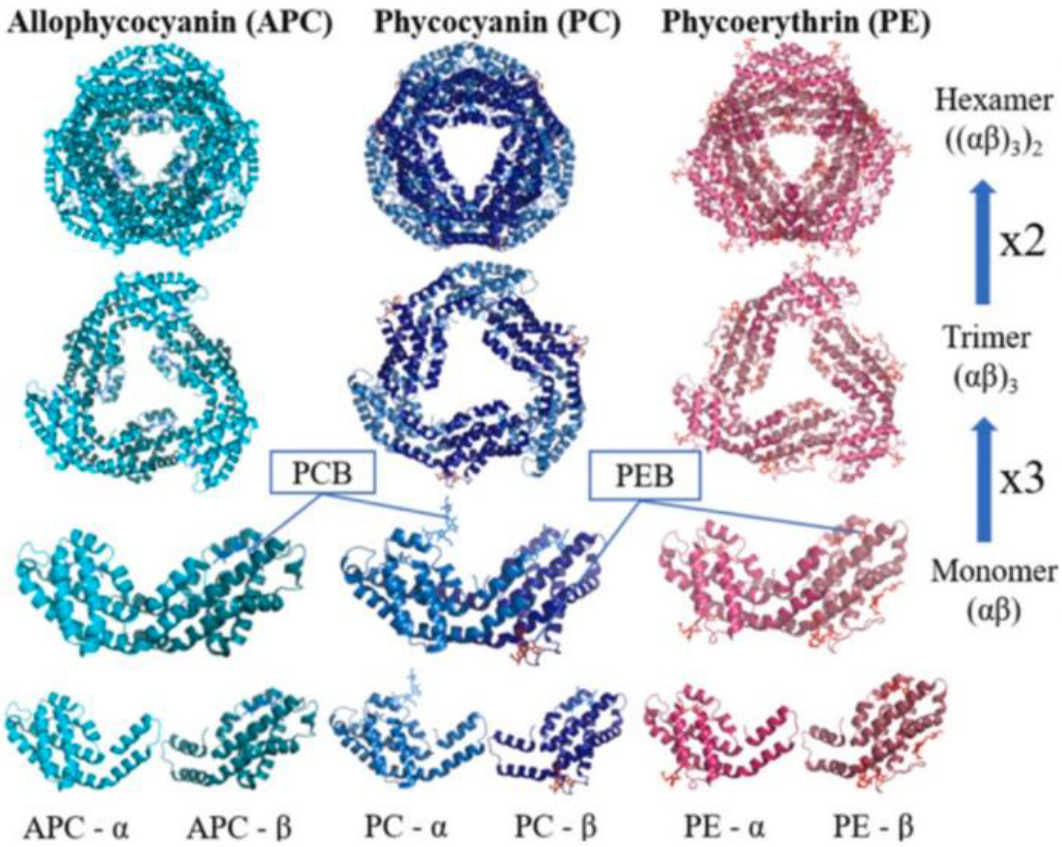
Figure 4 - Phycobilisome (PBS) structure model.



Source: Blankenship (2021); Ganesan (2022)

These pigments, such as phycocyanobilin and phycoerythrobilin, are bound to proteins known as biliproteins. The primary classes of biliprotein complexes include allophycocyanin, phycocyanin, and phycoerythrin (Figure 5), which are formed by monomers of α and β proteins fold into trimers and are arranged in hexamers in the PBS (Nguyen *et al.*, 2024). While bilins share structural similarities among themselves, the specific configuration of the biliproteins to which they are attached alters their light absorption properties, imparting unique characteristics to each complex (Blankenship, 2014; Ma *et al.*, 2020).

Figure 5 - Detailed protein structures of phycobiliproteins (allophycocyanin (APC), phycocyanin (PC), and phycoerythrin (PE), from subunits to hexamers.



Source: Nguyen *et al.* (2024)

An interesting adaptive aspect is chromatic acclimation, where some cyanobacteria can adjust the composition of their phycobilisomes in response to the quality of ambient light. By altering the expression levels of different biliproteins, these organisms optimize light absorption under varying conditions, enhancing their photosynthetic efficiency (Blankenship, 2021).

Bilin pigments, particularly phycobilins, along with carotenoids and chlorophyll, have garnered significant attention in the market due to their diverse applications across various industries. Their vibrant colors and light-absorbing properties make them valuable as natural colorants in the food, cosmetics, and pharmaceutical sectors, where there is a growing demand for natural alternatives to synthetic dyes (Aly; Rizk; Shams, 2023; Chen, C. *et al.*, 2022; Costa *et al.*, 2019).

Carotenoids, known for their yellow to orange hues, also contribute to the visual appeal of products while providing health benefits such as antioxidant properties. Similarly, chlorophyll is

utilized not only for its color but also for its potential health benefits, often featured in dietary supplements and green products (Benavente-Valdés *et al.*, 2021). As consumer awareness of sustainability and natural products continues to rise, the market for bilins, carotenoids, and chlorophyll is expected to expand, highlighting their potential as multifunctional ingredients in a wide range of applications (Aly; Rizk; Shams, 2023).

4.2 MICROALGAL AND CYANOBACTERIA CULTIVATION

The composition and productivity of biomass and compounds of interested produced by microalgae are directly influenced by cultivation conditions. Strategies such as nutrient reduction (N, P, and minerals), osmotic pressure adjustments, photoperiod variations, light intensity, the presence of heavy metals, and temperature all play significant roles in the production of these polymers (Garza-Rodríguez *et al.*, 2022). Another determining factor for the synthesis of biomass and molecules of interest is the intrinsic characteristics of the microalgae (Laroche, 2022). The optimal conditions for one species may be unfavorable for another. For instance, in the case of the *Spirulina* sp. strain, an increase in salinity stimulates the production of EPS (Lee; Chen; Peng, 2012) In contrast, for *Anabaena* sp., increased salinity acts as an inhibitor of EPS production. (Moreno *et al.*, 1998).

4.2.1 Carbon dioxide in microalgae/cyanobacteria production

The carbon fixation in microalgae occurs through three main pathways: the active and direct uptake of HCO_3^-, an active CO_2 transport mechanism, and enzymatic pathways involving carbonic anhydrase external to the plasma membrane. Various factors influence the photosynthetic efficiency of microalgae and CO_2 assimilation, including heat, light, and the mass transfer of CO_2 and nutrients. The physicochemical profiles (pH, temperature, salinity, turbidity), the composition of culture media, CO_2 concentration, light wavelengths and intensity, the design of bioreactors, and the selection of microalgal species significantly impact the biofixation capacity of CO_2 in these microorganisms (Daneshvar *et al.*, 2022; Zhang; Liu, 2021).

The optimal average concentration of CO_2 for microalgal growth ranges from 2% to 6%. Direct injection of high levels of CO_2 into microalgal cultures and bioreactors can lead to a decrease

in the pH of the culture medium. Elevated CO_2 levels (>10%) and the resulting acidification can damage RuBisCO in the carbon-concentrating mechanisms (CCMs) of microalgae, which are the primary enzymatic catalysts of photosynthesis. This damage can result in inhibited growth and cell death (Daneshvar *et al.*, 2022).

CO_2 has low solubility in water, resulting in significant losses of the gas to the atmosphere once added to the medium. Various strategies can be employed to minimize this loss. Among these strategies is the addition of chemical absorbents, such as monoethanolamine (MEA), which boasts an absorption efficiency of over 90% for CO_2. Additionally, the use of physical adsorbents, such as nanofibers, can be effective; these materials act as physical barriers that trap the gas due to their large surface area. (Comitre *et al.*, 2021; Daneshvar *et al.*, 2022).

The use of nanoparticles in microalgal cultivation is reported to increase biofixation, dissolved inorganic carbon, and biomass accumulation, as well as, change the macromolecule biomass profile (Cardias; Morais; Costa, 2024; Comitre *et al.*, 2021; Vaz; Mastrantonio; *et al.*, 2019). The authors usually attribute this behavior to the carbon availability in the media. The functional properties of these nanofibers are inherently determined by their constituent materials; specifically, the choice of polymers, metals, or chemical functionalization contributes to their distinct characteristics, such as surface charge and specific chemical binding affinities, so to maximize functionality, new components are tested (Vaz; Costa; *et al.*, 2019).

Amine-based absorbents are organic derivatives of ammonia characterized by their ability to reversibly bind acidic gases, such as CO_2, to form carbamates and bicarbonates. These compounds facilitate carbon recovery, as they can be regenerated through thermal treatment or pressure reduction (Said *et al.*, 2020). Previous studies have demonstrated that integrating amine absorbents, specifically monoethanolamine (MEA) and diethanolamine (DEA), into microalgal cultures enhances dissolved inorganic carbon (DIC) levels and modulates biomass composition (Rosa; Morais; Costa, 2018; Rosa *et al.*, 2016). Consequently, the synergy between the high specific surface area of nanofibers and the chemical affinity of MEA may function as a dual mechanism for carbon sequestration. This approach potentially increases carbon availability, thereby stimulating biomass productivity and inducing significant shifts in macromolecular profiles.

4.2.2 Magnetic fields in microalgal culture

The application of magnetic fields in microorganism cultivation is a technological alternative to enhance biomass production and the synthesis of compounds of interest. Magnetic fields can influence biological systems by affecting enzymatic activity, metabolism, membrane permeability, and gene transcription, being considered an environmental stressor that triggers cellular defense responses (Deamici *et al.*, 2022a; Santos *et al.*, 2022).

The mechanisms of action of magnetic fields (MF) are related to the magnetic properties of the atoms and molecules within the system. Properties such as paramagnetism (weakly influenced in the same direction as the external MF), diamagnetism (weakly magnetized in the opposite direction of the MF), and ferromagnetism (strongly influenced in the same direction as the MF) are key to understanding these interactions. These mechanisms influence biologic systems are: (1) magnetic induction, (2) the magneto-mechanical effect, and (3) the formation of radical pairs (Font *et al.*, 2023).

The first mechanism, magnetic induction, is theoretically grounded in the "Hall effect." This phenomenon generates a transverse electric field (E) across a conductor, which is perpendicular to an external magnetic field (B) applied at a right angle to the direction of current flow . The electric field E = vB is generated by the Lorentz force acting to shift charges to one side as they move with speed v through the magnetic field (Font *et al.*, 2023). This mechanism can act on the on the liquid-gas boundary layer effecting the mass transfer increasing gas distribution in the liquid (Pazur; Winklhofer, 2008).

The magneto-mechanical effect is another mechanism, primarily associated with ferromagnetic materials present in the cell. When exposed to an external magnetic field (MF), specific molecules or ferromagnetic substances undergo mechanical movements to align their magnetic moments with the direction of the applied field. In nature these molecules are based in the presence of magnetite (Fe_3O_4) usually present in bacteria, sharks, pigeons, and phyctoplankton responsible for their ability to navigation in response to Earth’s magnetic field. (Font *et al.*, 2023; Monteil; Lefevre, 2020).

The last mechanism is related to the formation of radical pairs. The reorientation of spins and the formation of radical pairs under the influence of an MF are intricately linked to the electronic configuration of each atom and, consequently, its intrinsic magnetic properties. This

mechanism involves magnetically sensitive intermediate molecules due to the existence of radical pairs. The only two molecules for magnetoreception associated with radical pair in photosynthetic organisms are cryptochrome and chlorophylls, which are related to the photosynthetic system (Hore; Mouritsen, 2016).

The effects in microalgae cells might be related to the previously described mechanisms; for this affirmation, more evidence is needed. Most studies associate the effect of an increase in the cell concentration of the cultures, variations in growth parameters, changes in the biochemical composition of the biomass, and improvement in the photosynthetic capacity of the microorganisms are associated to genetics, metabolic, and physiological changes in microorganisms (Font *et al.*, 2023).

The application of MF to microbial cultivation can be manipulated depending on the objective of the study. MF can be applied statically (homogeneous during the time of application), and dynamically (brief but strong pulsation of MF). Other parameters are MF intensity, time of exposure, and spatial distribution (homo- or heterogeneous). The main parameters studied are time and intensity, the latter ranging from 10 to 500 mT, with an intensity of up to 100 mT being more common, while in relation to time authors vary mostly from 1, 12 and 24 hours per day. (Santos *et al.*, 2022)

The role of MF in microalgae is complex and has been associated to changes in hormones, enzymatic activity, the transport of membrane ions, transcription of DNA, increasing the growth rate, counteracting the toxic effect, changes in the production of proteins and carbohydrates content, altering the intracellular macromolecule profile, increasing nutrient intake, and photosynthesis (Deamici *et al.*, 2016; Li, C. *et al.*, 2022; Shao *et al.*, 2018; Veiga *et al.*, 2020). All those described as results of MF influence in the microalgae culture.

The application of magnetic fields (MF), particularly static magnetic fields (SMF), has been shown to influence photosynthesis by affecting the photochemistry of Photosystem II (PSII). The MF enhances the respiration rate and increases the photosynthetic production of oxygen, which is linked to the light absorption and photochemical processes occurring in PSII. Specifically, MF impacts the photolysis of water in PSII, where water molecules are split into hydrogen, electrons, and oxygen through light energy (Font *et al.*, 2023).

When exposure to SMF 1h and 24h d^{-1} *Arthrospira platensis* SAG 21.99 improved the maximum quantum yield of primary photochemistry (φpo) in PSII, enhancing electron transport

efficiency (φeo) and increasing the likelihood of exciton movement along the electron transport chain beyond Q_A. Additionally, SMF decreases the absorption flux per reaction center (ABS/RC), *indica*ting an increase in the number of active reaction centers (RCs). This is associated with a rise in oxidized chlorophyll (P680+), which promotes the formation of radical pairs (P680•+ and Phe•−) in PSII, a key factor in improving photosynthetic efficiency under magnetic treatment (Deamici *et al.*, 2019).

Chlorella sp. and *Spirulina sp.* showed an increase in the concentration of carbohydrates when exposed to MF between 30 and 60 mT up to 24 h/day, while for *N. oculata* (when submitted to 15 mT) they responded with a reduction of 23% in carbohydrates. The application of MF seems to stimulate the production of pigments such as chlorophyll *a* as well as carotenoids and phycocyanin (Deamici *et al.*, 2022b; Deamici; Santos; Costa, 2018; Menestrino *et al.*, 2021; Veiga *et al.*, 2020).

4.3 MICROALGAE EXOPOLYSACCHARIDES EXTRACTION AND PURIFICATION

After cultivation, the microalgal EPS is extracted and purified. During the cultivation process, the environmental factors to which the microalgae are exposed will influence both the composition and the amount of EPS produced. Harvesting involves the separation of the biomass from the culture medium, while the extraction and purification steps are performed to isolate the EPS solubilized in the medium and those bound to the microalgal cell wall (Laroche, 2022).

Extraction and purification methods for EPS are crucial for optimizing the production yield. The main methods for separating solubilized EPS from the medium include centrifugation or microfiltration to separate biomass from the culture medium. This supernatant can be directly subjected to dialysis, ultrafiltration or precipitated using absolute alcohols (methanol, ethanol, or isopropanol) at a 2:1 ratio. Alcohol precipitation tends to co-precipitate salts along with the EPS, which can then be desalted through dialysis or membrane-based techniques. For analytical investigations, contaminants such as proteins, pigments, and salts must be removed, which can be achieved through treatments with trichloroacetic acid, tangential ultrafiltration, or selective alcohol precipitation. EPS acquired through ultrafiltration is directly influenced by the molecular weight cut out (MWCO) of the pores; a high MWCO offers a higher purity of EPS but lower the yield due

to loss of smaller EPS molecules. After purification, the extract is dried to obtain high-purity EPS. (Delattre *et al.*, 2016; Laroche, 2022).

The exopolysaccharides bound to the cell wall (BPS) can account for up to 50% of the total exopolysaccharides produced by microalgae. Therefore, various extraction methods have been studied, including the use of formaldehyde, ethylenediaminetetraacetic acid (EDTA), sodium hydroxide, sonication, heat, water washing, complexation treatments, ion-exchange resins, and mixed methods for BPS isolation. (Delattre *et al.*, 2016).

Among the methods used, washing with heated water is the most common due to its technical simplicity and efficiency. However, the parameters must be optimized for each type of microalgae and BPS, as they vary in temperature (ranging from 30 to 95°C), pH (2 to 9.5), and exposure time to heat (1 to 4 hours) to maximize the extraction potential of the polymer. The main disadvantage of this method is the potential disruption of the cell wall, which can lead to contamination of the EPS with polar compounds such as proteins, starch, and chrysolaminarin. As a result, additional purification steps are often required; low molecular weight compounds can be separated with alcoholic precipitation, but for EPS, similar molecules (e.g. protein) are almost impossible to separate. (Delattre *et al.*, 2016; El-Naggar *et al.*, 2020; Pessôa *et al.*, 2021).

4.4 MICROALGAE POLYSACHARIDES

EPS produced by microalgae are complex molecules, predominantly heteropolymers with a high molecular weight (>10^6 Da), composed of up to 12 different monosaccharides. In terms of their composition, these EPS may also incorporate non-glycosidic compounds into their backbone, including pyruvates, phosphates, sulphates, and O-acetyl or O-methyl groups (Babiak; Krzemińska, 2021; Laroche, 2022; Rahman *et al.*, 2019).

Microalgal exopolysaccharides can be found free in the media (RPS) or bound to the cell wall of the microalgae acting as a capsule (BPS). They are classified by their location in the media (RPS and BPS) and/or by their composition (neutral, acidic, sulfated). Sulfated and acidic exopolysaccharides, in particular, are of significant interest to the food, pharmaceutical, and technology industries due to their diverse functionalities, including bioactivity, emulsifying, thickening, and biosurfactant properties. (Ai *et al.*, 2023; Rahman *et al.*, 2019; Xiao; Zheng, 2016).

Polysaccharides produced by microalgae primarily consist of L-rhamnose, L-fucose, D-arabinose, D-glucose, D-mannose, D-xylose, and D-galactose, with galactose, glucose, and xylose being the most frequently encountered (Babiak; Krzemińska, 2021; Naveed *et al.*, 2019). These polysaccharides are characterized by α-(1-3), β-(1-3), β-(1-4), and (2-1)-β glycosidic linkages, resulting in complex linear or branched configurations. These structures are associated with the rheological and bioactive properties of the EPS (Babiak; Krzemińska, 2021).

Uronic acids in exopolysaccharides (EPS), specifically galacturonic and glucuronic acids, can constitute up to 40% of their polymeric composition. The EPS produced by the microalgae *Closterium* sp (Domozych *et al.*, 1993), *Amphora sp*. (Jin *et al.*, 2018), *Anabaena spiroides* (Gouvêa; Vieira; Lombardi, 2005), *Aphanothece halophytica* (Li, P.; Liu; Xu, 2001), *Arthrospira platensis* (Filali Mouhim *et al.*, 1993), *Cyanospira capsulata* (Vincenzini *et al.*, 1993) e *Fischerella maior* (Bellezza *et al.*, 2006) contain these monosaccharides as their primary components. EPS characterized by high concentrations of acidic sugars, sulfate groups, and rhamnose are linked to antiviral, antibacterial, antioxidant, and immunoregulatory properties as well as gel formation (Ai *et al.*, 2023; Costa *et al.*, 2021; Wang, M.; Yin; Zeng, 2022).

In photosynthetic organisms, sulphate is assimilated into organic compounds through two primary mechanisms. The first is the reduction process, which predominates in plants, where sulphur is reduced to sulfide and subsequently incorporated into cysteine. The second mechanism involves sulphation, where sulphur in its oxidized form is integrated earlier in the metabolic sequence. For sulphur incorporation into polysaccharides, cysteine is transformed into 3-phosphoadenosine-5-phosphosulphate (PAPS), which then acts as a substrate for sulphotransferases (ST) to synthesize sulphated polysaccharides (Keidan *et al.*, 2006).

Medina-Cabrera et al. (2020) characterized *Porphyridium sodidum* and *Porphyridium purpureum* EPS, and the major monosaccharides found were xylose, galactose, glucose and glucuronic acid, and the third more present component was sulfates. The primary difference between the two species was the higher concentration of sulfates and the presence of methyl pentose and hexose in *P. sordidum*, whereas *P. purpureum* exclusively exhibited methylated uronic acid hexose dimers, likely related to the methyl group linked to the uronic acid.

4.5 TECHNOLOGICAL PROPERTIES OF POLYSACCHARIDES

Polysaccharides are macromolecules composed of monosaccharide units linked by glycosidic bonds, characterized by their high molecular weight and complex structures. These characteristics confer polysaccharides various physicochemical and rheological properties, making them widely used in the food, pharmaceutical, and chemical industries. (Caetano *et al.*, 2022; Xie *et al.*, 2021). These polysaccharides are mainly known as gums and can be divided according to their origin: plant-based (guar gum, legume gum, etc); secretion (gum arabic and tragacanth); mucilage (psyllium); microbial (xanthan, gellan, and dextran gum); and algae (alginate and carrageenan) (Eghbaljoo *et al.*, 2022).

In the food industry, polysaccharides are used as technological ingredients with diverse functionalities. They serve as gelling and thickening agents, emulsifiers for stabilizing texture, and can control crystallization, producing films, inhibiting syneresis, and acting as encapsulating agents. Xanthan gum is the most widely used polysaccharide due to its ability to exhibit all of these functions. It remains stable under high temperatures, pH variations, and changes in ionic strength, while also possessing desirable rheological properties such as pseudoplasticity and thixotropy (Eghbaljoo *et al.*, 2022).

The main algae-derived polysaccharides used as gelling/thickening agents are alginate, carrageenan, agarose and agaropectin produced by macroalgae of the phylum *Rhodophyta* (*Gracilaria* and *Gelidium*). Several microalgae produce polysaccharides, which may have similar characteristics or distinct functionalities compared to those from macroalgae. These compounds are thus actively investigated for their potential applications. *Porphyridium* sp BPS has a similar rheological behavior as potential to xanthan gum (Bernaerts *et al.*, 2018). *Anabaena* sp., *Nostoc* sp. and *Arthrospira platenses* were submitted to the same tests, but they did not present potential for the formation of solid structures of gels (Bernaerts *et al.*, 2019). Similar EPS of *Chlororella* sp and *Neochloris oleoabundans* were investigated, but even with the addition of NaCl to the solution, which drastically increases its viscosity, it did not demonstrate gelling potential as relevant as *Porphyridium* sp (Wu, N.; Li; Lan, 2011).

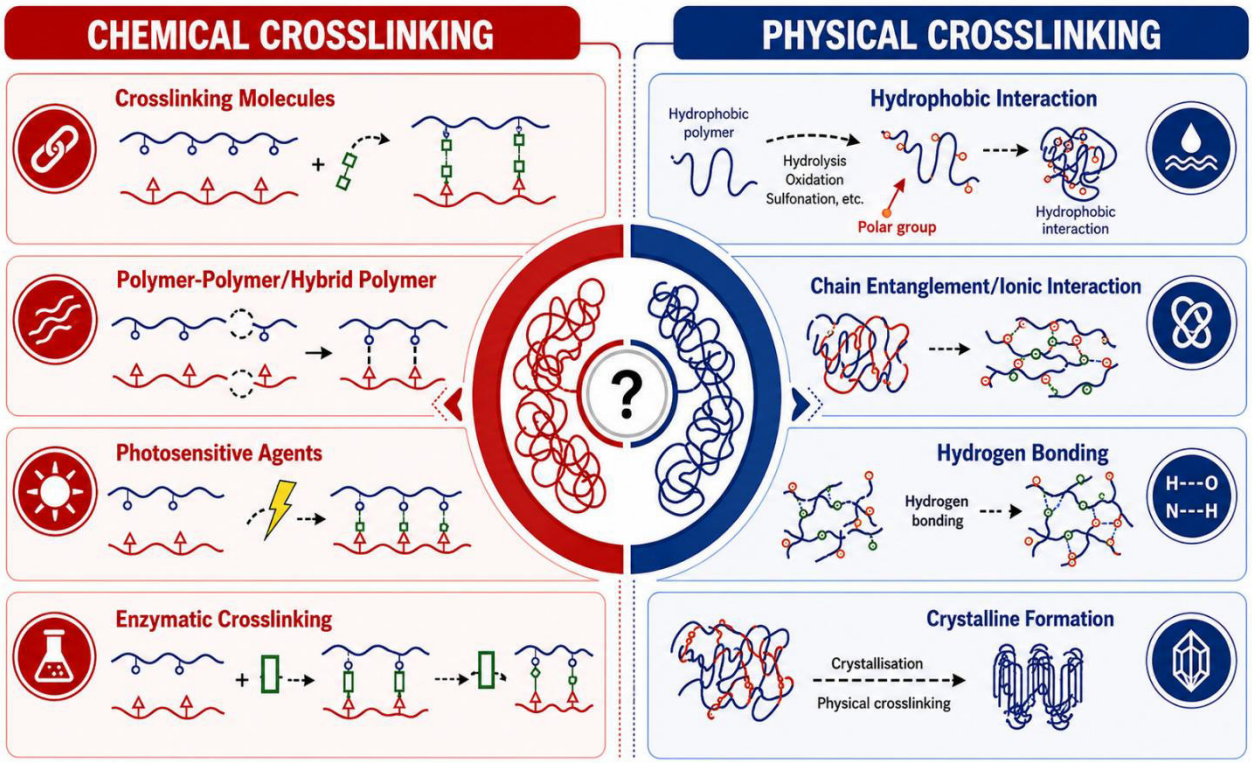
Compounds with gelling potential often also exhibit thickening properties, primarily due to their ability to increase solution viscosity. Gelling is defined as the ability of polymers to form three-dimensional networks, primarily through ionic bonds. These networks cause a sharp increase in viscosity, effectively turning the solution into a gel with reduced fluidity (Ju *et al.*, 2022).

Thickening occurs due to the physical behavior of the molecules, where intermolecular interactions within the solution restrict fluidity, thereby increasing viscosity (Saha; Bhattacharya, 2010).

Gelling can be triggered by 3 pathways: ionic gelation; when exposed to cationic solutions, such as Ba^{2+}, Ca^{2+}, K^{+}, and Fe^{2+}, polysaccharides capable of gelling undergo ionic interactions between the polymer chains and the cations (Ju *et al.*, 2022). Cold-set gelation; the polymer solution is first heated, usually, to alter its configuration and then cooled. As the solution cools, hydrogen bonding, hydrophobic interactions, and/or ionic bonding occur, resulting in the formation of the gel structure (Saha; Bhattacharya, 2010). Heat-set gelation occurs upon heating, where the thermal energy modifies the polymer structure, ultimately forming a gel (Ju *et al.*, 2022; Saha; Bhattacharya, 2010).

Hydrogel networks are broadly classified into two main categories based on their crosslinking strategy: physical and chemical (Figure 6). Physical hydrogels rely on reversible interactions between polymer chains, including hydrogen bonds, ionic bonds, hydrophobic interactions, and hydrophilic interactions. Because no permanent chemical reactions take place during their formation, these gels can respond to external stimuli and are considered reversible (Ju *et al.*, 2022; Stojkov *et al.*, 2021). A classic example is the addition of divalent calcium chloride to alginate, where the mechanical properties can be tuned by controlling the crosslinking density. While physical hydrogels offer the advantage of not requiring potentially toxic crosslinking agents, they tend to lack the mechanical strength and long-term stability of their chemically crosslinked counterparts (Stojkov *et al.*, 2021).

Figure 6 -Schematic representation of various types of physical and chemical crosslinking in hydrogels.



Source: Stojkov *et al.* (2021).

Covalently crosslinked hydrogels form irreversible networks that generally exhibit superior mechanical properties such as higher elastic moduli, and can be synthesized through photopolymerization, enzymatic crosslinking, and various click chemistry approaches. Beyond these two primary categories, there are interpenetrating networks that represent a special subclass of chemically crosslinked hydrogels in which two or more polymers are crosslinked simultaneously in each other's presence, without phase separation, to yield a new polymeric profile with distinct properties, such as the reported fibrous polyisocyanide and thermoresponsive PNIPAM that can become up to 50 times stiffer upon temperature changes. Whereas Composite hydrogels combine two different types of materials, typically an organic hydrogel matrix with an inorganic filler, to synergistically enhance mechanical and biological properties, as demonstrated by a polyvinyl alcohol/poly acrylic acid composite designed to mimic the load-bearing behavior of cartilage. (Stojkov *et al.*, 2021).

The mechanism on which the hydrogel is formed influences its network architecture. fundamentally governs mechanical and transport properties. These networks can take various forms, from the relatively homogeneous ionic networks of alginate and the fibrous helix-aggregated structures of agarose, to the interconnected macroporous sponge-like architectures of chitosan. Increasingly, researchers are engineering ordered structures through directional freezing, magnetic field alignment, 3D printing, and self-assembly to achieve enhanced and anisotropic properties. For instance, directional freezing produces aligned porous structures with directional mechanical behavior, while magnetically aligned cellulose nanofibrils yield oriented network architectures with tailored properties (Nie *et al.*, 2019).

More complex architectures, such as double-network and nanocomposite hydrogels, further expand the range of achievable properties. Double-network hydrogels feature two interpenetrating networks at different length scales: a rigid, highly crosslinked first network providing mechanical strength paired with a flexible, loosely crosslinked second network that dissipates energy. This results in exceptional toughness and fatigue resistance (Tan *et al.*, 2024). In nanocomposite gels, the spatial distribution and alignment of nanofillers like cellulose nanocrystals within the polymer matrix create percolating networks that enhance stress transfer and mechanical performance. Across all these architectures, crosslinking density plays a decisive role, with denser networks exhibiting lower swelling and slower degradation, while more porous networks show the opposite behavior (Xia *et al.*, 2024).

4.5.1 Technological properties of microalgal EPS.

Most of the studies related to the rheological properties of microalgae EPS have been carried out in solutions of polymers produced by microalgae of the genus *Rhodella* and *Porphyridium sp.* (Laroche, 2022). These solutions mostly showed characteristics of non-Newtonian fluids (Sun *et al.*, 2009), high viscosity (Bernaerts *et al.*, 2018), and viscoelastic behavior (Medina-Cabrera *et al.*, 2020). The rheological character of the EPS produced by *Porphyridium* was characterized as stable in pH ranges from 2 to 9 and temperatures up to 75ºC (Medina-Cabrera *et al.*, 2021). These technological characteristics of EPS are attributed to o-acetyl- and/or o-methyl-ester groups linked to peptides, presenting hydrophobic characteristics that give them the character of gums (Laroche, 2022; Rahman *et al.*, 2019).

Wang et al. (2022) report that thermal pre-treatment combined with high shear homogenization produces a suspension of *Synechococcus* sp. PCC 7002 has high viscosity and viscoelasticity, and they relate these characteristics to the bound exopolysaccharides (BPS) attached to the cell wall of the microalga. Jesus *et al*. (2019) characterized the exopolysaccharides (EPS) of *Spirulina* sp. LEB 18 and reported that the EPS exhibits properties of a non-Newtonian pseudoplastic anionic fluid (Colla *et al.*, 2020). As for EPS from *Porphyridium* sp, it forms a viscous solution at a relatively low concentration of 0.25%, comparable to xanthan gum and carrageenan. This EPS remains stable across a wide range of pH (2-9) and temperatures (20-150°C), as well as in the presence of cations such as Na^+, K^+, and $CaCl_2$/NaCl (Bayu *et al.*, 2023; Bernaerts *et al.*, 2018). Polymers with these characteristics possess significant technological potential, such as emulsifying, gelling, and thickening agents.

Additionally, EPS exhibit a broad spectrum of biological functionalities, including antiviral, antibacterial, immunomodulatory, antioxidant, and antithrombotic activities (Ai *et al.*, 2023; Casas-Arrojo *et al.*, 2021; Fimbres-Olivarría *et al.*, 2016; Gargouch *et al.*, 2021; Sun; Wang; Zhou, 2012). The antioxidant capacity of microalgal EPS, demonstrated both in vitro and in vivo, is primarily linked to the mitigation of oxidative damage and the upregulation of antioxidant enzymes. Meanwhile, immunomodulatory effects are mediated through the activation of mitogen-activated protein kinase (MAPK) and nuclear factor κB (NF-κB) pathways, which enhance host immune responses (Ai *et al.*, 2023; Wu, X. *et al.*, 2020). Regarding antiviral mechanisms, EPS, particularly from enveloped viruses like HSV-1, HSV-2, and VZV, act by mimicking cellular receptors, thereby obstructing viral attachment, entry, and subsequent replication (Bello-Morales *et al.*, 2022). These bioactivities are closely correlated with structural parameters, specifically sulfate content and molecular weight; EPS exceeding 10% sulfation demonstrates significant potency, which can be further enhanced in lower molecular weight polymers due to superior bioavailability (Han *et al.*, 2024; Sun; Wang; Zhou, 2012).

4.6 SUSTAINABLE DEVELOPMENT OBJECTIVES

The Sustainable Development Goals (SDGs) are the global goals to end poverty, protect the environment, and the climate so that all people can live in peace and prosperity. Divided into 17, the SDGs encompass the most basic problems, from the end of hunger to economic growth and infrastructure (UNITED NATIONS [UN], 2016). This project fits into six of the objectives: the

use of microalgae for food production fits into goal 2, Zero hunger and sustainable agriculture, by producing food ingredients with all essential nutrients in a sustainable way. In addition to compounds considered functional, such as fatty acids (omega 3), bioactive peptides, and sulfated polysaccharides, falling under goal 3 of Health and well-being (CHEN et al., 2022).

The cultivation of microalgae consumes CO2 and is therefore considered carbon negative, in line with goal 13 (Action against global climate change). Together with goal 12 (Responsible consumption and production) making full use of the microalgae parts of EPS production. Harnessing co-products (biomass) as an ingredient for food enrichment and new product development promoting new industries covering goals 9 and 8 (Industry, innovation and infrastructure, and Decent work and economic growth).

CHAPTER III

WORK OVERVIEW

The research presented in this thesis was developed across three distinct stages during the doctoral period. Experimental procedures and tests were conducted at the Pascal Institute (INP) of the University of Clermont Auvergne (UCA) and the School of Chemistry and Food (EQA) at the Federal University of Rio Grande (FURG).

In the first section, the study focused on the production of PAN nanofibers, both with and without MEA, through conventional electrospinning to be applied in microalgal cultivation. Cultivations of *Limnospira indica* PCC 8005 were performed in the presence and absence of these nanofibers, allied with a static magnetic field (SMF). In addition to monitoring growth kinetics, the harvested biomass was characterized, and BPS were extracted and subjected to biochemical and structural analysis (Scientific Paper I).

The second stage involved similar cultivations using *Porphyridium purpureum* to observe the impact of nanofibers and SMF on growth behavior. Following the harvest, exopolysaccharides (EPS) were extracted, purified, and characterized (Scientific Paper II).

In the third section, the mechanical behavior, hydrogel structure, and thermal properties of EPS from *P. purpureum* were evaluated (Scientific Paper III).

Scientific Paper I: Production of biomass and biomolecules in *Limnospira indica* PCC 8005 cultivation under magnetic fields and polymeric nanofibers

Scientific Paper II: Production of β-phycoerythrin and exopolysaccharide in *Porphyridium purpureum* modulated via static magnetic fields and polymeric nanofibers.

Scientific Paper III: Cultivation conditions drive divergent rheological behavior and Hydrogel architecture in *Porphyridium purpureum* exopolysaccharides.

PAPER I

PRODUCTION OF BIOMASS AND BIOMOLECULES IN *Limnospira indica* PCC 8005 CULTIVATION UNDER MAGNETIC FIELDS AND POLYMERIC NANOFIBERS

CARVALHO, M. P. de; MORAIS, M. G. de; SANTOS, L. O. dos; LAROCHE, C.; COSTA, J. A. V. **Journal of Biotechnology**, vol. 405, no. October 2024, pp. 48–56, Sep. 2025. DOI: 10.1016/j.jbiotec.2025.05.004. Available at: https://linkinghub.elsevier.com/retrieve/pii/S0168165625001142.

PRODUCTION OF BIOMASS AND BIOMOLECULES IN *Limnospira indica* PCC 8005 CULTIVATION UNDER MAGNETIC FIELDS AND POLYMERIC NANOFIBERS

ABSTRACT

Researchers often apply physical, chemical, or biological stresses to cyanobacteria cultivation to enhance biomass production by triggering cellular adaptation mechanisms, increasing growth, or boosting target compound synthesis. Static magnetic fields (SMF) offer a non-toxic, cost-effective way to modulate microalgal growth, alter biomass composition, and promote metabolite production. Polymeric nanofibers (Nano) function as a physical barrier in cultivation, while monoethanolamine (MEA) acts as a chemical absorbent, reducing CO_2 loss and enhancing biofixation. This study investigated the effects of SMF and nanofibers on the biomass yield and molecular composition of *Limnospira indica* PCC 8005. The combined SMF and Nano treatment achieved the highest biomass yield (5.87 ± 0.06 g L^{-1}), a 28% increase compared to the control. SMF application increased protein content by 16% but reduced carbohydrate levels by 73% relative to the nanofiber-only treatment (39.58 ± 0.98% ww^{-1}). Exopolysaccharide (EPS) produced under the SMF+NanoMEA treatment contained 39.9% uronic acid, while the Nano-only treatment had the highest sulphate content (8.4%) but the lowest uronic acid concentration (25.4%). The EPS were identified as acidic, sulphated polysaccharides. SMF and nanofibers significantly enhances biomass production, alters the carbohydrate and protein proportions in biomass, and influences the composition of sugars, acids, and sulphate in exopolysaccharides.

Keywords: Exopolysaccharides, microalgal pigments, sulphated polysaccharides, *Spirulina*;

1. INTRODUCTION

Global CO_2 emissions related to energy production grew by 1.1% in 2023, reaching 37.4 Gt. CO_2 is the main compound related to the greenhouse effect. The need to mitigate its concentration in the atmosphere is crucial (International Energy Agency, 2023). Common strategies for CO_2 mitigation described in the literature include reducing emissions through greener energy sources, capturing and storing CO_2 directly at the emission site (e.g., exhaust chimneys),

and utilizing direct air capture techniques that remove CO_2 from the atmosphere (Hanifa *et al.*, 2023). The CO_2 captured from these techniques can be processed through five main routes: conversion into chemicals and fuels, mineral carbonation, oil recovery, direct use of CO_2, and biological conversion. The latter, primarily carried out by microalgae and plants through photosynthesis, converts CO_2 into organic carbon to produce cellular biomass (Ghiat; Al-Ansari, 2021).

Due to the low solubility of CO_2 in water, a significant portion is lost to the atmosphere when introduced into the growth medium. To improve CO_2 retention and availability for microalgal cells, strategies involving chemical absorbents such as monoethanolamine (MEA) and physical adsorbents like polymeric nanofibers have shown promising results (Daneshvar *et al.*, 2022; Rosa *et al.*, 2015, 2016; Vaz; Costa; Morais, 2020). These approaches have been reported to enhance microalgal growth, CO_2 dissolution and fixation, and may also influence the macronutrient profile of the biomass (Cardias; Morais; Costa, 2024; Rosa; Morais; Costa, 2018; Rosa *et al.*, 2016; Vaz; Costa; Morais, 2020). The integration of monoethanolamine-functionalized nanofibers offers a dual mechanism for enhancing CO_2 capture: the nanofibers' high surface area facilitates physical adsorption of CO_2, while the monoethanolamine component acts as a chemical absorbent. Together, these properties can significantly improve CO_2 solubility and availability, thereby promoting greater biofixation efficiency and biomass production.

Cyanobacteria are prokaryote unicellular or multicellular microorganisms capable of oxygenic photosynthesis; oxidizing water molecules to hydrogen and oxygen while reducing CO_2 to organic matter (Majhi, 2024). Cyanobacteria are widely cultivated due to valuable compounds in the biomass, which are rich in proteins, polyunsaturated fatty acids, carbohydrates, natural pigments and active exopolysaccharides. These compounds are suitable for human and animal nutrition and have applications in the pharmaceutical and chemical industries (Aly; Rizk; Shams, 2023). Commonly marketed as "Spirulina," cyanobacteria from the genera *Arthrospira* and *Liminospira* thrive in high alkalinity and exhibit greater temperature resistance, which helps minimize contamination and facilitate production (Nowicka-Krawczyk; Mühlsteinová; Hauer, 2019). Several strategies are used to enhance the biomass production of cyanobacteria to increase the yield of high-value compounds, including nutrient manipulation and physical stress such as osmotic stress and more recently magnetic fields.

Magnetic fields can affect biological systems by enhancing production and altering the composition of biomass. This technique is low-cost, non-toxic, and easy to apply (Deamici; Morais; *et al.*, 2022). The effect in biological systems is generally associated with three phenomena: magnetic induction, by the "Hall Effect" on electrons, holes and/or ions, interfering with the positions and stability of charges, magneto-mechanical effect on ferromagnetic substances, aligning them to the direction of the applied magnetic field. Formation of radical pairs that act on magnetically sensitive intermediate molecules (e.g. cryptochrome and chlorophylls), changing the energy levels and spin orientation of electrons to create pairs of radicals, thus influencing photosynthesis (Font *et al.*, 2023). The exact effects of SMF on microalgae cells are not completely elucidated. Most studies associate it to growth behavior, structural composition, and metabolite production (Deamici; Santos; Costa, 2021; Font *et al.*, 2023; Santos *et al.*, 2022; Veiga *et al.*, 2020). These metabolic responces are linked to photosyntesis modulation (Deamici *et al.*, 2019), better nitrogen absorpions (Deamici; Morais; *et al.*, 2022) and hormonal, DNA and enzymatic changes (Luo *et al.*, 2020).

The use of static magnetic fields (SMF) in combination with polymeric nanofibers represents a novel and promising strategy that has yet to be thoroughly investigated. These two approaches may act synergistically, complementing each other to further enhance microalgal growth, protein synthesis, and CO_2 biofixation. The magnetic field can stimulate cellular activity and metabolic pathways, while the nanofibers improve CO_2 availability in the medium. Therefore, the present study aims to evaluate the production of biomass and biomolecules by *Limnospira indica* PCC 8005 cultivated under the combined influence of SMF and polymeric nanofibers.

2. MATERIALS AND METHODS

2.1 MICROORGANISM INOCULUM

The strain used was *Limnospira indica* PCC 8005 acquired from the culture collection of the Pasteur Institute (France) grown in modified Zarrouk medium (Cogne *et al.*, 2003) composed of (g L^{-1}): 16.8 $NaHCO_3$, 2.5 $NaNO_3$, 1.0 NaCl, 1.0 $K2SO_4$, 0.5 $K2HPO_4$, 0.04 $CaCl_2$, 0.08 EDTA, 0.08 $MgSO_4 \cdot 7H_2O$, 0.01 $FeSO_4 \cdot 7H2O$ and 1.0 mL mineral solutions (g L^{-1}): 0.23 $MnCl_2 \cdot 4H_2O$, 0.11 $ZnSO_4 \cdot 7H_2O$ and 0.03 $CuSO_4 \cdot H_2O$ and kept at 30 ± 2ºC in natural light.

2.2 NANOFIBER PRODUCTION AND STATIC MAGNETIC FIELD APPLICATION

Nanofibers solutions were made as described by Cardias et al. (2024), with 11.5% (p v^{-1}) of polyacrylonitrile (PAN Molecular weight 150,000 g mol^{-1} Sigma-Aldrich®) in dimethylformamide, as solvent (Synth). Monoethanolamine (MEA) (Sigma-Aldrich®) were added to the previous solution in a concentration of 1% (p v^{-1}). To produce the nanofibers electrospinning technique was used, injecting the polymeric solutions at a rate of 800 μL h^{-1} through a 0.55 mm diameter capillary at 25 kV electrical potential. The distance between the collector and the capillary was 180 mm at 20-23 ºC and humidity between 50 - 58%.

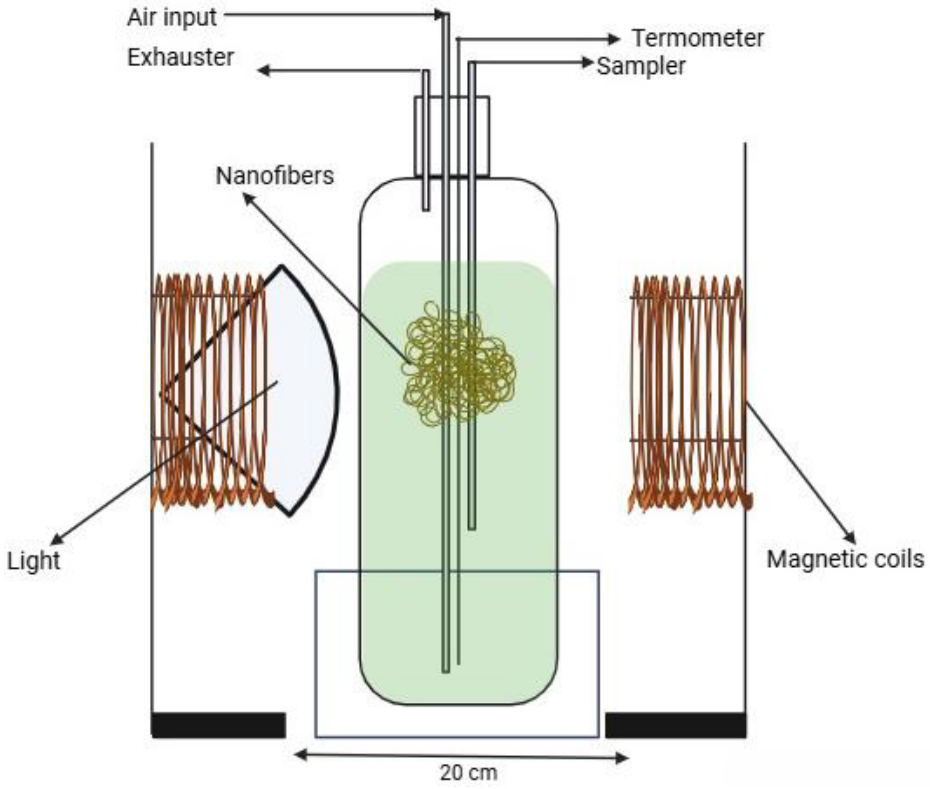
The static magnetic fields (SMF) were generated by two coils with 400 turns connected to an electric current of 3 A, creating a homogeneous SMF at the center of the 11 ± 2 mT bioreactors as described by Deamici et al., (2022) .

2.3 EXPERIMENT DESIGN

Experiments were performed in triplicate within 600 mL rectangular bioreactors (Figure 1), connected to condensers to minimize evaporation (APPENDIX A). The experiments were carried out in the previously media described (2.2) for 14 days, at 30 ºC, with irradiation of 150 μmol of photons m^{-2} s^{-1}, injection of sterile compressed air with a flow of 1.5 L min^{-1} for homogenization. CO_2 was injected for 2 min every hour with a flow rate of 0.06 mL^{-1} min^{-1}. To increase the contact time with the gas, the aeration was turned off 1 min before and after the addition of CO_2 (Rosa *et al.*, 2015; Vaz; Costa; Morais, 2020). $NaHCO_3$ and CO_2 was added to maximize biomass production since the focus is to study the influence of PAN nanofibers with/out MEA and SMF application in the cultivation.

Polymeric nanofibers were added in the proportion of 0.1 mg mL^{-1} of media to increase carbohydrate concentration (Vaz; Costa; Morais, 2020). The experiments were named: Control (culture without application of SMF or nanofibers), static magnetic field (SMF), only nanofibers (Nano), nanofibers and static magnetic field (Nano+SMF), nanofiber produced with monoethanolamine (NanoMEA) and addition of nanofiber with monoethanolamine and static magnetic field (NanoMEA+SMF).

Figure 1 - Bioreactor diagram.



2.4 GROWTH KINETICS

Biomass progression during cultivation was tracked daily by reading the optical density (OD) at 750 nm in a spectrophotometer (V730m Jasco) compared with the correlation of OD and dry mass obtained at the end of the cultivation, thus determining the concentration of biomass (X). pH was monitored with the aid of a pH meter (SevenEasy S20, Mettler Toledo). Nitrate Consumption during cultivation was determined by Cawse, (1967) modified by American Public Health Association (1971).

The biomass concentration (X), productivity (P) and doubling time (D_t) were calculated from the daily reads. The final mass of cells was added to the biomass production calculations. Daily productivity was obtained by the equation:

$$P = (X_t - X_0)/\, t \qquad (1)$$

Where X_t = biomass concentration of the day, X_0 = biomass concentration at the beginning of the culture and t = time in days. The maximum growth rate (μ_{max}) was determinate by the logarithmic regression of the exponential phase of the lnX vs t graph, and the doubling time Dt was determined by ln(2)/ μ_{max} (Deamici; Morais; et al., 2022).

As biomass is retained in the nanofibers at the end of the experiments (APPENDIX A), the nanofibers were dried at 50 ºC until stable weight. To create a linear biomass production in the nanofibers experiments, the equation:

$$P_{Nano} = (N_{final} - N_{inital})/\ 14 \quad (2)$$

Where $N_{initial}$ is the initial weight of nanofiber, N_{final} is the dry nanofiber at the end of the experiment. P_{Nano} was multiplied by t, then added to daily X.

2.5 BIOMASS CHARACTERIZATION

After 14 days the culture was centrifuged (10.000 x g for 15 min at 15 ºC), the biomass was washed with distilled water (to remove the culture medium), lyophilized and kept at -20 ºC until further analysis. The extract for analysis was made by resuspending 10 mg of lyophilized biomass in 10 mL of ultrapure water and subjected to an ultrasonic probe for 10 min at 100% amplitude in an on/off cycle of 59s (UP100H, Hielscher), to break the cell wall enabling the measurement of intracellular components. Carbohydrates were determined by the method described by DuBois et al. (1956) with standard glucose curve. For the determination of the proteins, the sonicated extract was submitted to treatment with 1 M NaOH for protein solubilization (Safi et al., 2014), followed and determined by the method described for Lowry et al. (1951) against an albumin curve. The lipid content was extracted from 10 mg of lyophilized biomass and measured by Bligh & Dyer, (1959) method modified by Ba et al. (2020).

To evaluate the pigments, calcium chloride was added to the extract at a concentration of 6 g L^{-1}, shaken for an hour, then centrifuged at 10.000 x g for 5 minutes, and the absorbance of the supernatant was read at 615 and 652 nm. The results were obtained by the correlation c-phycocyanin (PC) (Bennett; Bogorad, 1973)

$$PC = (ABS_{615} - 0.474\ ABS_{652})/5.34 \quad (3)$$

For the Chlorophylls the pellet was resuspended in acetone 80 % and centrifuged, this process was repeated until the pellet turned white. The absorbance of the acetone supernatant was read at 663.2 and 646.8 nm and the chlorophyll a (Chl a) was determined by the correlation (Porra, 2002):

$$\text{Chl a} = 12.25\ ABS_{663.2} - 2.79\ ABS_{646.8} \quad (4)$$

2.6 CELL WALL BOUND EXOPOLYSACCHARIDES (BPS) EXTRACTION AND CHARACTERIZATION

The extraction of exopolysaccharides adhered to the cell wall (BPS) was performed as described by Filali Mouhim et al. (1993) modified by Phélippé et al. (2019). 0.5 g of lyophilized biomass was suspended in 100 mL of TAPS buffer solution (0.05M) EDTA (0.025 M) at pH 8.15 heated to 100 ºC for 20 min, in which the supernatant was reserved while the precipitate was resubmitted to the previous step. The supernatants were mixed and added 3 times the volume of Cetyltrimethylammonium bromide 3% (CTAB), kept overnight. The solutions were centrifuged (10,000 x g for 15 min), the precipitate was resolubilized 4 times in KCl solutions of decreasing molarities (1.5 M, 0.75 M, 0.3 M) and finally in water. In each re-solubilization, 3 times the volume of ethanol at 96º was added and kept for 24 hours at -20 ºC for precipitation. Finally, it was resolubilized in water, submitted to dialysis with 10 kDa of MWCO (molecular weight cut-off) membrane and lyophilized.

Neutral sugars were determined by the resorcinol method, as described by Monsigny et al. (1988). Acidic sugars were determined with metahydroxydiphenyl as described by Blumenkrantz & Asboe-Hansen (1973) versus a standard curve of glucose and glucuronic acid, respectively. Quantification of neutral sugars was corrected by the formula described by Montreuil et al. (1963) . Sulphate content was determined by the turbidimetric method described by Dogson and Price (1962) with a K_2SO_4 standard curve, and the results were expressed in mg g^{-1} of SO_4 equivalent.

Fourier transform infrared (FT-IR) was performed using a VERTEX 70 FT-IR instrument. The EPS were dispersed in the ATR A225 diamond. Infrared spectra (50 scans. resolution 4 cm^{-1}) were recorded at room temperature (referenced against air) in the wavenumber range of 500–4000 cm^{-1}. The spectra were analyzed with the OPUS 7.2 software (Bruker Optics).

2.7 STATISTICAL ANALYSIS

All analyses and experiments were performed in triplicates. The data were analyzed using one-way ANOVA followed by Tukey's post hoc test, with a significance level of $p < 0.05$. Results are presented as mean ± standard deviation (SD).

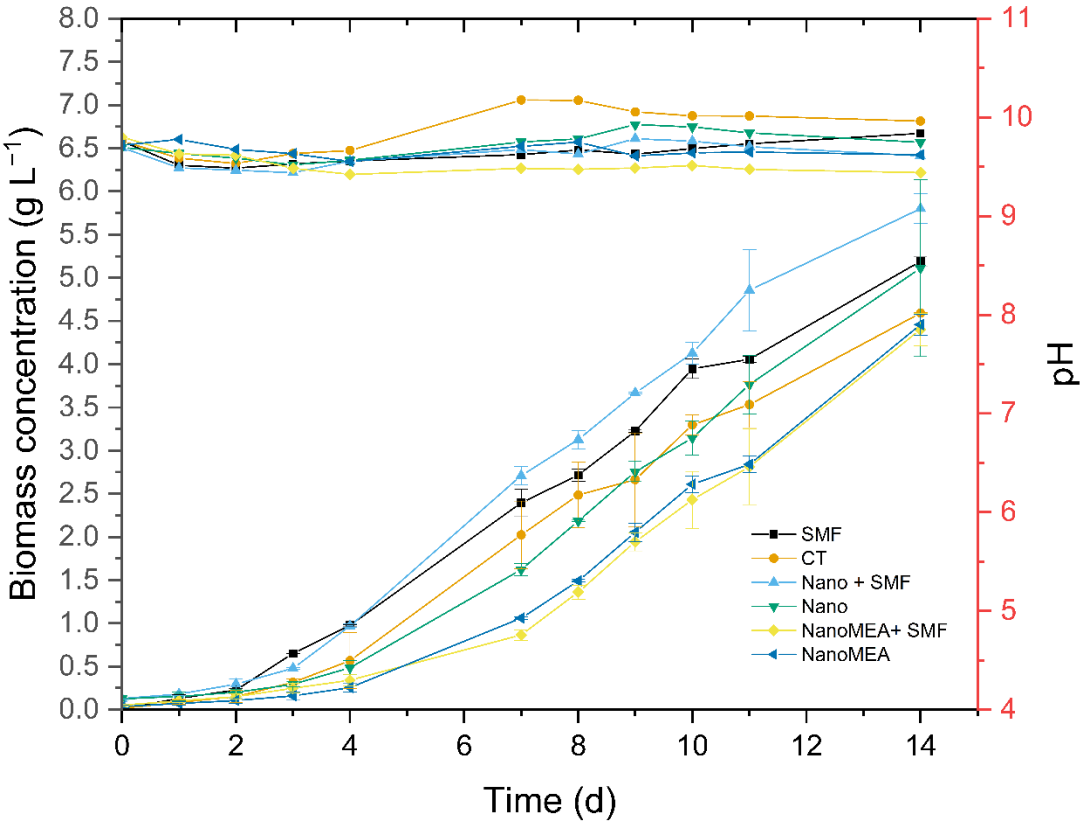
3. RESULTS AND DISCUSSION

3.1 *Limnospira indica* GROWTH

The pH during cultivation ranged from 9.4 to 10.1, with the lowest being found in the assays with nanofibers and SMF. The pH profiles of "*Spirulina*" cultivation may vary over time, but tend to remain relatively stable, within pH values ranging from 9 to 10 (Deamici; Santos; Costa, 2018, 2019; Veiga *et al.*, 2020).

The increase in pH during microalgae growth is primarily due to changes in the carbonate balance system, which tends to raise the pH in the medium. During photosynthesis, dissolved CO_2 consumption reduces the formation of carbonic acid, while the HCO_3 results in the formation of hydroxide ions (OH-). Hydroxide is also a product of NH_{4+} metabolic pathway (Blankenship, 2014). When CO_2 is added to the cultivation system, this shifts the carbonate equilibrium towards CO_2 and bicarbonate (HCO_3^-), resulting in a decrease in pH (Richmond, 2003). In the experiments using nanofibers, a lower pH was observed. The nanofibers effectively trap CO_2, leading to a higher concentration of CO_2 in the medium. This increase in CO_2 concentration may contribute to a reduction in pH if the carbonate balance shifts toward CO_2 and HCO_3^-. A similar reduction in pH was noted in experiments involving static magnetic fields (SMF). These results can be attributed to the Hall Effect, which affects ionic solutes present in the medium. This effect stabilizes the gas-liquid dielectric boundary layer, thereby mitigating temperature effects and enhancing the solubility of CO_2 (Pazur; Winklhofer, 2008).

Figure 2 -Growth curves and pH values of *Limnospira indica* PCC8005 cultures under magnetic field, nanofibers, and control treatments.



All experiments have shown similar growth behavior without lag phase. The exponential phase lasted from 1st to the 8th day of cultivation in the experiments without SMF. For the ones with SMF lasted from 1st to 4th day but SMF+ NanoMEA which lasted from 1st to 7th day. The maximum specific growth rates (μ_{max}) ranged from 0.380 ± 0.01 to 0.787 ± 0.01 d^{-1}, Nano and SMF experiments, respectively. As the addition of nanofibers in microalgae production tends to adsorb biomass during growth the concentration actually measured by optical density isn't accurate affecting the nano fibers experiment growth kinetic data (Vaz; Mastrantonio; *et al.*, 2019). In the present study around 9.5 – 15% of the biomass remained attached to the nanofibers.

The treatment yielding the highest final biomass production (X_{final}) was SMF + Nano, which reached of 5.9 g L^{-1} (Table 1). This was followed by the SMF + NanoMEA treatment at 5.2 g L^{-1} and the SMF treatment at 5.1 g L^{-1}. Notably, the SMF + Nano treatment resulted in an average increase of 21% in biomass production compared to Control treatment confirming a positive impact of combining magnetic fields with nanofibers on microalgae growth. Not just against the Control

but as well against individual application of Nano and SMF with an increase of 20 and 12%, respectively, of X_{final}.

Table 1 - Growth parameters of *Limnospira indica* PCC 8005 cultivated under the influence of SMF and nanofibers. SMF- Magnetic field 1h day^{-1}; SMF + Nano – added nanofiber magnetic field; Nano – Added nanofibers; SMF +NanoMEA – Magnetic field and nanofiber produced with MEA; NanoMEA - Nanofiber addition produced with MEA. The results are expressed as mean (n=3) ± standard deviation. Different letters on the same line indicate a significant difference between p-values <0.05 (Tukey's test).

		Control	SMF	SMF+Nano	Nano	SMF + NanoMEA	NanoMEA
X_{final}	g L^{-1}	4.6±0.1^{d}	5.2±0.1^{b}	5.9±0.1^{a}	4.7±0.1^{cd}	5.1±0.1^{b}	4.8±0.1^{c}
μ_{max}	d^{-1}	0.464±<0.01^{c}	0.786±0.01^{a}	0.547±0.04^{b}	0.380±0.01^{d}	0.394±0.03^{d}	0.405±0.02^{d}
P_{max}	mg L^{-1} d^{-1}	329±0.7^{d}	394.6±4.0^{b}	433.5±5.1^{a}	326±3.8^{d}	351±8.4^{c}	334.2±2.7^{d}
D_t	d	1.49±0.01^{c}	0.88±0.01^{a}	1.27±0.17^{b}	1.82±0.25^{e}	1.77±0.25^{de}	1.63±0.16^{cd}
R^2		0.97±0.01	0.97±<0.01	0.99±<0.01	0.99±<0.01	0.99±<0.01	0.99±<0.01
Δt	d	1-8	1-4	1-4	1-8	1-7	1-8
N	g d^{-1}	0.25±0.01^{ab}	0.26±0.03^{ab}	0.22±0.02^{b}	0.23±0.02^{b}	0.3±0.05^{a}	0.3±0.03^{a}

All experimental setups, but Nano, demonstrated an increase in maximum biomass production compared to the control. The higher yield in biomass production can be associated with the effect of SMF nanofibers or both in the cultivation of *L. indica*.

Similar results were reported for Spirulina sp. (Deamici; Costa; Santos, 2016; Hirano; Ohta; Abe, 1998; Li, Z.-Y. et al., 2007; Shao et al., 2018) and *Arthrospira plantensis* (Deamici; Santos; Costa, 2019) that describe final biomass increase between 10% to 95% when compared to their control assays, when exposed to SMF. Meanwhile, Cardias et al.(2024) reported an improvement of 17% in biomass production in Spirulina sp. LEB 18 cultivated with PAN nanofibers (0.2 mg/mL).

The application of SMF enhanced ($p \leq 0.05$) the maximum productivity (Pmax) of microalgal cultures compared to the control. SMF alone (394.6 ± 4.0 mg L^{-1} d^{-1}) and in combination with nanofibers (SMF+Nano, 433.5 ± 5.1 mg L^{-1} d^{-1}) yielded the highest productivity values ($p \leq 0.05$), suggesting that magnetic stimulation effectively boosts biomass formation rates. In contrast, the use of nanofibers without SMF (Nano and NanoMEA) resulted in P_{max} values similar to the Control ($p \leq 0.05$), indicating that nanofibers alone do not significantly impact productivity in this study. These findings demonstrate that SMF is the primary factor responsible for enhancing microalgal productivity, while the presence of nanofibers may exert a supportive but limited effect when not associated with magnetic fields.

The highest concentrations of final biomass were observed in cultures exposed to SMF. These results can be explained by three distinct hypotheses: (1) metabolic and/or genetic alterations, (2) structural changes, and (3) modifications in electron transition dynamics. (Font et al., 2023).

Changes in metabolic pathways can modify DNA transcription, enzymes, and hormonal interaction. Luo et al. (2020) relate the improvement in cell density in *C. vulgaris*, grown under SMF 80 mT for 2 h d^{-1}, to increase in enzyme activity due to paramagnetic transition metal ions element. Deamici, *et al*. (2022) link the higher *L. indica* biomass production exposed to SMF to higher N consumption due to increased membrane permeability. By alterations in the nutrient transport channels, facilitating the metabolization of these components, thus increasing the production of biomass. Deamici *et al*., (2019) also report the positive effect of SMF on photosystem II in *Arthrospira platensis* SAG 21.99 as SMF 30 mT for 1h d^{-1} increased the quantum yield by

facilitating the energy flow process of the oxide-reduction reaction, stimulating photosynthesis, which led to an increase of 49% in final biomass and 15% in carbohydrates in the biomass element.

The SMF seems to have a higher effect on the growth of *L. indica* than the polymeric nanofibers studied; the best growth result was the application of PAN nanofiber and SMF together (SMF+Nano); the same could not be seen for nanofibers made with MEA. These results indicate that nanofibers allied to SMF positively impact the growth of *L. indica* under the studied conditions. Although *Spirulina* sp. LEB 18 cultivations with MEA up to 25 mg L^{-1} were reported to achieve a higher growth rate (Rosa et al., 2015). The addition of the absorbent in PAN nanofibers does not carry the same effect in the tested concentration (1 mg L^{-1}), further studies are needed to develop nanofibers with higher concentrations of MEA aiming to increase their effect in growth rate.

3.2 BIOMASS CHARACTERIZATION

The composition of protein, carbohydrates, and lipids in the biomass studied is presented in Table 2. These macronutrients serve as the primary carbon substrates in microalgae, and their metabolic production pathways are interconnected, as the metabolized carbon will ultimately be allocated to one of these pathways (Blankenship, 2014; Li, C. *et al.*, 2022; Richmond, 2003).

The assays exposed to static magnetic fields (SMF) demonstrated the highest protein concentrations, with no significant differences ($p \leq 0.05$) among them. The maximum protein content recorded was 65 ± 1.4% ww^{-1} in the biomass for the SMF treatment. In contrast, assays incorporating nanofibers exhibited lower protein concentrations, with the minimum observed being 42 ± 0.33% ww^{-1} for the treatment with nanofibers alone. These results suggest magnetic fields positively influence protein formation in the biomass of *L. indica* PCC 8005.

Table 2- Macronutrient composition of biomass *Limnospira* grown under SMF and nanofibers. SMF - Magnetic field 1h day^{-1}; SMF + Nano – added nanofiber magnetic field; Nano – Added nanofibers; SMF +NanoMEA – Magnetic field and nanofiber produced with MEA; NanoMEA - Nanofiber addition produced with MEA. The results are expressed as mean (n=3) ± standard deviation. Different letters on the same line *indica*te a significant difference between p-values <0.05 (Tukey's test).

		Control	SMF	SMF+Nano	Nano	SMF+NanoMEA	NanoMEA
Protein	%,ww^{-1}	55.2±1.8^{b}	65.5±1.4^{a}	62.8±1.7^{a}	42.4±0.3^{c}	61.7±1.6^{a}	53.6±5.8^{b}
Carbohydrates	%,ww^{-1}	28.3±2.2^{bc}	25.6±2.5^{b}	26.0±1.4^{bc}	39.6±1.0^{a}	20.2±1.6^{c}	30.4±3.3^{b}
Lipids	%,ww^{-1}	6.3±0.9^{a}	6.1±1.2^{a}	7.5±0.4^{a}	8.1±0.2^{a}	7.8±0.6^{a}	7.3±1.3^{a}

Proteins in cyanobacteria are produced for both biochemical and structural purposes. They play essential roles in regulating and controlling gene expression, metabolic pathways, and cellular responses to environmental stimuli. This regulation is crucial for maintaining cellular homeostasis and facilitating adaptation to changing conditions (Berges; Mulholland, 2008).

Protein formation in cyanobacteria is primarily attributed to nitrogen (N) assimilation. This nutrient can be present in the medium in both inorganic forms, such as ammonium and nitrates, and organic forms, such as urea and amino acids. Once absorbed, nitrogen is enzymatically converted to ammonium within the cytoplasm, where it is incorporated into carbon skeletons to facilitate the synthesis of proteins (Berges; Mulholland, 2008; Muro-Pastor; Reyes; Florencio, 2005). The higher concentration of proteins in the biomass in this study indicates that SMF induces intracellular carbon partitioning to the metabolic pathway of protein formation.

The high protein content in the biomass is a positive result, since the biomass of *L. indica* can be used for human and animal nutrition. The increase in protein concentration in cultures under SMF, when compared to controls, is reported for *Spirulina sp.* (16%) (Deamici; Costa; Santos, 2016), *Chlorella fusca (Desmodesmus abundans)* (28%) (Deamici; Santos; Costa, 2021) and

Tribonema sp. (16%) (Huo *et al.*, 2020). Deamici, Morais, et al. (2022) observed protein content in biomass of *L. indica* when grown under SMF 1h d^{-1} (similar parameters) of 67 % ww^{-1}, an increase of 12% when compared to the control assay. The present study obtained similar results in the trials with SMF increasing 16% of the protein content in the biomass when compared to the Control.

The increase in protein concentration in the biomass of microalgae cultivated under SMF is related to the influence of magnetic fields that facilitate enzymatic activity by their action on paramagnetic cofactors and changes in transport channels in the cell membrane, increasing its permeability to nutrients (Deamici; Morais; *et al.*, 2022; Deamici; Costa; Santos, 2016; Deamici; Santos; Costa, 2021; Huo *et al.*, 2020).

The highest carbohydrate content ($p \leq 0.05$) was observed in the biomass from the Nano treatments, reaching 39.6 ± 0.98% (ww^{-1}), while the SMF treatments exhibited the lowest carbohydrate levels ($p \leq 0.05$), ranging from 20.2% to 25.6% (ww^{-1}). Since nanofibers alter the

N/C balance by increasing CO_2 availability, a higher production of carbon-rich macronutrients is expected. Cardias et al. (2024) reported an average decrease of 45% in carbohydrate content during the cultivation of *Spirulina* sp. LEB 18 with PAN nanofibers, with and without MEA (0.2 g L^{-1}), an effect opposite to what was observed in the present study. In opposition, Vaz et al. (2019) shown an increase of carbohydrate portion in *Chlorella fusca* LEB 111 biomass cultivated with Fe_2O_3 nanoparticles enriched PAN nanofibers (0.1 g L^{-1}). The authors attributed this increase to enhanced carbon availability due to the adsorption properties of the nanofibers. These results suggest that the

Nano treatment in the present study stimulated the metabolic pathway toward carbohydrate accumulation.

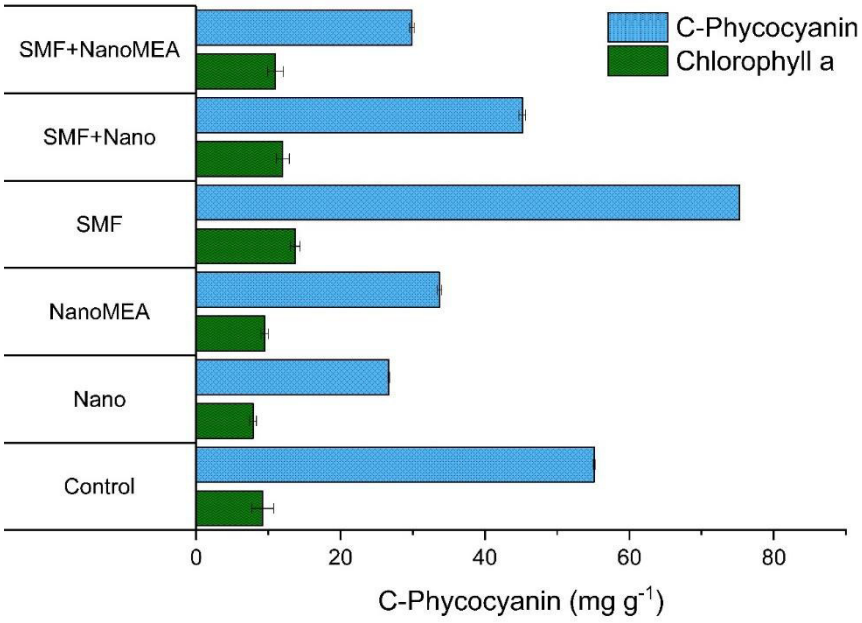
Carbohydrates present in microalgae biomass are mainly composed of polysaccharides used as structural components strongly linked to the cell wall and/or energy storage, such as glycogen. Carbohydrate formation in cyanobacteria is metabolized by the Calvin-Benson-Bassham cycle (CBB) from inorganic carbon, photorespiration, and enzymatically polymerized in the cellular cytoplasm (Rossi; Philippis, 2016; Xiong *et al.*, 2017). The results *indica*ted an inversely proportional correlation between protein and carbohydrate concentrations, reaffirming the competitive nature of these metabolic pathways involved in carbon fixation (Li et al., 2022). Carbon (C) is essential for the metabolic pathways involved in forming the main components of

microalgal biomass, which include carbohydrates, proteins, and lipids. The flow of carbon tends to maintain equilibrium to ensure stable cellular maintenance. However, when microalgae cultures are under stress, this balance can be disrupted, leading to increased production of certain metabolites as a means of maintaining cellular homeostasis. Consequently, when more carbon is directed toward nitrogen fixation (for protein synthesis), less is available for carbohydrate production.

Cardias et al. (2024) reports an increase of 37% in lipid content in cultivation of *Spirulina sp.* LEB 18 with PAN nanofibers with and without MEA (0.2 g L^{-1}). In contrast, the proposed assays did not affect ($p \leq 0.05$) the total lipid production in the biomass of *Limnospira indica* PCC 8005.

The pigment concentrations in the biomass of *L. indica* PCC 8005 are illustrated in Figure 3. The highest concentration of c-phycocyanin (PC) was observed in the SMF assay, reaching 75.2 ± 0.1 mg g^{-1}, followed by the control group at 55 ± 1.2 mg g^{-1}. For chlorophyll a (Chl a), the highest concentration recorded was 13.7 ± 0.2 mg g^{-1} in the SMF assay, followed by 12 ± 0.4 mg g^{-1} in the SMF+Nano treatment and 11 ± 1.1 mg g^{-1} in the SMF+NanoMEA treatment (Figure 2).

Figure 3 - Phycocyanin c and chlorophyll a concentration in L. indica biomass.SMF - Magnetic field 1h day^{-1}; SMF + Nano – added nanofiber magnetic field; Nano – Added nanofibers; SMF +NanoMEA – Magnetic field and nanofiber produced with MEA; NanoMEA - Nanofiber addition produced with MEA. The results are expressed as mean (n=3) ± standard deviation. Different letters on the same line indicate a significant difference between p-values <0.05 (Tukey's test).



Comparing the Control treatment with the SMF and Nano treatments, distinct effects on the production of PC and Chl a were observed. The addition of nanofibers resulted in a significant negative impact, with a reduction of -103% in PC synthesis and -16% in Chl a production, compared to CT. In opposition, the SMF treatment had a positive effect, enhancing PC synthesis by 36% and increasing Chl a levels by 49%. These results indicate that the incorporation of polymeric nanofibers wields a more substantial influence on PC production compared to Chl a while the beneficial effects of SMF are more pronounced in Chl a production.

The pigment content in microalgae is influenced by various environmental stimuli, including nutrient availability, temperature, irradiance, light-dark cycles, and pH levels. Additionally, the intrinsic characteristics of the species also play a significant role in determining pigment composition. Garcia-Gragera *et al*. (2022) characterized pigments in *L. indica* biomass cultured under light intensities of 163 µmol photons m^{-2} s^{-1}, reporting chlorophyll a concentrations

of 16 ± 2 mg g^{-1} and c-phycocyanin 75 ± 6 mg g^{-1}. Meanwhile, Deamici *et al*. (2022) found a 161% increase in chlorophyll a in biomass grown under the influence of SMF, when compared to control.

The metabolic pathway for the synthesis of pigments in photosynthetic microorganisms is a complex reaction involving enzymes and co-factors in which can show magnetic behavior, such as Fe^{2+} and Mg^{2+}. The orientation of the magnetic field can influence the activity of enzymes involved in these pathways, promoting pigment production. Chlorophylls are particularly known for forming radical pairs (P $680^{\bullet+}$ and $Phe^{\bullet-}$) when exposed to static magnetic fields (SMF), which can alter their behavior and modulate photosynthesis by increasing the activity in reaction centers in Photosystem II, ultimately increasing quantum yield. Additionally, PC is a biliprotein, and the previous results showed an increase in its concentration in treatments exposed to SMF, aligning with the overall rise in protein levels under these conditions (Deamici *et al.*, 2019; Font *et al.*, 2023; Yu, Z. *et al.*, 2024).

Despite the promising potential of static magnetic fields (SMF) and polymeric nanofibers for enhancing microalgae cultivation, several barriers must be addressed before large-scale application is feasible. For SMF, although generally considered low-cost, the economic viability at industrial scale depends on balancing increased productivity against the costs of magnets, installation, and maintenance(Santos *et al.*, 2022). Moreover, life cycle assessments have reported mixed environmental impacts, with some indicators improving and others remaining unchanged or worsening. The mechanisms underlying SMF's effects on microalgae also remain poorly understood, with most research limited to laboratory or pilot scales and little information available on long-term performance or reproducibility (Xu, S. *et al.*, 2024). Similarly, the use of polymeric nanofibers faces significant challenges, including the difficulty of producing high-quality fibers at scale, operational complexity, environmental variability, and economic constraints. Overcoming these barriers—particularly through the development of scalable, cost-effective electrospinning or electrospraying technologies—is critical for practical deployment in industrial systems (Almeida *et al.*, 2024).

In this context, SMF was found to enhance microalgal metabolism, increasing protein content by 16% and boosting photosynthetic pigments by 36–49% (phycocyanin and chlorophyll *a*). In contrast, nanofiber treatments promoted carbohydrate accumulation (39%) but suppressed pigment synthesis, revealing a trade-off between growth stimulation and metabolic balance. These findings suggest that while both technologies offer unique advantages, their optimization and

integration require careful consideration to maximize benefits for biomass and biomolecule production.

3.3 CHARACTERIZATION OF BOUND EXOPOLYSACCHARIDES (BPS)

The profile of bound exopolysaccharides (BPS) extracted from the biomass of *Limnospira indica* PCC 8005 is shown in Table 3. Total sugars and proteins are *indica*tors of purity in BPS, while sulphate groups, neutral sugars, and uronic acid composition. The effects of nanofibers and SMF on BPS production parallel to those observed in carbohydrate synthesis. The BPS extracted in this study mainly consisted of neutral sugars, ranging from 69.4 ± 0.58% (SMF treatment) to 56.1 ± 1.71% (SMF+NanoMEA) while uronic acid content varied from 39.9 ± 2.49% (SMF+Nano) to 25.4 ± 0.71% (Nano).

Table 3 - Characterization of the EPS extracted from *L. Indica* biomass cultivated with nanofibers under the influence of SMF. SMF - Magnetic field 1h day^{-1}; SMF + Nano – added nanofiber magnetic field; Nano – Added nanofibers; SMF +NanoMEA – Magnetic field and nanofiber produced with MEA; NanoMEA - Nanofiber addition produced with MEA. The results are expressed as mean (n=3) ± standard deviation. Different letters on the same line indicate a significant difference between p-values <0.05 (Tukey's test).

	% Total Sugars	% Protein	% Neutral sugars	% Uronic Acid	% Sulphated groups (eq. SO4)
	Samples (%Mass)		EPS (Mass (g 100g^{-1} EPS)		
Control	31±0.01^{c}	25.3±0.3^{bc}	64.5±1.56^{bc}	34.2 ± 1.26^{b}	1.37 ± 0.4^{d}
SMF	34±0.01^{bc}	20.3±2.7^{a}	69.4±0.58^{d}	25.6±0.96^{cd}	4.4±0.96^{bc}
SMF+Nano	40±0.01^{a}	25.5±0.60^{bc}	62.2±0.48^{b}	36.4±0.51^{b}	1.42±0.08^{d}
Nano	38±0.04^{ab}	21.2±2.40^{ab}	66.2±0.80^{c}	25.4±0.71^{d}	08.41±0.15^{a}
SMF+Nano MEA	42±0.01^{a}	26.5±0.1^{c}	56.1±1.71^{a}	39.9±2.49^{a}	3.78±0.52^{c}
NanoMEA	40±0.03^{a}	19.3±2.8^{a}	67.8±0.17^{cd}	28.4±0.28^{c}	4.0±0.47^{b}

The application of static magnetic fields (SMF) and nanofibers (Nano) in microalgae cultivation induced significant alterations in the structural composition of extracellular polysaccharides (RPS). Compared to the control, treatment with SMF alone resulted in a notable increase in neutral sugars (69.4 ± 0.58%), but was accompanied by reductions in uronic acids (25.61 ± 0.96 %) and sulfonated groups (4.4 ± 0.96%). This profile suggests the formation of structurally simpler RPS, with lower functional complexity, possibly due to the induction of metabolic pathways aimed at producing reserve carbohydrates.

On the other hand, Nano treatment resulted in the highest expression of sulphated groups (08.41 ± 0.15%) among all treatments, associated with a slight reduction in neutral sugars (66.2 ± 0.80%) and uronic acids (25.39 ± 0.71%). This behavior indicates a metabolic redirection toward the synthesis of sulphated RPS with greater bioactive potential (Ai *et al.*, 2023; Phélippé *et al.*,

2019). Comparatively, while SMF favored the production of simpler RPS rich in structural carbohydrates, treatment with nanofibers stimulated the generation of polymers with bioactive characteristics. Thus, the two treatments distinctly modify the composition of RPS: SMF stands out for increasing neutral carbohydrates, while Nano proves to be more promising for obtaining biopolymers with biotechnological applications.

The primary neutral sugars found in *L. indica* are glucose, rhamnose, fucose, arabinose and xylose comprising 40% to 90% of the polymer, while uronic acids, which can make up to 60%, are predominantly composed of glucuronic acid (Laroche, 2022; Van Camp *et al.*, 2022). Phélippe *et al*., (2019) compiled studies characterizing the EPS of *Arthrospira platensis*, which reports the effects of temperature, nitrates and light intensity during cultivation in the EPS composition and productions as well as extraction methods. The study concludes low light intensity (< 200 µmol of photons m^{-2} s^{-1}) effect the polysaccharide profile, decreases uronic acid content and modifying neutral sugars makeup in BPS, particularly the content of mannose and rhamnose, the latter highly linked with bioactivity (Ai *et al.*, 2023). Van Camp et al. (2022) presented the profile of EPS produced by *L. indica,* for BPS its was found to be just glucose (40%) and glucuronic acid (60%). Uronic acids have anionic nature and hydrophobic behavior, therefore enhance viscosity, suggesting potential applications as biosurfactants, bioemulsifiers, and bioflocculants (Laroche, 2022; Wang et al., 2021). Therefore, the presence of these compounds *indica*te the potential bioactivity of the BPS extracted from the SMF+NanoMEA assay.

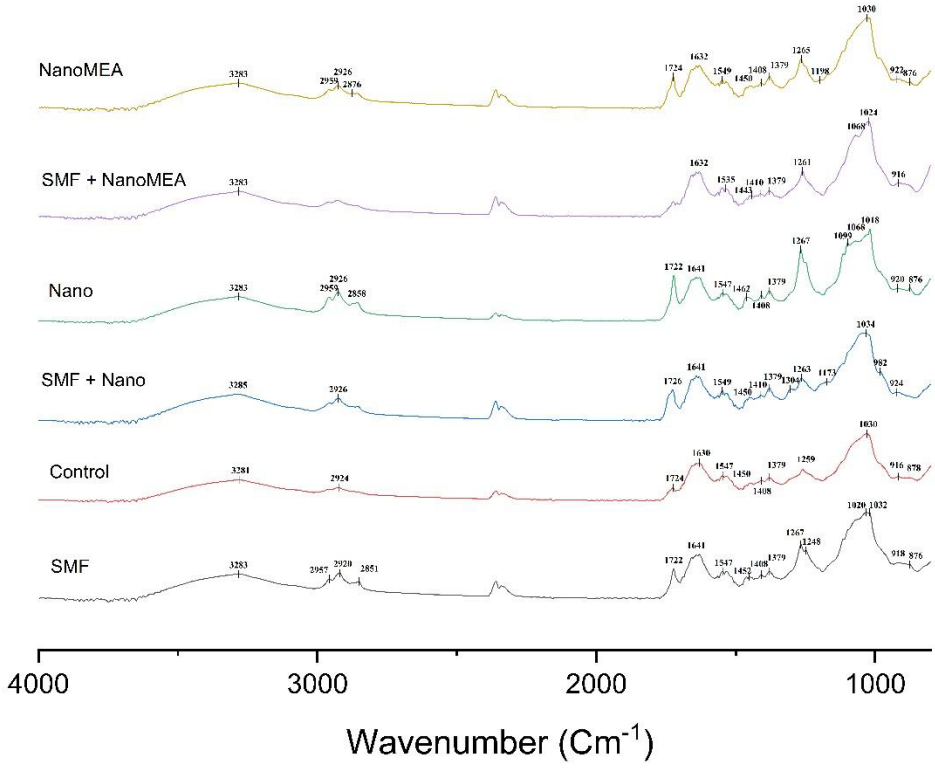
The proportion of acidic, neutral, and sulphated components in these polymers depends on cultivation conditions, extraction methods, and whether the EPS is bound or released (Laroche, 2022; Phélippé *et al.*, 2019). Sulphate groups in *Limnospira indica* are not well documented. Phélippe *et al*. (2019) reported a mean sulphate concentration of 4% for *Arthrospira platensis*. Sulphate, along with methylation and uronic acids, serve as important *indica*tors of biological and technological potential due to their reactive nature (Pierre *et al.*, 2019; Zhang, J. *et al.*, 2019). Indeed exopolysaccharides may exhibit antiviral, antibacterial, immunomodulatory, antioxidant, and antithrombotic activities, along with gel-forming capabilities (Ai *et al.*, 2023; Fimbres-Olivarría *et al.*, 2016). The bioactive properties of EPS from cyanobacteria, reported in literature, describe its antioxidant capacity, both in vitro and in vivo, is linked to the inhibition of oxidative damage and the enhancement of antioxidant enzyme functions. Immunomodulatory effects are primarily associated with cellular stimulation through activation of mitogen-activated protein

kinase and nuclear factor κB pathways, thereby improving immune system functions (Ai *et al.*, 2023; Wu, X. *et al.*, 2020). The antiviral and antibacterial properties of EPS are attributed to preventing cytopathic effects and syncytium formation, obstructing viral binding and entry into host cells, and inhibiting virus replication (Ai *et al.*, 2023; Hayashi; Hayashi; Kojima, 1996). In addition, sulphated polysaccharides and their derivatives exhibit significant anticoagulant properties, contributing to their antithrombotic effects (Majdoub *et al.*, 2009).

The FT-IR (Fourier Transform Infrared) spectra of the extracted EPS, covering the range from 4000 to 400 cm^{-1}, are presented in Figure 4. The results in the functional group region (4000 – 1500 cm^{-1}) are characteristic of a polysaccharide with soft peaks around 3282 cm^{-1} related to the stretching vibration of the hydrogen bonds in the O-H (Wang *et al*., 2007). Followed by CH_3 peaks around 2960 cm^{-1} for symmetrical vibration elongation and around 2870 cm^{-1} for asymmetrical, showing a degree of methylation in the extracted BPS (Maréchal, 1997). Methyl groups can be associated with methylated amino acids or sugars such as 3-O-methyl rhamnose (acofriose), 3-O-methyl xylose, 2-O-methyl-glucuronic acid or 3-O-methyl galactose present in their structures (Esqueda; Gardarin; Laroche, 2022). Peaks found around 2920 cm^{-1} are associated with CH vibration directed to an indication of the total sugar content in the samples (Chopin; Kerin; Mazerolle, 1999). Bands between 1725 to 1740 cm^{-1} are associated with O-Acetyl groups and were found in all samples. Peaks ranging from 1430 to 1660 cm^{-1} are related to amide groups present in proteins and ester sulphate (Chopin; Kerin; Mazerolle, 1999; Maréchal, 1997), likely derived from the biomass during the extraction of BPS, which was not completely removed.

As for the region between 400 - 1500 cm^{-1}, peaks around 1260 cm^{-1} is related to the sulphated ester (S=O) and is an indicator of the sulphate content in polysaccharides, it is present in all samples but at different intensities (Chopin; Kerin; Mazerolle, 1999), in agreement with the previously assays.

Figure 4 - FT-IR spectrum of BPS extracted from *L. indica* biomass. SMF - Magnetic field 1h day^{-1}; SMF + Nano – added nanofiber magnetic field; Nano – Added nanofibers; SMF +NanoMEA – Magnetic field and nanofiber produced with MEA; NanoMEA - Nanofiber addition produced with MEA.



The bands in the 1000-1200 cm^{-1} range suggest the presence of lateral C-O-H groups, vibration of the C-O-C glycosidic band, and C-C bonds related to the pyran rings of sugars (Chopin; Kerin; Mazerolle, 1999; Esqueda; Gardarin; Laroche, 2022; Molaei; Jahanbin, 2017). This band is the most prominent in all samples, and peaks at around 1030 cm^{-1} for all samples except for the Nano assay (1018 cm^{-1}). However, it is possible to notice the formation of a shoulder at wavelengths above 1018 cm^{-1}, suggesting hidden specific C-bonds peaks.

In addition, the FTIR analysis is in accordance with the characterization in Table 3. The RPS with the highest concentration of sugars showed the highest peak around 1030 cm^{-1}. The same applies to sulphate content; the RPS of the Nano assay had the highest peak in the 1260 cm^{-1} band; the presence of acetyl and carboxyl groups indicates acidic sugars; and the presence of amide

(protein) bonds. Therefore, RPS extracted from *L. indica* biomass can be characterized as acidic sulphated polysaccharides.

4. CONCLUSION

This study demonstrates that integrating static magnetic fields (SMF) and polymeric nanofibers synergistically enhances *Limnospira indica* PCC 8005 biomass production (28% increase) while differentially modulating its biochemical profile: SMF elevated protein content (16%) and photosynthetic pigments (36 – 49% for phycocyanin and chlorophyll a), whereas nanofibers favored carbohydrate accumulation (39%). However, nanofibers suppressed pigment synthesis, revealing critical trade-offs between growth stimulation and metabolic balance. EPS exhibited treatment-specific functional traits, including uronic acid-rich (39.9%) or highly sulphated (8.4%) profiles, suggesting tailored applications in biomaterials or bioactive compounds. Future work must resolve mechanistic conflicts between SMF and nanofiber effects, optimize scalability, and characterize EPS functionality to unlock the full potential of this approach for sustainable bioproduct development.

Author contributions: CRediT: Matheus Pereira de Carvalho: Conceptualization, Formal analysis, Investigation, Writing – original draft. **Michele Greque de Morais:** Methodology, Conceptualization. **Lucielen Oliveira** dos **Santos:** Methodology, Conceptualization. **Céline Laroche:** Supervision, Writing – review and editing, Methodology, Funding acquisition, Conceptualization: **Jorge Alberto Vieira Costa**: Supervision, writing – review and editing, Funding acquisition, Conceptualization.

Funding sources This study was financed in part by the Coordenação de Aperfeiçoamento de Pessoal de Nível Superior—Brasil (CAPES)—Finance Code 001. This research was funded by the Program CAPES-COFECUB (Sv 945/19)

REFERENCE

AI, X.; YU, P.; LI, X.; LAI, X.; YANG, M.; LIU, F.; LUAN, F.; MENG, X. Polysaccharides from : Extraction methods, structural features and bioactivities diversity. **International Journal of Biological Macromolecules**, vol. 231, no. 1166, p. 123211, Mar. 2023. DOI:

10.1016/j.ijbiomac.2023.123211. Available at: https://doi.org/10.1016/j.ijbiomac.2023.123211.

ALMEIDA, A. C. A. de; VAZ, S.; COSTA, J. A. V.; MORAIS, M. G. de. Innovative technology for microalgal cell preservation through immobilization in polylactic acid nanofibers. **Algal Research**, vol. 84, no. May, p. 103781, 2024. DOI: 10.1016/j.algal.2024.103781. Available at: https://doi.org/10.1016/j.algal.2024.103781.

ALY, H. F.; RIZK, M. Z.; SHAMS, S. G. E. Microalgae in food and feed: Safety and toxicological aspects. **Handbook of Food and Feed from Microalgae: Production, Application, Regulation, and Sustainability**. Elsevier, 1 Jan. 2023. pp. 549–565. https://doi.org/10.1016/B978-0-323-99196-4.00004-8.

AMERICAN PUBLIC HEALTH ASSOCIATION. **Standard Methods for the Examination of Water and Wastewater**. Washington DC,USA: American Public Health Association, 1971. 237–239 pp.

BA, F.; FOISSARD, A.; LEBERT, A.; DJELVEH, G.; LAROCHE, C. Polyethyleneimine as a tool for compounds fractionation by flocculation in a microalgae biorefinery context. **Bioresource Technology**, vol. 315, p. 123857, Nov. 2020. DOI: 10.1016/j.biortech.2020.123857. Available at: https://linkinghub.elsevier.com/retrieve/pii/S0960852420311299.

BENNETT, A.; BOGORAD, L. Complementary chromatic adaptation in a filamentous blue-green alga. **The Journal of Cell Biology**, vol. 58, no. 2, pp. 419–435, 1 Aug. 1973. DOI: 10.1083/jcb.58.2.419. Available at: https://rupress.org/jcb/article/58/2/419/18179/COMPLEMENTARY-CHROMATIC-ADAPTATION-IN-A.

BERGES, J. A.; MULHOLLAND, M. R. Enzymes and Nitrogen Cycling. **Nitrogen in the Marine Environment**. Elsevier, 2008. pp. 1385–1444. DOI: 10.1016/B978-0-12-372522-6.00032-3. Available at: https://linkinghub.elsevier.com/retrieve/pii/B9780123725226000323.
BLANKENSHIP, R. E. **Molecular Mechanisms of Photosynthesis**. II. Tempe: Wiley, 19 Dec. 2014. 1–321 pp. DOI: 10.1002/9780470758472. Available at: https://onlinelibrary.wiley.com/doi/book/10.1002/9780470758472.

BLIGH, E. G.; DYER, W. J. A rapid method of total lipid extraction and purification. **Canadian Journal of Biochemistry and Physiology**, vol. 37, no. 8, pp. 911–917, 1 Aug. 1959. DOI: 10.1139/o59-099. Available at: http://www.nrcresearchpress.com/doi/10.1139/o59-099.
BLUMENKRANTZ, N.; ASBOE-HANSEN, G. New method for quantitative determination of uronic acids. **Analytical Biochemistry**, vol. 54, no. 2, pp. 484–489, Aug. 1973. https://doi.org/10.1016/0003-2697(73)90377-1.

BORJAS ESQUEDA, A.; GARDARIN, C.; LAROCHE, C. Exploring the Diversity of Red Microalgae for Exopolysaccharide Production. **Marine Drugs**, vol. 20, no. 4, p. 246, 31 Mar. 2022. DOI: 10.3390/md20040246. Available at: https://www.mdpi.com/1660-3397/20/4/246/htm. Accessed: 1 Aug. 2022.

CARDIAS, B. B.; MORAIS, M. G. de; COSTA, J. A. V. Increased biomass and biomolecule productivity of *Spirulina sp*. LEB 18 cultivated with CO_2 adsorbent nanofibers. **Clean Technologies and Environmental Policy**, no. 0123456789, 15 Jun. 2024. DOI: 10.1007/s10098-024-02907-x. Available at: https://doi.org/10.1007/s10098-024-02907-x.

CAWSE, P. A. The determination of nitrate in soil solutions by ultraviolet spectrophotometry. **The Analyst**, vol. 92, no. 1094, p. 311, 1967. https://doi.org/10.1039/an9679200311.

CHOPIN, T.; KERIN, B. F.; MAZEROLLE, R. Phycocolloid chemistry as a taxonomic *indica*tor of phylogeny in the Gigartinales, Rhodophyceae: A review and current developments using Fourier transform infrared diffuse reflectance spectroscopy. **Phycological Research**, vol. 47, no. 3, pp. 167–188, Sep. 1999. DOI: 10.1046/j.1440-1835.1999.00170.x. Available at: http://doi.wiley.com/10.1046/j.1440-1835.1999.00170.x.

COGNE, G.; LEHMANN, B.; DUSSAP, C.; GROS, J. Uptake of macrominerals and trace elements by the cyanobacterium *Spirulina platensis* (*Arthrospira platensis* PCC 8005) under photoautotrophic conditions: Culture medium optimization. **Biotechnology and Bioengineering**, vol. 81, no. 5, pp. 588–593, 5 Mar. 2003. https://doi.org/10.1002/bit.10504.

DANESHVAR, E.; WICKER, R. J.; SHOW, P.-L.; BHATNAGAR, A. Biologically-mediated carbon capture and utilization by microalgae towards sustainable CO_2 biofixation and biomass valorization – A review. **Chemical Engineering Journal**, vol. 427, p. 130884, 1 Jan. 2022. DOI: 10.1016/j.cej.2021.130884. Available at: https://linkinghub.elsevier.com/retrieve/pii/S1385894721024682.

DEAMICI, K. M.; COSTA, J. A. V.; SANTOS, L. O. Magnetic fields as triggers of microalga growth: evaluation of its effect on *Spirulina sp*. **Bioresource Technology**, vol. 220, pp. 62–67, 1 Nov. 2016. https://doi.org/10.1016/J.BIORTECH.2016.08.038.

DEAMICI, K. M.; CUELLAR-BERMUDEZ, S. P.; MUYLAERT, K.; SANTOS, L. O.; COSTA, J. A. V. Quantum yield alterations due to the static magnetic fields action on *Arthrospira platensis* SAG 21.99: Evaluation of photosystem activity. **Bioresource Technology**, vol. 292, p. 121945, Nov. 2019. DOI: 10.1016/j.biortech.2019.121945. Available at: https://linkinghub.elsevier.com/retrieve/pii/S0960852419311757. Accessed: 14 May 2024.

DEAMICI, K. M.; MORAIS, M. G. de; DOS SANTOS, L. O.; GROS, F.; COSTA, J. A. V.; LAROCHE, C. Magnetic Field Action on *Limnospira indica* PCC8005 Cultures: Enhancement of Biomass Yield and Protein Content. **Applied Sciences**, vol. 12, no. 3, p. 1533, 31 Jan. 2022. DOI: 10.3390/app12031533. Available at: https://www.mdpi.com/2076-3417/12/3/1533.

DEAMICI, K. M.; SANTOS, L. O.; COSTA, J. A. V. Magnetic field action on outdoor and indoor cultures of *Spirulina*: Evaluation of growth, medium consumption and protein profile. **Bioresource Technology**, vol. 249, pp. 168–174, 1 Feb. 2018. https://doi.org/10.1016/J.BIORTECH.2017.09.185.

DEAMICI, K. M.; SANTOS, L. O.; COSTA, J. A. V. Magnetic field as promoter of growth in outdoor and indoor assays of *Chlorella fusca*. **Bioprocess and Biosystems Engineering**, vol. 44,

no. 7, pp. 1453–1460, 2021. DOI: 10.1007/s00449-021-02526-6. Available at: https://doi.org/10.1007/s00449-021-02526-6.

DEAMICI, K. M.; SANTOS, L. O.; COSTA, J. A. V. Use of static magnetic fields to increase CO_2 biofixation by the microalga *Chlorella fusca*. **Bioresource Technology**, vol. 276, no. November 2018, pp. 103–109, 1 Mar. 2019. DOI: 10.1016/j.biortech.2018.12.080. Available at: https://linkinghub.elsevier.com/retrieve/pii/S0960852418317516. Accessed: 10 Mar. 2023.

DOGSON, K.; PRICE, R. A note on the determination of the ester sulphate content of sulphated polysaccharides. **Biochemical Journal**, vol. 84, no. 1, pp. 106–110, 1 Jul. 1962. DOI: 10.1042/bj0840106. Available at: https://portlandpress.com/biochemj/article/84/1/106/52792/A-note-on-the-determination-of-the-ester-sulphate.

DUBOIS, M.; GILLES, K. A.; HAMILTON, J. K.; REBERS, P. A.; SMITH, F. Colorimetric Method for Determination of Sugars and Related Substances. **Analytical Chemistry**, vol. 28, no. 3, pp. 350–356, 1 Mar. 1956. DOI: 10.1021/ac60111a017. Available at: https://pubs.acs.org/doi/abs/10.1021/ac60111a017. Accessed: 27 Jan. 2022.

FILALI MOUHIM, R.; CORNET, J. F.; FONTANE, T.; FOURNET, B.; DUBERTRET, G. Production, isolation and preliminary characterization of the exopolysaccharide of the cyanobacterium *Spirulina platensis*. **Biotechnology Letters 1993 15:6**, vol. 15, no. 6, pp. 567–572, 1993. DOI: 10.1007/BF00138541. Available at: https://link.springer.com/article/10.1007/BF00138541. Accessed: 12 Sep. 2022.

FIMBRES-OLIVARRÍA, D.; LÓPEZ-ELÍAS, J. A.; CARVAJAL-MILLÁN, E.; MÁRQUEZ-ESCALANTE, J. A.; MARTÍNEZ-CÓRDOVA, L. R.; MIRANDA-BAEZA, A.; ENRÍQUEZ-OCAÑA, F.; VALDÉZ-HOLGUÍN, J. E.; BROWN-BOJÓRQUEZ, F. Navicula sp. Sulfated Polysaccharide Gels Induced by Fe(III): Rheology and Microstructure. **International Journal of Molecular Sciences 2016, Vol. 17, Page 1238**, vol. 17, no. 8, p. 1238, 30 Jul. 2016. DOI: 10.3390/IJMS17081238. Available at: https://www.mdpi.com/1422-0067/17/8/1238/htm. Accessed: 31 Oct. 2022.

FONT, Y. S.; DÍAZ, Y. O.; CUYPERS, A.; ALEMÁN, E. I.; VANDAMME, D. The effect of magnetic field treatment on the cultivation of microalgae: An overview of involved mechanisms. **Journal of Applied Phycology**, vol. 35, no. 4, pp. 1525–1536, 1 Aug. 2023. https://doi.org/10.1007/s10811-023-02994-1.

GHIAT, I.; AL-ANSARI, T. A review of carbon capture and utilisation as a CO_2 abatement opportunity within the EWF nexus. **Journal of CO_2 Utilization**, vol. 45, p. 101432, 1 Mar. 2021. DOI: 10.1016/j.jcou.2020.101432. Available at: https://linkinghub.elsevier.com/retrieve/pii/S2212982020310623.

HANIFA, M.; AGARWAL, R.; SHARMA, U.; THAPLIYAL, P. C.; SINGH, L. P. A review on CO_2 capture and sequestration in the construction industry: Emerging approaches and commercialised technologies. **Journal of CO_2 Utilization**, vol. 67, p. 102292, 1 Jan. 2023. DOI: 10.1016/j.jcou.2022.102292. Available at: https://linkinghub.elsevier.com/retrieve/pii/S2212982022004115.

HAYASHI, K.; HAYASHI, T.; KOJIMA, I. A natural sulfated polysaccharide, calcium spirulan, isolated from Spirulina platensis: In vitro and ex vivo evaluation of anti-herpes simplex virus and anti-human immunodeficiency virus activities. **AIDS Research and Human Retroviruses**, vol. 12, no. 15, pp. 1463–1471, 1996. https://doi.org/10.1089/aid.1996.12.1463.

HIRANO, M.; OHTA, A.; ABE, K. Magnetic Field Effects on Photosynthesis and Growth of the Cyanobacterium *Spirulina platensis*. **JOURNAL OF FERMENTATION AND BIOENGINEERING**, vol. 86, no. 3, pp. 313–316, 1998.

HUO, S.; CHEN, X.; ZHU, F.; ZHANG, W.; CHEN, D.; JIN, N.; COBB, K.; CHENG, Y.; WANG, L.; RUAN, R. Magnetic field intervention on growth of the filamentous microalgae *Tribonema sp*. in starch wastewater for algal biomass production and nutrients removal: Influence of ambient temperature and operational strategy. **Bioresource Technology**, vol. 303, no. January, p. 122884, May 2020. DOI: 10.1016/j.biortech.2020.122884. Available at: https://doi.org/10.1016/j.biortech.2020.122884.

INTERNATIONAL ENERGY AGENCY, I. **CO_2 Emissions in 2023**. [*N.d.*]. Available at: www.iea.org. Accessed: 22 Apr. 2024.
LAROCHE, C. Exopolysaccharides from Microalgae and Cyanobacteria: Diversity of Strains, Production Strategies, and Applications. **Marine Drugs**, vol. 20, no. 5, p. 336, 21 May 2022. DOI: 10.3390/md20050336. Available at: https://doi.org/10.3390/md20050336. Accessed: 29 Jul. 2022.

LI, C.; HU, Z.; GAO, Y.; MA, Y.; PAN, X.; LI, X.; LIU, S.; CHU, B. Bioeffects of static magnetic fields on the growth and metabolites of *C. pyrenoidosa* and *T. obliquus*. **Journal of Biotechnology**, vol. 351, no. November 2021, pp. 1–8, Jun. 2022. DOI: 10.1016/j.jbiotec.2022.04.004. Available at: https://doi.org/10.1016/j.jbiotec.2022.04.004.

LI, Z.-Y.; GUO, S.-Y.; LI, L.; CAI, M.-Y. Effects of electromagnetic field on the batch cultivation and nutritional composition of *Spirulina platensis* in an air-lift photobioreactor. **Bioresource Technology**, vol. 98, no. 3, pp. 700–705, Feb. 2007. DOI: 10.1016/j.biortech.2006.01.024. Available at: https://linkinghub.elsevier.com/retrieve/pii/S0960852406000678. Accessed: 14 May 2024.

LOWRY, O.; ROSEBROUGH, N.; FARR, A. L.; RANDALL, R. Protein Measurement with The Folin Phenol Reagent. **Journal of Biological Chemistry**, vol. 193, no. 1, pp. 265–275, Nov. 1951. DOI: 10.1016/S0021-9258(19)52451-6. Available at: https://linkinghub.elsevier.com/retrieve/pii/S0021925819524516. Accessed: 10 Apr. 2023.

LUO, X.; ZHANG, H.; LI, Q.; ZHANG, J. Effects of static magnetic field on *Chlorella vulgaris*: growth and extracellular polysaccharide (EPS) production. **Journal of Applied Phycology**, vol. 32, no. 5, pp. 2819–2828, 19 Oct. 2020. DOI: 10.1007/s10811-020-02164-7. Available at: https://link.springer.com/10.1007/s10811-020-02164-7. Accessed: 14 May 2024.

MAJDOUB, H.; MANSOUR, M. Ben; CHAUBET, F.; ROUDESLI, M. S.; MAAROUFI, R. M. Anticoagulant activity of a sulfated polysaccharide from the green alga *Arthrospira platensis*.

Biochimica et Biophysica Acta - General Subjects, vol. 1790, no. 10, pp. 1377–1381, 2009. https://doi.org/10.1016/j.bbagen.2009.07.013.

MAJHI, B. K. Cyanobacteria : Photosynthetic Cell Factories for Biofuel Production. **Journal of Bioresources and Bioproducts**, pp. 0–28, 2024. DOI: 10.1016/j.jobab.2024.10.001. Available at: https://doi.org/10.1016/j.jobab.2024.10.001.

MARÉCHAL, Y. Interaction configurations of H_2O molecules in a protein (Stratum Corneum) by infrared spectrometry. **Journal of Molecular Structure**, vol. 416, nos. 1–3, pp. 133–143, Oct. 1997. DOI: 10.1016/S0022-2860(97)00032-X. Available at: https://linkinghub.elsevier.com/retrieve/pii/S002228609700032X. Accessed: 11 Apr. 2024.

MOLAEI, H.; JAHANBIN, K. Structural features of a new water-soluble polysaccharide from the gum exudates of *Amygdalus scoparia* Spach (Zedo gum). 2017. DOI: 10.1016/j.carbpol.2017.10.099. Available at: www.elsevier.com/locate/carbpol. Accessed: 21 May 2024.

MONSIGNY, M.; PETIT, C.; ROCHE, A.-C. Colorimetric determination of neutral sugars by a resorcinol sulfuric acid micromethod. **Analytical Biochemistry**, vol. 175, no. 2, pp. 525–530, Dec. 1988. https://doi.org/10.1016/0003-2697(88)90578-7.

MONTREUIL, J.; SPIK, G.; CHOSSON, A.; SEGARD, E.; SCHEPPLER, N. Methods Of Study Of The Structure Of Glycoproteins. **Journal de pharmacie de Belgique**, vol. 18, pp. 529–46, 1963. Available at: http://www.ncbi.nlm.nih.gov/pubmed/14096752.

MURO-PASTOR, M. I.; REYES, J. C.; FLORENCIO, F. J. Ammonium assimilation in cyanobacteria. **Photosynthesis Research**, vol. 83, no. 2, pp. 135–150, Feb. 2005. DOI: 10.1007/s11120-004-2082-7. Available at: http://link.springer.com/10.1007/s11120-004-2082-7.

NOWICKA-KRAWCZYK, P.; MÜHLSTEINOVÁ, R.; HAUER, T. Detailed characterization of the Arthrospira type species separating commercially grown taxa into the new genus *Limnospira* (Cyanobacteria). **Scientific Reports**, vol. 9, no. 1, p. 694, 24 Jan. 2019. DOI: 10.1038/s41598-018-36831-0. Available at: https://www.nature.com/articles/s41598-018-36831-0.

PAZUR, A.; WINKLHOFER, M. Magnetic effect on CO_2 solubility in seawater: A possible link between geomagnetic field variations and climate. **Geophysical Research Letters**, vol. 35, no. 16, 30 Aug. 2008. DOI: 10.1029/2008GL034288. Available at: https://agupubs.onlinelibrary.wiley.com/doi/10.1029/2008GL034288.

PHÉLIPPÉ, M.; GONÇALVES, O.; THOUAND, G.; COGNE, G.; LAROCHE, C. Characterization of the polysaccharides chemical diversity of the cyanobacteria *Arthrospira platensis*. **Algal Research**, vol. 38, no. December 2018, p. 101426, 2019. DOI: 10.1016/j.algal.2019.101426. Available at: https://doi.org/10.1016/j.algal.2019.101426.

PIERRE, G.; DELATTRE, C.; DUBESSAY, P.; JUBEAU, S.; VIALLEIX, C.; CADORET, J. P.; PROBERT, I.; MICHAUD, P. What is in store for EPS microalgae in the next decade? **Multidisciplinary Digital Publishing Institute**, vol. 24, no. 23, p. 4296, 25 Nov. 2019. DOI:

10.3390/molecules24234296. Available at: https://www.mdpi.com/1420-3049/24/23/4296/htm. Accessed: 13 Oct. 2022.

PORRA, R. J. The chequered history of the development and use of simultaneous equations for the accurate determination of chlorophylls a and b. **Photosynthesis research**, vol. 73, nos. 1–3, pp. 149–56, 2002. DOI: 10.1023/A:1020470224740. Available at: http://www.ncbi.nlm.nih.gov/pubmed/16245116.

RICHMOND, A. **Handbook of Microalgal Culture**. Oxford, UK: Wiley, 25 Nov. 2003. DOI: 10.1002/9780470995280. Available at: https://onlinelibrary.wiley.com/doi/book/10.1002/9780470995280.

ROSA, G. M. da; MORAES, L.; CARDIAS, B. B.; SOUZA, M. da R. A. Z. de; COSTA, J. A. V. Chemical absorption and CO_2 biofixation via the cultivation of Spirulina in semicontinuous mode with nutrient recycle. **Bioresource Technology**, vol. 192, pp. 321–327, Sep. 2015. https://doi.org/10.1016/j.biortech.2015.05.020.

ROSA, G. M. da; MORAIS, M. G. de; COSTA, J. A. V. Green alga cultivation with monoethanolamine: Evaluation of CO_2 fixation and macromolecule production. **Bioresource Technology**, vol. 261, no. April, pp. 206–212, 2018. https://doi.org/10.1016/j.biortech.2018.04.007.

ROSA, G. M.; MORAES, L.; DE SOUZA, M. da R. A. Z.; COSTA, J. A. V. *Spirulina* cultivation with a CO_2 absorbent: Influence on growth parameters and macromolecule production. **Bioresource Technology**, vol. 200, pp. 528–534, 1 Jan. 2016. https://doi.org/10.1016/J.BIORTECH.2015.10.025.

ROSSI, F.; PHILIPPIS, R. De. **The Physiology of Microalgae**. Cham: Springer International Publishing, 2016. DOI: 10.1007/978-3-319-24945-2. Available at: http://link.springer.com/10.1007/978-3-319-24945-2.

SAFI, C.; ZEBIB, B.; MERAH, O.; PONTALIER, P. Y.; VACA-GARCIA, C. Morphology, composition, production, processing and applications of *Chlorella vulgaris*: A review. **Renewable and Sustainable Energy Reviews**, vol. 35, pp. 265–278, 2014. https://doi.org/10.1016/j.rser.2014.04.007.

SANTOS, L. O.; SILVA, P. G. P.; MACHADO, B. R.; SALA, L.; DEAMICI, K. M. Update on the application of magnetic fields to microalgal cultures. **World Journal of Microbiology and Biotechnology**, vol. 38, no. 11, pp. 1–10, 2 Nov. 2022. DOI: 10.1007/s11274-022-03398-y. Available at: https://link.springer.com/article/10.1007/s11274-022-03398-y. Accessed: 3 Oct. 2022.

SHAO, W.; EBAID, R.; ABOMOHRA, A. E.-F.; SHAHEN, M. Enhancement of *Spirulina* biomass production and cadmium biosorption using combined static magnetic field. **Bioresource Technology**, vol. 265, pp. 163–169, Oct. 2018. DOI: 10.1016/j.biortech.2018.06.009. Available at: https://linkinghub.elsevier.com/retrieve/pii/S0960852418307880. Accessed: 14 May 2024.

VAN CAMP, C.; FRAIKIN, C.; CLAVERIE, E.; ONDERWATER, R.; WATTIEZ, R. Capsular polysaccharides and exopolysaccharides from *Gloeothece verrucosa* under various nitrogen regimes and their potential plant defence stimulation activity. **Algal Research**, vol. 64, p. 102680, 1 May 2022. DOI: 10.1016/j.algal.2022.102680. Available at: https://linkinghub.elsevier.com/retrieve/pii/S2211926422000510.

VAZ, B. da S.; COSTA, A. V.; MORAIS, M. G. de. Physical and biological fixation of CO_2 with polymeric nanofibers in outdoor cultivations of Chlorella fusca LEB 111. **International Journal of Biological Macromolecules**, vol. 151, pp. 1332–1339, May 2020. DOI: 10.1016/j.ijbiomac.2019.10.179. Available at: https://linkinghub.elsevier.com/retrieve/pii/S0141813019357472.

VAZ, B. da S.; MASTRANTONIO, D. J. da S.; COSTA, J. A. V.; MORAIS, M. G. de. Green alga cultivation with nanofibers as physical adsorbents of carbon dioxide: Evaluation of gas biofixation and macromolecule production. **Bioresource Technology**, vol. 287, no. May, p. 121406, Sep. 2019. DOI: 10.1016/j.biortech.2019.121406. Available at: https://linkinghub.elsevier.com/retrieve/pii/S0960852419306364.

VEIGA, M. C.; FONTOURA, M. M.; DE OLIVEIRA, M. G.; COSTA, J. A. V.; SANTOS, L. O. Magnetic fields: biomass potential of *Spirulina sp*. for food supplement. **Bioprocess and Biosystems Engineering**, vol. 43, no. 7, pp. 1231–1240, 2020. DOI: 10.1007/s00449-020-02318-4. Available at: https://doi.org/10.1007/s00449-020-02318-4.

WANG, S. C.; BLIGH, S. W. A.; SHI, S. S.; WANG, Z. T.; HU, Z. B.; CROWDER, J.; BRANFORD-WHITE, C.; VELLA, C. Structural features and anti-HIV-1 activity of novel polysaccharides from red algae *Grateloupia longifolia* and *Grateloupia filicina*. **International Journal of Biological Macromolecules**, vol. 41, no. 4, pp. 369–375, Oct. 2007. DOI: 10.1016/j.ijbiomac.2007.05.008. Available at: https://doi.org/10.1016/j.ijbiomac.2007.05.008.

WANG, W. N.; LI, Y.; ZHANG, Y.; XIANG, W. Z.; LI, A. F.; LI, T. Comparison on characterization and antioxidant activity of exopolysaccharides from two *Porphyridium* strains. **Journal of Applied Phycology**, vol. 33, no. 5, pp. 2983–2994, 1 Oct. 2021. DOI: 10.1007/s10811-021-02518-9. Available at: https://link.springer.com/article/10.1007/s10811-021-02518-9. Accessed: 26 Aug. 2022.

WU, X.; LIU, Z.; LIU, Y.; YANG, Y.; SHI, F.; CHEONG, K.-L.; TENG, B. Immunostimulatory Effects of Polysaccharides from *Spirulina platensis* In Vivo and Vitro and Their Activation Mechanism on RAW246.7 Macrophages. **Marine Drugs**, vol. 18, no. 11, p. 538, 28 Oct. 2020. DOI: 10.3390/md18110538. Available at: https://www.mdpi.com/1660-3397/18/11/538.

XIONG, W.; CANO, M.; WANG, B.; DOUCHI, D.; YU, J. The plasticity of cyanobacterial carbon metabolism. **Current Opinion in Chemical Biology**, vol. 41, pp. 12–19, 2017. DOI: 10.1016/j.cbpa.2017.09.004. Available at: http://dx.doi.org/10.1016/j.cbpa.2017.09.004.

XU, S.; JIANG, Y.; LIU, Y.; ESAKKIMUTHU, S.; CHEN, H.; WANG, S. Impact of constant magnetic field on enhancing the microalgal biomass and biomolecules accumulations and life cycle assessment of the approach. **Algal Research**, vol. 80, p. 103563, Jun. 2024. DOI:

https://doi.org/10.1016/j.algal.2024.103563. Available at: https://www.sciencedirect.com/science/article/pii/S2211926424001759.

YU, Z.; ZHAO, W.; SUN, H.; MOU, H.; LIU, J.; YU, H.; DAI, L.; KONG, Q.; YANG, S. Phycocyanin from microalgae: A comprehensive review covering microalgal culture, phycocyanin sources and stability. **Food Research International**, vol. 186, no. December 2023, p. 114362, Jun. 2024. DOI: 10.1016/j.foodres.2024.114362. Available at: https://doi.org/10.1016/j.foodres.2024.114362.

ZHANG, J.; LIU, L.; REN, Y.; CHEN, F. Characterization of exopolysaccharides produced by microalgae with antitumor activity on human colon cancer cells. **International Journal of Biological Macromolecules**, vol. 128, pp. 761–767, 2019. DOI: 10.1016/j.ijbiomac.2019.02.009. Available at: https://doi.org/10.1016/j.ijbiomac.2019.02.009.

PAPER II

PRODUCTION OF B-PHYCOERYTHRIN AND EXOPOLYSACCHARIDE IN *Porphyridium purpureum* MODULATED VIA STATIC MAGNETIC FIELDS AND POLYMERIC NANOFIBERS.

CARVALHO, M. P.; DE MORAIS, M. G.; GARDARIN, C.; DOS SANTOS, L. O.; COSTA, J. A. V.; LAROCHE, C. Production of β-Phycoerythrin and Exopolysaccharide in Porphyridium purpureum Modulated via Static Magnetic Fields and Polymeric Nanofibers. **Applied Sciences**, vol. 16, no. 14, p. 7311, 21 Jul. 2026. DOI: 10.3390/app16147311. Available at: https://www.mdpi.com/2076-3417/16/14/7311.

PRODUCTION OF B-PHYCOERYTHRIN AND EXOPOLYSACCHARIDE IN *Porphyridium purpureum* MODULATED VIA STATIC MAGNETIC FIELDS AND POLYMERIC NANOFIBERS.

ABSTRACT

Trade-offs between biomass productivity and metabolite accumulation constrain microalgae cultivation for high-value biomolecules due to nutrient competition and concurrent metabolic pathways. This study evaluated the independent and combined effects of static magnetic fields (SMF) and polymeric nanofibers on growth performance, biomass composition, and exopolysaccharide (EPS) profiles of *Porphyridium purpureum*. A process intensification strategy was applied by integrating external physical forcing and structured functional materials to enhance mass transfer and carbon utilization efficiency. Cultivations were conducted under controlled photobioreactor conditions using SMF exposure for 1 h d^{-1} or 24 h d^{-1}, combined with polyacrylonitrile (PAN) nanofibers or monoethanolamine-functionalized nanofibers (MEA). Intermittent SMF increased maximal biomass concentration by 36% compared to the control, whereas continuous SMF, MEA nanofibers, and combined conditions reduced biomass accumulation by up to 45%. SMF promoted metabolic reallocation toward carbon-rich fractions, increasing released polysaccharides by 83% and lipid content by 38%. Nanofibers strongly enhanced pigment biosynthesis, with β-phycoerythrin reaching 41.3 mg g^{-1}, threefold higher than the control. EPS characterization showed increased purity, uronic acid content, and sulfation depending on treatment. Overall, SMF and nanofibers acted as selective intensification tools, enabling tunable modulation of growth, metabolism, and product formation.

Key-words: Sulphated polysaccharides, pigments, phycobiliprotein, microalgal cultivation.

1. INTRODUCTION

Microalgae function as the primary agent for global carbon sequestration, mediating approximately 50% of the planet's oxygenic photosynthesis (Hoque *et al.*, 2025). Their carbon

assimilation rates often exceed those of vascular plants by 10 to 50 times, attributed to the Carbon Concentrating Mechanism (CCM). CCM increases inorganic carbon assimilation through carbon dioxide (CO_2) supersaturation around the RuBisCO enzyme, facilitating photosynthesis (Dao *et al.*, 2025; Xu, P. *et al.*, 2023). Beyond their ecological significance, these microorganisms present a compelling alternative to terrestrial crops. They bypass the "food vs. fuel" trilemma by thriving on marginal lands, exhibiting high nutrient-use efficiency, and high valor biomass production (Hoque *et al.*, 2025).

Industrial microalgae biomass is mostly derived from *Chlorella* sp. and the cyanobacteria *Arthrospira* (commercially "Spirulina") summing up to 90% of the total production, due to their lipid and protein content, respectively (Ang *et al.*, 2025). However, the pursuit for other high value molecules has increased the interest toward genera such as *Crypthecodinium* and *Nannochloropsis* for long-chain polyunsaturated fatty acids (PUFAs), and *Haematococcus* for astaxanthin (Liu, L. *et al.*, 2022; Navalho *et al.*, 2025; Nur *et al.*, 2021). Among these microalgae, the rhodophyte *Porphyridium purpureum* is characterized by the synthesis of exopolysaccharides (EPS), phycoerythrin, carotenoids, and PUFAs (Schoeters *et al.*, 2023). The structural complexity of these EPS gives them characteristics ranging from their viscoelastic behavior, bioactivity, and antioxidant potential. *P. purpureum* is a promising candidate for food, pharmaceutics, and cosmetic industries due to EPS antiviral, immune regulatory, and thickening behavior, as well as phycoerythrin pink-red pigments (Laroche, 2022; Medina-Cabrera *et al.*, 2020; Wang, W. N. *et al.*, 2021).

The transition to industrial-scale production of microalgae is typically hindered by productivity, since traditional strategies to enhance high-value molecules, such as nitro-gen or phosphorus starvation, decrease biomass production (Maizatul *et al.*, 2021). Consequently, the development of strategies to mitigate the low biomass productivity while increasing the synthesis of high-value molecules is necessary. Hence, Static Magnetic Fields (SMF) have emerged as a promising alternative as an easy-to-apply, non-toxic, and low-cost method to improve microalgal cultivation (Deamici; Dziergowska; *et al.*, 2022). SMF stimulus acts upon biological systems via magnetic induction, magneto-mechanical effect, and the radical pair mechanism, potentially modulating DNA transcription, enzymatic flux, metabolic pathways, photosynthesis, and oxidation levels (Deamici *et al.*, 2019; Font *et al.*, 2023; Santos *et al.*, 2022).

Most of the data available on the effect of SMF on microalgae and cyanobacteria are derived from observational, whole-culture experiments interpreted through general bio-chemical and biophysical principles, rather than from direct mechanistic investigation, highlighting the need for research targeting the specific metabolic pathways through which this stimulus acts. In these organisms, the reported effects of magnetic fields can be broadly grouped into three categories: metabolic and/or genetic changes, structural changes at the cellular level, and changes in electron transport linked to the photosynthetic reaction centers (Font *et al.*, 2023). Metabolic and genetic changes are typically inferred from experiments in which SMF exposure increases the growth rate or alters protein content, indicating a shift in cellular metabolism. Structural changes are mostly associated with increased membrane permeability, which enhances nutrient uptake from the medium into the cytoplasm and, consequently, metabolic efficiency. Effects on the reaction centers, in turn, have been linked to an increase in the quantum yield of photosystem II, stimulating energy flow and electron transfer during photosynthesis (Font *et al*., 2023). The microalgae response to SMF stimuli is highly dependent on the source, intensity, and duration of exposure, as well as the microorganism being exposed, suggesting the need for specific studies of how SMF acts in different microalgae (Font *et al.*, 2023; Santos *et al.*, 2022).

In parallel, the optimization of interfacial mass transfer of CO_2 remains a critical challenge in high-density cultivation. Chemical absorbents, specifically alkanolamines such as monoethanolamine (MEA) and diethanolamine (DEA), are well-documented for their ability to increase CO_2 retention in liquid media through the formation of carbamates (Daneshvar *et al.*, 2022; Rosa; Morais; Costa, 2018; Rosa *et al.*, 2016). Also, to amplify the bioavailability of inorganic carbon, the use of polymeric nanofibers can be employed. Due to the high surface area of these structures, they act as physical adsorbents of CO_2 in the microalgal cultivation (Vaz; Costa; *et al.*, 2019; Vaz; Costa; Morais, 2020). At the same time, nanofiber production allows for personalizing its components; therefore, the production of polymeric nanofibers with MEA is possible. These nanofibers theoretically have a double-retention mechanism: the nanofiber matrix provides a dense network of physical adsorption sites, while the functionalized MEA enables localized chemisorption, increasing CO_2 availability for microalgal cultivation (Cardias; Morais; Costa, 2024). Enhanced CO_2 availability during cultivation can stimulate carbon fixation by increasing Calvin-cycle activity and photosynthetic oxygen evolution. It may also enhance bicarbonate transport, carbonic anhydrase function, and pyrenoid-based CO_2 concentrating

mechanisms, improving CO_2 supply to Rubisco and thereby favoring metabolic activity and growth (Yao et al., 2024).

The combined SMF and polymeric nanofibers represents a novel and largely unexplored strategy in microalgal biotechnology. SMF have been reported to influence cellular activity and metabolic regulation, whereas polymeric nanofibers improve CO_2 availability at the cell–medium interface (Cardias; Morais; Costa, 2024; Font *et al.*, 2023). In this context, this study aims to evaluate the independent and combined effects of SMF and MEA-nanofibers on the cultivation of *Porphyridium purpureum*. Specifically, investigating how these stimuli modulate growth kinetics and the biosynthesis of high-value β-phycoerythrin and EPS, while seeking alternatives to conventional stress-based induction strategies.

2. MATERIALS AND METHODS

2.1 INOCULUM

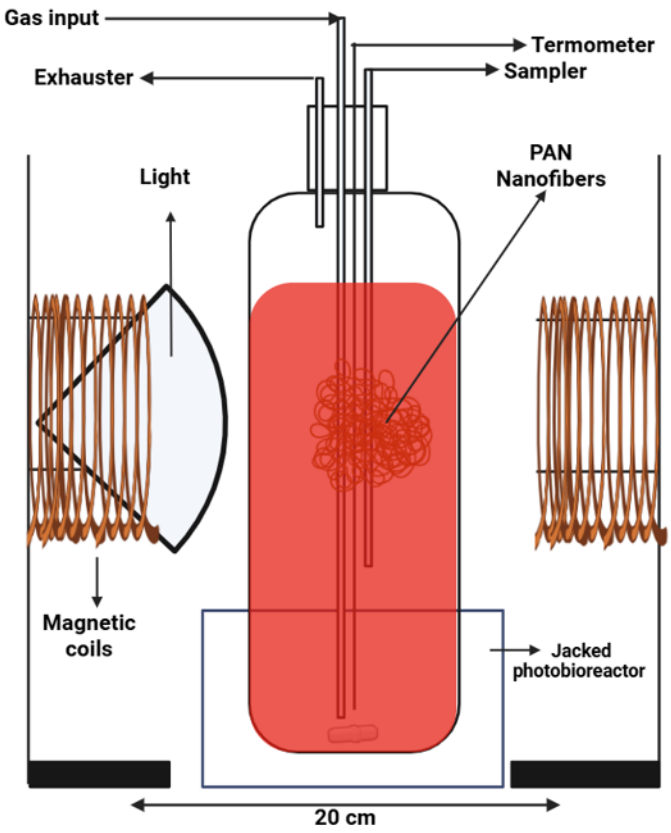
The strain used was *Porphyridium purpureum* CCAP 1380/1A acquired from the Culture Collection of Algae and Protozoa (www.ccap.ac.uk) grown in modified artificial sea water (ASW) medium (Soanen et al., 2016) composed of g L^{-1}; 28 NaCl, 1.85 NaNO3, 0.95 K2HPO4, 7.20 MgSO47H2O, 1.55 CaCl2 2H2O, 100 µL mineral solution (g L^{-1}); 1.5 MnSO4H2O, 0.15 (NH4)6Mo7O244H2O, 0.15 CoSO4,7H2O 0.5 CuSO45H2O, 2.5 ZnSO47H2O, and 100 Fer-EDTA and vitamins (g L^{-1}); 0.1 B12, 0.25 thiamine, and 0.4 biotin and kept at 21 °C. Medium was sterilized by filtration on 0.22µm membranes and kept at room temperature.

2.2 EXPERIMENTAL DESIGN

All experiments were performed in triplicate in 600 mL rectangular jacked photobioreactors connected to condensers to minimize evaporation (Figure 1) (APPENDIX B). Cultivations were homogenized using a magnetic stirrer and sterile airflow; the temperature was controlled by an immersed electrode. The experiments lasted 15 days with modified ASW medium (Soanen *et al.*, 2016). Cultures were maintained at 21±1 °C under continuous (24h) irradiation of 200 µmol photons·m^{-2}·s^{-1} (Carvalho *et al.*, 2025). Homogenization was ensured by sterile compressed air at a flow rate of 0.3 vvm (mL_{air}·mL_{medium}^{-1}·min^{-1}). A gas mixture of 7.5% CO_2 was

injected for 2 minutes hourly, with aeration paused for 1 minute before and after injection to enhance mass transfer (Rosa *et al.*, 2016).

Figure 1 - Used photobioreactor schematic for the proposed experiments.



A static magnetic field (SMF) of 11±2 mT was generated by coils connected to electric current (3A) at the center of the bioreactors and applied intermittently (1 h d^{-1}) or continuously (24 h d^{-1}) (Deamici; Morais; *et al.*, 2022). Nanofiber solutions were prepared according to Cardias *et al.* (2024). Polyacrylonitrile (PAN; 150,000 g mol-1, Sigma-Aldrich®) was dissolved in dimethylformamide (DMF; Synth) at 11.5% (w v-1), followed by the addition of monoethanolamine (MEA; Sigma-Aldrich®) at 1% (w v-1). Electrospinning was performed at a flow rate of 800 µL h-1 using a 0.55 mm capillary, with an applied voltage of 425 kV and a tip-to-collector distance of 180 mm. The process was conducted at 20–23 °C and 50–58% relative humidity. Polymeric nanofibers were added in the proportion of 0.1 mg mL_{medium}^{-1} (Vaz; Vieira Costa; Greque De Morais, 2018).

The experiments had 7 conditions: Control (CT), static magnetic field 1 h d^{-1} (M1), static magnetic field 24 h (M24), with only PAN nanofibers (N), PAN nanofibers and static magnetic field 1 h d^{-1} (MN), PAN monoethanolamine nanofiber (NE), and PAN monoethanolamine nanofiber with static magnetic field 1 h d^{-1} (MNE).

2.3 GROWTH KINETICS

Culture growth was tracked daily by cell counting in Malassez chamber, which was linearly correlated to gravimetric dry mass. The culture pH was monitored with pH meter (SevenEasy S20, Mettler Toledo). The biomass concentration (X), productivity (P) and doubling time (D_t) were calculated from the daily readings. The final mass of cells was added to the biomass production calculations. Daily productivity was obtained by the equation:

$$P = (X_t - X_0)/\, t \tag{1}$$

Where X_t = biomass concentration of the day, X_0 = biomass concentration at the beginning of the culture and t = time in days. The maximum growth rate (μ_{max}) was estimated by linear regression of the exponential growth phase in the lnX vs t graph, and the doubling time Dt was determined by ln(2)/ μ_{max} (Deamici; Morais; *et al*., 2022).

For treatments containing nanofibers, a correction was applied to account for adhered biomass. At the end of the cultivation, nanofibers were collected, dried at 50 °C until a constant weight (N_{inital}) was achieved (APPENDIX B). A daily linear biomass accumulation rate on the nanofibers (P_{Nano}) was assumed and calculated using the equation:

$$P_{Nano} = (N_{final} - N_{inital})/t_{final} \tag{2}$$

Where N_{inital} is the initial mass of the nanofibers and t_{final} is the total cultivation duration in days. The corrected daily biomass concentration ($X_{corrected}$) was then calculated by adding this linear accumulation to the measured suspended biomass(Carvalho *et al.*, 2025):

$$X_{corrected} = X_t + (P_{Nano}.t) \quad (3)$$

2.4 BIOMASS AND EPS HARVEST

After 15 days the culture was centrifuged (10.000 × g for 15 min at 5 ºC), the biomass was washed 2 times with NaCl solution (18 g L^{-1}) to reduce salt content and wash RPS while avoiding cell lysis, the supernatant was separated for released polysaccharides (RPS) extraction while the pellet (biomass) was frozen at -80 ºC for 48h, then lyophilized and kept at -20ºC until further analysis..

EPS was separated into released polysaccharides (RPS) and bound polysaccharides (BPS). RPS was harvested by ultrafiltration of the supernatant at the end of the experiments with Vivaflow 200 system with 10 kDa NMWCO (molecular weight cut-off) membrane for desalination and purification of EPS up to the conductivity measured < 5 µS cm^{-1}, after which the sample was frozen at -80 ºC for 48 h, then lyophilized and kept at -20ºC until further analysis.

BPS extraction was performed as described by Filali Mouhim *et al.* (1993) modified by Phélippé *et al.*, (2019) . A 0.5 g sample of lyophilized biomass was suspended in 200 mL of TAPS buffer (50 mM, pH 8.15) containing 25 mM EDTA and heated to 100 ºC for 20 minutes. After centrifugation (10,000×g for 15 min), the supernatant was reserved, and the pellet was subjected to a second extraction under identical conditions. The two supernatants were pooled, and the BPS was precipitated by adding three volumes of 3% (w/v) cetyltrimethylammonium bromide (CTAB) and incubating overnight. The precipitated BPS-CTAB complex was recovered by centrifugation (10,000×g for 15 min at 0 ºC) and purified through three sequential resolubilization-precipitation cycles. The pellet was first dissolved in 1.5 M KCl, then reprecipitated with three volumes of 96% (v/v) ethanol (24 h at −20 ºC). This process was repeated using 0.75 M KCl and 0.3 M KCl. Finally, BPS pellet was dissolved in MilliQ water, submitted to ultrafiltration as previously described, and then lyophilized.

2.5 BIOMASS CHARACTERIZATION

For macronutrient quantification, a cellular lysate was prepared by resuspending 10 mg of lyophilized biomass in 10 mL of distilled water. The suspension was then subjected to ultrasonication for 10 minutes (UP100H, Hielscher) at 100% amplitude using a 30-second on, 29-second off pulse cycle to ensure complete cell lysis. In order to prevent molecular degradation, the tube was maintained in ice during the process. In order to prevent molecules degradation, the tube was maintained in ice during the process.

Total carbohydrates were quantified from the lysate using the phenol-sulfuric acid method described by (DuBois *et al.*, 1956) and modified as previously described by (Esqueda; Gardarin; Laroche, 2022) with glucose as the standard. For total protein analysis, the lysate was first treated with 1 M NaOH (1:1) and incubated for 5 minutes at 100 °C for solubilization of protein (Safi *et al.*, 2014), and followed by (Lowry *et al.*, 1951) method against an albumin standard curve. The lipid content was extracted from 10 mg of lyophilized biomass and measured by the colorimetric method described by (Marsh; Weinstein, 1966) with chloroform and methanol as solvents.

To evaluate the pigments, 0.1 g of dried biomass was diluted in 7 mL of sodium phosphate 20 mM buffer (pH 7.2). The cells were lysed by subjecting the suspension to three freeze-thaw cycles, followed by ultrasonication for 3 minutes at 100% amplitude (UP100H, Hielscher) in an ice bath. This extraction was centrifuged 10.000 x g for 30 min and the supernatant absorbance was measured at 545, 620, and 650. The B-phycoerythrin (BPE) concentration (mg L^{-1}) was calculated with the correlation equations between R-phycocyanin (RPC) and allophycocyanin (APC) (Bermejo Román *et al.*, 2002):

$$RPC = (\mathrm{Abs}_{620\,nm} - 0.7\,\mathrm{Abs}_{650\,nm})/7.38 \quad (4)$$

$$\mathrm{APC} = (\mathrm{Abs}_{650\,nm} - 0.19\,\mathrm{Abs}_{620\,nm})/5.65 \quad (5)$$

$$\mathrm{BPE} = (\mathrm{Abs}_{545\,nm} - 2.8[\mathrm{RPC}] - 1.34\,[\mathrm{APC}]\,)/12.7 \quad (6)$$

Subsequently, liposoluble compounds were extracted from the pellets subjected to repeated extractions with 80% (v/v) acetone, with centrifugation after each step, until the pellet was

colorless. The absorbance of the pooled acetone supernatants was measured at 470, 646.8, and 663.2 nm. Concentration (mg L^{-1}) of carotenoids (TC), chlorophyll a and b (Chl a and Chl b) was determined by the correlation (Lichtenthaler, 1987):

$$Chl\ a = 12{,}25\ Abs_{663.2\ nm} - 2.79\ Abs_{646.8\ nm} \quad (7)$$

$$Chl\ b = 21.50\ Abs_{646.8\ nm} - 5.1\ Abs_{663\ nm} \quad (8)$$

$$TC = (1000 Abs_{470\ nm} - 1{,}82[Chl\ a] - 85.02[Chl\ b])/198 \quad (9)$$

B-PE concentration, initially obtained on a culture volume basis (mg L^{-1}), was normalized to biomass concentration to express B-PE content (mg BPE g dw^{-1}). B-PE volumetric productivity (mg BPE L^{-1} d^{-1}) was then calculated by multiplying this content by the maximum biomass productivity (Pmax, g L^{-1} d^{-1}) obtained for each treatment.

2.6 EPS BIOCHEMICAL CHARACTERIZATION

For detailed monosaccharide composition, EPS samples were first hydrolyzed in 2 M trifluoroacetic acid (TFA) for 90 minutes at 120 °C, followed by neutralization with 2 M NH_4OH (pH~7). The hydrolysates were filtered (0.2 µm) prior to analysis by High-Performance Anion-Exchange Chromatography with Pulsed Amperometric Detection (HPAEC-PAD) on a Dionex ICS 3000 system equipped with an AS 50 autosampler as described by Borjas-Esqueda; Gardarin; Laroche (2022).

A 25 µL aliquot of each sample was injected onto a CarboPac PA1 guard column (4×50 mm) connected to a CarboPac PA1 analytical column (4×250 mm) maintained at 25∘C. The column was equilibrated with 18 mM NaOH for 15 minutes before each injection. Monosaccharides were eluted at a constant flow rate of 1 mL min^{-1} using an isocratic step of 18 mM NaOH for 25 minutes to separate neutral sugars, followed by a 20-minute linear gradient from 0 to 0.5 M sodium acetate in 200 mM NaOH to elute acidic sugars. A final 15-minute wash with 200 mM NaOH was performed to regenerate the column. Data were collected and analyzed using Chromeleon 6.80 software. Monosaccharide peaks were identified by comparing their elution

times to a standard mixture (L-Rha, D-Rib, L-Fuc, L-Ara, D-Xyl, D-Man, D-Gal, D-Glc, D-GalN, D-GalNAc, D-GlcNAc, D-GlcA, D-GalA). Peak identities were subsequently confirmed by co-elution (spiking) of samples with the corresponding authentic standards.

The global composition and sulfate content of the exopolysaccharide (EPS) fractions were determined using established colorimetric and turbidimetric assays. Total neutral sugars were quantified using the resorcinol-sulfuric acid method (Monsigny; Petit; Roche, 1988; Montreuil *et al.*, 1963), and total uronic (acidic) sugars were quantified using the metahydroxydiphenyl method (Blumenkrantz; Asboe-Hansen, 1973). Sulfate content was determined via the turbidimetric method of Dogson and Price (1962) against a K_2SO_4 standard curve, with results expressed as mg SO_4 equivalent per g EPS.

2.7 STATISTICAL ANALYSIS

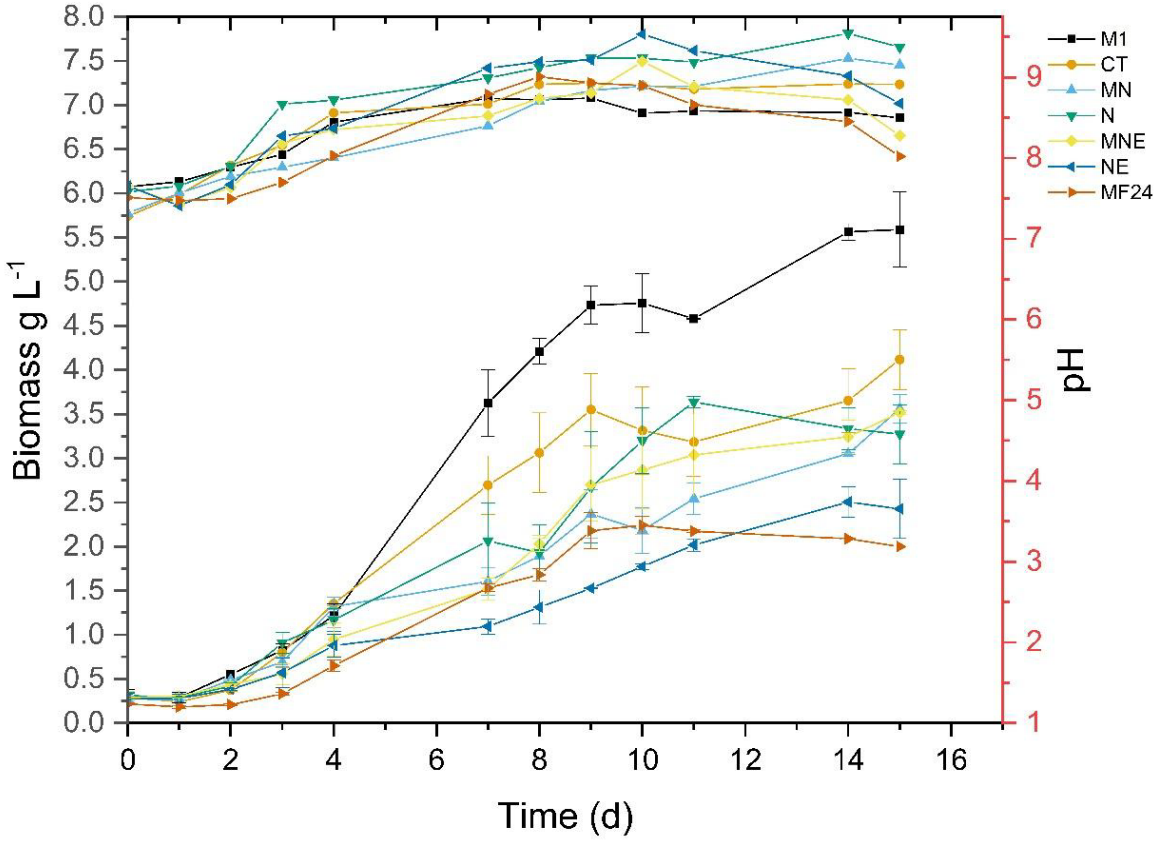
All experiments were conducted using at least three independent biological replicates ($n \geq 3$), and the results are presented as the mean ± standard deviation (SD). Statistical significance between experimental groups was assessed by a one-way analysis of variance (ANOVA) followed by Tukey's post hoc test a p-value < 0.05 was considered statistically significant.

3. RESULTS

3.1 *Porphyridium purpureum* GROWTH KINETICS

Throughout the cultivation, the pH varied from 7.3 to 9.5 (Figure 1), and the experiments with added nanofibers showed a higher pHmax (> 9.2) than the assays without nanofibers (pHmax < 8.9.) The experiments under SMF tend to show a lower pH than their non-MF counterparts (e.g., MN x N).

Figure 2- Growth curves of *Porphyridium purpureum* under magnetic field, nanofibers, and control culture.



All experiments follow a similar behavior for growth (Figure 2), with the start of the exponential phase on day 1 (Table 1). They differed in the duration of this phase, varying from 1 to 8 days, with the longest being the experiment M1. M1 was the assay with the highest ($p \leq 0.05$) maximal biomass (X_{max}) of 5.59 g L^{-1} an increase of 36% when compared to CT, while for the experiments MNE, NE, and M24 showed decreases of 15, 39, and 45%, respectively.

Table 1 - Growth parameters and produced RPS of Porphyridium purpureum under the influence of SMF and nanofibers. CT- Control; M1- Magnetic field 1 h day^{-1}; MN – added nanofiber magnetic field; N – Added nanofibers; MNE – Magnetic field and nanofiber produced with MEA; NE- Nanofiber addition produced with MEA; M24 Magnetic field 24 h day^{-1}. The results are expressed as mean (n = 3) ± standard deviation. Different letters on the same line show a significant difference between treatments p-values < 0.05 (Tukey's test).

	CT	M1	MN	N	MNE	NE	M24
X_{max} (g L^{-1})	4.12±0.34^{b}	5.59±0.42^{a}	3.56±0.16^{bc}	3.64±0.06^{bc}	3.52±0.02^{c}	2.5 ±0.17^{d}	2.27±0.1^{d}
μ_{max} d^{-1})	0.59±0.04	0.34±0.03^{c}	0.51±0.01^{ab}	0.5±0.03^{b}	0.39±0.05^{c}	0.38±0.08^{c}	0.4±0.01^{c}
P_{max} (gL^{-1} d^{-1})	0.36±0.04^{b}	0.48±0.04^{a}	0.26±0.02^{cd}	0.3±0.01^{bc}	0.27±0.05^{cd}	0.16±0.01^{de}	0.2±0.01^{e}
D_t (d)	1.19±0.09	2.04±0.19^{bc}	1.36±0.02^{a}	1.43±0.1^{a}	2.14±0.21^{b}	1.9±0.37^{b}	2.33±0.03^{c}
R^2	0.97	0.98	0.98	0.96	0.98	0.99	0.98
Δt (d)	1---4	1---8	1---4	1---4	1---4	1--4	1---7
RPS (g L^{-1})	0.36±0.05^{c}	0.66±0.11^{a}	0.60±0.16^{ab}	0.28±0.02^{c}	0.40±0.04^{bc}	0.36±0.02^{c}	0.41±0.02^{bc}

The maximum specific growth (μ_{max}) was the highest from CT, MN, and N (0.59, 0.51, and 0.50 g d^{-1}) due to the shorter exponential phase (1-4 days). Similarly, for the doubling time (Dt), the lowest value corresponds to the one with the highest μ_{max}. At the end, the released polysaccharide (RPS) concentration varied from 0.66 – 0.28 g L^{-1} for M1 and N assays, respectively.

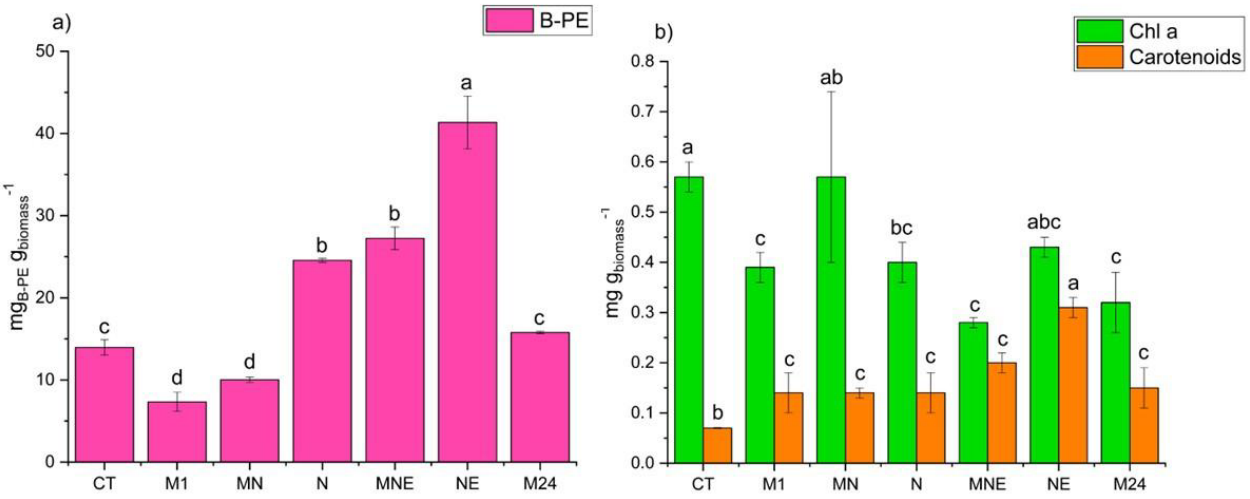
3.2 BIOMASS CHARACTERIZATION

Analysis of the P. *purpureum* biomass *indica*tes that carbohydrates constituted the primary macromolecular fraction across all experimental groups (Table 2). The M24 treatment yielded the maximal carbohydrate concentration at 52.4%, representing a 21% increase relative to the control (CT). This was followed by the MN treatment (49.3%), whereas the M1 group exhibited the lowest carbohydrate content at 40.1%. Protein concentrations were highest in the MNE and CT treatments, both stabilizing at approximately 37%. The M24 treatment showed the lowest protein levels at 28.5%. Regarding the lipid fraction, values fluctuated between ~19% (CT and M24) and ~26% (MN and M1).

Table 2 - Main compounds of *Porphyridium purpureum* biomass. CT- Control; M1- Magnetic field 1 h day^{-1}; MN – added nanofiber magnetic field; N – Added nanofibers; MNE – Magnetic field and nanofiber produced with MEA; NE- Nanofiber addition produced with MEA; M24 Magnetic field 24 h day^{-1}. The results are expressed as mean (n = 3) ± standard deviation. Different letters on the same line show a significant difference between treatments, p-values < 0.05 (Tukey's test).

	CT	M1	MN	N	MNE	NE	M24
Protein (%)	37.16±0.48^{a}	33.83±0.76^{b}	23.81±0.86^{e}	33.87±0.46^{b}	37.69±0.27^{a}	31.39±0.65^{c}	28.53±0.27^{d}
Carbohydrates (%)	43.39±0.48^{e}	40.06±1.25^{f}	49.3±0.85^{b}	47.46±0.75^{c}	41.09±0.32^{f}	45.59±0.73^{d}	52.39±0.48^{a}
Lipids (%)	19.44±0.81^{d} e	26.11±1.66^{a}	26.9±0.83^{a}	18.67±0.39^{e}	21.22±0.41^{cd}	23.01±0.74^{bc}	19.08±0.57^{e}

Figure 3 - Concentration of phycoerythrin (a), chlorophyll, and carotenoids (b) in produced P. purpureum biomass. CT- Control; M1- Magnetic field 1 h day^{-1}; MN – added nanofiber magnetic field; N – Added nanofibers; MNE – Magnetic field and nanofiber produced with MEA; NE- Nanofiber addition produced with MEA; M24 Magnetic field 24 h day^{-1}. The results are expressed as mean (n = 3) ± standard deviation. Different letters on different graphs represent a significant difference between treatments, p-values < 0.05 (Tukey's test).



The main pigments present in *P. purpureum* are phycobilin, chlorophylls, and carotenoids. Phycoerythrin is divided into β-phycoerythrin (β-PE) and α-phycoerythrin, where β-PE is considered the core pigment (Ma *et al.*, 2020; Marcati *et al.*, 2014). The higher ($p \leq 0.05$) B-PE content was in treatments with only nanofibers, in particular, the NE assay (41.3 ± 3.22 mg gdw^{-1}) (Figure 3a.), which presented a 196% increase when compared to CT (13.9 ± 0.95 mg gdw^{-1}). While treatments with only SMF had no difference (M24) or a decrease ($p \leq 0.05$) of 47% when compared to CT. Carotenoid content (Figure 3b) in the biomass was affected in all experiments, showing an increase (~100%) when compared to CT, but NE treatment had the highest increase (342%) when compared to CT.

Considering biomass production across the treatments and assuming that B-PE content at harvest is representative of content during the period of maximal biomass productivity, volumetric B-PE productivity was still higher in the NE treatment, reaching 6.61 mg β-PE L^{-1} d^{-1}, compared with 5.02 mg β-PE L^{-1} d^{-1} in CT. The N and MNE treatments showed the highest β-PE productivity among all conditions, both reaching 7.35 mg β-PE L^{-1} d^{-1}. These results indicate that, despite lower

biomass productivity, treatments enhancing β-PE content still translate into a net gain in volumetric pigment production relative to the control.

3.3 EPS CHARACTERIZATION

EPS purity can be *indica*ted by the results of the total sugars assay (Table 3), which shows a higher purity of the RPS (60-92%) than BPS (40-52%), due to the hot extraction of the BPS from the biomass, which increases the protein content of the purified EPS. Assays with nanofibers, in general, have shown a higher ($p \leq 0.05$) RPS purity (~20%) when compared to M1 and CT of the produced EPS (both RPS and BPS), varying between 62-77%.

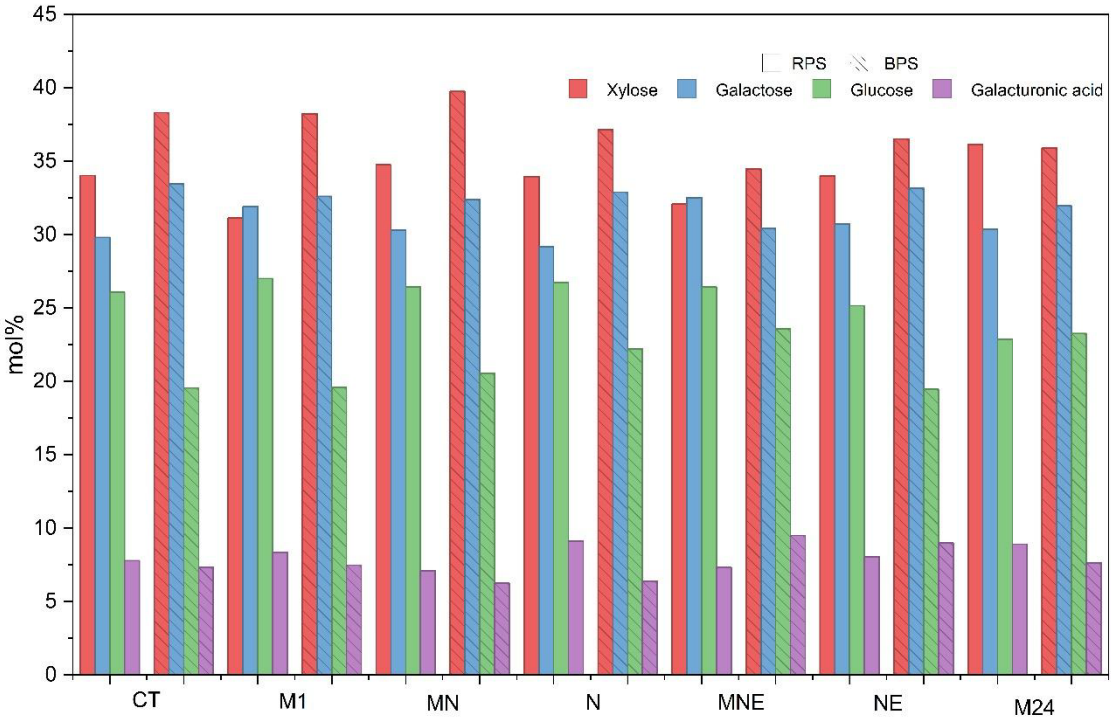
MNE treatment RPS showed the highest ($p \leq 0.05$) acid sugar ratio (28%). Treatment M24 had the highest ($p \leq 0.05$) sulphated content (16.9%) and the second-highest uronic acid concentration (21.1%). BPS biochemical profile differed from RPS mostly by the higher ($p \leq 0.05$) sulphate ratio (15-21%) and lower acid sugars (10-18%). BPS of all assays showed a higher acid sugar content than CT, but not for sulphates. Sulphate ratio was equal for CT, M1, MN, MNE, where M1 assay showed high sulphate (19%) and uronic acid (18%) ratios simultaneously.

Table 3 - Biochemical composition of released/bound polysaccharide. CT- Control; M1- Magnetic field 1 h day^{-1}; MN – added nanofiber magnetic field; N – Added nanofibers; MNE – Magnetic field and nanofiber produced with MEA; NE- Nanofiber produced with MEA; M24 Magnetic field 24 h day^{-1}. The results are expressed as mean (n = 3) ± standard deviation. Different letters on the same column and EPS section show a significant difference between p-values < 0.05 (Tukey's test).

	% Total Sugars	% Protein	% Sulphated groups (eq. SO_4)	% Neutral sugars	% Uronic Acid
	Samples (%Mass)		EPS (%Mass (g 100gEPS^{-1})		
Released polysaccharides (RPS)					
CT	67.5±2.71^{c}	7.0±0.83^{ab}	13.0±0.96^{b}	75.6±0.69^{ab}	11.4±0.9^{c}
M1	60.6±2.16^{c}	6.6±0.85^{c}	13.4±0.01^{b}	70.8±0.97^{ab}	15.8±0.86^{c}
MN	78.8±2.29^{b}	6.3±1.76^{ab}	11.9±0.38^{bc}	77.2±2.81^{a}	10.9±0.58^{d}
N	92.2±2.91^{a}	6.8±1.22^{e}	13.2±0.65^{b}	77.3±4.35^{a}	9.5±0.99^{d}
MNE	75.5±3.47^{b}	5.8±0.98^{a}	10.9±0.78^{c}	61.0±3.01^{c}	28.0±2.39^{a}
NE	89.6±1.66^{a}	7.4±0.49^{d}	9.3±0.6^{d}	69.7±3.82^{b}	21.1±3.72^{b}
M24	87.6±4.19^{a}	7.9±0.21^{bc}	16.9±0.38^{a}	62.1±1.53^{c}	21.1±1.37^{b}
Bound polysaccharides (BPS)					
CT	47.7±1.94^{ab}	21.8±0.83^{ab}	20.5±1.33^{a}	69.4±1.09^{a}	10.0±0.86^{c}
M1	40.1±2.51^{c}	19.1±0.85^{c}	19.2±0.43^{ab}	62.3±0.25^{a}	18.5±1.09^{a}
MN	51.5±4.85^{a}	21.8±1.76^{ab}	17.0±3.39^{abc}	69.6±5.18^{a}	13.4±0.27^{b}
N	52.2±3.07^{a}	11.3±1.22^{e}	15.0±0.26^{c}	70.9±2.43^{a}	14.1±0.4^{b}
MNE	48.9±1.32^{a}	23.9±0.98^{a}	19.7±0.06^{ab}	68.0±1.88^{a}	12.3±0.98^{b}
NE	41.9±0.74^{bc}	15.2±0.49^{d}	16.2±1.25^{bc}	70.4±6.57^{a}	13.5±0.81^{b}
M24	40.4±1.48^{c}	21.1±0.21^{bc}	16.8±0.01^{bc}	71.0±4.94^{a}	12.3±0.56^{b}

The monosaccharide profile of the extracted exopolysaccharides (EPS) confirms a heteropolymeric structure dominated by xylose, galactose, glucose, and galacturonic acid (Figure 3). These findings align with established benchmarks for P. *purpureum* (Esqueda; Gardarin; Laroche, 2022; Guerreiro *et al.*, 2026). Neutral sugars accounted for over 90% of the total mass, following abundance order: xylose > galactose > glucose. However, the apparent backbone stability across treatments covers some divergences between the released (RPS) and bound (BPS) fractions. Notably, RPS exhibited an 18% higher glucose proportion compared to BPS, whereas the latter showed a higher xylose (10%) and galactose (6%). These differences suggest that glucose is preferentially associated with released polymers, whereas xylose characterizes cell wall-bound polymers.

Figure 4 - Monosaccharide profile composition of RPS and BPS in % molar ratios. CT- Control; M1- Magnetic field 1 h day^{-1}; MN – added nanofiber magnetic field; N – Added nanofibers; MNE – Magnetic field and nanofiber produced with MEA; NE- Nanofiber produced with MEA; M24 Magnetic field 24 h day^{-1}.



4. DISCUSSION

4.1 *Porphyridium purpureum* GROWTH KINETICS AND EPS PRODUCTION

The effect of the treatments on growth kinetics can be associated with the SMF, nanofibers, or a combination of both treatments. MF can act by enhancing CO_2 solubility by physically stabilizing the dielectric gas-liquid layer through the Hall effect (Pazur; Winklhofer, 2008) acidifying the media. This behavior is desirable from a biotechnological point of view since it would be necessary to use less CO_2 for pH control, increasing the efficiency of CO_2 assimilation. Meanwhile, nanofiber experiments show an increase in pH during cultivation, but the MNE assays show a sharp drop in pH during the last two days, probably due to metabolic decline saturating CO_2 in the media. Nanofibers in microalgae cultivations are shown to increase the pH due to the adsorption of CO_2, decreasing the formation of carbonic acid (Comitre et al., 2021).

The increase in pH during microalgae cultivation is expected, since the consumption of CO_2 during photosynthesis tends to influence the carbonate balance by assimilating the carbonic acid via carbonic anhydrase, as well as the production of hydroxide during the NH3+ metabolism, which increases the pH (Blankenship, 2021). Followed by a drop in pH due to CO_2 accumulation and the end of nitrates in the media after the exponential phase, reducing the consumption of carbonic acid and the production of hydroxide. The rise and fall of pH during cultivation behavior were seen in all experiments. Once they achieved the higher biomass content, the pH followed the tendency to be the highest.

Growth in microalgae cultivation is a multifactorial process depending on cultivation parameters such as temperature, bioreactor, light, salinity, and other stresses. SMF its not linear and can act as a stimulatory, inhibitory or non-existent effect depends on the intensity, time, source, and microorganism on which is being applied (Santos et al., 2022; Serrano et al., 2021). It influences physical and biochemical mechanisms, such as enzymatic activation and photosynthesis (Deamici et al., 2019). This broad aspect of SMF makes it difficult to determine a specific factor for the response of biological systems.

SMF can increase the oxygen species beyond the cell capacity of antioxidation, disruption of paramagnetic enzymatic centers, and increase cell wall permeability, deeming its application inhibitory (Serrano et al., 2021) as observed in M24. At the same time, if used properly (time and intensity) it can have the opposite effect (M1), increasing biomass production, antioxidant

response, and photosynthesis via enzymatic response, membrane permeability, and/or ion transfer (Deamici et al., 2019; Font et al., 2023; Serrano et al., 2021). It is worth noting that M1 combined the lowest specific growth rate (μ_{max}) with the highest volumetric productivity (P_{max}) among all treatments (Table 1). This apparent contradiction is explained by the distinct nature of these two parameters: μmax reflects the relative rate of biomass increase during the exponential phase, whereas P_{max} reflects the absolute biomass gain over time, which depends on both growth rate and the duration of active growth. M1 sustained an exponential phase markedly longer than the other treatments (8 days, versus 1–4 days), allowing it to reach the highest Xmax (5.59 g L^{-1}) despite a comparatively lower specific rate. This indicates that, under M1 conditions, SMF prolonged the period of active growth rather than accelerating it, resulting in the greatest overall biomass gain.

At the molecular level, the effects of SMF on microalgal and cyanobacterial cells can be broadly attributed to three non-mutually exclusive mechanisms. First, the radical pair mechanism proposes that magnetic fields modulate the singlet-triplet interconversion of light-generated radical pairs, such as those formed in flavin- and cryptochrome-based photoreceptors, thereby altering local reactive oxygen species levels and downstream redox-sensitive signaling pathways (Evans *et al.*, 2013; Müller; Ahmad, 2011). Second, SMF may influence redox enzymes and electron-transfer reactions, including antioxidant defenses such as superoxide dismutase, thereby affecting cellular oxidative balance (Yoon *et al.*, 2026). Third, magnetic-field-induced effects on ion transport and membrane-associated signaling may contribute to changes in Ca^{2+} homeostasis, nutrient uptake, and gene expression, although this mechanism remains less directly validated in microalgae (Gartzke; Lange, 2002; Santos *et al.*, 2022). In a more mechanistic bacterial model, proteomic analysis of *Listeria monocytogenes* exposed to pulsed magnetic field showed coordinated disruption of nutrient transport and key metabolic pathways, including carbohydrate, amino acid, and nicotinate/nicotinamide metabolism, supporting the idea that magnetic fields can perturb membrane-linked transport and intracellular metabolism (Chen, Di *et al.*, 2025). Together, these mechanisms provide a plausible molecular basis for the responses observed in the present study, but species- and dose-specific validation is still needed.

X_{max} for the nanofiber-only treatments (MN and N) did not differ significantly from either CT or the MNE treatment, occupying an intermediate position between them. CT, in turn, was significantly higher than MNE and NE, which showed reductions of 15% and 39%, respectively, relative to CT (Table 1). This gradient, from CT, through the intermediate MN/N, to the reduced

MNE/NE, suggests that the bio-mass-limiting effect intensifies with MEA functionalization rather than being caused by the presence of nanofibers alone, possibly because MEA promotes a more pronounced cell–surface interaction. This is consistent with the tendency of *P. purpureum* to aggregate on surfaces, which could reduce cell/media interaction and limit nutrient uptake.

Studies in *Porphyridium* under SMF or nanofibers are not available in the literature, the main strategies to increase production of biomass and biocompounds are manipulation of parameters such as nutrients, light, pH, hormones, etc. (Nguyen et al., 2024). Yi et al. (Yi et al., 2024) increased biomass production to ~5.97 g L-1, an increase of 132% compared to their control, using experimental optimization for cultivation with calcium gluconate, magnesium gluconate, and peptides ratios. The authors associate the increase in biomass production with the high-quality plant peptides and the extra organic carbon supplied.

In contrast, adding nanofibers into microalgae cultivation has its downside; the adsorption of biomass during growth (APPENDIX B) makes the concentration calculation inaccurate and hard to compare to the experiments without nanofibers (Vaz; Mastrantonio; et al., 2019). Carvalho et al. (Carvalho et al., 2025) reported a 9-15% of *Limnospira* biomass attached to nanofibers. In our study, the biomass attached to the nanofibers varied from 15 – 19% of the X_{max} , this increase was expected for *P. purpureum* since this microalga tends to produce EPS and attach to surfaces. This biomass was weighed at the end of the experiment to be considered in the final biomass and kinetics calculation.

The EPS production is linked to physical and chemical stress, such as osmotic pressure and nitrogen deprivation (Esqueda; Gardarin; Laroche, 2022). For the M1 and MN assays, SMF seems to act as a physical stressor, inducing the formation of RPS. It is relevant to notice that the M24 treatment showed an RPS concentration statistically similar to CT, despite having 45% less biomass, which may indicate an increase in the RPS/biomass ratio. SMF seems to increase carbohydrate production towards RPS; this effect could be associated with the influence of the SMF in microalgae cultivation associated with carbon assimilation metabolic pathways, enzymatic activity, an increase in cell wall permeability, and improved nutrient intake (Deamici; Dziergowska; *et al.*, 2022). During the SMF experiments, a more homogeneous cultivation was visually observed (APPENDIX B), which could help explain the higher RPS concentration in the medium: with less cell clustering, a smaller fraction of EPS remains attached to the cell wall,

favoring its release into the medium as RPS. Further studies are needed to evaluate the homogenizing effect of SMF on *Porphyridium* cultivation

4.2 BIOMASS CHARACTERIZATION

Carbohydrate accumulation in the biomass did not respond uniformly across SMF treatments: it increased under continuous SMF (M24) and the combined MN treatment, but decreased under intermittent SMF alone (M1). Nanofiber-only treatments also increased carbohydrate content despite the absence of SMF. This pattern suggests that carbohydrate accumulation in the biomass is not an exclusive SMF effect, but rather a broader stress-associated metabolic response, potentially involving carbon assimilation pathways, enzymatic activity, and cell wall permeability, triggered to different extents by both SMF and nanofiber exposure. Carbohydrates in *Porphyridium* are found mainly in three groups: sulfated cell-wall polysaccharides, floridean starch, and low–molecular-weight carbohydrates (primarily floridoside) (Arad; Levy-Ontman, 2013; Yu, Y. *et al.*, 2021). Synthesized through photosynthesis and the Calvin-Benson-Bassham cycle, their production is influenced by countless reasons, such as nutrients, temperature, and stress (Blankenship, 2021). Complex biological systems are susceptible to magnetic forces that act in paramagnetic molecules, electric charges, and radical pairs (Font *et al.*, 2023).The increase in biomass carbohydrates has been reported for other microalgae by Deamici *et al.* (2019) for *Chlorella fusca* with an increase of 31% when compared to the control in cultivation under 30 mT SMF for 1 h d^{-1}. Similar behavior was found by Menestrino *et al.* (2020) for *Chlorella minutissima* cultivation under 30 mT 24 h d^{-1} continuous SMF, with a twofold increase in carbohydrate content when compared to its control.

Comparing intracellular and extracellular carbohydrate pools across treatments suggests that SMF duration influences how carbon is partitioned between the two. M1 (intermittent SMF) combined the lowest biomass carbohydrate content (40.1%) with the highest RPS concentration (0.66 g L^{-1}), whereas M24 (continuous SMF) showed the inverse profile, the highest biomass carbohydrate content (52.4%) alongside an RPS concentration close to CT. This is consistent with intermittent SMF favoring carbon release into the medium, while continuous exposure favors intracellular carbohydrate accumulation instead. This inverse relationship, however, was specific to the SMF-only treatments and did not extend to MN, which combined a high biomass

carbohydrate content with a high RPS concentration, suggesting that the addition of nanofibers alters this partitioning independently of the SMF duration effect described above.

As with carbohydrates, lipid metabolism is also part of carbon fixation and is related to nitrogen limitation or stress, and is used as energy storage and structural molecules. Lipids are formed through the enzymatic transformation of triose phosphate from the CBB cycle, which is synthesized into fatty acids and then assembled into triacylglycerols by the Kennedy pathway. The lipid content in *Porphyridium sp.* is 9 - 14% dw^{-1} and characterized by a high ratio of PUFAs up to 33% when under stress, which is seen as a high-value product (Nguyen *et al.*, 2024). In the present study, the biomass lipid ratio got an increase of 38% for M1 and MN assays when compared to the Control.

The lowest protein ratio was observed in MN treatment (23.81%), suggesting a faster diversion of metabolic routes to lipid and carbohydrate production, a common behavior under nitrogen depletion, when compared to CT and MNE (37%). Protein content is directly related to nitrogen intake, nitrates or ammonia, and carbon availability, due to the carbon skeleton in the center of these molecules. Proteins in *Porphyridium* are found mostly as enzymes and phycobiliproteins, the latter of which are building blocks for the photosynthetic system. They are complex protein structures that play an important part in light harvesting, being represented by phycoerythrin, phycocyanin, and allophycocyanin (Blankenship, 2021).

The production of B-PE is related to many factors, such as temperature, light color, and intensity (Guihéneuf; Stengel, 2015; Ji *et al.*, 2025), phosphorus, nitrogen, and mineral content (Gargouch *et al.*, 2018; Yi *et al.*, 2024). Since this pigment is a phycobiliprotein, it is directly linked to the synthesis of proteins; the nitrogen metabolic pathway seems to be prioritized when nanofibers are added to *P. purpureum* cultivation. The use of nanofiber to increase protein content in *Chlorella fusca* biomass is reported by Comitre et al. (Comitre *et al.*, 2021), and for *Spirulina sp.* LEB 18 by Cardias et al. (2024). These authors link protein increase to the influence of nanofibers on the C/N ratio, which can act directly in their synthesis; similar behavior was seen in our study for *P. purpureum*.

The mechanistic basis for the nanofiber effects differs from that of SMF, acting primarily through enhanced carbon availability rather than direct molecular interaction with cellular components. PAN nanofibers increase local CO_2 retention at the cell-medium interface through physical adsorption, while MEA functionalization adds a chemisorption route via carbamate

formation, together increasing the pool of dissolved inorganic carbon accessible to the cells (Cardias; Morais; Costa, 2024). The extra carbon appears to favor glycolytic flux and amino acid precursor supply (Ala, Leu, and Val) for phycoerythrin biosynthesis in *P. purpureum* cultivation. Even though the total protein of the biomass does not reflect the results of B-PE, phycobiliproteins are just a small part of the total protein content (Gargouch *et al.*, 2018).

At the same time, the physical presence of the nanofiber matrix promotes cell attachment and aggregation at the fiber surface, which may reduce the effective cell-medium contact area available for nutrient exchange, offering a plausible explanation for the concurrent reduction in biomass accumulation observed in the MEA nanofiber treatments. This trade-off between enhanced carbon capture for pigment biosynthesis and reduced nutrient exchange for biomass growth illustrates how the same physical structure can exert opposing effects on distinct metabolic outputs.

The B-PE increase in biomass is a positive effect since this compound has high value due to its color, fluorescence, antioxidant, and anti-inflammatory properties, with potential use in food, biomedical research, nutraceuticals, and pharmaceuticals (Nguyen *et al.*, 2024). Although this increase in B-PE content coincided with lower biomass accumulation, a profile generally associated with low-growth physiological states, volumetric B-PE productivity remained higher than the control in all pigment-enhancing treatments (Section 3.1), indicating that the reduction in biomass did not translate into a net loss of pigment output. Strategies to increase phycoerythrin in *Porphyridium* biomass include high nitrate concentration (Zhang, A. H. *et al.*, 2022), light control (wavelength/intensity), minerals, phosphate deficiency (Gargouch *et al.*, 2018; Yi *et al.*, 2024), and peptides (Yi *et al.*, 2024). Yi *et al.* (2024).reported ~44 mg g_{dw}^{-1} of B-PE in *P. purpureum* biomass on the 16th day of cultivation with calcium gluconate (3 g L^{-1}), but with a decrease in biomass production (~2.7 g L^{-1}) when compared to the control. Similarly, Gargouch *et al.* (2018) reported low biomass productivity but a higher concentration of B-PE (~41 mg g_{dw}^{-1}) in *P. purpureum* cultivated with higher nitrates, minerals, lower light intensities, and phosphorus deficiency. The same pattern was observed in the NE treatment, where higher B-PE concentration coincided with reduced biomass production relative to CT.

The increase in carotenoid content in all treatments suggests a conserved metabolic response to the induction of oxidative stress, notably in NE treatment. Carotenoids present in *P. purpureum* are primarily zeaxanthin and β-carotene (Schubert; García-Mendoza; Pacheco-Ruiz, 2006). These pigments play a crucial role in protection against solar radiation and oxidative stress.

They are natural antioxidants and colorants, which make them a valuable compound for the cosmetic, food, and pharmaceutical industries (Nguyen *et al.*, 2024).

In the present study, cultures were subjected to high light intensity (200 μmol photons·m^{-2}·s^{-1}) and moderate temperatures (21 ºC). Under these conditions, Guihéneuf and Stengel (Guihéneuf; Stengel, 2015) reported a decrease in pigments, in agreement with our control. The authors linked this behavior to the thylakoid membrane area shrinkage, minimizing pigment content in the biomass. They also reported that the opposite occurs in low-temperature (10 ºC) and low-intensity-light (30 μmol photons·m^{-2}·s^{-1}) systems shift the metabolic pathway to increase the production of pigments over primary biomass accumulation. These results suggest that the stress caused by nanofibers with/without MEA may have a similar effect to low light and low-temperature strategies, increasing photosynthetic unit size, thus boosting pigment concentration in the biomass of *P. purpureum*.

Taken together, the results indicate that SMF and nanofiber treatments do not act as uniform "enhancers" of *P. purpureum* metabolism, but instead redirect carbon and nitrogen flux toward specific outputs, often at the expense of others. Three trade-offs illustrate this pattern. First, M1 achieved the highest biomass production (X_{max}) but did not improve B-PE content relative to CT, indicating that the conditions favoring rapid biomass accumulation did not simultaneously favor phycobiliprotein synthesis. Second, NE showed the opposite profile: the highest B-PE content of all treatments, but with reduced biomass accumulation, consistent with the general association between phycoerythrin enrichment and lower growth performance already reported for *P. purpureum* under nutrient-limiting conditions (Guihéneuf; Stengel, 2015). It is worth noting, however, that this reduction in biomass did not offset the pigment gain in volumetric terms, as B-PE productivity in NE still exceeded that of CT once corrected for biomass output (Section 3.1). Third, M24 combined the highest carbohydrate content with the lowest protein content, pointing to a metabolic shift away from nitrogen-dependent biosynthesis and toward carbon storage under prolonged SMF exposure. A similar partitioning logic was observed for the extracellular versus intracellular carbohydrate pools, where the highest RPS release (M1) coincided with the lowest intracellular carbohydrate content, and the reverse was true for M24, suggesting that the same carbon pool can be preferentially allocated to either storage or release depending on SMF duration.

These trade-offs suggest that SMF and nanofiber exposure act as selective metabolic switches rather than general growth promoters, with the specific outcome (biomass, pigment,

carbohydrate, or EPS accumulation) depending on the type, intensity, and duration of the stimulus applied. From an applied perspective, this indicates that no single treatment condition tested here maximizes all valuable outputs simultaneously; rather, treatment selection should be guided by the target product, intermittent SMF (M1) for biomass-driven applications, MEA-functionalized nanofibers (NE) for B-PE-enriched biomass, and continuous SMF (M24) for carbohydrate-rich biomass or RPS-lean conditions. This treatment-specific tunability, rather than a single optimal condition, represents the central practical outcome of the present study.

4.3 EPS CHARACTERIZATION

The EPS produced had neutral sugars as a major group, already expected since *P. purpureum* EPS has as major monosaccharides xylose, galactose, and glucose (Esqueda; Gardarin; Laroche, 2022). Acid sugar (uronic acids) in *P. purpureum* EPS are D-glucuronic and galacturonic acid. The primary metabolic pathway for uronic acid and its derivatives involves the enzymatic oxidation of the C-6 hydroxyl group, resulting in a carboxylic acid group (-COOH) linked to the former C-6 position. This is usually triggered by stress, such as osmotic, nutritional uptake, carbon availability, and heavy metals, as a response to fix redox equilibrium, the balance between neutral and acidic sugars, increase water retention (viscosity), and gene regulation (Guerreiro *et al.*, 2026; Laroche, 2022). This response was observed in M24 and the treatments with nanofiber with MEA, peaking in the combined treatment MNE, suggesting resonance between the combined treatment to increase production of uronic acid.

Uronic acid and sulphated groups in EPS are indicative of reactivity: mechanical, chemical, and biological activity (Laroche, 2022). This distribution of uronic acids and sulphate groups increases the overall anionic character of EPS, which controls its rheological behavior, chemical reactivity, and diverse bioactivities such as metal binding, antioxidant, and antiviral properties (Bello-Morales *et al.*, 2022; Laroche, 2022; Wang, W. N. *et al.*, 2021). Uronic acid in *Porphyridium* EPS is usually found as D-glucuronic or galacturonic acid and its acetylated/methylated form (Gargouch *et al.*, 2021). Sulphation in these polymers arises from SO_4^{-2} groups covalently attached to sugar residues (Usov; Zelinsky, 2013).

SMF 24h exposure seems to have promoted the sulphation metabolism of RPS as a stress response. Via the secondary enzymatic pathway for sulphate assimilation: increasing the activity

of ATP sulfurylase and APS kinase, producing the intermediary for the carbohydrate sulfotransferase to attach sulphate groups in the hydroxyl residues present in the EPS backbone, which for *Porphyridium* are usually the glucose O-6 and galactose O-6/O-3 (Prioretti *et al.*, 2014; Usov; Zelinsky, 2013; Wójcik-Augustyn; Johansson; Borowski, 2019). Whereas for BPS, the SMF influence seems to be higher in the acid-sugar portion; hence, most SMF assays increase the synthesis of uronic acids. This indicates that SMF stress stimulates this compound metabolic pathway.

The ratio and concentration of sulphated EPS are highly susceptible to environmental changes, such as nutrition limitation (Laroche, 2022), oxidative stress (Bont *et al.*, 2022), and osmotic stress (Decamp *et al.*, 2023). As SMF can act by magnet induction through the Hall effect, interfering with ions and charges in molecules, it can act directly with the electronegativity of these groups (Font *et al.*, 2023).

Porphyridium EPS has been shown to have bioactivity, such as antiviral activity for enveloped viruses (HSV-1, HSV-2, and VZV) by emulating cell receptors and blocking viral entry (Bello-Morales *et al.*, 2022), antioxidant due to scavenging activity (Gargouch *et al.*, 2021) and immunomodulatory via cytokine release stimuli (Casas-Arrojo *et al.*, 2021; Sun; Wang; Zhou, 2012). The bioactivity is especially correlated with sulphate content and molecular weight. EPS with more than 10% of sulphate groups already exhibits these properties, which can be enhanced in lower molecular weight polymers due to better bioavailability (Han *et al.*, 2024; Sun; Wang; Zhou, 2012). Beyond its bioactivity, sulphates and acid groups grant singular rheological characteristics to the EPS. Arad and Levy-Ontman, (2013) report the rheological behavior of *Porphyridium* EPS, particularly its potential as a thickening agent, biolubricant, and weak gel formation. They associate these potentials in *Porphyridium* EPS with its high intrinsic viscosity, low friction coefficients, wear protection, and structural stability across a broad range of shear velocities. These unique physicochemical attributes demonstrate the potential of the *Porphyridium* EPS produced in our study to be used as a candidate for specialized applications in the pharmaceutical, food, mechanical, and biochemical industries.

The higher xylose and galactose ratios observed in BPS relative to RPS (Section 3.3) could shift its functional properties, since xylose tends to introduce branching and additional substituents (sulphates, methyl, acetyl groups) to the polymer backbone, affecting rheological behavior such as gel formation through increased electronegative character (Usov; Zelinsky, 2013). Despite these

compositional differences between fractions, the treatments did not significantly alter the monosaccharide backbone composition, indicating that RPS and BPS differences are intrinsic to the polymer's biosynthetic origin rather than treatment-dependent. Discrepancies between colorimetric and chromatographic quantification of uronic acids may result from monosaccharide modifications (methoxylation, acetylation, sulfation) not detected by chromatographic standards, as previously reported for P. purpureum EPS (Guerreiro *et al.*, 2026; Medina-Cabrera *et al.*, 2020).

5. CONCLUSION

This study demonstrates that static magnetic fields (SMF) and polymeric nanofibers modulate *Porphyridium purpureum* physiology in distinct and complementary ways. Intermittent SMF application (M1) significantly enhanced growth performance, yielding the highest maximal biomass (5.59 g L^{-1}), a 36% increase relative to the control, whereas prolonged exposure or combination with MEA nanofibers reduced biomass accumulation. SMF exposure also influenced carbon allocation in a treatment-dependent manner: intermittent SMF (M1 and MN) favored the release of extracellular polysaccharides (RPS) and increased the lipid fraction, whereas continuous exposure (M24) instead favored intracellular carbohydrate storage, indicating that carbon partitioning under SMF depends on the duration of exposure rather than on SMF application alone. In contrast, nanofiber-based systems markedly enhanced pigment biosynthesis, particularly β-phycoerythrin, with the MEA-functionalized nanofiber treatment alone (NE) reaching a 196% increase in B-PE content compared to the control. Although this was accompanied by lower biomass accumulation, volumetric B-PE productivity, when corrected for biomass output, still exceeded the control in all pigment-enhancing treatments, indicating a genuine net gain in pigment production rather than a simple biomass-productivity trade-off. Regarding extracellular polysaccharides, nanofiber-containing treatments improved RPS purity and promoted higher uronic acid content, especially in the combined static magnetic field and MEA-nanofiber condition (MNE), while extended SMF exposure (M24) favored RPS sulfation, suggesting stress-mediated regulation of polysaccharide functionalization. Bound polysaccharides (BPS) generally showed a higher sulphation ratio than released polysaccharides (RPS). The monosaccharide profile indicates that the treatments did not alter the major EPS composition, suggesting that RPS and BPS differences are intrinsic to the polymer's biosynthetic origin rather than treatment-dependent.

Collectively, these results indicate that SMF and nanofiber treatments act as selective, tunable stimuli rather than uniform growth enhancers, with SMF duration governing the balance between biomass accumulation and carbon release or storage, and nanofiber functionalization governing the balance between biomass growth and pigment accumulation, highlighting their combined potential to tailor biomass composition and high-value metabolite production in *P. purpureum* cultivation.

Author Contributions: Matheus Pereira de Carvalho: investigation, writing - original draft, formal analysis, conceptualization **Michele Greque de Morais**: conceptualization, methodology **Lucielen Oliveira dos Santos**: conceptualization, methodology **Jorge Alberto Vieira Costa**: funding acquisition, project administration, supervision, resources, writing - review & editing **Céline Laroche**: funding acquisition, project administration, supervision, resources, writing - review & editing.

Funding: This research received no external funding.

Institutional Review Board Statement: Not applicable.

Informed Consent Statement: Not applicable.

Data Availability Statement: Data will be made available on request.

Acknowledgments: This study was financed in part by the Coordenação de Aperfeiçoamento de Pessoal de Nível Superior—Brasil (CAPES)—Finance Code 001. This research was funded by the Program CAPES-COFECUB (Sv 945/19).

Conflicts of Interest: The authors declare that they have no known competing financial interests or personal relationships that could have appeared to influence the work reported in this paper.

REFERENCES

ANG, W. S.; KEE, P. E.; LAN, J. C.-W.; CHEN, W.-H.; CHANG, J.-S.; KHOO, K. S. Unveiling the rise of microalgae-based foods in the global market: Perspective views and way forward. **Food Bioscience**, vol. 66, p. 105390, Apr. 2025. DOI: 10.1016/j.fbio.2024.105390. Available at: https://linkinghub.elsevier.com/retrieve/pii/S2212429224018212.

ARAD, S. (Malis); LEVY-ONTMAN, O. Sulfated Polysaccharides in the Cell Wall of Red Microalgae. **Handbook of Biopolymer-Based Materials**. Wiley, 24 Apr. 2013. pp. 351–370. DOI: 10.1002/9783527652457.ch12. Available at: https://onlinelibrary.wiley.com/doi/10.1002/9783527652457.ch12.

BELLO-MORALES, R.; ANDREU, S.; RUIZ-CARPIO, V.; RIPA, I.; LÓPEZ-GUERRERO, J. A. Extracellular Polymeric Substances: Still Promising Antivirals. **Viruses**, vol. 14, no. 6, 2022. https://doi.org/10.3390/v14061337.

BERMEJO ROMÁN, R.; ALVÁREZ-PEZ, J. M.; ACIÉN FERNÁNDEZ, F. G.; MOLINA GRIMA, E. Recovery of pure B-phycoerythrin from the microalga Porphyridium cruentum. **Journal of Biotechnology**, vol. 93, no. 1, pp. 73–85, Jan. 2002. DOI: 10.1016/S0168-1656(01)00385-6. Available at: https://linkinghub.elsevier.com/retrieve/pii/S0168165601003856.

BLANKENSHIP, R. E. **Molecular Mechanisms of Photosynthesis**. III. Tempe: Wiley & Sons, 2021. 1–352 pp. Available at: https://www.wiley.com/en-us/Molecular+Mechanisms+of+Photosynthesis%2C+3rd+Edition-p-9781119800019.

BLUMENKRANTZ, N.; ASBOE-HANSEN, G. New method for quantitative determination of uronic acids. **Analytical Biochemistry**, vol. 54, no. 2, pp. 484–489, Aug. 1973. https://doi.org/10.1016/0003-2697(73)90377-1.

BONT, L. de; DONNAY, N.; COUTURIER, J.; ROUHIER, N. Redox regulation of enzymes involved in sulfate assimilation and in the synthesis of sulfur-containing amino acids and glutathione in plants. **Frontiers in Plant Science**, vol. 13, no. August, pp. 1–12, 16 Aug. 2022. DOI: 10.3389/fpls.2022.958490. Available at: https://www.frontiersin.org/articles/10.3389/fpls.2022.958490/full.

CARDIAS, B. B.; MORAIS, M. G. de; COSTA, J. A. V. Increased biomass and biomolecule productivity of *Spirulina sp*. LEB 18 cultivated with CO_2 adsorbent nanofibers. **Clean Technologies and Environmental Policy**, no. 0123456789, 15 Jun. 2024. DOI: 10.1007/s10098-024-02907-x. Available at: https://doi.org/10.1007/s10098-024-02907-x.

CARVALHO, M. P. de; MORAIS, M. G. de; SANTOS, L. O. dos; LAROCHE, C.; COSTA, J. A. V. Production of biomass and biomolecules in *Limnospira indica* PCC 8005 cultivation under magnetic fields and polymeric nanofibers. **Journal of Biotechnology**, vol. 405, no. October 2024, pp. 48–56, Sep. 2025. DOI: 10.1016/j.jbiotec.2025.05.004. Available at: https://linkinghub.elsevier.com/retrieve/pii/S0168165625001142.

CASAS-ARROJO, V.; DECARA, J.; ARROJO-AGUDO, M. de los Á.; PÉREZ-MANRÍQUEZ, C.; ABDALA-DÍAZ, R. T. Immunomodulatory, antioxidant activity and cytotoxic effect of sulfated polysaccharides from porphyridium cruentum. (s.f.gray) nägeli. **Biomolecules**, vol. 11, no. 4, 2021. https://doi.org/10.3390/biom11040488.

CHEN, D.; QIAN, J.; HUO, S.; WANG, F.; MA, H.; LIU, S. Proteomic Analysis of Listeria monocytogenes Subjected to Pulsed Magnetic Field. **Foods**, vol. 14, no. 11, p. 1871, 24 May 2025. DOI: 10.3390/foods14111871. Available at: https://www.mdpi.com/2304-8158/14/11/1871.

COMITRE, A. A.; VAZ, B. da S.; COSTA, J. A. V.; MORAIS, M. G. de. Renewal of nanofibers in *Chlorella fusca* microalgae cultivation to increase CO_2 fixation. **Bioresource Technology**, vol. 321, no. November 2020, p. 124452, Feb. 2021. DOI: 10.1016/j.biortech.2020.124452. Available

at: https://doi.org/10.1016/j.biortech.2020.124452.

DANESHVAR, E.; WICKER, R. J.; SHOW, P.-L.; BHATNAGAR, A. Biologically-mediated carbon capture and utilization by microalgae towards sustainable CO_2 biofixation and biomass valorization – A review. **Chemical Engineering Journal**, vol. 427, p. 130884, 1 Jan. 2022. DOI: 10.1016/j.cej.2021.130884. Available at: https://linkinghub.elsevier.com/retrieve/pii/S1385894721024682.

DAO, O.; BERTRAND, M.; ALSEEKH, S.; VEILLET, F.; AUROY, P.; NGUYEN, P.-C.; LÉGERET, B.; EPTING, V.; MORIN, A.; CUINÉ, S.; MONTEIL, C. L.; MACKINDER, L. C. M.; BURLACOT, A.; KRIEGER-LISZKAY, A.; WEBER, A. P. M.; FERNIE, A. R.; PELTIER, G.; LI-BEISSON, Y. The green algae CO_2 concentrating mechanism and photorespiration jointly operate during acclimation to low CO_2. **Nature Communications**, vol. 16, no. 1, p. 5296, 17 Jun. 2025. DOI: 10.1038/s41467-025-60525-7. Available at: doi.org/10.1038/s41467-025-60525-7.

DEAMICI, K. M.; CUELLAR-BERMUDEZ, S. P.; MUYLAERT, K.; SANTOS, L. O.; COSTA, J. A. V. Quantum yield alterations due to the static magnetic fields action on *Arthrospira platensis* SAG 21.99: Evaluation of photosystem activity. **Bioresource Technology**, vol. 292, p. 121945, Nov. 2019. DOI: 10.1016/j.biortech.2019.121945. Available at: https://linkinghub.elsevier.com/retrieve/pii/S0960852419311757. Accessed: 14 May 2024.

DEAMICI, K. M.; DZIERGOWSKA, K.; SILVA, P. G. P.; MICHALAK, I.; SANTOS, L. O.; DETYNA, J.; KATARIA, S.; BRESTIC, M.; SARRAF, M.; ISLAM, M. Microalgae Cultivated under Magnetic Field Action: Insights of an Environmentally Sustainable Approach. **Sustainability**, vol. 14, no. 20, p. 13291, 16 Oct. 2022. DOI: 10.3390/su142013291. Available at: https://www.mdpi.com/2071-1050/14/20/13291.

DEAMICI, K. M.; MORAIS, M. G. de; DOS SANTOS, L. O.; GROS, F.; COSTA, J. A. V.; LAROCHE, C. Magnetic Field Action on *Limnospira indica* PCC8005 Cultures: Enhancement of Biomass Yield and Protein Content. **Applied Sciences**, vol. 12, no. 3, p. 1533, 31 Jan. 2022. DOI: 10.3390/app12031533. Available at: https://www.mdpi.com/2076-3417/12/3/1533.

DEAMICI, K. M.; SANTOS, L. O.; COSTA, J. A. V. Use of static magnetic fields to increase CO_2 biofixation by the microalga *Chlorella fusca*. **Bioresource Technology**, vol. 276, no. November 2018, pp. 103–109, 1 Mar. 2019. DOI: 10.1016/j.biortech.2018.12.080. Available at: https://linkinghub.elsevier.com/retrieve/pii/S0960852418317516. Accessed: 10 Mar. 2023.

DECAMP, A.; MARTINEAU, E.; GRIZEAU, D.; PRUVOST, J.; GONÇALVES, O. Effects of the salinity on the biosynthesis of the polysaccharides of the marine microalgae *Porphyridium cruentum*. **Algal Research**, vol. 71, no. April, p. 103089, Apr. 2023. DOI: 10.1016/j.algal.2023.103089. Available at: https://linkinghub.elsevier.com/retrieve/pii/S2211926423001224.

DOGSON, K.; PRICE, R. A note on the determination of the ester sulphate content of sulphated polysaccharides. **Biochemical Journal**, vol. 84, no. 1, pp. 106–110, 1 Jul. 1962. DOI: 10.1042/bj0840106. Available at: https://portlandpress.com/biochemj/article/84/1/106/52792/A-note-on-the-determination-of-the-ester-sulphate.

DUBOIS, M.; GILLES, K. A.; HAMILTON, J. K.; REBERS, P. A.; SMITH, F. Colorimetric Method for Determination of Sugars and Related Substances. **Analytical Chemistry**, vol. 28, no. 3, pp. 350–356, 1 Mar. 1956. DOI: 10.1021/ac60111a017. Available at: https://pubs.acs.org/doi/abs/10.1021/ac60111a017. Accessed: 27 Jan. 2022.

ESQUEDA, A. B.; GARDARIN, C.; LAROCHE, C. Exploring the Diversity of Red Microalgae for Exopolysaccharide Production. **Marine Drugs**, vol. 20, no. 4, p. 246, 31 Mar. 2022. DOI: 10.3390/md20040246. Available at: https://www.mdpi.com/1660-3397/20/4/246/htm. Accessed: 1 Aug. 2022.

EVANS, E. W.; DODSON, C. A.; MAEDA, K.; BISKUP, T.; WEDGE, C. J.; TIMME, C. R. Magnetic field effects in flavoproteins and related systems. **Interface Focus**, vol. 3, no. 5, p. 20130037, 6 Oct. 2013. DOI: 10.1098/RSFS.2013.0037. Available at: https://pmc.ncbi.nlm.nih.gov/articles/PMC3915827/. Accessed: 1 Jul. 2026.

FILALI MOUHIM, R.; CORNET, J. F.; FONTANE, T.; FOURNET, B.; DUBERTRET, G. Production, isolation and preliminary characterization of the exopolysaccharide of the cyanobacterium *Spirulina platensis*. **Biotechnology Letters 1993 15:6**, vol. 15, no. 6, pp. 567–572, 1993. DOI: 10.1007/BF00138541. Available at: https://link.springer.com/article/10.1007/BF00138541. Accessed: 12 Sep. 2022.

FONT, Y. S.; DÍAZ, Y. O.; CUYPERS, A.; ALEMÁN, E. I.; VANDAMME, D. The effect of magnetic field treatment on the cultivation of microalgae: An overview of involved mechanisms. **Journal of Applied Phycology**, vol. 35, no. 4, pp. 1525–1536, 1 Aug. 2023. https://doi.org/10.1007/s10811-023-02994-1.

GARGOUCH, N.; ELLEUCH, F.; KARKOUCH, I.; TABBENE, O.; PICHON, C.; GARDARIN, C.; RIHOUEY, C.; PICTON, L.; ABDELKAFI, S.; FENDRI, I.; LAROCHE, C. Potential of exopolysaccharide from *Porphyridium marinum* to contend with bacterial proliferation, biofilm formation, and breast cancer. **Marine Drugs**, vol. 19, no. 2, 2021. https://doi.org/10.3390/md19020066.

GARGOUCH, N.; KARKOUCH, I.; ELLEUCH, J.; ELKAHOUI, S.; MICHAUD, P.; ABDELKAFI, S.; LAROCHE, C.; FENDRI, I. Enhanced B-phycoerythrin production by the red microalga *Porphyridium marinum*: A powerful agent in industrial applications. **International Journal of Biological Macromolecules**, vol. 120, pp. 2106–2114, 2018. https://doi.org/10.1016/j.ijbiomac.2018.09.037.

GARTZKE, J.; LANGE, K. Cellular target of weak magnetic fields: ionic conduction along actin filaments of microvilli. **American Journal of Physiology-Cell Physiology**, vol. 283, no. 5, pp. C1333–C1346, 1 Nov. 2002. DOI: 10.1152/ajpcell.00167.2002. Available at: https://journals.physiology.org/doi/10.1152/ajpcell.00167.2002.

GUERREIRO, M.; EMMANUEL, C.; DUPUITS, C.; GARDARIN, C.; MOUZEYAR, S.; ROCHE, J.; LAROCHE, C. Transcriptomic Insights into Metabolic Reprogramming and Exopolysaccharide Synthesis in *Porphyridium purpureum* Under Gradual Nitrogen Deprivation.

pp. 1–28, 2026.

GUIHÉNEUF, F.; STENGEL, D. B. Towards the biorefinery concept: Interaction of light, temperature and nitrogen for optimizing the co-production of high-value compounds in *Porphyridium purpureum*. **Algal Research**, vol. 10, pp. 152–163, Jul. 2015. DOI: 10.1016/j.algal.2015.04.025. Available at: http://dx.doi.org/10.1016/j.algal.2015.04.025.

HAN, S. Il; HEO, Y. M.; JEON, M. S.; KYUNG, S.; KANG, S.; KWON, S. J.; RYU, J. H.; KIM, J. H.; AHN, J. W. The effect of exopolysaccharides from EMS-induced *Porphyridium cruentum* mutant on human epidermal and dermal layers. **Frontiers in Marine Science**, vol. 11, no. May, pp. 1–12, 2024. https://doi.org/10.3389/fmars.2024.1365311.

HOQUE, M. M.; IANNELLI, V.; PADULA, F.; RADICE, R. P.; SAHA, B. K.; MARTELLI, G.; SCOPA, A.; DROSOS, M. Microalgae: Green Engines for Achieving Carbon Sequestration, Circular Economy, and Environmental Sustainability—A Review Based on Last Ten Years of Research. **Bioengineering**, vol. 12, no. 9, pp. 1–23, 2025. https://doi.org/10.3390/bioengineering12090909.

JI, L.; LIU, Y.; LUO, J.; FAN, J. Freeze-thaw-assisted aqueous two-phase system as a green and low-cost option for analytical grade B-phycoerythrin production from unicellular microalgae *Porphyridium purpureum*. **Algal Research**, vol. 67, no. June, p. 102831, 2022. DOI: 10.1016/j.algal.2022.102831. Available at: https://doi.org/10.1016/j.algal.2022.102831.

LAROCHE, C. Exopolysaccharides from Microalgae and Cyanobacteria: Diversity of Strains, Production Strategies, and Applications. **Marine Drugs**, vol. 20, no. 5, p. 336, 21 May 2022. DOI: 10.3390/md20050336. Available at: https://doi.org/10.3390/md20050336. Accessed: 29 Jul. 2022.

LICHTENTHALER, H. K. [34] Chlorophylls and carotenoids: Pigments of photosynthetic biomembranes. **Methods in Enzymology**. 1987. vol. 148, no. C, pp. 350–382. DOI: 10.1016/0076-6879(87)48036-1. Available at: https://linkinghub.elsevier.com/retrieve/pii/0076687987480361.

LOWRY, O.; ROSEBROUGH, N.; FARR, A. L.; RANDALL, R. Protein Measurement With The Folin Phenol Reagent. **Journal of Biological Chemistry**, vol. 193, no. 1, pp. 265–275, Nov. 1951. DOI: 10.1016/S0021-9258(19)52451-6. Available at: https://linkinghub.elsevier.com/retrieve/pii/S0021925819524516. Accessed: 10 Apr. 2023.

MA, J.; YOU, X.; SUN, S.; WANG, X.; QIN, S.; SUI, S.-F. Structural basis of energy transfer in *Porphyridium purpureum* phycobilisome. **Nature**, vol. 579, no. 7797, pp. 146–151, 5 Mar. 2020. DOI: 10.1038/s41586-020-2020-7. Available at: http://dx.doi.org/10.1038/s41586-020-2020-7.

MAIZATUL, A. Y.; RADIN, M. S. R.; MOHAMED, A. A.; AMBATI, R. A.; RANGA, R. Influence of nitrogen and phosphorus on microalgal growth, biomass, lipid, and fatty acid production: An overview. **Cells**, vol. 10, no. 393, pp. 10–20, 2021.

MARCATI, A.; URSU, A. V.; LAROCHE, C.; SOANEN, N.; MARCHAL, L.; JUBEAU, S.;

DJELVEH, G.; MICHAUD, P. Extraction and fractionation of polysaccharides and B-phycoerythrin from the microalga *Porphyridium cruentum* by membrane technology. **Algal Research**, vol. 5, no. 1, pp. 258–263, Jul. 2014. DOI: 10.1016/j.algal.2014.03.006. Available at: http://dx.doi.org/10.1016/j.algal.2014.03.006.

MARSH, J. B.; WEINSTEIN, D. B. Simple charring method for determination of lipids. **Journal of Lipid Research**, vol. 7, no. 4, pp. 574–576, 1966. https://doi.org/10.1016/s0022-2275(20)39274-9.

MEDINA-CABRERA, E. V.; RÜHMANN, B.; SCHMID, J.; SIEBER, V. Characterization and comparison of *Porphyridium sordidum* and *Porphyridium purpureum* concerning growth characteristics and polysaccharide production. **Algal Research**, vol. 49, no. October 2019, p. 101931, Aug. 2020. DOI: 10.1016/j.algal.2020.101931. Available at: https://doi.org/10.1016/j.algal.2020.101931.

MENESTRINO, B. da C.; PINTOS, T. H. C.; SALA, L.; COSTA, J. A. V.; SANTOS, L. O. Application of Static Magnetic Fields on the Mixotrophic Culture of *Chlorella minutissima* for Carbohydrate Production. **Applied Biochemistry and Biotechnology**, vol. 192, no. 3, pp. 822–830, 29 Nov. 2020. DOI: 10.1007/s12010-020-03364-0. Available at: https://link.springer.com/10.1007/s12010-020-03364-0.

MONSIGNY, M.; PETIT, C.; ROCHE, A.-C. Colorimetric determination of neutral sugars by a resorcinol sulfuric acid micromethod. **Analytical Biochemistry**, vol. 175, no. 2, pp. 525–530, Dec. 1988. https://doi.org/10.1016/0003-2697(88)90578-7.

MONTREUIL, J.; SPIK, G.; CHOSSON, A.; SEGARD, E.; SCHEPPLER, N. Methods of study of the structure of glycoproteins. **Journal de pharmacie de Belgique**, vol. 18, pp. 529–46, 1963. Available at: http://www.ncbi.nlm.nih.gov/pubmed/14096752.

MÜLLER, P.; AHMAD, M. Light-activated cryptochrome reacts with molecular oxygen to form a flavin-superoxide radical pair consistent with magnetoreception. **Journal of Biological Chemistry**, vol. 286, no. 24, pp. 21033–21040, 17 Jun. 2011. DOI: 10.1074/jbc.M111.228940. Available at: https://pubmed.ncbi.nlm.nih.gov/21467031/. Accessed: 1 Jul. 2026.

NAVALHO, S.; FERRER-LEDO, N.; BARBOSA, M. J.; VARELA, J. Nannochloropsis Lipids and Polyunsaturated Fatty Acids: Potential Applications and Strain Improvement. **Marine Drugs**, vol. 23, no. 3, pp. 1–34, 2025. https://doi.org/10.3390/md23030128.

NGUYEN, A. Q.; MOHAMMADI, M.; ALIAN, M.; MURALITHARAN, G.; CHAUHAN, V. S.; BALAN, V. Exploring the versatility of Porphyridium sp.: A comprehensive review of cultivation, bio-product extraction, purification, and characterization techniques. **Biotechnology Advances**, vol. 77, no. October, p. 108471, 2024. DOI: 10.1016/j.biotechadv.2024.108471. Available at: https://doi.org/10.1016/j.biotechadv.2024.108471.

NUR, S.; OSLAN, H.; SHOPARWE, N. F.; YUSOFF, A. H.; RAHIM, A. A.; CHANG, C. S.; TAN, J. S.; OSLAN, S. N.; ARUMUGAM, K.; ARIFF, A. Bin; SULAIMAN, A. Z.; MOHAMED, M. S. A Review on *Haematococcus pluvialis* Bioprocess Optimization of Green

and Red Stage Culture Conditions for the Production of Natural Astaxanthin. **Biomolecules**, vol. 11, no. 256, pp. 1–15, 2021.

PAZUR, A.; WINKLHOFER, M. Magnetic effect on CO_2 solubility in seawater: A possible link between geomagnetic field variations and climate. **Geophysical Research Letters**, vol. 35, no. 16, 30 Aug. 2008. DOI: 10.1029/2008GL034288. Available at: https://agupubs.onlinelibrary.wiley.com/doi/10.1029/2008GL034288.

PHÉLIPPÉ, M.; GONÇALVES, O.; THOUAND, G.; COGNE, G.; LAROCHE, C. Characterization of the polysaccharides chemical diversity of the cyanobacteria *Arthrospira platensis*. **Algal Research**, vol. 38, no. December 2018, p. 101426, 2019. DOI: 10.1016/j.algal.2019.101426. Available at: https://doi.org/10.1016/j.algal.2019.101426.

PRIORETTI, L.; GONTERO, B.; HELL, R.; GIORDANO, M. Diversity and regulation of ATP sulfurylase in photosynthetic organisms. **Frontiers in Plant Science**, vol. 5, no. November, pp. 1–12, 5 Nov. 2014. DOI: 10.3389/fpls.2014.00597. Available at: http://journal.frontiersin.org/article/10.3389/fpls.2014.00597/abstract.

ROSA, G. M. da; MORAIS, M. G. de; COSTA, J. A. V. Green alga cultivation with monoethanolamine: Evaluation of CO_2 fixation and macromolecule production. **Bioresource Technology**, vol. 261, no. April, pp. 206–212, 2018. https://doi.org/10.1016/j.biortech.2018.04.007.

ROSA, G. M.; MORAES, L.; DE SOUZA, M. da R. A. Z.; COSTA, J. A. V. *Spirulina* cultivation with a CO_2 absorbent: Influence on growth parameters and macromolecule production. **Bioresource Technology**, vol. 200, pp. 528–534, 1 Jan. 2016. https://doi.org/10.1016/J.BIORTECH.2015.10.025.

SAFI, C.; ZEBIB, B.; MERAH, O.; PONTALIER, P. Y.; VACA-GARCIA, C. Morphology, composition, production, processing and applications of *Chlorella vulgaris*: A review. **Renewable and Sustainable Energy Reviews**, vol. 35, pp. 265–278, 2014. https://doi.org/10.1016/j.rser.2014.04.007.

SANTOS, L. O.; SILVA, P. G. P.; MACHADO, B. R.; SALA, L.; DEAMICI, K. M. Update on the application of magnetic fields to microalgal cultures. **World Journal of Microbiology and Biotechnology**, vol. 38, no. 11, pp. 1–10, 2 Nov. 2022. DOI: 10.1007/s11274-022-03398-y. Available at: https://link.springer.com/article/10.1007/s11274-022-03398-y. Accessed: 3 Oct. 2022.

SCHUBERT, N.; GARCÍA-MENDOZA, E.; PACHECO-RUIZ, I. Carotenoid composition of marine red algae. **Journal of Phycology**, vol. 42, no. 6, pp. 1208–1216, 16 Dec. 2006. DOI: 10.1111/j.1529-8817.2006.00274.x. Available at: https://onlinelibrary.wiley.com/doi/10.1111/j.1529-8817.2006.00274.x.

SERRANO, G.; MIRANDA-OSTOJIC, C.; FERRADA, P.; WULFF-ZOTELLE, C.; MAUREIRA, A.; FUENTEALBA, E.; GALLARDO, K.; ZAPATA, M.; RIVAS, M. Response to static magnetic field-induced stress in *Scenedesmus obliquus* and *Nannochloropsis gaditana*.

Marine Drugs, vol. 19, no. 9, 2021. https://doi.org/10.3390/md19090527.

SOANEN, N.; DA SILVA, E.; GARDARIN, C.; MICHAUD, P.; LAROCHE, C. Improvement of exopolysaccharide production by *Porphyridium marinum*. **Bioresource Technology**, vol. 213, pp. 231–238, 2016. DOI: 10.1016/j.biortech.2016.02.075. Available at: http://dx.doi.org/10.1016/j.biortech.2016.02.075.

SUN, L.; WANG, L.; ZHOU, Y. Immunomodulation and antitumor activities of different-molecular-weight polysaccharides from *Porphyridium cruentum*. **Carbohydrate Polymers**, vol. 87, no. 2, pp. 1206–1210, 2012. DOI: 10.1016/j.carbpol.2011.08.097. Available at: http://dx.doi.org/10.1016/j.carbpol.2011.08.097.

USOV, A. I.; ZELINSKY, N. D. Chemical structures of algal polysaccharides. **Functional Ingredients from Algae for Foods and Nutraceuticals**. Elsevier, 2013. no. 2011, pp. 23–86. DOI: 10.1533/9780857098689.1.23. Available at: http://dx.doi.org/10.1533/9780857098689.1.23.

VAZ, B. da S.; COSTA, A. V.; MORAIS, M. G. de. Physical and biological fixation of CO_2 with polymeric nanofibers in outdoor cultivations of *Chlorella fusca* LEB 111. **International Journal of Biological Macromolecules**, vol. 151, pp. 1332–1339, May 2020. DOI: 10.1016/j.ijbiomac.2019.10.179. Available at: https://linkinghub.elsevier.com/retrieve/pii/S0141813019357472.

VAZ, B. da S.; MASTRANTONIO, D. J. da S.; COSTA, J. A. V.; MORAIS, M. G. de. Green alga cultivation with nanofibers as physical adsorbents of carbon dioxide: Evaluation of gas biofixation and macromolecule production. **Bioresource Technology**, vol. 287, no. May, p. 121406, Sep. 2019. DOI: 10.1016/j.biortech.2019.121406. Available at: https://linkinghub.elsevier.com/retrieve/pii/S0960852419306364.

VAZ, B. da S.; VIEIRA COSTA, J. A.; GREQUE DE MORAIS, M. Innovative nanofiber technology to improve carbon dioxide biofixation in microalgae cultivation. 2018. DOI: 10.1016/j.biortech.2018.11.054. Available at: https://doi.org/10.1016/j.biortech.2018.11.054. Accessed: 15 May 2024.

WANG, W. N.; LI, Y.; ZHANG, Y.; XIANG, W. Z.; LI, A. F.; LI, T. Comparison on characterization and antioxidant activity of exopolysaccharides from two *Porphyridium* strains. **Journal of Applied Phycology**, vol. 33, no. 5, pp. 2983–2994, 1 Oct. 2021. DOI: 10.1007/s10811-021-02518-9. Available at: https://link.springer.com/article/10.1007/s10811-021-02518-9. Accessed: 26 Aug. 2022.

WÓJCIK-AUGUSTYN, A.; JOHANSSON, A. J.; BOROWSKI, T. Mechanism of Sulfate Activation Catalyzed by ATP Sulfurylase - Magnesium Inhibits the Activity. **Computational and Structural Biotechnology Journal**, vol. 17, pp. 770–784, 2019. DOI: 10.1016/j.csbj.2019.06.016. Available at: https://linkinghub.elsevier.com/retrieve/pii/S2001037018303118.

XIE, L.; SHEN, M.; WANG, Z.; XIE, J. Structure, function and food applications of

carboxymethylated polysaccharides: A comprehensive review. **Trends in Food Science and Technology**, vol. 118, no. PA, pp. 539–557, 2021. DOI: 10.1016/j.tifs.2021.09.016. Available at: https://doi.org/10.1016/j.tifs.2021.09.016.

XU, P.; LI, J.; QIAN, J.; WANG, B.; LIU, J.; XU, R.; CHEN, P.; ZHOU, W. Recent advances in CO_2 fixation by microalgae and its potential contribution to carbon neutrality. **Chemosphere**, vol. 319, p. 137987, Apr. 2023. DOI: 10.1016/j.chemosphere.2023.137987. Available at: https://linkinghub.elsevier.com/retrieve/pii/S0045653523002540.

YAO, D.; WU, L.; TAN, D.; YU, Y.; JIANG, Q.; WU, Y.; WANG, H.; LIU, Y. Enhancing CO_2 fixation by microalgae in a Photobioreactor: Molecular mechanisms with exogenous carbonic anhydrase. **Bioresource Technology**, vol. 408, no. February, p. 131176, Sep. 2024. DOI: 10.1016/j.biortech.2024.131176. Available at: https://doi.org/10.1016/j.biortech.2024.131176.

YI, S.; ZHANG, A. H.; HUANG, J.; YAO, T.; FENG, B.; ZHOU, X.; HU, Y.; PAN, M. Maximizing Polysaccharides and Phycoerythrin in *Porphyridium purpureum* via the Addition of Exogenous Compounds: A Response-Surface-Methodology Approach. **Marine Drugs**, vol. 22, no. 3, 2024. https://doi.org/10.3390/md22030138.

YOON, S.; CHANG, S. C.; PAYNE, G. F.; LEE, S.; KYHM, K.; PARK, S. G.; KANG, M. Effect of a magnetic field on the activity of superoxide dismutase studied at the enzyme level. **RSC Advances**, vol. 16, no. 28, pp. 25395–25401, 15 May 2026. DOI: 10.1039/D5RA10059C. Available at: https://dx.doi.org/10.1039/d5ra10059c. Accessed: 1 Jul. 2026.

ZHANG, A. H.; FENG, B.; ZHANG, H.; JIANG, J.; ZHANG, D.; DU, Y.; CHENG, Z.; HUANG, J. Efficient cultivation of *Porphyridium purpureum* integrated with swine wastewater treatment to produce phycoerythrin and polysaccharide. **Journal of Applied Phycology**, vol. 34, no. 5, pp. 2315–2326, 2022. https://doi.org/10.1007/s10811-022-02785-0

PAPER III

CULTIVATION CONDITIONS DRIVE DIVERGENT RHEOLOGICAL BEHAVIOR AND HYDROGEL ARCHITECTURE IN *Porphyridium purpureum* EXOPOLYSACCHARIDES

CULTIVATION CONDITIONS DRIVE DIVERGENT RHEOLOGICAL BEHAVIOR AND HYDROGEL ARCHITECTURE IN *Porphyridium purpureum* EXOPOLYSACCHARIDES

ABSTRACT

This study evaluated the effects of static magnetic field exposure and polymeric nanofiber on the physicochemical and thermal properties of released and bound exopolysaccharides, as well as rheological and hydrogel-forming properties of the released and exopolysaccharides from *Porphyridium purpureum*. Cultures were grown under control conditions, static magnetic field exposure for 1 or 24 h day^{-1}, or static magnetic field combined with nanofibers, and the polysaccharides produced were characterized by FTIR spectroscopy, zeta potential, thermal analysis, rheology, and scanning electron microscopy. All fractions exhibited spectral features consistent with sulfated heteropolysaccharides and strong colloidal stability, with zeta potential values < -30 mV. Thermal analysis revealed multistep degradation above 220 C and predominantly amorphous structures, indicating suitability for low-temperature processing. The released polysaccharides displayed pseudoplastic, gel-like behavior, and continuous magnetic field exposure produced the strongest viscoelastic network, with a storage modulus of 17.10 Pa, approaching 66% of the value observed for commercial xanthan. Hydrogel morphology was strongly affected by cultivation conditions, ranging from sheet-like macroporous structures to fibrillar and hierarchical nanofibrillar networks with honeycomb-like pores. Overall, static magnetic field and nanofiber-assisted cultivation modulated the structural and functional properties of *P. purpureum* exopolysaccharides, highlighting their potential for applications in food, pharmaceutical, and biomedical formulations.

Keywords: Sulfated polysaccharides, biopolymer, hydrogel morphology, rheology, ionic gelation.

1. INTRODUCTION

Valuable compounds produced by microalgae are secondary metabolites, the accumulation of which is often triggered or enhanced by stress-related stimuli. Conventional strategies to increase the yield of these compounds include nutrient deprivation, modulation of light intensity and photoperiod, osmotic stress, and temperature shifts (Barizão *et al.*, 2025). More recently, novel approaches have been explored to further enhance productivity and modulate the biochemical composition of microalgal biomass. Among these, the use of plant hormone precursors (Leal *et al.*, 2026), cell immobilization systems (Efremenko *et al.*, 2025), polymeric nanofibers, and exposure to static magnetic fields (SMF) (Carvalho *et al.*, 2025) have attracted growing interest. Among these approaches, several target carbon assimilations, the main metabolic route for forming carbon-based macromolecules such as EPS. Thus, understanding how these treatments influence the structure and properties of the target biomolecules is essential for their rational application in industrial contexts.

Exopolysaccharides produced by *P. purpureum* are complex heteropolymers characterized by a high degree of sulfation (typically 8–20%), uronic acid content (10-15%), and branched polysaccharide backbone (Maulina *et al.*, 2025). These structural features confer on the EPS a strongly anionic character, which underlies both their biological activities and their rheological behavior (Guerreiro *et al.*, 2026). Due to this complex structure, EPS synthesis is environmentally sensitive, particularly regarding substituent groups and structural features (sulfation, uronic acid content, methylation, glycoprotein attachment, etc.) (Maulina *et al.*, 2025). SMF during cultivation is a multifactorial stress-inducing strategy that acts upon charged and paramagnetic particles and molecules; this stress could affect substituent group formation due to their anionic character (Carvalho *et al.*, 2025). Conversely, polymeric nanofibers in microalgae cultivation are intended to increase CO_2 availability through gas entrapment, which improves liquid-gas mass transfer, thereby enhancing carbon fixation by acting directly on carbon assimilation pathways and increasing production of carbon-based macromolecules(Cardias; Morais; Costa, 2024).

EPS can be classified as released polysaccharides (RPS), secreted into the culture medium, or bound polysaccharides (BPS), which remain associated with the cell wall (Phélippé *et al.*, 2019). These two fractions differ substantially in chemical ratios, molecular weight, and functional properties. Both have been studied for their bioactive potential (antioxidant, antitumor, antiviral

activities) and as functional ingredients with viscosity-enhancing and emulsifying capacities(Bernaerts *et al.*, 2018, 2019; Laroche, 2022; Maulina *et al.*, 2025; Zhang, J. *et al.*, 2019). RPS are usually easier to extract and purify, yielding higher amounts of longer polymers with more predictable structural formation (Bernaerts *et al.*, 2018). The rheological properties of *P. purpureum* EPS underpin their potential as functional biopolymers, analogous to commercial gums, for food, pharmaceutical, and cosmetic applications.

Gel formation in polysaccharides can occur through thermally induced mechanisms (cold-set or heat-set gelation) or ionic cross-linking, where multivalent cations (Ba^{2+}, Ca^{2+}, K^{+}, Fe^{3+}) interact with negatively charged polymer groups to form three-dimensional networks (Fu *et al.*, 2024; Ju *et al.*, 2022). Cation selection introduces both technical and biological functionality; for instance, Fe^{3+} is relevant in hemostasis and wound healing, opening avenues for EPS-based hydrogels as drug-delivery vehicles, wound dressings, or bioactive scaffolds (Stojkov *et al.*, 2021; Xu, H. *et al.*, 2024; Xu, P. *et al.*, 2023). Gel morphology (pore size, wall thickness, network architecture) governs mechanical stiffness, swelling behavior, permeability, and cell colonization suitability (Stojkov *et al.*, 2021), determined by polymer molecular properties (degree of sulfation, charge density, chain flexibility) and gelation conditions (Ju *et al.*, 2022; Xia *et al.*, 2024). Therefore, understanding how SMF and nanofiber cultivation treatments alter EPS molecular architecture, and consequently gel-forming behavior, is critical for assessing technological potential.

We hypothesized that cultivation-stage modulation of carbon assimilation, via SMF and nanofiber treatments, alters the structural features (sulfation, branching, charge density) of the EPS and consequently their rheological and gelation behavior. Therefore, this study evaluated the effect of SMF and polymeric nanofiber on the physicochemical properties and hydrogel-forming capacity of EPS produced by *P. purpureum*, using FTIR spectroscopy, dynamic light scattering, thermal analysis (TGA and DSC), steady-state and oscillatory rheology, and scanning electron microscopy of hydrogels.

2. MATERIALS AND METHODS

2.1 NANOFIBERS AND MAGNETIC FIELD

Nanofiber solutions were prepared following Cardias et al. (2024).using 11.5% (p v^{-1}) polyacrylonitrile (PAN, 150,000 g mol^{-1}, Sigma-Aldrich®). Nanofibers were produced by electrospinning at a flow rate of 800 µL h^{-1} through a 0.55 mm capillary under 25 kV, with a 180 mm tip-to-collector distance at 20–23 °C and 50–58% humidity.

Static magnetic fields (SMF) were generated using two 400-turn coils supplied with 3 A electric current, producing a homogeneous field of 11 ± 2 mT (FH 51 gaussmeter, Magnet-Physik, DE)in the center of the bioreactor as described by Deamici et al. (2022).

2.2 EXOPOLYSACCHARIDES PRODUCTION

The strain used in this study was *Porphyridium purpureum* CCAP 1380/1A acquired from the Culture Collection of Algae and Protozoa (www.ccap.ac.uk) maintained in modified artificial seawater (ASW) medium composed of g L^{-1}; 28 NaCl, 1.85 $NaNO_3$, 0.95 K_2HPO_4, 7.20 $MgSO_47H_2O$, 1.55 $CaCl_2$ $2H_2O$, 100 µL mineral solution (g L^{-1}); 1.5 $MnSO_4H_2O$, 0.15 $(NH_4)6Mo7O_244H_2O$, 0.15 $CoSO_4,7H_2O$ 0.5 $CuSO_45H_2O$, 2.5 $ZnSO_47H_2O$, and 100 Fer-EDTA and vitamins (g L^{-1}); 0.1 B12, 0.25 thiamine, and 0.4 biotin and kept at 21 °C (Soanen *et al.*, 2016). The media were sterilized by filtration on 0.22µm membranes and kept at room temperature. *P. Purpureum* was cultivated under SMF (11 ± 2 mT) and PAN nanofiber 0.1 mg $mL^{-1}{}_{media}$ added directly to the media at the beginning of the cultivation.

The culture was conducted for 15 days in triplicate at 21 ± 1 °C under continuous irradiation (200 µmol photons m^{-2} s^{-1}, 24 h) in 600 mL rectangular jacketed bioreactors. Homogenization was achieved using sterile compressed air at 0.3 vvm ($mL_{air} \cdot mL_{medium}^{-1} \cdot min^{-1}$). A gas mixture containing 7.5% CO_2 was injected for 2 minutes every hour, with aeration paused for 1 minute before and after injection to enhance mass transfer.

The experiment comprised four treatments, each yielding one released polysaccharide (RPS) and one bound polysaccharide (BPS) sample: a control (CT) without SMF or nanofibers, SMF exposure for 1 h d^{-1} (M1), SMF exposure for 24 h d^{-1} (M24), and SMF exposure for 1 h d^{-1} with nanofibers (MN). At the end of cultivation, the cultures were centrifuged. The supernatant

was collected for RPS separation, and the biomass pellet was frozen at −80 °C for 48h, lyophilized, and stored at −20 °C for subsequent BPS extraction.

RPS was obtained from the supernatant at the end of cultivation by ultrafiltration with Vivaflow 200 system with 10 kDa NMWCO (molecular weight cut-off) membrane for desalination and purification of EPS up to the conductivity measured < 5 μS cm^{-1} (Mettler Toledo SevenEasy, EUA) , after which the sample was frozen at -80 ºC for 48h, then lyophilized and kept at -20ºC until analysis.

Hot extraction of BPS was performed as described by Filali Mouhim et al. (1993) modified by Phélippé et al. (2019). A 0.5 g of freeze-dried biomass was resuspended in 200 mL of 50 mM TAPS buffer (pH 8.15) containing 25 mM EDTA and heated to 100 ºC for 20 minutes., After centrifugation (10,000×g for 15 min), the supernatant was collected and the pellet was re-extracted under the same conditions. The two supernatants were combined, and BPS was precipitated by adding three volumes of 3% (w/v) cetyltrimethylammonium bromide (CTAB), followed by incubation overnight. The resulting BPS–CTAB complex was recovered by centrifugation (10,000×g for 15 min at 0 °C) and purified through three consecutive solubilization–precipitation cycles. In each cycle, the pellet was dissolved in KCl solution (first 1.5 M, then 0.75 M, and finally 0.3 M) and reprecipitated with three volumes of 96% (v/v) ethanol (24 h at −20 °C). The purified BPS pellet was dissolved in Milli-Q water, subjected to ultrafiltration, and lyophilized under the same conditions as previously described.

2.3 FOURIER TRANSFORM INFRARED (FTIR)

FTIR spectra were measured by VERTEX70 FTIR instrument (Bruker, USA). 50 mg of lyophilized EPS was spread on the ATR A225 diamond to be read. 50 scans resolution 4 cm^{-1} infrared spectra were recorded at room temperature, referenced against air, in the wavenumber range of 500–4000 cm-1. Then the spectra were analyzed with OPUS 7.2 software (Bruker Optics).

2.4 DYNAMIC LIGHT SCATTERING (DLS)

EPS solutions of 0.01 % w v^{-1} were made in MiliQ water at 25 °C at pH 7. To determine the ionic charge of the EPS, the zeta potential was measured in triplicate at 25ºC and a Refractive

Index of 1.53, by dynamic light scattering with a Zetasizer Ultra-Red (Malvern Panalytical,UK) (Alvarez *et al.*, 2021).

2.5 THERMAL ANALYSIS TGA AND DSC

The thermogravimetric analysis (TGA) of the EPS was performed using a TGA instrument (Shimadzu DTG-60, Japan) in accordance with ASTM D3850-12 (2013) methodology. Shortly, ~ 4 mg of sample were heated to a rate of 10 °C min^{-1} from 25 ºC to 600 °C in an inert nitrogen atmosphere, with a flow rate of 30 mL min^{-1}.

The thermal transitions and melting temperatures of the EPS were analyzed using differential scanning calorimetry (DSC) in a Shimadzu DSC-60 instrument (Japan). 4 mg of freeze-dried EPS was placed in aluminum containers, sealed, and analyzed under a nitrogen atmosphere (flow rate of 50 mL/min), with a constant heating rate of 10 ºC min^{-1} from 25 ºC to 300 ºC.

2.6 RHEOLOGY ASSAYS

RPS, xanthan, and guar gum were hydrated and homogenized in Milli-Q water at 1% (w v^{-1}) 24 h before analysis to ensure complete dissolution (Medina-Cabrera *et al.*, 2020). Steady shear and dynamic oscillatory shear measurements were performed using an Anton Paar MCR 92 controlled-stress rheometer (Anton Paar, AT) equipped with a B-CC27 concentric cylinder geometry to minimize evaporation and edge effects. Flow curves were obtained by measuring the apparent viscosity (η) over a shear rate (γ) range of 1 to 100 s^{-1} using 100 logarithmically spaced points. Apparent viscosity versus shear rate data were fitted to the power-law model using logarithmic transformation, Equation 1:

$$\log \eta = \log(K) + n - 1 \log(\gamma) \quad (1)$$

The flow behavior (n) was calculated from the slope of the log (η) versus log (γ) plot, and the consistency index (K) was obtained from the intercept. Where when $n < 1$ indicates pseudoplastic behavior.

Viscoelastic behavior was evaluated by frequency sweep experiments. The strain amplitude was maintained at 2%, while the angular frequency (ω) was decreased from 100 to 0.1 rad s^{-1}. All rheological analyses were performed at 25 °C.

The frequency dependence of G′ was determined from the slope of the linear regression obtained from the log–log plot of G′ as a function of angular frequency, ω. The slope was calculated according to the relationship log G′ = m log ω + b, where m represents the frequency dependence of the storage modulus.

2.7 HYDROGELS PREPARATION AND MORPHOLOGY

RPS gelation was achieved through ionic gelation by mixing equal volumes (500 µL) of 1% (w v^{-1}) EPS and 0.3% (w v^{-1}) $Fe_2(SO_4)_3$ aqueous solutions. The mixtures were homogenized and left overnight at 25 ºC to promote the formation of a three-dimensional gel network. The hydrogels were then immersed in liquid nitrogen (to preserve structural integrity), kept in -80ºC, and lyophilized.

The lyophilized hydrogels were sliced with a scalpel into 1–5 mm sections. The slices were placed on carbon tape mounted on metal stubs for scanning electron microscopy (SEM) analysis. The morphology was analyzed using a JEOL JSM-6610LV SEM (JEOL Ltd., Japan). The stubs were gold-coated using a sputter metallizer (Denton Vacuum CAR001–0038, USA) according to ASTM E986-04, (2004). SEM images were acquired at an acceleration voltage of 15 kV, a working distance of 13 mm, and magnifications of up to 500×. The maximum Feret diameters of the pores were measured using ImageJ software with n > 30 per sample.

2.8 STATISTICAL ANALYSIS

Statistical significance between experimental groups was assessed by a one-way analysis of variance (ANOVA) followed by Tukey's post hoc test a *p*-value < 0.05 was considered statistically significant with assistance of Origin 2026 software.

3. RESULTS AND DISCUSSION

3.1 MOLECULAR CHARACTERISTICS OF EPS

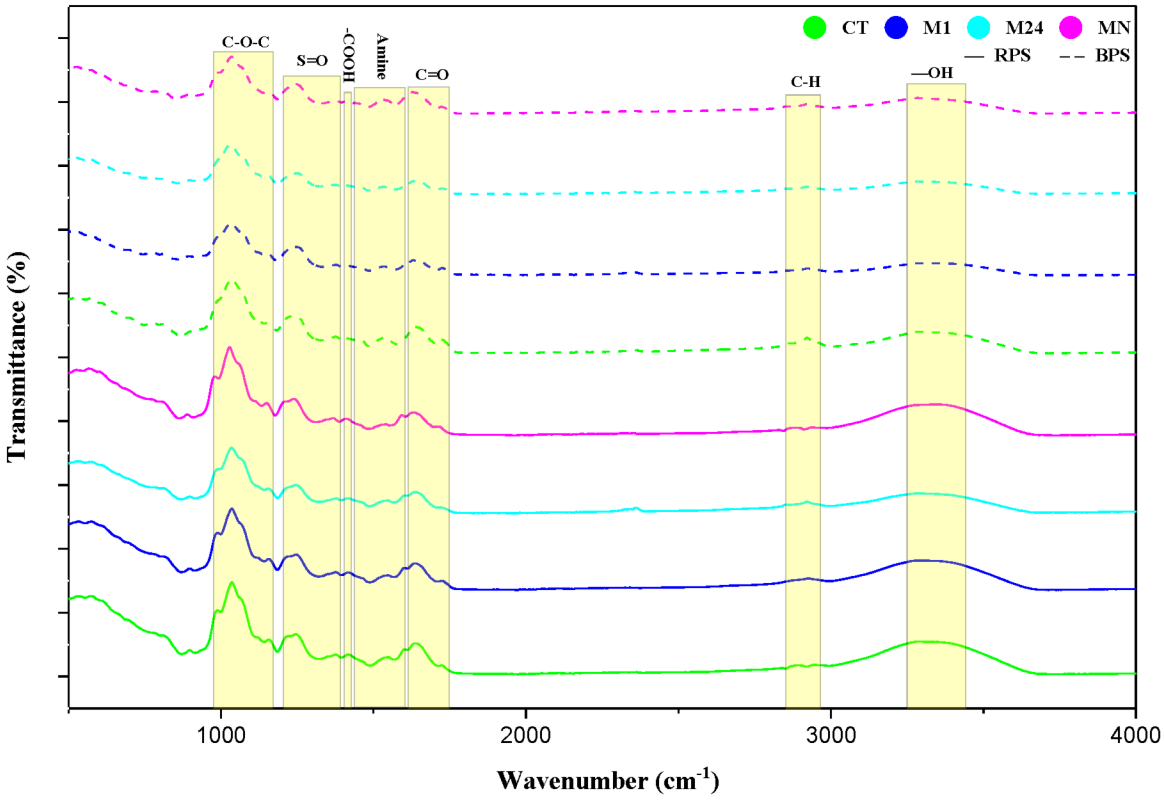
3.1.1 Fourier Transform Infrared (FT-IR) of EPS produced by *P. Purpureum*

The FT-IR (Fourier Transform Infrared) spectra of RPS and BPS, covering the range from 4000 to 400 cm^{-1}, are presented in Figure 1. The functional group region (4000 – 1500 cm^{-1}) is typical of a polysaccharide, with soft peaks between 3285-3352 cm^{-1} associated with the stretching vibration of the hydrogen bonds in the -OH group (Chopin; Kerin; Mazerolle, 1999; Maréchal, 1997). Peaks in 2920 cm^{-1} and 2850 cm^{-1}, can be linked to the C-H stretching vibrations, indicating methylation in the polymer from amino acids or methylated sugars, such as 2-O-methyl-glucuronic acid, 3-O-methyl xylose, or 3-O-methyl galactose (Esqueda; Gardarin; Laroche, 2022). Most noticeable in BPS, M24 and M1 RPS treatments presented these peaks, probably due to lower intensity in the 3285-3352 cm^{-1} peak, suggesting higher amino acid content, making the CH_3 peaks more noticeable.

Carbonyl bands peaks (1730 – 1630 cm^{-1}) can be indication of carboxylic acid ester (1722 cm^{-1}) C=O stretching vibration of -CHO and (1641 cm^{-1}) carboxylate anion of COO- present in all samples (Gómez-Ordóñez; Rupérez, 2011; Li, T. *et al.*, 2021). Bands around 1570 -1430 cm^{-1} relate to amide groups (N-H, N-H···O=C, N-D, N-D···O=C and N-D), from proteins (Maréchal, 1997) . Peaks at 1416 cm^{-1} indicate -COOH stretching present in glucuronic acid (Kim *et al.*, 2021). Bands between 1370- 1210 cm^{-1} are present in all EPS; these peaks are indicative of sulphate groups by the asymmetric stretching vibration of S=O (Wang, X. *et al.*, 2013).

The strong peaks around 1000-1200 cm^{-1} refer to the C-O-C glycosidic band vibration and the C-O-H side groups (Molaei; Jahanbin, 2017). A peak at 1034 cm^{-1} with a shoulder peak around 980 cm^{-1} is present in all samples, indicating the C-O, C-C, and β(C-OH) vibrations in xylose and glucose (Wiercigroch *et al.*, 2017). 897 cm^{-1} band appeared in all samples, which can be associated to unsulphated β-D-galactose/ 6–0-methylgalactose commonly present in Porphyridium. EPS (Chopin; Kerin; Mazerolle, 1999; Usov; Zelinsky, 2013). FTIR of the samples suggests that the extracted EPS can be characterized as a sulphated acid polymer with alpha- and beta-glycosidic bonds.

Figure 1- FT-IR spectra of RPS and BPS produced by *P. purpureum*. CT: control; M1: magnetic field 1 h d^{-1}; M24: magnetic field 24 h d^{-1}; MN: magnetic field 1 h d^{-1} with nanofibers.



3.1.2 Zeta Potential of EPS produced by *P. purpureum*

The zeta potential analysis revealed the electrostatic characteristics and dispersion stability of the EPS fractions. All studied samples showed a ZP < -30 mV (Table 1), which indicates a highly stable colloidal dispersion with strong electrostatic repulsion between particles, preventing aggregation and sedimentation. This is an excellent result for both food and pharmaceutical applications (Cano-Sarmiento *et al.*, 2018; Rawat *et al.*, 2025). Varying from -44.4 mV to -68.3 mV, this negative nature of the EPS can be associated with substituent groups in the polymeric chain, which for *P. purpureum* EPS derived from sulphate and uronic acid groups (Laroche, 2022).

Table 1 - Zeta potential of the studied EPS. CT: control; M1- Magnetic field 1 h day^{-1}; M24 Magnetic field 24 h day^{-1}; MN – added nanofiber magnetic field. The results are expressed as mean (n = 3) ± standard deviation. Different letters show a significant difference between samples, *p*-values < 0.05 (Tukey's test).

	CT	M1	M24	MN
RPS (mV)	-44.4±3^{c}	-65.2±2.9^{a}	-60.3±8.3^{ab}	-54.8±2.8^{bc}
BPS (mV)	-62.8±3.3^{ab}	-53.8±1.1^{bc}	-61.5±2.6^{ab}	-68.3±5.2^{a}

When comparing the two factions within each treatment, CT and MN showed that BPS was more anionic (more negative zeta potential) than RPS ($p < 0.05$). In contrast, M1 showed the opposite pattern, with RPS displaying a higher anionic charge (more negative zeta potential) ($p < 0.05$). In M24, the ZP values of RPS and BPS were not significantly different ($p > 0.05$), indicating that the two fractions have very similar charge characteristics. This suggests that nanofiber exposure may have decreased negative groups associated with the RPS produced, while increasing these groups in BPS, compared to M1. Meanwhile, SMF exposure time influences the EPS charge profile: short exposure (M1) results in a more negative ZP for RPS, whereas continuous exposure (M24) makes both fractions similar in ZP.

The strongly anionic, highly stable profile of the produced EPS is comparable to alginate and pectin (-29,94 mV and -16.6 mV, respectively), both of which are extensively used in encapsulation, controlled drug release, edible films, and emulsion stabilization. Polysaccharides with high negative ZP are excellent candidates for forming interpolyelectrolyte complexes with cationic polymers (e.g., chitosan), for stabilizing oil-in-water emulsions, and for mucoadhesive or gastro-resistant delivery systems (Barbosa *et al.*, 2019; Cano-Sarmiento *et al.*, 2018).

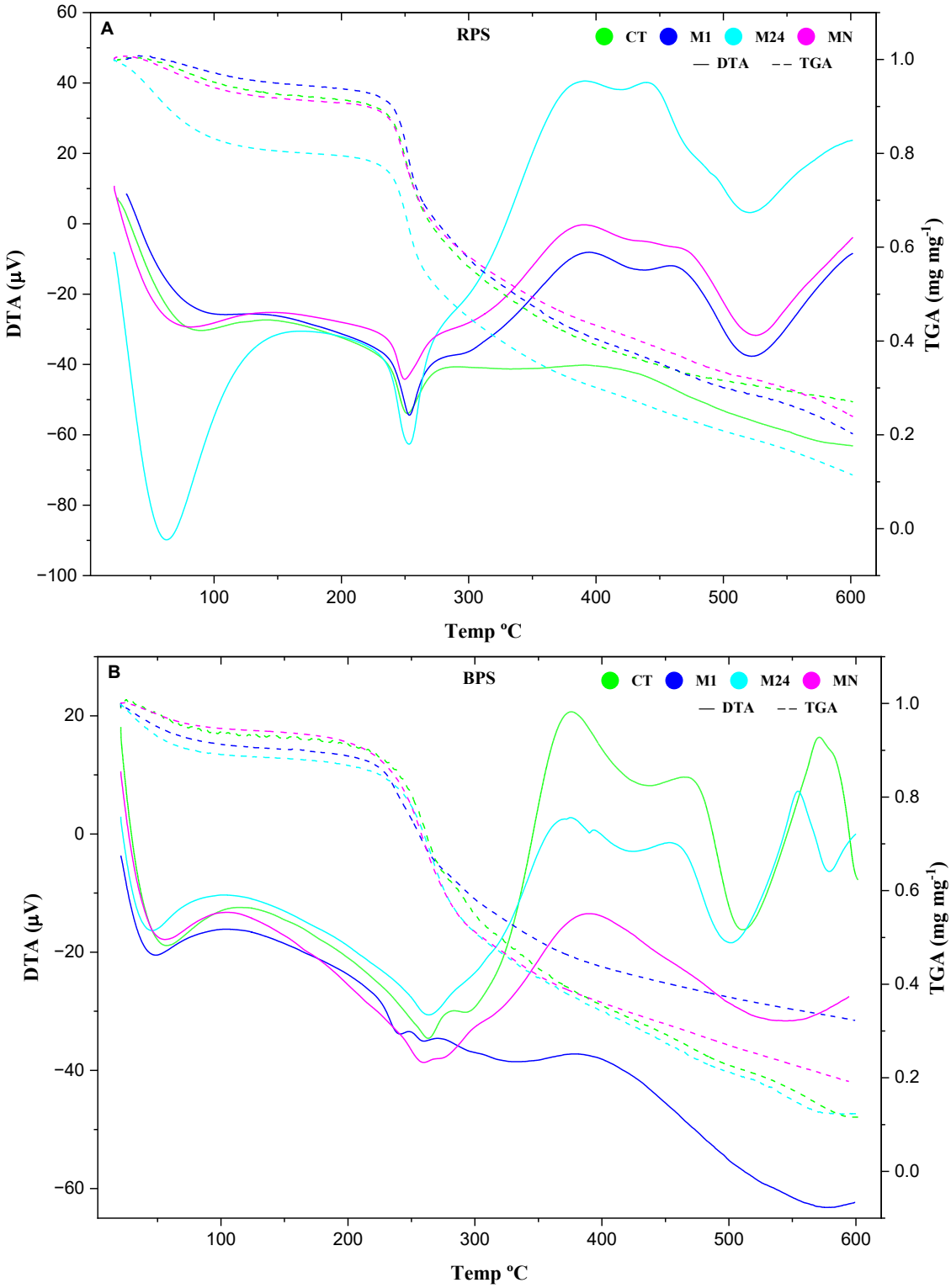
All treatments produced highly negative zeta potential values, suggesting that these treatments may enhance the functional potential of the EPS. The high anionic character of P. purpureum EPS can be associated with the degree of sulfation in the polymer.(Laroche, 2022). In polymers such as κ-carrageenan (a sulfated polysaccharide from marine algae), these groups derive from sulfuric acid and dissociate completely across a wide pH range, granting pH-independent colloidal stability (Barbosa et al., 2019).

3.2 EPS THERMAL ANALYSIS

3.2.1 Thermogravimetric analysis (TGA)

The Thermogravimetric Analysis (TGA) curves of *Porphyridium purpureum* RPS (Figure 2A) and BPS (Figure 2B) revealed a multistep thermal degradation profile consistent with the complex chemical composition of these extracellular polysaccharides (EPS). Three main degradation stages were identified: an initial moisture loss below 120 °C, a primary decomposition event between approximately 220 and 400 °C attributed to glycosidic bond cleavage and polysaccharide backbone depolymerization, and a broader high-temperature degradation region extending up to 600 °C associated with progressive breakdown of thermally stable structures and char formation (Blanco; Siracusa, 2021). The residual mass observed at temperatures above 600 °C reflects the presence of thermally stable carbonaceous material and inorganic ash, with inter-sample differences indicating compositional and structural variation among treatments.

Figure 2 - TGA of RPS (A) and BPS (B). CT: control; M1: magnetic field 1 h d^{-1}; M24: magnetic field 24 h d^{-1}; MN: magnetic field 1 h d^{-1} with PAN nanofibers.



Among RPS samples (Figure 2A), an initial mass loss of approximately 8% was observed up to 120 °C for most samples, attributed to the removal of moisture and weakly bound water (Koçer *et al.*, 2021). The M24 sample exhibited a higher initial mass loss of 22%, suggesting a greater water-binding capacity and/or a higher proportion of labile volatile compounds, which may reflect differences in chain conformation or sulfate group distribution induced by the M24 treatment conditions. The main degradation event, occurring between approximately 220 and 400 °C with the peak rate at around 380 °C, corresponded to approximately 53% mass loss across all samples and is attributed to the cleavage of glycosidic bonds and depolymerization of the polysaccharide backbone (Maulina *et al.*, 2025). A subsequent gradual degradation stage between 400 and 600 °C resulted in an additional 20% mass loss for most samples, except CT, which showed only 12% mass loss, suggesting a higher degree of crosslinking or more compact chain packing.(Nurazzi *et al.*, 2021). The residual mass at the end of the assay among the RPS samples was approximately 11% for M24, 27% for CT, 20% for M1, and 24% for MN. The higher residual mass in CT, M1, and MN suggests a greater tendency toward thermally stable char formation, protein, and/or higher inorganic ash content, consistent with reports for polysaccharides from cashew gum (Mothé; Freitas, 2018) and *Bacillus licheniformis* (Maulina *et al.*, 2025). The lower char residue formed by the M24 treatment may be attributed to the higher moisture content present in the sample at the beginning of the assay.

For BPS (Figure 2B), the CT and MN samples showed approximately 8% moisture loss, whereas M1 and M24 exhibited approximately 12% moisture loss, again suggesting treatment-related differences in water-binding affinity. The primary degradation stage (220–400 °C), corresponding to glycosidic bond cleavage, resulted in approximately 58% mass loss for CT, M24, and MN samples, whereas M1 showed a lower mass loss of 47% in this region, indicating comparatively greater thermal stability of the M1 BPS fraction. In the gradual degradation range (400–600 °C), M1 BPS showed 12% mass loss, whereas CT, M24, and MN presented 24%, 22%, and 17% mass loss, respectively. These differences resulted in variable residual masses at the end of the assay: CT and M24 retained approximately 12%, while MN and M1 showed 19% and 32% residual mass, respectively.

Among BPS samples, M1 appears to be the most thermally stable, exhibiting lower mass loss in the primary degradation region (47% vs. approximately 58% for CT, M24, and MN) and lower residual degradation in the high-temperature zone (400–600 °C). This enhanced thermal

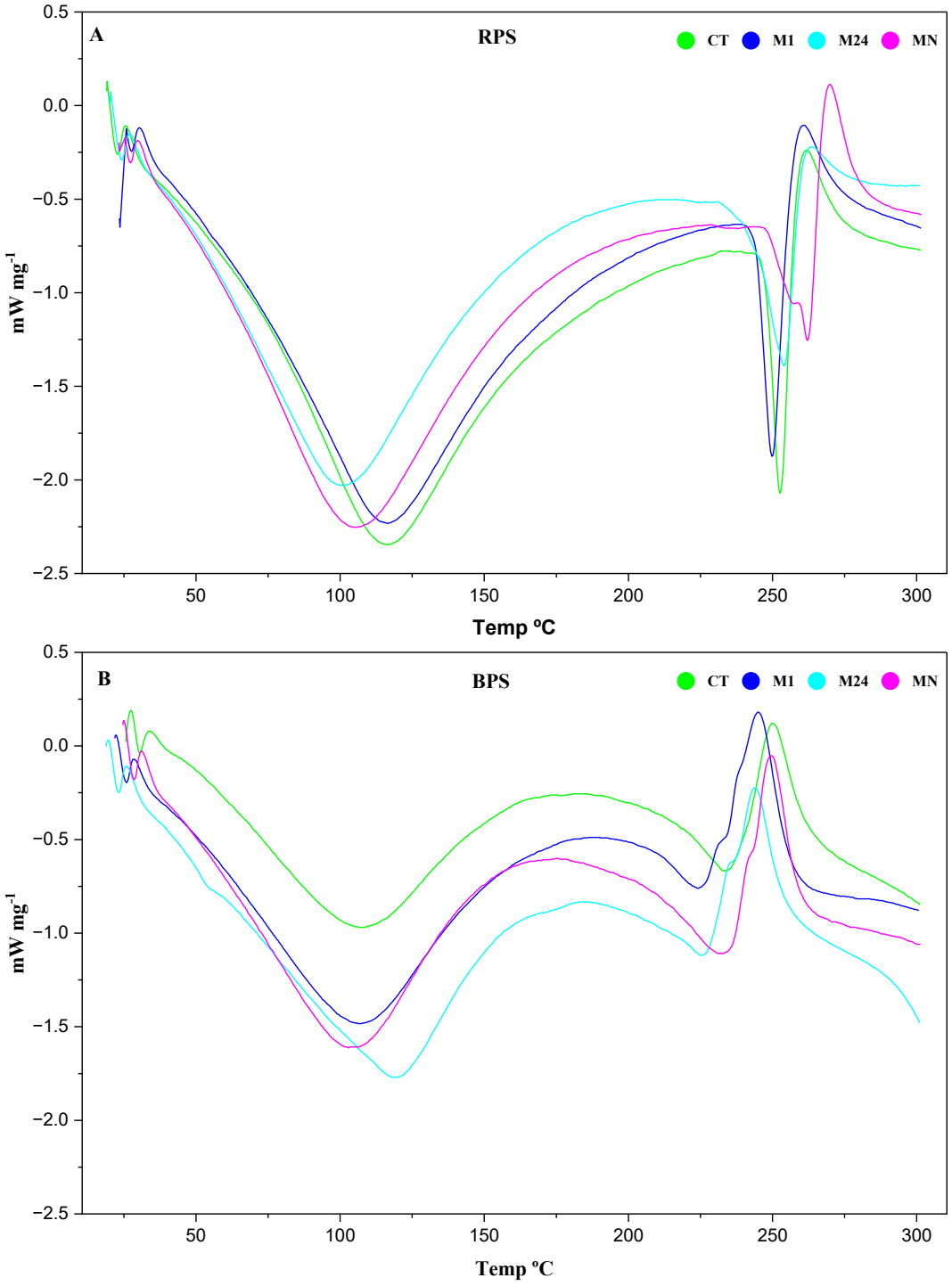
stability is consistent with a more compact or ordered chain arrangement, possibly involving changes in branching patterns or side-group composition that delay the onset of thermal degradation (Barboríková *et al.*, 2019). The higher char residue formed by M1 at elevated temperatures indicates that M1 treatment may have produced a polymer with high protein content and inorganic salt content, which are known to favor carbonaceous residue formation during pyrolysis (Lezcano *et al.*, 2025).

Overall, *P. purpureum EPS* behaves as a heteropolysaccharide exhibiting a characteristic multistep degradation profile, with distinct thermal events arising from glycosidic bond cleavage and further contributions from substituted groups, including sulfates and uronic acids, as well as the protein fraction associated with the polymer matrix. This pattern is consistent with the thermal behavior reported for other microbial and plant-derived EPS (Koçer *et al.*, 2021; Leal *et al.*, 2026; Mothé; Freitas, 2018). In microalgae, the thermally stable char-forming fraction is generally associated with proteins and carbohydrate fractions with higher mineral content, which collectively favor carbonaceous residue formation during thermal decomposition (Lezcano *et al.*, 2025). The influence of magnetic field exposure and nanofiber supplementation on cultivation conditions, represented by the M1, M24, and MN treatments, appears to modulate these structural features to varying degrees, as evidenced by the inter-sample differences in moisture content, degradation temperature, and residual mass observed across both fractions.

3.2.2 Differential Scanning Calorimetry (DSC)

Differential scanning calorimetry (DSC) analysis of the EPS (Figure 3) corroborated the thermal events identified by TGA, revealing two apparent thermal transitions. A low-temperature endothermic event observed between 100 and 118 °C is attributed to the release of strongly bound water retained within the polysaccharide matrix, consistent with the initial mass loss stage identified in TGA (Dong *et al.*, 2026). A broader high-temperature transition between 225 and 281 °C corresponds to structural relaxation and thermal degradation of the polysaccharide network, in agreement with the primary glycosidic bond cleavage event observed by TGA in the 220–400 °C range. The range of both DSC events reflects the chemical heterogeneity of the EPS, likely arising from variation in branching degree, sulfate group distribution along the polymer chains, and compositional differences between the released and bound fractions.

Figure 3-DSC curves of RPS (A) and BPS (B). CT: control; M1: magnetic field 1 h d^{-1}; M24: magnetic field 24 h d^{-1}; MN: magnetic field 1 h d^{-1} with nanofibers.



The absence of sharp melting peaks or crystallization exotherms in the DSC profiles confirms the predominantly amorphous character of the *P. purpureum* EPS. This is expected for highly branched, associated with protein fraction, in which the structural irregularity of the backbone prevents the formation of ordered crystalline domains (Akter *et al.*, 2026). Taken together, the DSC and TGA profiles characterize the EPS as an amorphous biopolymer with moderate thermal stability. The onset of major decomposition above approximately 250 °C indicates that the material can tolerate common drying procedures and low-temperature processing steps without significant structural degradation (Jakhu *et al.*, 2021).

Although RPS and BPS share a similar overall thermal behavior, differences in transition intensity, peak breadth, and apparent structural ordering suggest that the two fractions are not identical in molecular organization. These differences likely reflect fractionation-related divergences in molecular packing and hydration state, rather than a fundamentally different polysaccharide backbone. Further characterization by complementary techniques, such as modulated DSC (MDSC) or X-ray diffraction, would be valuable to resolve potential subtle differences in chain ordering and to confirm the absence of crystalline domains.

From an applied perspective, the thermal behavior of *P. purpureum* EPS supports its suitability for low-temperature processing applications, including the drying, formulation of films, gels, stabilizers, coatings, and active delivery matrices. The combination of moderate thermal stability, high water-binding capacity, and predominantly amorphous structure is consistent with the use of this EPS as a bioactive ingredient in food, cosmetic, aquaculture, and biomedical formulations, rather than as a high-temperature structural polymer (Benalaya *et al.*, 2024; Maulina *et al.*, 2025).

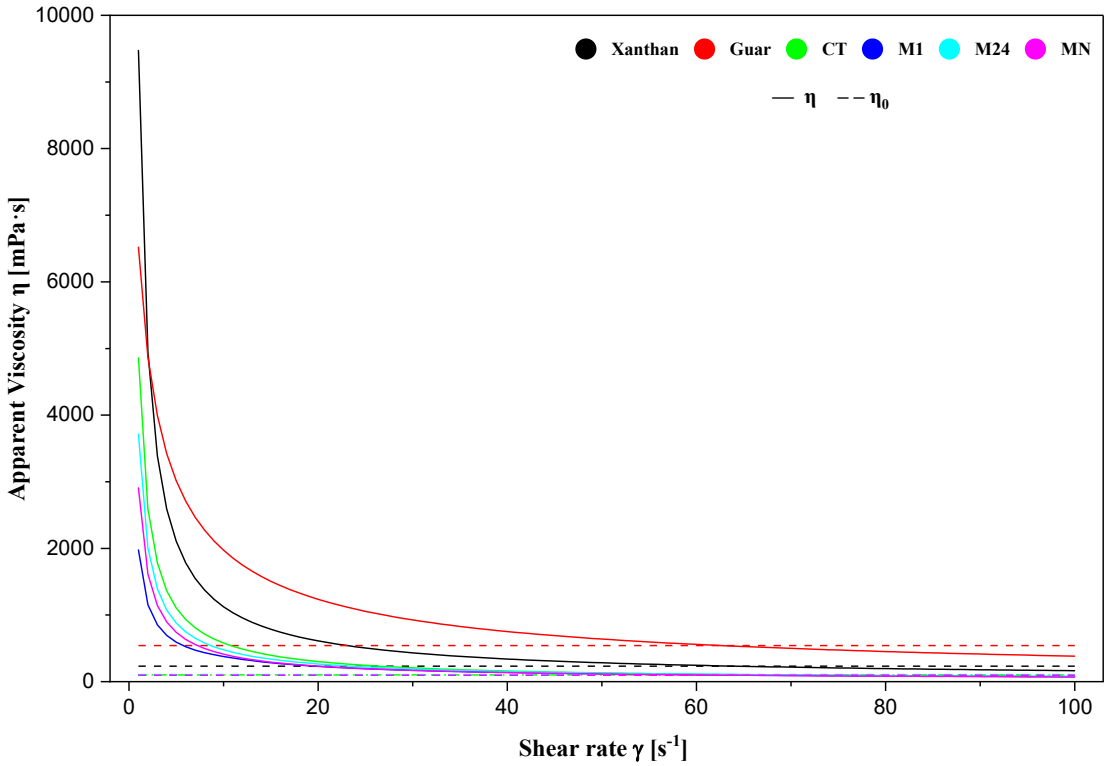
3.3 RHEOLOGY ASSAYS

3.3.1 Apparent viscosity assay

The apparent viscosity (η) and frequency sweep of RPS compared to xanthan and guar gum 1% (w v^{-1}) aqueous solution are shown in Figure 4. BPS was not evaluated due to the low-yielding production. The viscosity (η) decreased continuously with increasing shear rate over the range of 1 to 100 s^{-1}, confirming the non-Newtonian, pseudoplastic character of all biopolymers tested. Xanthan gum showed the highest η (9471.4 mPa·s) at a shear rate of 1 s^{-1}, while the lowest was

observed for M1 (1975.5 mPa·s). CT (4860.4 mPa·s) showed the highest η among the tested RPS samples. The results indicate a higher molecular weight and/or greater stiffness of the xanthan gum polymer chains compared with the *P. purpureum* RPS under low shear rates (Yunus; Parisi, 2024). The studied treated RPS showed a lower viscosity than CT, probably due to alterations in the polymeric chain, caused by the treatments increasing chain flexibility. By shear rate 100 s^{-1}, viscosity had decreased substantially for all samples, converging toward a narrow band of η values between 68.7 and 162.6 mPa·s, reflecting the progressive disruption of polymer network structure under increasing hydrodynamic stress (Wang, M.; Yin; Zeng, 2022).

Figure 4- Flow curves of the studied polymeric solutions 1% m v^{-1}.CT: control; M1: magnetic field 1 h d^{-1}; M24: magnetic field 24 h d^{-1}; MN: magnetic field 1 h d^{-1} with nanofibers.



All samples approached their respective Newtonian plateau(η_0) at shear rates of approximately 54–58 s^{-1}. The Newtonian regression plateaus confirmed limiting high-shear viscosity, not exhibiting thixotropic behavior (Hu *et al.*, 2026). The convergence of apparent viscosities toward the Newtonian plateau in the range of 54–58 s^{-1} across all RPS samples, despite their differing absolute viscosities and flow indices, suggests that complete network disruption

occurs within a similar window of hydrodynamic stress for all treatments, which may reflect a common backbone chemistry and molecular architecture of the *Porphyridium* RPS regardless of cultivation condition.

Flow curves were fitted to the power-law model in the shear-thinning region up to 54 s^{-1}, which adequately described the experimental data(Yunus; Parisi, 2024) The flow behavior index (n) and consistency index (K) were then determined, with lower n values indicating stronger pseudoplastic behavior. The control RPS (CT) exhibited the strongest shear-thinning behavior among all samples (n = 0.0644, K = 4952.221 mPa·s^n), followed by xanthan gum (n = 0.1134, K = 8820.638 mPa·s^n) and M24 (n = 0.1468, K = 3461.784 mPa·s^n). MN and M1 showed progressively weaker shear-thinning behavior with n = 0.1764 and 0.2819, respectively. In contrast, guar gum displayed the highest flow behavior index (n = 0.3565, K = 8214.857 mPa·s^n). Therefore, CT exhibited the strongest shear-thinning behavior, indicated by the lowest n value, meaning its viscosity decreased most rapidly as shear rate increased. Xanthan gum, despite having a higher K value, showed slightly weaker shear-thinning behavior, indicating greater viscosity at low shear but less sensitivity to changes in shear rate than CT. Guar gum displayed the weakest shear-thinning behavior, with the highest n value, consistent with a more gradual reduction in viscosity under shear. The viscosity reduction between 1 and 100 s^{-1} was most pronounced for CT (98.5%) and xanthan gum (98.3%), followed by M24 (98.0%), MN (97.6%), M1 (96.3%), and guar gum (94.2%).

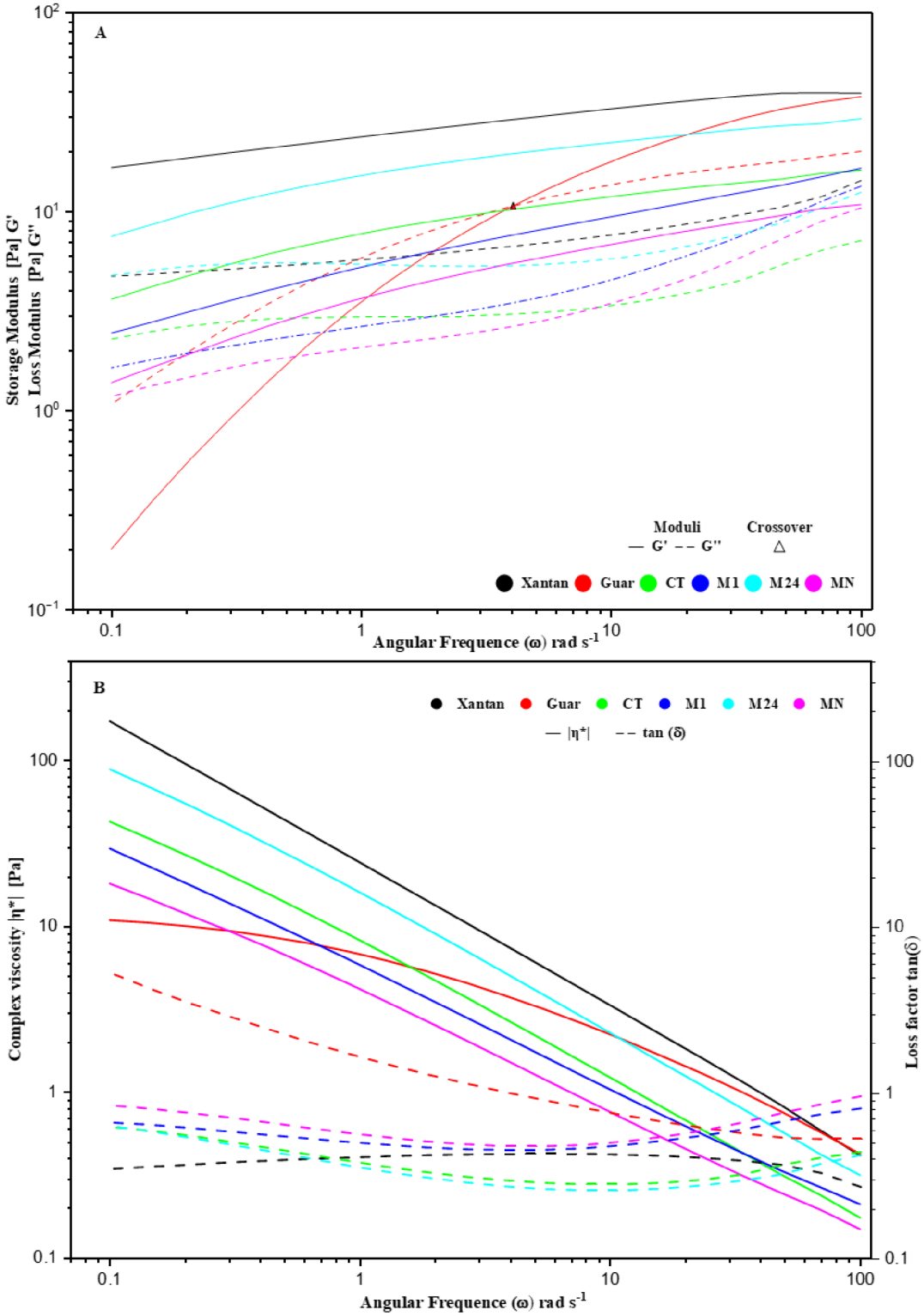
3.3.2 Frequency sweep

The viscoelastic profile of the *Porphyridium purpureum* RPS solutions was evaluated by oscillatory frequency sweep at 25 °C and compared against xanthan and guar gum as commercial reference biopolymers (Figure 5A). Comparing the rheological properties of *P. purpureum* RPS against these commercial standards is therefore essential to assess its functional competitiveness and applied potential.

For all RPS samples and xanthan gum, the storage modulus (G′) exceeded the loss modulus (G″) across the entire angular frequency range tested (0.1–100 rad s^{-1}), confirming a predominant elastic, gel-like character (Caccavo *et al.*, 2018). In contrast, guar gum exhibited a gel-to-solution transition with a crossover point (G′ = G″ ≈ 11.54 Pa) at approximately 4.04 rad s^{-1}, indicating

liquid-like behavior at low deformation frequencies and a transition to elastic-dominant behavior only at higher frequencies (Yunus; Parisi, 2024).

Figure 5 - Frequency sweeps of elastic and viscous moduli (A) and complex viscosity (|η*|), loss factor vs angular frequency (B) of the studied polymeric solutions 1% m v^{-1}. CT: control; M1: magnetic field 1 h d^{-1}; M24: magnetic field 24 h d^{-1}; MN: magnetic field 1 h d^{-1} with nanofibers.



Among the RPS samples, the continuous magnetic field condition (M24) produced the strongest viscoelastic network, with G′ values of 17.10 Pa and 22.56 Pa at 1 and 10 rad s^{-1}, respectively, approaching approximately 66% of the G′ values recorded for xanthan gum (25.89 and 33.32 Pa at the same frequencies). The control RPS (CT) showed intermediate elasticity (G′ = 8.86 Pa at 1 rad s^{-1}), whereas the intermittent magnetic field treatment (M1) yielded slightly lower G′ values (6.23 Pa at 1 rad s^{-1}), suggesting that short daily exposure to magnetic fields does not enhance and may slightly reduce the structural organization of the RPS network relative to the control. The combined treatment with nanofibers (MN) produced the lowest G′ among all conditions (G′ = 4.43 Pa at 1 rad s^{-1}), indicating that the addition of nanofibers, in combination with the magnetic field stimulus, reduced the storage modulus and weakened gel-like behavior of the RPS solutions. This behavior may be associated with differences in the molecular structure of the RPS produced under these treatments.

The frequency dependence of G′ is reflected in the calculated slopes, which ranged from 0.186 for M24 to 0.291 for MN, compared with 0.133 for xanthan gum. This suggests that the EPS networks are physically cross-linked rather than chemically fixed, relying on non-covalent interactions such as hydrogen bonding, electrostatic associations, and polymer chain entanglements(Stojkov *et al.*, 2021). Such behavior is well documented for sulfated microalgal polysaccharides, whose gel character is largely governed by the degree of sulfation, molecular weight distribution, and the presence of uronic acid and glycoproteins that promote inter-chain associations(Bernaerts *et al.*, 2019; Eteshola *et al.*, 1998; Medina-Cabrera *et al.*, 2020). The relatively shallow frequency dependence of M24 (slope = 0.186) suggests that continuous magnetic field exposure during cultivation may promote the formation of a more interactive and entangled network than intermittent exposure (M1, slope = 0.269) or the combined nanofiber treatment (MN, slope = 0.291), both of which show greater G′ sensitivity to frequency and therefore less developed network structures. The frequency sweep profiles obtained for all *P. purpureum* RPS samples are consistent with the rheological behavior of weak-to-intermediate physical gels, characterized by a predominance of G′ over G″(Figure 5A) across the entire frequency window examined (Duarte *et al.*, 2026).

A significant discrepancy emerges when comparing the flow curve (Figure 4) and oscillatory data (Figure 5A) for the CT and M24 samples: despite CT exhibiting higher apparent viscosity than M24 (4860.4 vs. 3712.6 mPa·s at 1 s^{-1}), M24 consistently showed higher storage

modulus values in the frequency sweep (G' = 17.10 vs. 8.86 Pa at 1 rad s^{-1}). This contradiction can be understood by recognizing that apparent viscosity under steady shear and elastic modulus under oscillatory strain probe fundamentally different aspects of polymer network behavior. High apparent viscosity at low shear rates reflects resistance to flow. It is strongly influenced by hydrodynamic volume, polymer concentration, and molecular entanglement density. In contrast, G' reflects the capacity of the network to store elastic energy, which depends more critically on the strength and lifetime of physical cross-links and junction zones (Saiev *et al.*, 2023).

Therefore, CT RPS might consist of higher molecular weight or more extended polymer chains that generate substantial hydrodynamic resistance under flow, yet form fewer or weaker physical cross-links capable of sustaining elastic stress under oscillatory deformation. In contrast, M24 treatment may have produced an RPS with a more organized network architecture, probably due to a higher density of branching points that participate in junction formation (Sorichetti *et al.*, 2023), a greater abundance of associative functional groups, stronger inter-chain interaction (Xue *et al.*, 2024), or a larger fraction of ordered helical segments that promote helix–helix aggregation (Liu, G. *et al.*, 2022). As a result, M24 behaves more elastically, even if its individual chains are not maximized in hydrodynamic volume, because its elasticity is dominated by the strength and connectivity of the network rather than by single-chain coil size. Similar behavior has been reported for associative polysaccharide systems, where introducing additional binding sites or promoting ordered segments modulates G′ and shear-thinning without a proportional increase in hydrodynamic volume (Blanco-López *et al.*, 2021; Yunus; Parisi, 2024). This would explain the lower flow behavior index of CT (n = 0.079) compared to M24 (n = 0.176): the more abrupt viscosity collapse of CT under shear is indicative of a network that disrupts easily, yielding rapidly to flow alignment, whereas the more gradual thinning of M24 reflects a network that resists disruption more progressively (Münstedt, 2021). However, direct structural evidence through techniques such as SEC-MALS, HPGPC, or NMR would be required to confirm this interpretation.

All samples exhibited pronounced shear-thinning behavior, with complex viscosity ($|\eta^*|$) decreasing monotonically with increasing angular frequency (Figure 5B). At 0.1 rad s^{-1}, $|\eta^*|$ followed the order: xanthan (172.81 Pa·s) > M24 (88.92 Pa·s) > CT (42.89 Pa·s) > M1 (29.55 Pa·s) > MN (18.16 Pa·s) > guar (10.95 Pa·s). The power-law slopes of the $|\eta^*|$–ω curves ranged from −0.866 (xanthan) to −0.472 (guar), with the EPS treatments falling between −0.708 (MN) and

−0.828 (M24), indicating M24 treatment produces RPS that flow behavior most closely resembles xanthan gum among the samples tested.

The loss factor profiles (Figure 5B) provided further information on the differences in molecular network between the polymer solutions studied. M24 presented the lowest tan δ values among the RPS samples, ranging from 0.261 to 0.637, with a minimum recorded at mid-range frequencies (7.85–11.3 rad s^{-1}), a pattern consistent with a well-developed, frequency-stable elastic network (Yunus; Parisi, 2024). The CT and M1 samples showed progressively higher tan δ values (minima of 0.274 and 0.457, respectively), confirming weaker but still gel-like structures. The MN treatment approached the gel–sol threshold, with tan δ reaching 0.962 at 100 rad s^{-1}, indicating that elasticity is substantially compromised at high deformation rates. Xanthan gum maintained tan δ values between 0.274 and 0.434 throughout the frequency range, reflecting its well-known robust network structure (Yunus; Parisi, 2024). Guar gum presented the highest tan δ values (0.532 – 5.328), indicating the viscous response and a less elastic network under low shear conditions.

The proximity of M24 to xanthan gum in tan δ is particularly noteworthy, as xanthan is among the most widely used biopolymer thickeners and gelling agents in food, cosmetic, and pharmaceutical industries, prized precisely for its high elastic modulus and shear-thinning behavior (Eghbaljoo *et al.*, 2022). *P. Purpureum* RPS produced under continuous magnetic field stimulation approaches xanthan's elastic dominance without chemical modification, suggesting meaningful biotechnological potential. Guar gum, by contrast, behaved as a viscoelastic fluid at low frequencies, with the gel-to-solution crossover occurring at approximately 4.04 rad s^{-1}, confirming that it lacks a stable gel network under still or low shear conditions, a well-known limitation of galactomannan-based gums relative to bacterial exopolysaccharides (Dille; Haug; Draget, 2021).

The contrasting rheological outcomes between M1 and M24 merit mechanistic consideration. Magnetic fields have been reported to influence microalgal physiology through multiple pathways, including alterations in membrane permeability(Deamici; Morais; *et al.*, 2022), modulation of reactive oxygen species signaling, and upregulation of carbohydrate biosynthesis genes (Font *et al.*, 2023; Santos *et al.*, 2022). The substantial improvement in gel strength observed under continuous exposure (M24) relative to intermittent exposure (M1) suggests that the cellular response to the magnetic field stimulus is time-dependent, requiring sustained activation to positively affect RPS weak gel behavior, which might occur due to branching, active substitute groups, and/or the increase of polymerization. The latter is a key element since higher molecular

weight polysaccharides form more entanglements per chain, directly increasing *G'* and reducing frequency dependence, which is consistent with the rheological data (Eghbaljoo *et al.*, 2022). The absence, and even slight deterioration, in weak gel properties of MN RPS indicates that nanofibers alter the culture's physicochemical environment in a way that disrupts EPS chain assembly. This could be due to the increased turbulence, altered light distribution, or adsorption of secreted polysaccharide onto the nanofiber surface, of the higher molecular weight, or before its complete formation.

The pronounced shear-thinning behavior exhibited by all samples, with power-law slopes of $|\eta^*|$ (Figure 5B) between −0.708 and −0.866, is a highly desirable property for industrial applications as it implies ease of pumping and processing at high shear rates while recovering structural integrity and viscosity at rest (Sayko; Jacobs; Dobrynin, 2021). The steeper slope of M24 (−0.824) relative to M1 (−0.714) and MN (−0.780) is consistent with the hypothesis of a more branched or structurally organized polymer network in M24; however, direct structural evidence through techniques such as SEC-MALS or NMR would be required to confirm this interpretation. Especially, the large dynamic range of complex viscosity for M24, from 88.92 Pa·s at 0.1 rad s^{-1} to 0.32 Pa·s at 100 rad s^{-1}, spanning nearly three orders of magnitude, is comparable to the behavior of xanthan gum (172.81 to 0.42 Pa·s) and substantially greater than that of guar gum (10.95 to 0.43 Pa·s), reinforcing the suitability of M24-derived EPS as a functional biopolymer ingredient. Therefore, the results indicate that continuous magnetic field exposure represents a promising, non-invasive cultivation strategy to enhance the rheological functionality of *Porphyridium Purpureum* RPS, requiring further investigation into the underlying biosynthetic mechanisms and the structural characterization of the polysaccharide fractions responsible for the observed differences.

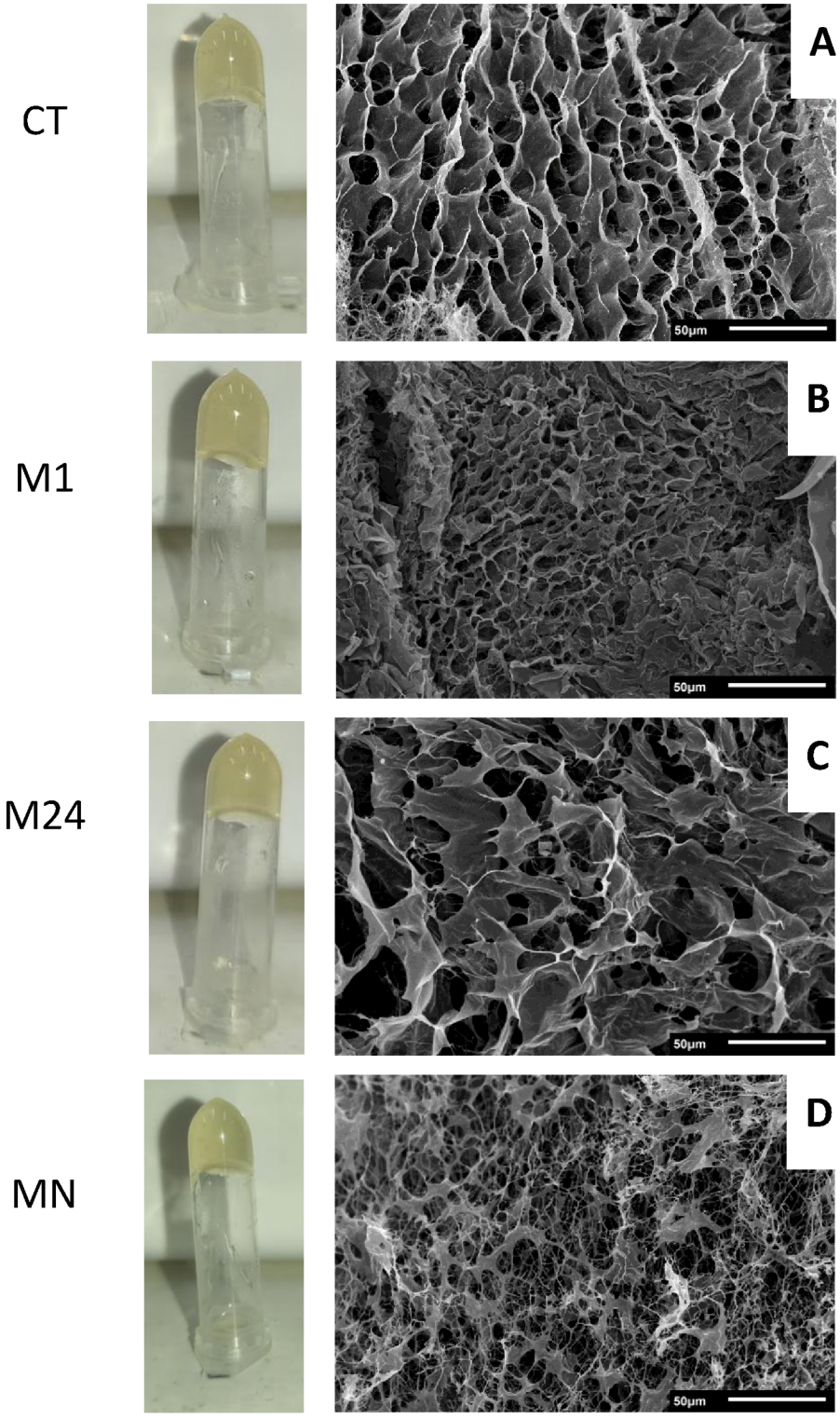
3.4 HYDROGELS MORPHOLOGY

Physical hydrogel networks rely on reversible interactions between polymer chains, including hydrogen bonds, ionic bonds, hydrophobic, and hydrophilic interactions (Stojkov *et al.*, 2021). The main gelation mechanism in this study was ionic cross-linking, using Fe^{3+} as binding sites, forming structural gels as shown in Figure 6.

CT RPS (Figure 6A) formed a well-developed, interconnected macroporous network with thick, predominantly sheet-like walls arranged in a vertically elongated orientation, with relatively

uniform pore sizes (Feret diameter 11.09 ± 2.4 μm). The continuity and thickness of the walls suggest a high local polymer density at the junction zones established by Fe^{3+} coordination, consistent with the higher apparent viscosity of CT EPS observed in flow curve measurements, which reflects the large hydrodynamic volume of its native polymer chains. A uniform macroporous architecture supports a possible, predictable, direction-independent mass transport and a consistent mechanical response, properties that favor applications requiring reproducible diffusion characteristics, such as controlled drug release matrices (Ong *et al.*, 2018; Stojkov *et al.*, 2021). The thick walls also increase resistance to pore collapse during swelling or *compressive* loading, improving handling stability (Ong *et al.*, 2018).

Figure 6 - Hydrogels SEM images of RPS solution 1% (w v^{-1}) added of 0.3% (w v^{-1}) $Fe_2(SO_4)_3$. CT: control; M1: magnetic field 1 h d^{-1}; M24: magnetic field 24 h d^{-1}; MN: magnetic field 1 h d^{-1} with nanofibers.



M1 RPS (Figure 6B) produced a structurally similar but slightly less ordered macroporous network with comparable pore dimensions (10.09 ± 2.09 μm) and sheet-like walls of moderate thickness. The wall surfaces appeared rougher and more folded than those of CT RPS, indicating a less homogeneous polymer matrix. Given that M1 RPS exhibited lower elastic modulus and higher loss factor than CT RPS in oscillatory rheology, the less consolidated wall morphology is consistent with a weaker or less extensive cross-linked network in the precursor polymer (Stojkov *et al.*, 2021). Nonetheless, the overall macroporous connectivity of M1 RPS is preserved, suggesting adequate gelation capacity for scaffold applications where absolute stiffness is less critical than structural openness.

M24 RPS (Figure 6C) displayed a different macrostructure of larger pores with substantially greater size heterogeneity (16.06 ± 6.66 μm Feret diameter), thinner and more angular walls with sharp edges, and a prominent fibrillar component decorating and bridging wall structures. The combination of broad pore-size distribution, angular wall geometry, and fibrils is indicative of a gel formed from a compositionally complex, heterogeneous polymer population in which network coalescence was spatially incomplete (Annabi *et al.*, 2010; Tan *et al.*, 2024). Fibrillar architectures of this type are commonly observed in hydrogels derived from heteropolymers or from polymers capable of forming ordered secondary structures, such as helical assemblies or β-sheet-like aggregates, that preferentially segregate into elongated fibers rather than homogeneous lamellae during cross-linking (Tan *et al.*, 2024). This morphology would produce an anisotropic, strain-dependent mechanical response governed not only by the wall structure but also by fiber stretching, bending, and junction rearrangement at small and intermediate strains (Martikainen *et al.*, 2020). developed walls in M24 is consistent with the higher storage modulus and lower apparent viscosity observed relative to CT, as a smaller effective polymer volume fraction forming thinner walls, combined with increased branching and functional group density, would favor a more flexible yet resilient network in which fibrils contribute significantly to resistance under oscillatory deformation. Fibrous scaffolds are widely exploited in tissue engineering for their ability to guide cell migration, provide contact guidance cues, and mimic the architecture of collagen-rich extracellular matrices (Xia *et al.*, 2024).

MN RPS (Figure 6D) presented the most architecturally distinctive morphology of all RPS samples: a hierarchical dual-scale structure in which a dense nanofibrillar mesh forms the thin walls of well-defined, uniformly sized honeycomb-like pores (12.15 ± 2.3 μm Feret diameter). This

organization's nanoscale fiber network superimposed on a micrometer-scale pore matrix closely resembles the architecture of native soft-tissue extracellular matrices, where nanofibrillar collagen and glycosaminoglycan networks define the mechanical microenvironment around cells (Xia *et al.*, 2024) . The origin of the fibrillar character in MN RPS can be attributed to the chemical complexity of the polymer produced under the combined magnetic field and nanofiber cultivation condition: polysaccharide matrices with heterogeneous monosaccharide composition, sulfation ratio, and significant protein or proteoglycan content are known to self-assemble into fibrillar architectures during solution gel transitions rather than forming homogeneous sheets. This structure happens due to local chain segments with complementary conformations that can nucleate fibril cores while adjacent incompatible segments are excluded to the interfibrillar space (Chen, Dongning *et al.*, 2020; Pletikapić *et al.*, 2014). This dual-scale porosity confers a mechanically adaptive, strain-stiffening behavior characteristic of fiber-reinforced biological gels, in which compliance at small strains (fiber bending) transitions to stiffening at larger strains (fiber stretching and network locking) (Xia *et al.*, 2024), making MN RPS therefore represents a candidate scaffold material warranting further mechanical characterization and biocompatibility assessment.

The treatments applied to *P. purpureum* directly influenced the architecture of the resulting hydrogels. In the control (CT), thicker wall layers formed a stiffer network, whereas intermittent SMF application (M1) produced thinner walls while largely preserving the CT-like morphology, which may be suitable for matrices designed for slow, controlled release. In contrast, the combined SMF and nanofiber treatment (MN) generated a predominantly fibrillar hydrogel, more consistent with architectures typically exploited for biological and tissue-engineering purposes.

4. CONCLUSION

This study demonstrated that static magnetic field exposure and polymeric nanofiber supplementation during cultivation of *Porphyridium purpureum* meaningfully modulate the molecular architecture, rheological functionality, and hydrogel-forming capacity of released (RPS). FTIR spectroscopy confirmed the structural hallmarks of sulfated heteropolymers across all fractions, while zeta potential values below −30 mV indicated strong colloidal stability driven by sulfate and uronic acid substituents, with treatment-dependent differences in charge density reflecting variation in functional group profile. Thermal analysis confirmed that all fractions are

predominantly amorphous and stable up to approximately 220–250 °C, consistent with suitability for low-temperature processing and formulation into gels, films, coatings, and active delivery matrices.

Rheological characterization revealed that all RPS fractions exhibit shear-thinning behavior and a predominantly elastic, gel-like viscoelastic character comparable to established commercial biopolymers. Continuous magnetic field exposure (M24) consistently produced the most developed viscoelastic network, approaching xanthan gum in elastic dominance and complex viscosity dynamic range without chemical modification. Intermittent exposure (M1) and the combined nanofiber condition (MN) yielded progressively weaker networks, indicating that the RPS produced under magnetic stimulation is cumulative and that nanofiber co-exposure does not synergize with RPS network assembly under the conditions tested.

Scanning electron microscopy of Fe^{3+} ionic gels revealed that cultivation conditions substantially govern hydrogel network architecture. RPS gels ranged from uniform macroporous sheet-like networks (CT, M1) to fibrillar-laminar hybrid structures (M24) and hierarchical nanofibrillar meshes with uniform micrometer-scale pores (MN), the latter presenting a tissue-mimetic architecture of particular interest for biomedical scaffold applications.

These results establish continuous magnetic field (M24) exposure as a promising non-invasive strategy for enhancing the rheological performance of *P. purpureum* RPS, and nanofiber co-treatment as a route toward biomimetic gel architectures (MN). Key limitations include the absence of molecular weight data and quantitative gel rheometry, which constrain mechanistic interpretation. Future work should prioritize SEC-MALS characterization, oscillatory rheology of the gel state, and in vitro biocompatibility assessment, positioning *P. purpureum* EPS as a competitive, sustainably sourced alternative to conventional biopolymers in food, cosmetic, and biomedical applications.

ACKNOWLEDGEMENT

This study was financed in part by the Coordenação de Aperfeiçoamento de Pessoal de Nível Superior—Brasil (CAPES)—Finance Code 001. This research was funded by the Program CAPES-COFECUB (Sv 945/19).

REFERENCES

AHMAD, N. H.; AHMED, J.; HASHIM, D. M.; MANAP, Y. A.; MUSTAFA, S. Oscillatory and steady shear rheology of gellan/dextran blends. **Journal of Food Science and Technology**, vol. 52, no. 5, pp. 2902–2909, 1 May 2015. DOI: 10.1007/s13197-014-1330-x. Available at: http://link.springer.com/10.1007/s13197-014-1330-x.

AKTER, F.; MONDAL, A. K.; MESTRES, G.; GUSTAFSSON, J.; RALPH, P. J.; KUZHIUMPARAMBIL, U. Unravelling Rheology and Structural Properties of Polysaccharides from *Porphyridium Purpureum* After Alkali Pre-Treatment. **Macromolecular Bioscience**, vol. 26, no. 3, pp. 1–17, 2026. https://doi.org/10.1002/mabi.202500522.

ALVAREZ, X.; ALVES, A.; RIBEIRO, M. P.; LAZZARI, M.; COUTINHO, P.; OTERO, A. Biochemical characterization of Nostoc sp. exopolysaccharides and evaluation of potential use in wound healing. **Carbohydrate Polymers**, vol. 254, no. June 2020, p. 117303, Feb. 2021. DOI: 10.1016/j.carbpol.2020.117303. Available at: https://doi.org/10.1016/j.carbpol.2020.117303.

ANNABI, N.; NICHOL, J. W.; ZHONG, X.; JI, C.; KOSHY, S.; KHADEMHOSSEINI, A.; DEHGHANI, F. Controlling the porosity and microarchitecture of hydrogels for tissue engineering. vol. 16, no. 4, pp. 371–383, 2010. https://doi.org/10.1089/ten.teb.2009.0639.

ASTM INTERNATIONAL. D3850–12:Standard test method for rapid thermal degradation of solid electrical insulating materials by thermogravimetric method (TGA) West Conshohocken: **ASTM**, 2013.

ASTM INTERNATIONAL. E986-04:Standard Practice for Scanning Electron Microscope Beam Size Characterization. 2004.

BARBORÍKOVÁ, J.; ŠUTOVSKÁ, M.; KAZIMIEROVÁ, I.; JOŠKOVÁ, M.; FRAŇOVÁ, S.; KOPECKÝ, J.; CAPEK, P. Extracellular polysaccharide produced by *Chlorella vulgaris* – Chemical characterization and anti-asthmatic profile. **International Journal of Biological Macromolecules**, vol. 135, no. 7, pp. 1–11, Aug. 2019. DOI: 10.1016/j.ijbiomac.2019.05.104. Available at: https://linkinghub.elsevier.com/retrieve/pii/S0141813019322536.

BARBOSA, J. A. C.; ABDELSADIG, M. S. E.; CONWAY, B. R.; MERCHANT, H. A. Using zeta potential to study the ionisation behaviour of polymers employed in modified-release dosage forms and estimating their pKa. **International Journal of Pharmaceutics: X**, vol. 1, no. March, p. 100024, Dec. 2019. DOI: 10.1016/j.ijpx.2019.100024. Available at: https://doi.org/10.1016/j.ijpx.2019.100024.

BARIZÃO, A. C. de L.; BRANDÃO, L. L.; GOMES, L. E. de O.; OLIVEIRA, J. P. de; CASSINI, S. T. Optimizing microalgae culture conditions for high-value biomolecules production. **Algae Biotechnology for Biomedical and Nutritional Applications**. Elsevier, 2025. pp. 325–347. DOI: 10.1016/B978-0-443-24006-5.00008-0. Available at: https://linkinghub.elsevier.com/retrieve/pii/B9780443240065000080.

BENALAYA, I.; ALVES, G.; LOPES, J.; SILVA, L. R. A Review of Natural Polysaccharides: Sources, Characteristics, Properties, Food, and Pharmaceutical Applications. **International Journal of Molecular Sciences**, vol. 25, no. 2, 2024. https://doi.org/10.3390/ijms25021322.

BERNAERTS, T. M. M.; GHEYSEN, L.; FOUBERT, I.; HENDRICKX, M. E.; VAN LOEY, A. M. The potential of microalgae and their biopolymers as structuring ingredients in food: A review. **Biotechnology Advances**, vol. 37, no. 8, p. 107419, Dec. 2019. DOI: 10.1016/j.biotechadv.2019.107419. Available at: https://doi.org/10.1016/j.biotechadv.2019.107419.

BERNAERTS, T. M. M.; KYOMUGASHO, C.; VAN LOOVEREN, N.; GHEYSEN, L.; FOUBERT, I.; HENDRICKX, M. E.; VAN LOEY, A. M. Molecular and rheological characterization of different cell wall fractions of *Porphyridium cruentum*. **Carbohydrate Polymers**, vol. 195, no. February, pp. 542–550, 2018. DOI: 10.1016/j.carbpol.2018.05.001. Available at: https://doi.org/10.1016/j.carbpol.2018.05.001.

BLANCO-LÓPEZ, M.; GONZÁLEZ-GARCINUÑO, Á.; TABERNERO, A.; MARTÍN DEL VALLE, E. M. Steady and Oscillatory Shear Flow Behavior of Different Polysaccharides with Laponite®. **Polymers**, vol. 13, no. 6, p. 966, 22 Mar. 2021. DOI: 10.3390/polym13060966. Available at: https://www.mdpi.com/2073-4360/13/6/966.

BLANCO, I.; SIRACUSA, V. The Use of Thermal Techniques in the Characterization of Bio-Sourced Polymers. **Materials**, vol. 14, no. 7, p. 1686, 30 Mar. 2021. DOI: 10.3390/ma14071686. Available at: https://www.mdpi.com/1996-1944/14/7/1686.

BORJAS ESQUEDA, A.; GARDARIN, C.; LAROCHE, C. Exploring the Diversity of Red Microalgae for Exopolysaccharide Production. **Marine Drugs**, vol. 20, no. 4, p. 246, 31 Mar. 2022. DOI: 10.3390/md20040246. Available at: https://www.mdpi.com/1660-3397/20/4/246/htm. Accessed: 1 Aug. 2022.

CACCAVO, D.; CASCONE, S.; LAMBERTI, G.; BARBA, A. A. Hydrogels: Experimental characterization and mathematical modelling of their mechanical and diffusive behaviour. **Chemical Society Reviews**, vol. 47, no. 7, pp. 2357–2373, 2018. DOI: 10.1039/c7cs00638a. Available at: http://dx.doi.org/10.1039/C7CS00638A.

CANO-SARMIENTO, C.; TÉLLEZ-MEDINA, D. I.; VIVEROS-CONTRERAS, R.; CORNEJO-MAZÓN, M.; FIGUEROA-HERNÁNDEZ, C. Y.; GARCÍA-ARMENTA, E.; ALAMILLA-BELTRÁN, L.; GARCÍA, H. S.; GUTIÉRREZ-LÓPEZ, G. F. Zeta Potential of Food Matrices. **Food Engineering Reviews**, vol. 10, no. 3, pp. 113–138, 5 Sep. 2018. DOI: 10.1007/s12393-018-9176-z. Available at: http://link.springer.com/10.1007/s12393-018-9176-z.

CARDIAS, B. B.; MORAIS, M. G. de; COSTA, J. A. V. Increased biomass and biomolecule productivity of *Spirulina sp.* LEB 18 cultivated with CO_2 adsorbent nanofibers. **Clean Technologies and Environmental Policy**, no. 0123456789, 15 Jun. 2024. DOI: 10.1007/s10098-024-02907-x. Available at: https://doi.org/10.1007/s10098-024-02907-x.

CARVALHO, M. P. de; MORAIS, M. G. de; SANTOS, L. O. dos; LAROCHE, C.; COSTA, J.

A. V. Production of biomass and biomolecules in *Limnospira indica* PCC 8005 cultivation under magnetic fields and polymeric nanofibers. **Journal of Biotechnology**, vol. 405, no. October 2024, pp. 48–56, Sep. 2025. DOI: 10.1016/j.jbiotec.2025.05.004. Available at: https://linkinghub.elsevier.com/retrieve/pii/S0168165625001142.

CHEN, D.; SMITH, L. R.; KHANDEKAR, G.; PATEL, P.; YU, C. K.; ZHANG, K.; CHEN, C. S.; HAN, L.; WELLS, R. G. Distinct effects of different matrix proteoglycans on collagen fibrillogenesis and cell-mediated collagen reorganization. **Scientific Reports**, vol. 10, no. 1, pp. 1–13, 2020. DOI: 10.1038/s41598-020-76107-0. Available at: https://doi.org/10.1038/s41598-020-76107-0.

CHOPIN, T.; KERIN, B. F.; MAZEROLLE, R. Phycocolloid chemistry as a taxonomic indicator of phylogeny in the *Gigartinales*, Rhodophyceae: A review and current developments using Fourier transform infrared diffuse reflectance spectroscopy. **Phycological Research**, vol. 47, no. 3, pp. 167–188, Sep. 1999. DOI: 10.1046/j.1440-1835.1999.00170.x. Available at: http://doi.wiley.com/10.1046/j.1440-1835.1999.00170.x.

DEAMICI, K. M.; MORAIS, M. G. de; DOS SANTOS, L. O.; GROS, F.; COSTA, J. A. V.; LAROCHE, C. Magnetic Field Action on *Limnospira indica* PCC8005 Cultures: Enhancement of Biomass Yield and Protein Content. **Applied Sciences**, vol. 12, no. 3, p. 1533, 31 Jan. 2022. DOI: 10.3390/app12031533. Available at: https://www.mdpi.com/2076-3417/12/3/1533.

DILLE, M. J.; HAUG, I. J.; DRAGET, K. I. Gelatin and collagen. **Handbook of Hydrocolloids**. Elsevier, 1 Jan. 2021. pp. 1073–1097. DOI: 10.1016/B978-0-12-820104-6.00028-0. Available at: https://linkinghub.elsevier.com/retrieve/pii/B9780128201046000280. Accessed: 31 Oct. 2022.

DONG, W.; MAZZARA, E.; SÁNCHEZ-BACA, A.; MONDAL, K.; VILLAMIEL, M.; BABU, R.; SUN, D.-W.; TIWARI, B. K. A comparative study on heterogeneous deacetylation of chitin to chitosan under various ultrasound irradiation and characterization. **Ultrasonics Sonochemistry**, vol. 128, no. November 2025, p. 107794, May 2026. DOI: 10.1016/j.ultsonch.2026.107794. Available at: https://linkinghub.elsevier.com/retrieve/pii/S1350417726000593.

DUARTE, M. M.; SUPRINOVYCH, A.; VEIGA, A.; LOPES, A. I.; TAVARIA, F. K.; MORAIS, R. C.; OLIVEIRA, A. L. Hydrogel-Forming Ability and Biological Characterization of Exopolysaccharide (EPS) from *Porphyridium cruentum*. **Gels**, vol. 12, no. 5, p. 352, 23 Apr. 2026. DOI: 10.3390/gels12050352. Available at: https://www.mdpi.com/2310-2861/12/5/352.
EFREMENKO, E.; SENKO, O.; TEPLOVA, K.; ASLANLI, A. Biomass of Microalgae and Other Phototrophic Microorganisms: Current Trends in Regulation of Its Accumulation and Application of Immobilized Forms. **Applied Sciences**, vol. 15, no. 23, p. 12775, 2 Dec. 2025. DOI: 10.3390/app152312775. Available at: https://www.mdpi.com/2076-3417/15/23/12775.

EGHBALJOO, H.; SANI, I. K.; SANI, M. A.; RAHATI, S.; MANSOURI, E.; MOLAEE-AGHAEE, E.; FATOUREHCHI, N.; KADI, A.; ARAB, A.; SARABANDI, K.; SAMBORSKA, K.; JAFARI, S. M. Advances in plant gum polysaccharides; Sources, techno-functional properties, and applications in the food industry - A review. **International Journal of Biological Macromolecules**, vol. 222, no. PB, pp. 2327–2340, Dec. 2022. DOI:

10.1016/j.ijbiomac.2022.10.020. Available at: https://doi.org/10.1016/j.ijbiomac.2022.10.020.

ETESHOLA, E.; KARPASAS, M.; ARAD, S.; GOTTLIEB, M. Red microalga exopolysaccharides: 2. Study of the rheology, morphology and thermal gelation of aqueous preparations. **Acta Polymerica**, vol. 49, nos. 10–11, pp. 549–556, Oct. 1998. DOI: 10.1002/(SICI)1521-4044(199810)49:10/11<549::AID-APOL549>3.0.CO;2-T. Available at: https://onlinelibrary.wiley.com/doi/10.1002/(SICI)1521-4044(199810)49:10/11%3C549::AID-APOL549%3E3.0.CO;2-T.

FILALI MOUHIM, R.; CORNET, J. F.; FONTANE, T.; FOURNET, B.; DUBERTRET, G. Production, isolation and preliminary characterization of the exopolysaccharide of the cyanobacterium *Spirulina platensis*. **Biotechnology Letters 1993 15:6**, vol. 15, no. 6, pp. 567–572, 1993. DOI: 10.1007/BF00138541. Available at: https://link.springer.com/article/10.1007/BF00138541. Accessed: 12 Sep. 2022.

FONT, Y. S.; DÍAZ, Y. O.; CUYPERS, A.; ALEMÁN, E. I.; VANDAMME, D. The effect of magnetic field treatment on the cultivation of microalgae: An overview of involved mechanisms. **Journal of Applied Phycology**, vol. 35, no. 4, pp. 1525–1536, 1 Aug. 2023. https://doi.org/10.1007/s10811-023-02994-1.

GÓMEZ-ORDÓÑEZ, E.; RUPÉREZ, P. FTIR-ATR spectroscopy as a tool for polysaccharide identification in edible brown and red seaweeds. **Food Hydrocolloids**, vol. 25, no. 6, pp. 1514–1520, Aug. 2011. DOI: 10.1016/j.foodhyd.2011.02.009. Available at: http://dx.doi.org/10.1016/j.foodhyd.2011.02.009.

GUERREIRO, M.; EMMANUEL, C.; DUPUITS, C.; GARDARIN, C.; MOUZEYAR, S.; ROCHE, J.; LAROCHE, C. Transcriptomic Insights into Metabolic Reprogramming and Exopolysaccharide Synthesis in Porphyridium purpureum Under Gradual Nitrogen Deprivation. pp. 1–28, 2026.

HU, X.; DAI, S.; LIU, C.; ZHANG, C.; ZHAO, Z.; QIAO, L.; XU, J.; JIN, H.; XU, X.; YANG, Z.; LI, J.; HUANG, L.; MU, Y.; HUANG, H. Exploration into the structural characteristics and functional properties of exopolysaccharide synthesized by *Pseudoduganella armeniaca* ZMN–3. **International Journal of Biological Macromolecules**, vol. 366, no. April, p. 152375, 2026. DOI: 10.1016/j.ijbiomac.2026.152375. Available at: https://doi.org/10.1016/j.ijbiomac.2026.152375.

ILYIN, S. O. Structural Rheology in the Development and Study of Complex Polymer Materials. **Polymers**, vol. 16, no. 17, p. 2458, 29 Aug. 2024. DOI: 10.3390/polym16172458. Available at: https://www.mdpi.com/2073-4360/16/17/2458.

JAKHU, S.; SHARMA, Y.; SHARMA, K.; VAID, K.; DHAR, H.; KUMAR, V.; SINGH, R. P.; SHEKH, A.; KUMAR, G. Production and characterization of microalgal exopolysaccharide as a reducing and stabilizing agent for green synthesis of gold-nanoparticle: a case study with a *Chlorella sp*. from Himalayan high-altitude psychrophilic habitat. **Journal of Applied Phycology**, vol. 33, no. 6, pp. 3899–3914, 1 Dec. 2021. DOI: 10.1007/s10811-021-02580-3. Available at: https://link.springer.com/article/10.1007/s10811-021-02580-3. Accessed: 9 Sep.

2022.

KIM, T. H.; LEE, K.; OH, B. R.; LEE, M. E.; SEO, M.; LI, S.; KIM, J. K.; CHOI, M.; CHANG, Y. K. A novel process for the coproduction of biojet fuel and high-value polyunsaturated fatty acid esters from heterotrophic microalgae *Schizochytrium sp*. ABC101. **Renewable Energy**, vol. 165, pp. 481–490, 2021. DOI: 10.1016/j.renene.2020.09.116. Available at: https://doi.org/10.1016/j.renene.2020.09.116.

KOÇER, A. T.; İNAN, B.; KAPTAN USUL, S.; ÖZÇIMEN, D.; YILMAZ, M. T.; IŞILDAK, İ. Exopolysaccharides from microalgae: production, characterization, optimization and techno-economic assessment. **Brazilian Journal of Microbiology**, vol. 52, no. 4, pp. 1779–1790, 11 Dec. 2021. DOI: 10.1007/s42770-021-00575-3. Available at: https://link.springer.com/article/10.1007/s42770-021-00575-3. Accessed: 1 Aug. 2022.

LAROCHE, C. Exopolysaccharides from Microalgae and Cyanobacteria: Diversity of Strains, Production Strategies, and Applications. **Marine Drugs**, vol. 20, no. 5, p. 336, 21 May 2022. DOI: 10.3390/md20050336. Available at: https://doi.org/10.3390/md20050336. Accessed: 29 Jul. 2022.

LEAL, G. B. C.; SANTOS, K. N. dos; SARPAL, A. S.; COSTA, J. A. V. Two-stage cultivation of the microalga *Chlorella fusca* LEB 111 using the phytohormone indole-3-acetic acid and nitrogen reduction for assessment of aviation fuel applications. **Biomass and Bioenergy**, vol. 210, no. December 2025, p. 109046, 2026. DOI: 10.1016/j.biombioe.2026.109046. Available at: https://doi.org/10.1016/j.biombioe.2026.109046.

LEZCANO, G.; GAUTAM, R.; HITA, I.; YERRAYYA, A.; ALJAZIRI, J.; DE FREITAS, B. B.; SAMARAS, V. G.; LAUERSEN, K. J.; SARATHY, S. M.; CASTAÑO, P. Linking microalgae characteristics with their fast pyrolysis products. **Journal of Analytical and Applied Pyrolysis**, vol. 191, no. May, p. 107170, Oct. 2025. DOI: 10.1016/j.jaap.2025.107170. Available at: https://linkinghub.elsevier.com/retrieve/pii/S0165237025002232.

LI, T.; XU, J.; WANG, W.; CHEN, Z.; LI, C.; WU, H.; WU, H.; XIANG, W. A Novel Three-Step Extraction Strategy for High-Value Products from Red Algae *Porphyridium purpureum*. **Foods**, vol. 10, no. 9, p. 2164, 13 Sep. 2021. DOI: 10.3390/foods10092164. Available at: https://www.mdpi.com/2304-8158/10/9/2164.

LIU, G.; FU, K.; WANG, X.; QIAN, C.; LIU, J.; WANG, D.; WANG, H.; ZHU, L.; ZHAO, Y. One-Dimensional Helical Aggregates Organized from Achiral Imine-Based Polymers. **ACS Materials Letters**, vol. 4, no. 4, pp. 715–723, 4 Apr. 2022. DOI: 10.1021/acsmaterialslett.2c00111. Available at: https://pubs.acs.org/doi/10.1021/acsmaterialslett.2c00111.

MARÉCHAL, Y. Interaction configurations of H2O molecules in a protein (Stratum Corneum) by infrared spectrometry. **Journal of Molecular Structure**, vol. 416, nos. 1–3, pp. 133–143, Oct. 1997. DOI: 10.1016/S0022-2860(97)00032-X. Available at: https://linkinghub.elsevier.com/retrieve/pii/S002228609700032X. Accessed: 11 Apr. 2024.

MARTIKAINEN, L.; BERTULA, K.; TURUNEN, M.; IKKALA, O. Strain Stiffening and Negative Normal Force of Agarose Hydrogels. **Macromolecules**, vol. 53, no. 22, pp. 9983–9992, 24 Nov. 2020. DOI: 10.1021/acs.macromol.0c00601. Available at: https://pubs.acs.org/doi/10.1021/acs.macromol.0c00601.

MAULINA, D.; MUN'IM, A.; BAYU, A.; SETIAWAN, H.; MOHD HASHIM, N. Sulfated Exopolysaccharides from *Porphyridium purpureum*: A Review of Extraction, Structural Characterization, and Chemical Properties for Advanced Applications. **F1000Research**, vol. 14, p. 1323, 27 Nov. 2025. DOI: 10.12688/f1000research.173006.1. Available at: https://f1000research.com/articles/14-1323/v1.

MEDINA-CABRERA, E. V.; RÜHMANN, B.; SCHMID, J.; SIEBER, V. Characterization and comparison of *Porphyridium sordidum* and *Porphyridium purpureum* concerning growth characteristics and polysaccharide production. **Algal Research**, vol. 49, no. October 2019, p. 101931, Aug. 2020. DOI: 10.1016/j.algal.2020.101931. Available at: https://doi.org/10.1016/j.algal.2020.101931.

MOLAEI, H.; JAHANBIN, K. Structural features of a new water-soluble polysaccharide from the gum exudates of Amygdalus scoparia Spach (Zedo gum). 2017. DOI: 10.1016/j.carbpol.2017.10.099. Available at: www.elsevier.com/locate/carbpol. Accessed: 21 May 2024.

MOTHÉ, C. G.; FREITAS, J. S. de. Lifetime prediction and kinetic parameters of thermal decomposition of cashew gum by thermal analysis. **Journal of Thermal Analysis and Calorimetry**, vol. 131, no. 1, pp. 397–404, 28 Jan. 2018. DOI: 10.1007/s10973-017-6844-9. Available at: https://doi.org/10.1007/s10973-017-6844-9.

MÜNSTEDT, H. Rheological Measurements and Structural Analysis of Polymeric Materials. **Polymers**, vol. 13, no. 7, p. 1123, 1 Apr. 2021. DOI: 10.3390/polym13071123. Available at: https://www.mdpi.com/2073-4360/13/7/1123.

NURAZZI, N. M.; ASYRAF, M. R. M.; RAYUNG, M.; NORRRAHIM, M. N. F.; SHAZLEEN, S. S.; RANI, M. S. A.; SHAFI, A. R.; AISYAH, H. A.; RADZI, M. H. M.; SABARUDDIN, F. A.; ILYAS, R. A.; ZAINUDIN, E. S.; ABDAN, K. Thermogravimetric Analysis Properties of Cellulosic Natural Fiber Polymer Composites: A Review on Influence of Chemical Treatments. **Polymers**, vol. 13, no. 16, p. 2710, 13 Aug. 2021. DOI: 10.3390/polym13162710. Available at: https://www.mdpi.com/2073-4360/13/16/2710.

ONG, Y. X. J.; LEE, L. Y.; DAVOODI, P.; WANG, C. H. Production of drug-releasing biodegradable microporous scaffold using a two-step micro-encapsulation/supercritical foaming process. **Journal of Supercritical Fluids**, vol. 133, no. July 2017, pp. 263–269, 2018. DOI: 10.1016/j.supflu.2017.10.018. Available at: https://doi.org/10.1016/j.supflu.2017.10.018.

PHÉLIPPÉ, M.; GONÇALVES, O.; THOUAND, G.; COGNE, G.; LAROCHE, C. Characterization of the polysaccharides chemical diversity of the cyanobacteria *Arthrospira platensis*. **Algal Research**, vol. 38, no. December 2018, p. 101426, 2019. DOI: 10.1016/j.algal.2019.101426. Available at: https://doi.org/10.1016/j.algal.2019.101426.

PLETIKAPIĆ, G.; LANNON, H.; MURVAI, Ü.; KELLERMAYER, M. S. Z.; SVETLIČIĆ, V.; BRUJIC, J. Self-Assembly of Polysaccharides Gives Rise to Distinct Mechanical Signatures in Marine Gels. **Biophysical Journal**, vol. 107, no. 2, pp. 355–364, Jul. 2014. DOI: 10.1016/j.bpj.2014.04.065. Available at: https://linkinghub.elsevier.com/retrieve/pii/S0006349514006043.

RAWAT, E.; SHARMA, S.; VYAS, S.; ALSAIDAN, O. A.; KAPOOR, D. U.; PRAJAPATI, B. G. Advances in alginate-based nanoformulations: Innovative and effective strategies for targeting and treating brain disorders. **International Journal of Pharmaceutics**, vol. 681, no. May, p. 125851, Aug. 2025. DOI: 10.1016/j.ijpharm.2025.125851. Available at: https://doi.org/10.1016/j.ijpharm.2025.125851.

RAZAVI, S. M. A.; CUI, S. W.; GUO, Q.; DING, H. Some physicochemical properties of sage (*Salvia macrosiphon*) seedgum. **Food Hydrocolloids**, vol. 35, pp. 453–462, 2014. DOI: 10.1016/j.foodhyd.2013.06.022. Available at: http://dx.doi.org/10.1016/j.foodhyd.2013.06.022.

SAIEV, S.; BELJONNE, D.; LAZZARONI, R.; ROOSE, P. Decoding Elasticity Build-Up and Network Topology in Free-Radical Cross-Linking Polymerization: A Combined Experimental and Atomistic Approach. **Macromolecules**, vol. 56, no. 18, pp. 7396–7405, 26 Sep. 2023. DOI: 10.1021/acs.macromol.3c00644. Available at: https://pubs.acs.org/doi/10.1021/acs.macromol.3c00644.

SANTOS, L. O.; SILVA, P. G. P.; MACHADO, B. R.; SALA, L.; DEAMICI, K. M. Update on the application of magnetic fields to microalgal cultures. **World Journal of Microbiology and Biotechnology**, vol. 38, no. 11, pp. 1–10, 2 Nov. 2022. DOI: 10.1007/s11274-022-03398-y. Available at: https://link.springer.com/article/10.1007/s11274-022-03398-y. Accessed: 3 Oct. 2022.

SAYKO, R.; JACOBS, M.; DOBRYNIN, A. V. Quantifying Properties of Polysaccharide Solutions. **ACS Polymers Au**, vol. 1, no. 3, pp. 196–205, 8 Dec. 2021. DOI: 10.1021/acspolymersau.1c00028. Available at: https://pubs.acs.org/doi/10.1021/acspolymersau.1c00028.

SOANEN, N.; DA SILVA, E.; GARDARIN, C.; MICHAUD, P.; LAROCHE, C. Improvement of exopolysaccharide production by *Porphyridium marinum*. **Bioresource Technology**, vol. 213, pp. 231–238, 2016. DOI: 10.1016/j.biortech.2016.02.075. Available at: http://dx.doi.org/10.1016/j.biortech.2016.02.075.

SORICHETTI, V.; NINARELLO, A.; RUIZ-FRANCO, J.; HUGOUVIEUX, V.; ZACCARELLI, E.; MICHELETTI, C.; KOB, W.; ROVIGATTI, L. Structure and elasticity of model disordered, polydisperse, and defect-free polymer networks. **Journal of Chemical Physics**, vol. 158, no. 7, 2023. DOI: 10.1063/5.0134271. Available at: https://doi.org/10.1063/5.0134271.

STOJKOV, G.; NIYAZOV, Z.; PICCHIONI, F.; BOSE, R. K. Relationship between Structure and Rheology of Hydrogels for Various Applications. **Gels**, vol. 7, no. 4, p. 255, 9 Dec. 2021. DOI: 10.3390/gels7040255. Available at: https://www.mdpi.com/2310-2861/7/4/255.

TAN, T.; HOU, Y.; SHI, J.; WANG, B.; ZHANG, Y. Materials Today Bio Biostable hydrogels consisting of hybrid β -sheet fibrils assembled by a pair of enantiomeric peptides. **Materials Today Bio**, vol. 25, no. January, p. 100961, 2024. DOI: 10.1016/j.mtbio.2024.100961. Available at: https://doi.org/10.1016/j.mtbio.2024.100961.

USOV, A. I.; ZELINSKY, N. D. Chemical structures of algal polysaccharides. **Functional Ingredients from Algae for Foods and Nutraceuticals**. Elsevier, 2013. no. 2011, pp. 23–86. DOI: 10.1533/9780857098689.1.23. Available at: http://dx.doi.org/10.1533/9780857098689.1.23.

WANG, M.; YIN, Z.; ZENG, M. Microalgae as a promising structure ingredient in food: Obtained by simple thermal and high-speed shearing homogenization. **Food Hydrocolloids**, vol. 131, no. April, p. 107743, Oct. 2022. DOI: 10.1016/j.foodhyd.2022.107743. Available at: https://doi.org/10.1016/j.foodhyd.2022.107743.

WANG, X.; ZHANG, Z.; YAO, Q.; ZHAO, M.; QI, H. Phosphorylation of low-molecular-weight polysaccharide from *Enteromorpha linza* with antioxidant activity. **Carbohydrate Polymers**, vol. 96, no. 2, pp. 371–375, Jul. 2013. DOI: 10.1016/j.carbpol.2013.04.029. Available at: http://dx.doi.org/10.1016/j.carbpol.2013.04.029.

WIERCIGROCH, E.; SZAFRANIEC, E.; CZAMARA, K.; PACIA, M. Z.; MAJZNER, K.; KOCHAN, K.; KACZOR, A.; BARANSKA, M.; MALEK, K. Raman and infrared spectroscopy of carbohydrates: A review. **Spectrochimica Acta - Part A: Molecular and Biomolecular Spectroscopy**, vol. 185, pp. 317–335, 2017. DOI: 10.1016/j.saa.2017.05.045. Available at: http://dx.doi.org/10.1016/j.saa.2017.05.045.

XIA, P.; ZHANG, W.; PENG, C.; YIN, H.; WANG, D. M.; YANG, J.; TUAN, R. S.; JIANG, L.; WANG, J. A High-Order Double Network Hydrogel. **Macromolecules**, vol. 57, no. 23, pp. 11251–11265, 2024. https://doi.org/10.1021/acs.macromol.4c01880.

XUE, J.-T.; BAI, Y.; PENG, L.; HUANG, X.-B.; SUN, Z.-Y. Exploring the Interplay between Local Chain Structure and Stress Distribution in Polymer Networks. **Chinese Journal of Polymer Science**, vol. 42, no. 6, pp. 874–885, 7 Jun. 2024. DOI: 10.1007/s10118-024-3099-3. Available at: https://link.springer.com/10.1007/s10118-024-3099-3.

YUNUS, R. A. M.; PARISI, D. Scaling Laws in Polysaccharide Rheology: Comparative Analysis of Water and Ionic Liquid Systems. **Biomacromolecules**, vol. 25, no. 10, pp. 6883–6898, 14 Oct. 2024. DOI: 10.1021/acs.biomac.4c01125. Available at: https://pubs.acs.org/doi/10.1021/acs.biomac.4c01125.

ZHANG, J.; LIU, L.; REN, Y.; CHEN, F. Characterization of exopolysaccharides produced by microalgae with antitumor activity on human colon cancer cells. **International Journal of Biological Macromolecules**, vol. 128, pp. 761–767, 2019. DOI: 10.1016/j.ijbiomac.2019.02.009. Available at: https://doi.org/10.1016/j.ijbiomac.2019.02.009.

CHAPTER IV

GENERAL CONCLUSION

This thesis investigated the use of physical stimuli static magnetic fields (SMF) and functionalized polyacrylonitrile (PAN) nanofibers as tools for bioprocess intensification and product modulation in two microalgal species: *Limnospira indica* PCC8005 and *Porphyridium purpureum*.

The first study demonstrated that SMF and PAN nanofibers exert distinct and partially antagonistic effects on the metabolism of *L. indica*. SMF promoted biomass accumulation (+28%) and enhanced photosynthetic pigment synthesis, whereas nanofiber exposure redirected metabolic flux toward carbohydrate production (+39%) at the expense of pigment content. The combined treatment revealed that these stimuli engage independent metabolic pathways, establishing the basis for a combinatorial approach to bioprocess control.

The second study extended this framework to *P. purpureum* and demonstrated that the temporal pattern of SMF exposure is a critical variable. Intermittent SMF maximized biomass yield (+36%), while MEA-functionalized nanofibers induced a pronounced shift toward pigment synthesis, with β-phycoerythrin content increasing by 196% relative to control cultures. These results confirm that physical stimuli can be used to selectively favor either biomass or high-value metabolite production within the same organism, depending on the regime applied.

The third study examined the structural and rheological consequences of stimulus exposure on the EPS produced by *P. purpureum*. Prolonged SMF treatment (M24) yielded RPS forming a viscoelastic network with properties comparable to xanthan gum, while the RPS of the combined SMF-nanofiber (NM) treatment produced a hierarchical nanofibrillar hydrogel with tissue-mimetic architecture. These findings demonstrate that the studded physical stimuli do not merely influence the quantity of EPS produced, but also its molecular organization and functional properties. The polymers obtained exhibited thermal stability up to 220–250°C, amorphous character, and high colloidal stability (zeta potential < -30 mV), confirming their suitability for high-value applications.

Collectively, these results establish that the cultivation environment can be used as a molecular design parameter. Through the deliberate selection and combination of SMF regimes and functionalized nanofibers, it is possible to direct microalgal metabolism and pre-engineer the structural properties of the resulting biopolymers without genetic modification or chemical

induction. This positions physical stimulus-based bioprocess design as a viable strategy for the production of tailored, sustainable biopolymers from microalgal sources.

CONCLUSÃO GERAL

Esta tese investigou o uso de estímulos físicos campos magnéticos estáticos (CME) e nanofibras de poliacrilonitrila (PAN) funcionalizadas como ferramentas para a intensificação de bioprocessos e modulação de produtos em duas espécies de microalgas: *Limnospira indica* PCC8005 e *Porphyridium purpureum* CCAP 1380/1A.

O primeiro estudo demonstrou que o CME e as nanofibras de PAN exercem efeitos distintos e parcialmente antagônicos no metabolismo da *L. indica*. O CME promoveu o acúmulo de biomassa (+28%) e aumentou a síntese de pigmentos fotossintéticos, enquanto a exposição às nanofibras redirecionou o fluxo metabólico para a produção de carboidratos (+39%) em detrimento do conteúdo de pigmentos. O tratamento combinado revelou que esses estímulos acionam vias metabólicas independentes, estabelecendo a base para uma abordagem combinatória no controle de bioprocessos.

O segundo estudo estendeu esses estímulos para o cultivo de *P. purpureum* e demonstrou que o padrão temporal de exposição ao CME é uma variável crítica. O CME intermitente maximizou o rendimento de biomassa (+36%), enquanto as nanofibras funcionalizadas com MEA induziram uma mudança acentuada em direção à síntese de pigmentos, com o conteúdo de β-ficoeritrina aumentando-o 296% em relação às culturas de controle. Esses resultados confirmam que estímulos físicos podem ser usados para favorecer seletivamente a produção de biomassa ou de metabólitos de alto valor dentro do mesmo organismo, dependendo do regime aplicado.

O terceiro estudo examinou as consequências estruturais e reológicas da exposição aos estímulos nos EPS produzidos pela *P. purpureum*. O tratamento prolongado com CME (M24) resultou em RPS que formam uma rede viscoelástica com propriedades comparáveis à goma xantana, enquanto o RPS do tratamento combinado CME-nanofibra produziu um hidrogel nanofibrilar hierárquico com arquitetura biomimética tecidual. Esses achados demonstram que os estímulos físicos estudados não influenciam apenas a quantidade de EPS produzida, mas também sua organização molecular, e como consequência, nas propriedades funcionais. Os polímeros obtidos exibiram estabilidade térmica de até 220–250 °C, caráter amorfo e alta estabilidade coloidal (potencial zeta < −30 mV), confirmando sua adequação para processos com temperaturas moderadas e de alto valor agregada na indústria farmacêutica, alimentícia e biotecnológica.

Coletivamente, esses resultados *indica*m que o ambiente de cultivo pode ser utilizado como um parâmetro para modular metabolitos de alto valor agregado. Através da seleção deliberada e combinação de regimes de CME e nanofibras funcionalizadas, é possível direcionar o metabolismo microalgal e pré-projetar as propriedades estruturais dos biopolímeros resultantes sem modificação genética ou indução química. Isso posiciona o design de bioprocessos baseado em estímulos físicos como uma estratégia viável para a produção de biopolímeros sustentáveis e personalizados a partir de fontes microalgais.

CHAPTER V

GENERATED WASTE AND DESTINATION

During the experimental and analytical stages, liquid wastes consisting of solvents used for biomass and EPS characterization were generated. Upon completion of the analyses, these residues were stored in properly labeled vials and set aside by solvent type. Disposal was carried out in strict accordance with the current waste management regulations of the Federal University of Rio Grande (FURG) and the Université Clermont Auvergne (UCA).

SUGGESTIONS FOR FUTURE WORK

Several directions emerge naturally from this work, spanning stimulus optimization, polymer characterization, and applied material development.

Stimulus optimization for *P. purpureum*. - The results of this thesis were obtained under fixed stimulus intensities and exposure durations. A systematic investigation varying SMF intensity and application time would help define optimal windows for each metabolic outcome. Of particular interest is the potential of sequential stimulus strategies that adapt to the physiological state of the culture. For example, given that intermittent SMF (1 h/day) strongly promotes growth during the exponential phase, a two-stage protocol could be envisioned in which SMF exposure is extended to 24 h/day during the final days of cultivation to redirect metabolism toward EPS synthesis once biomass targets have been met. Similarly, the introduction of functionalized nanofibers after the exponential phase, rather than from inoculation, could decouple growth maximization from pigment development, potentially combining the benefits observed separately in Papers 2.

Deeper polymer characterization - The structural and rheological properties of the EPS described in Paper 3 warrant further investigation at the molecular level. Determination of molecular weight distribution and structural characterization would provide a more complete picture of how physical stimuli alter polymer chemistry. Equally important is the evaluation of low-temperature performance, which is relevant for cold-chain applications and cryopreservation contexts but has not yet been assessed for these polymers. The hydrogels obtained should also be characterized more thoroughly as functional materials, including measurements of gel strength, swelling capacity, water retention, and controlled release kinetics of encapsulated compounds, critical properties for any prospective application in delivery systems or biomaterials.

Applied material development. - The unique architectural and physicochemical properties of the stimulus-derived EPS open several applied research areas. Blending these polymers with other biopolymers or bioactive compounds could be explored to assess synergistic effects on antioxidant activity, antimicrobial performance, and hydration capacity. A particularly promising application is the development of wound dressings, where the combination of viscoelastic behavior, high water retention, colloidal stability, and potential bioactivity could meet the functional requirements of advanced wound care materials. Beyond biomedical uses, these EPS could serve

as wall materials in microencapsulation systems, providing protective matrices for high-value microorganisms or degradable compounds such as probiotics, antioxidants, phenolics, and vitamins, where their thermal stability and film-forming capacity would be clear assets.

Molecular signaling characterization - The mechanisms by which SMF and nanofibers are perceived at the cellular level remain to be elucidated. Transcriptomic or proteomic analyses conducted under defined stimulus conditions would identify the signaling pathways underlying the metabolic shifts observed, enabling more rational and targeted bioprocess design in future studies.

Techno-economic and life cycle assessment - A techno-economic analysis comparing physical stimulus-based production of microalgal EPS against conventional high-value microalgae compounds production would clarify the commercial feasibility of this approach and identify the process steps where efficiency gains are most needed, providing a practical roadmap for scale-up.

CHAPTER VI

REFERENCES

AI, X.; YU, P.; LI, X.; LAI, X.; YANG, M.; LIU, F.; LUAN, F.; MENG, X. Polysaccharides from Spirulina platensis: Extraction methods, structural features and bioactivities diversity. **International Journal of Biological Macromolecules**, vol. 231, no. 1166, p. 123211, Mar. 2023. DOI: 10.1016/j.ijbiomac.2023.123211. Available at: https://doi.org/10.1016/j.ijbiomac.2023.123211.

AKTER, F.; MONDAL, A. K.; MESTRES, G.; GUSTAFSSON, J.; RALPH, P. J.; KUZHIUMPARAMBIL, U. Unravelling Rheology and Structural Properties of Polysaccharides from *Porphyridium Purpureum* After Alkali Pre-Treatment. **Macromolecular Bioscience**, vol. 26, no. 3, pp. 1–17, 2026. https://doi.org/10.1002/mabi.202500522.

ALMEIDA, A. C. A. de; VAZ, S.; COSTA, J. A. V.; MORAIS, M. G. de. Innovative technology for microalgal cell preservation through immobilization in polylactic acid nanofibers. **Algal Research**, vol. 84, no. May, p. 103781, 2024. DOI: 10.1016/j.algal.2024.103781. Available at: https://doi.org/10.1016/j.algal.2024.103781.

ALVAREZ, X.; ALVES, A.; RIBEIRO, M. P.; LAZZARI, M.; COUTINHO, P.; OTERO, A. Biochemical characterization of *Nostoc sp*. exopolysaccharides and evaluation of potential use in wound healing. **Carbohydrate Polymers**, vol. 254, no. June 2020, p. 117303, Feb. 2021. DOI: 10.1016/j.carbpol.2020.117303. Available at: https://doi.org/10.1016/j.carbpol.2020.117303.

ALY, H. F.; RIZK, M. Z.; SHAMS, S. G. E. Microalgae in food and feed: Safety and toxicological aspects. **Handbook of Food and Feed from Microalgae: Production, Application, Regulation, and Sustainability**. Elsevier, 1 Jan. 2023. pp. 549–565. https://doi.org/10.1016/B978-0-323-99196-4.00004-8.

AMERICAN PUBLIC HEALTH ASSOCIATION. **Standard Methods for the Examination of Water and Wastewater**. Washington DC,USA: American Public Health Association, 1971. 237–239 pp.

ANG, W. S.; KEE, P. E.; LAN, J. C.-W.; CHEN, W.-H.; CHANG, J.-S.; KHOO, K. S. Unveiling the rise of microalgae-based foods in the global market: Perspective views and way forward. **Food Bioscience**, vol. 66, p. 105390, Apr. 2025. DOI: 10.1016/j.fbio.2024.105390. Available at: https://linkinghub.elsevier.com/retrieve/pii/S2212429224018212.

ANNABI, N.; NICHOL, J. W.; ZHONG, X.; JI, C.; KOSHY, S.; KHADEMHOSSEINI, A.; DEHGHANI, F. Controlling the porosity and microarchitecture of hydrogels for tissue engineering. vol. 16, no. 4, pp. 371–383, 2010. https://doi.org/10.1089/ten.teb.2009.0639.

ARAD, S. (Malis); LEVY-ONTMAN, O. Sulfated Polysaccharides in the Cell Wall of Red Microalgae. **Handbook of Biopolymer-Based Materials**. Wiley, 24 Apr. 2013. pp. 351–370. DOI: 10.1002/9783527652457.ch12. Available at: https://onlinelibrary.wiley.com/doi/10.1002/9783527652457.ch12.

ASTM INTERNATIONAL. D3850–12:Standard test method for rapid thermal degradation of solid electrical insulating materials by thermogravimetric method (TGA) West Conshohocken: **ASTM**, 2013.

ASTM INTERNATIONAL. E986-04:Standard Practice for Scanning Electron Microscope Beam Size Characterization. 2004.

BA, F.; FOISSARD, A.; LEBERT, A.; DJELVEH, G.; LAROCHE, C. Polyethyleneimine as a tool for compounds fractionation by flocculation in a microalgae biorefinery context. **Bioresource Technology**, vol. 315, p. 123857, Nov. 2020. DOI: 10.1016/j.biortech.2020.123857. Available at: https://linkinghub.elsevier.com/retrieve/pii/S0960852420311299.

BABIAK, W.; KRZEMIŃSKA, I. Extracellular Polymeric Substances (EPS) as Microalgal Bioproducts: A Review of Factors Affecting EPS Synthesis and Application in Flocculation Processes. **Energies 2021, Vol. 14, Page 4007**, vol. 14, no. 13, p. 4007, 2 Jul. 2021. DOI: 10.3390/EN14134007. Available at: https://www.mdpi.com/1996-1073/14/13/4007/htm. Accessed: 1 Aug. 2022.

BARBORÍKOVÁ, J.; ŠUTOVSKÁ, M.; KAZIMIEROVÁ, I.; JOŠKOVÁ, M.; FRAŇOVÁ, S.; KOPECKÝ, J.; CAPEK, P. Extracellular polysaccharide produced by *Chlorella vulgaris* – Chemical characterization and anti-asthmatic profile. **International Journal of Biological Macromolecules**, vol. 135, no. 7, pp. 1–11, Aug. 2019. DOI: 10.1016/j.ijbiomac.2019.05.104. Available at: https://linkinghub.elsevier.com/retrieve/pii/S0141813019322536.

BARBOSA, J. A. C.; ABDELSADIG, M. S. E.; CONWAY, B. R.; MERCHANT, H. A. Using zeta potential to study the ionisation behaviour of polymers employed in modified-release dosage forms and estimating their pKa. **International Journal of Pharmaceutics: X**, vol. 1, no. March, p. 100024, Dec. 2019. DOI: 10.1016/j.ijpx.2019.100024. Available at: https://doi.org/10.1016/j.ijpx.2019.100024.

BARIZÃO, A. C. de L.; BRANDÃO, L. L.; GOMES, L. E. de O.; OLIVEIRA, J. P. de; CASSINI, S. T. Optimizing microalgae culture conditions for high-value biomolecules production. **Algae Biotechnology for Biomedical and Nutritional Applications**. Elsevier, 2025. pp. 325–347. DOI: 10.1016/B978-0-443-24006-5.00008-0. Available at: https://linkinghub.elsevier.com/retrieve/pii/B9780443240065000080.

BAYU, A.; NOERDJITO, D. R.; RAHMAWATI, S. I.; PUTRA, M. Y.; KARNJANAKOM, S. Biological and technical aspects on valorization of red microalgae genera *Porphyridium*. **Biomass Conversion and Biorefinery**, vol. 13, no. 14, pp. 12395–12411, 16 Sep. 2023. DOI: 10.1007/s13399-021-02167-5. Available at: https://link.springer.com/10.1007/s13399-021-02167-5. Accessed: 27 Feb. 2024.

BELLEZZA, S.; ALBERTANO, P.; DE PHILIPPIS, R.; PARADOSSI, G. Exopolysaccharides of two cyanobacterial strains from *Roman hypogea*. Jul. 2006. **Geomicrobiology Journal**. Taylor & Francis Group, Jul. 2006. vol. 23, no. 5, pp. 301–310. DOI: 10.1080/01490450600761904. Available at: https://www.tandfonline.com/doi/abs/10.1080/01490450600761904. Accessed: 12 Sep. 2022.

BELLO-MORALES, R.; ANDREU, S.; RUIZ-CARPIO, V.; RIPA, I.; LÓPEZ-GUERRERO, J. A. Extracellular Polymeric Substances: Still Promising Antivirals. **Viruses**, vol. 14, no. 6, 2022. https://doi.org/10.3390/v14061337.

BENALAYA, I.; ALVES, G.; LOPES, J.; SILVA, L. R. A Review of Natural Polysaccharides: Sources, Characteristics, Properties, Food, and Pharmaceutical Applications. **International Journal of Molecular Sciences**, vol. 25, no. 2, 2024. https://doi.org/10.3390/ijms25021322.

BENAVENTE-VALDÉS, J. R.; MÉNDEZ-ZAVALA, A.; HERNÁNDEZ-LÓPEZ, I.; CARREÓN-GONZÁLEZ, B. A.; VELÁZQUEZ-ARELLANO, M. E.; MORALES-OYERVIDES, L.; MONTAÑEZ-SAÉNZ, J. C. Unconventional microalgae species and potential for their use in the food industry. **Cultured Microalgae for the Food Industry: Current and Potential Applications**, pp. 49–71, 2021. https://doi.org/10.1016/B978-0-12-821080-2.00010-1.

BENNETT, A.; BOGORAD, L. COMPLEMENTARY CHROMATIC ADAPTATION IN A FILAMENTOUS BLUE-GREEN ALGA. **The Journal of Cell Biology**, vol. 58, no. 2, pp. 419–435, 1 Aug. 1973. DOI: 10.1083/jcb.58.2.419. Available at: https://rupress.org/jcb/article/58/2/419/18179/COMPLEMENTARY-CHROMATIC-ADAPTATION-IN-A.

BERGES, J. A.; MULHOLLAND, M. R. Enzymes and Nitrogen Cycling. **Nitrogen in the Marine Environment**. Elsevier, 2008. pp. 1385–1444. DOI: 10.1016/B978-0-12-372522-6.00032-3. Available at: https://linkinghub.elsevier.com/retrieve/pii/B9780123725226000323.

BERMEJO ROMÁN, R.; ALVÁREZ-PEZ, J. M.; ACIÉN FERNÁNDEZ, F. G.; MOLINA GRIMA, E. Recovery of pure B-phycoerythrin from the microalga *Porphyridium cruentum*. **Journal of Biotechnology**, vol. 93, no. 1, pp. 73–85, Jan. 2002. DOI: 10.1016/S0168-1656(01)00385-6. Available at: https://linkinghub.elsevier.com/retrieve/pii/S0168165601003856.

BERNAERTS, T. M. M.; GHEYSEN, L.; FOUBERT, I.; HENDRICKX, M. E.; VAN LOEY, A. M. The potential of microalgae and their biopolymers as structuring ingredients in food: A review. **Biotechnology Advances**, vol. 37, no. 8, p. 107419, Dec. 2019. DOI: 10.1016/j.biotechadv.2019.107419. Available at: https://doi.org/10.1016/j.biotechadv.2019.107419.

BERNAERTS, T. M. M.; KYOMUGASHO, C.; VAN LOOVEREN, N.; GHEYSEN, L.; FOUBERT, I.; HENDRICKX, M. E.; VAN LOEY, A. M. Molecular and rheological characterization of different cell wall fractions of *Porphyridium cruentum*. **Carbohydrate Polymers**, vol. 195, no. February, pp. 542–550, 2018. DOI: 10.1016/j.carbpol.2018.05.001. Available at: https://doi.org/10.1016/j.carbpol.2018.05.001.

BLANCO-LÓPEZ, M.; GONZÁLEZ-GARCINUÑO, Á.; TABERNERO, A.; MARTÍN DEL VALLE, E. M. Steady and Oscillatory Shear Flow Behavior of Different Polysaccharides with Laponite®. **Polymers**, vol. 13, no. 6, p. 966, 22 Mar. 2021. DOI: 10.3390/polym13060966. Available at: https://www.mdpi.com/2073-4360/13/6/966.

BLANCO, I.; SIRACUSA, V. The Use of Thermal Techniques in the Characterization of Bio-Sourced Polymers. **Materials**, vol. 14, no. 7, p. 1686, 30 Mar. 2021. DOI: 10.3390/ma14071686.

Available at: https://www.mdpi.com/1996-1944/14/7/1686.

BLANKENSHIP, R. E. **Molecular Mechanisms of Photosynthesis**. II. Tempe: Wiley, 19 Dec. 2014. 1–321 pp. DOI: 10.1002/9780470758472. Available at: https://onlinelibrary.wiley.com/doi/book/10.1002/9780470758472.

BLANKENSHIP, R. E. **Molecular Mechanisms of Photosynthesis**. III. Tempe: Wiley & Sons, 2021. 1–352 pp. Available at: https://www.wiley.com/en-us/Molecular+Mechanisms+of+Photosynthesis%2C+3rd+Edition-p-9781119800019.

BLIGH, E. G.; DYER, W. J. A rapid method of total lipid extraction and purification. **Canadian Journal of Biochemistry and Physiology**, vol. 37, no. 8, pp. 911–917, 1 Aug. 1959. DOI: 10.1139/o59-099. Available at: http://www.nrcresearchpress.com/doi/10.1139/o59-099.

BLUMENKRANTZ, N.; ASBOE-HANSEN, G. New method for quantitative determination of uronic acids. **Analytical Biochemistry**, vol. 54, no. 2, pp. 484–489, Aug. 1973. https://doi.org/10.1016/0003-2697(73)90377-1.

BONT, L. de; DONNAY, N.; COUTURIER, J.; ROUHIER, N. Redox regulation of enzymes involved in sulfate assimilation and in the synthesis of sulfur-containing amino acids and glutathione in plants. **Frontiers in Plant Science**, vol. 13, no. August, pp. 1–12, 16 Aug. 2022. DOI: 10.3389/fpls.2022.958490. Available at: https://www.frontiersin.org/articles/10.3389/fpls.2022.958490/full.

BOROVKOV, A. B.; RYLKOVA, O. A.; GUDVILOVICH, I. N.; AVSIYAN, A. L. Growth and morphometric characteristics of the microalga *Porphyridium purpureum* (Bory) Ross using sodium bicarbonate as a carbon source. **Bioresource Technology Reports**, vol. 33, no. January, 2026. https://doi.org/10.1016/j.biteb.2026.102615.

CACCAVO, D.; CASCONE, S.; LAMBERTI, G.; BARBA, A. A. Hydrogels: Experimental characterization and mathematical modelling of their mechanical and diffusive behaviour. **Chemical Society Reviews**, vol. 47, no. 7, pp. 2357–2373, 2018. DOI: 10.1039/c7cs00638a. Available at: http://dx.doi.org/10.1039/C7CS00638A.

CAETANO, P. A.; TATIELE, C.; FERNANDES, S.; NASS, P. P.; VIEIRA, K. R.; MAR, M. R.; JACOB-LOPES, E.; ZEPKA, L. Q. Microalgae-based polysaccharides : Insights on production , applications , analysis , and future challenges. **Biocatalysis and Agricultural Biotechnology**, vol. 45, no. September, 2022. https://doi.org/10.1016/j.bcab.2022.102491.

CANO-SARMIENTO, C.; TÉLLEZ-MEDINA, D. I.; VIVEROS-CONTRERAS, R.; CORNEJO-MAZÓN, M.; FIGUEROA-HERNÁNDEZ, C. Y.; GARCÍA-ARMENTA, E.; ALAMILLA-BELTRÁN, L.; GARCÍA, H. S.; GUTIÉRREZ-LÓPEZ, G. F. Zeta Potential of Food Matrices. **Food Engineering Reviews**, vol. 10, no. 3, pp. 113–138, 5 Sep. 2018. DOI: 10.1007/s12393-018-9176-z. Available at: http://link.springer.com/10.1007/s12393-018-9176-z.

CARDIAS, B. B.; MORAIS, M. G. de; COSTA, J. A. V. Increased biomass and biomolecule productivity of *Spirulina sp.* LEB 18 cultivated with CO_2 adsorbent nanofibers. **Clean Technologies and Environmental Policy**, no. 0123456789, 15 Jun. 2024. DOI: 10.1007/s10098-

024-02907-x. Available at: https://doi.org/10.1007/s10098-024-02907-x.

CARVALHO, M. P. de; MORAIS, M. G. de; SANTOS, L. O. dos; LAROCHE, C.; COSTA, J. A. V. Production of biomass and biomolecules in *Limnospira indica* PCC 8005 cultivation under magnetic fields and polymeric nanofibers. **Journal of Biotechnology**, vol. 405, no. October 2024, pp. 48–56, Sep. 2025. https://doi.org/10.1016/j.jbiotec.2025.05.004.

CASAS-ARROJO, V.; DECARA, J.; ARROJO-AGUDO, M. de los Á.; PÉREZ-MANRÍQUEZ, C.; ABDALA-DÍAZ, R. T. Immunomodulatory, antioxidant activity and cytotoxic effect of sulfated polysaccharides from *Porphyridium cruentum*. (s.f.gray) nägeli. **Biomolecules**, vol. 11, no. 4, 2021. https://doi.org/10.3390/biom11040488.

CAWSE, P. A. The determination of nitrate in soil solutions by ultraviolet spectrophotometry. **The Analyst**, vol. 92, no. 1094, p. 311, 1967. https://doi.org/10.1039/an9679200311.

CHEN, C.; TANG, T.; SHI, Q.; ZHOU, Z.; FAN, J. The potential and challenge of microalgae as promising future food sources. **Trends in Food Science & Technology**, vol. 126, no. March, pp. 99–112, Aug. 2022. DOI: 10.1016/j.tifs.2022.06.016. Available at: https://linkinghub.elsevier.com/retrieve/pii/S0924224422002096.

CHEN, Di; QIAN, J.; HUO, S.; WANG, F.; MA, H.; LIU, S. Proteomic Analysis of Listeria monocytogenes Subjected to Pulsed Magnetic Field. **Foods**, vol. 14, no. 11, p. 1871, 24 May 2025. DOI: 10.3390/foods14111871. Available at: https://www.mdpi.com/2304-8158/14/11/1871.

CHEN, Dongning; SMITH, L. R.; KHANDEKAR, G.; PATEL, P.; YU, C. K.; ZHANG, K.; CHEN, C. S.; HAN, L.; WELLS, R. G. Distinct effects of different matrix proteoglycans on collagen fibrillogenesis and cell-mediated collagen reorganization. **Scientific Reports**, vol. 10, no. 1, pp. 1–13, 2020. DOI: 10.1038/s41598-020-76107-0. Available at: https://doi.org/10.1038/s41598-020-76107-0.

CHEN, J. H.; TANG, M.; JIN, X. Q.; LI, H.; CHEN, L. S.; WANG, Q. L.; SUN, A. Z.; YI, Y.; GUO, F. Q. Regulation of Calvin–Benson cycle enzymes under high temperature stress. **Springer**, vol. 3, no. 1, pp. 65–77, 1 Mar. 2022. DOI: 10.1007/s42994-022-00068-3. Available at: https://pmc.ncbi.nlm.nih.gov/articles/PMC9590453/. Accessed: 3 Mar. 2026.

CHOPIN, T.; KERIN, B. F.; MAZEROLLE, R. Phycocolloid chemistry as a taxonomic indicator of phylogeny in the Gigartinales, Rhodophyceae: A review and current developments using Fourier transform infrared diffuse reflectance spectroscopy. **Phycological Research**, vol. 47, no. 3, pp. 167–188, Sep. 1999. DOI: 10.1046/j.1440-1835.1999.00170.x. Available at: http://doi.wiley.com/10.1046/j.1440-1835.1999.00170.x.

COGNE, G.; LEHMANN, B.; DUSSAP, C.; GROS, J. Uptake of macrominerals and trace elements by the cyanobacterium *Spirulina platensis* (*Arthrospira platensis* PCC 8005) under photoautotrophic conditions: Culture medium optimization. **Biotechnology and Bioengineering**, vol. 81, no. 5, pp. 588–593, 5 Mar. 2003. https://doi.org/10.1002/bit.10504.

COLLA, E.; MENEGOTTO, A. L. L.; KALSCHNE, D. L.; DA SILVA-BUZANELLO, R. A.;

CANAN, C.; DRUNKLER, D. A. Microalgae: A new and promising source of food. **Handbook of Algal Science, Technology and Medicine**. Elsevier, 2020. pp. 507–518. DOI: 10.1016/B978-0-12-818305-2.00032-2. Available at: https://doi.org/10.1016/B978-0-12-818305-2.00032-2.

COMITRE, A. A.; VAZ, B. da S.; COSTA, J. A. V.; MORAIS, M. G. de. Renewal of nanofibers in *Chlorella fusca* microalgae cultivation to increase CO_2 fixation. **Bioresource Technology**, vol. 321, no. November 2020, p. 124452, Feb. 2021. DOI: 10.1016/j.biortech.2020.124452. Available at: https://doi.org/10.1016/j.biortech.2020.124452.

COSTA, J. A. V.; FREITAS, B. C. B.; ROSA, G. M.; MORAES, L.; MORAIS, M. G.; MITCHELL, B. G. Operational and economic aspects of *Spirulina*-based biorefinery. **Bioresource Technology**, vol. 292, no. July, p. 121946, 2019. DOI: 10.1016/j.biortech.2019.121946. Available at: https://doi.org/10.1016/j.biortech.2019.121946.

COSTA, J. A. V.; LUCAS, B. F.; ALVARENGA, A. G. P.; MOREIRA, J. B.; DE MORAIS, M. G. Microalgae Polysaccharides: An Overview of Production, Characterization, and Potential Applications. **Polysaccharides**, vol. 2, no. 4, pp. 759–772, 1 Oct. 2021. DOI: 10.3390/polysaccharides2040046. Available at: https://www.mdpi.com/2673-4176/2/4/46/htm. Accessed: 3 Aug. 2022.

DANESHVAR, E.; WICKER, R. J.; SHOW, P.-L.; BHATNAGAR, A. Biologically-mediated carbon capture and utilization by microalgae towards sustainable CO_2 biofixation and biomass valorization – A review. **Chemical Engineering Journal**, vol. 427, p. 130884, 1 Jan. 2022. DOI: 10.1016/j.cej.2021.130884. Available at: https://linkinghub.elsevier.com/retrieve/pii/S1385894721024682.

DAO, O.; BERTRAND, M.; ALSEEKH, S.; VEILLET, F.; AUROY, P.; NGUYEN, P.-C.; LÉGERET, B.; EPTING, V.; MORIN, A.; CUINÉ, S.; MONTEIL, C. L.; MACKINDER, L. C. M.; BURLACOT, A.; KRIEGER-LISZKAY, A.; WEBER, A. P. M.; FERNIE, A. R.; PELTIER, G.; LI-BEISSON, Y. The green algae CO_2 concentrating mechanism and photorespiration jointly operate during acclimation to low CO_2. **Nature Communications**, vol. 16, no. 1, p. 5296, 17 Jun. 2025. DOI: 10.1038/s41467-025-60525-7. Available at: doi.org/10.1038/s41467-025-60525-7.

DE JESUS, C. S.; DE JESUS ASSIS, D.; RODRIGUEZ, M. B.; MENEZES FILHO, J. A.; COSTA, J. A. V.; DE SOUZA FERREIRA, E.; DRUZIAN, J. I. Pilot-scale isolation and characterization of extracellular polymeric substances (EPS) from cell-free medium of *Spirulina sp*. LEB-18 cultures under outdoor conditions. **International Journal of Biological Macromolecules**, vol. 124, pp. 1106–1114, 2019. DOI: 10.1016/j.ijbiomac.2018.12.016. Available at: https://doi.org/10.1016/j.ijbiomac.2018.12.016.

DEAMICI, K. M.; CARDIAS, B. B.; COSTA, J. A. V.; SANTOS, L. O. Static magnetic fields in culture of *Chlorella fusca*: Bioeffects on growth and biomass composition. **Process Biochemistry**, vol. 51, no. 7, pp. 912–916, Jul. 2016. DOI: 10.1016/j.procbio.2016.04.005. Available at: http://dx.doi.org/10.1016/j.procbio.2016.04.005.

DEAMICI, K. M.; COSTA, J. A. V.; SANTOS, L. O. Magnetic fields as triggers of microalga growth: evaluation of its effect on *Spirulina sp*. **Bioresource Technology**, vol. 220, pp. 62–67, 1 Nov. 2016. https://doi.org/10.1016/J.BIORTECH.2016.08.038.

DEAMICI, K. M.; CUELLAR-BERMUDEZ, S. P.; MUYLAERT, K.; SANTOS, L. O.; COSTA, J. A. V. Quantum yield alterations due to the static magnetic fields action on *Arthrospira platensis* SAG 21.99: Evaluation of photosystem activity. **Bioresource Technology**, vol. 292, p. 121945, Nov. 2019. DOI: 10.1016/j.biortech.2019.121945. Available at: https://linkinghub.elsevier.com/retrieve/pii/S0960852419311757. Accessed: 14 May 2024.

DEAMICI, K. M.; DZIERGOWSKA, K.; SILVA, P. G. P.; MICHALAK, I.; SANTOS, L. O.; DETYNA, J.; KATARIA, S.; BRESTIC, M.; SARRAF, M.; ISLAM, M. Microalgae Cultivated under Magnetic Field Action: Insights of an Environmentally Sustainable Approach. **Sustainability**, vol. 14, no. 20, p. 13291, 16 Oct. 2022. DOI: 10.3390/su142013291. Available at: https://www.mdpi.com/2071-1050/14/20/13291.

DEAMICI, K. M.; MORAIS, M. G. de; DOS SANTOS, L. O.; GROS, F.; COSTA, J. A. V.; LAROCHE, C. Magnetic Field Action on *Limnospira indica* PCC8005 Cultures: Enhancement of Biomass Yield and Protein Content. **Applied Sciences**, vol. 12, no. 3, p. 1533, 31 Jan. 2022. DOI: 10.3390/app12031533. Available at: https://www.mdpi.com/2076-3417/12/3/1533.

DEAMICI, K. M.; SANTOS, L. O.; COSTA, J. A. V. Magnetic field action on outdoor and indoor cultures of *Spirulina*: Evaluation of growth, medium consumption and protein profile. **Bioresource Technology**, vol. 249, pp. 168–174, 1 Feb. 2018. https://doi.org/10.1016/J.BIORTECH.2017.09.185.

DEAMICI, K. M.; SANTOS, L. O.; COSTA, J. A. V. Magnetic field as promoter of growth in outdoor and indoor assays of *Chlorella fusca*. **Bioprocess and Biosystems Engineering**, vol. 44, no. 7, pp. 1453–1460, 2021. DOI: 10.1007/s00449-021-02526-6. Available at: https://doi.org/10.1007/s00449-021-02526-6.

DEAMICI, K. M.; SANTOS, L. O.; COSTA, J. A. V. Use of static magnetic fields to increase CO2 biofixation by the microalga *Chlorella fusca*. **Bioresource Technology**, vol. 276, no. November 2018, pp. 103–109, 1 Mar. 2019. DOI: 10.1016/j.biortech.2018.12.080. Available at: https://linkinghub.elsevier.com/retrieve/pii/S0960852418317516. Accessed: 10 Mar. 2023.

DECAMP, A.; MARTINEAU, E.; GRIZEAU, D.; PRUVOST, J.; GONÇALVES, O. Effects of the salinity on the biosynthesis of the polysaccharides of the marine microalgae *Porphyridium cruentum*. **Algal Research**, vol. 71, no. April, p. 103089, Apr. 2023. DOI: 10.1016/j.algal.2023.103089. Available at: https://linkinghub.elsevier.com/retrieve/pii/S2211926423001224.

DELATTRE, C.; PIERRE, G.; LAROCHE, C.; MICHAUD, P. Production, extraction and characterization of microalgal and cyanobacterial exopolysaccharides. **Biotechnology Advances**, vol. 34, no. 7, pp. 1159–1179, 2016. DOI: 10.1016/j.biotechadv.2016.08.001. Available at: http://dx.doi.org/10.1016/j.biotechadv.2016.08.001.

DILLE, M. J.; HAUG, I. J.; DRAGET, K. I. Gelatin and collagen. **Handbook of Hydrocolloids**. Elsevier, 1 Jan. 2021. pp. 1073–1097. DOI: 10.1016/B978-0-12-820104-6.00028-0. Available at: https://linkinghub.elsevier.com/retrieve/pii/B9780128201046000280. Accessed: 31 Oct. 2022.

DOGSON, K.; PRICE, R. A note on the determination of the ester sulphate content of sulphated

polysaccharides. **Biochemical Journal**, vol. 84, no. 1, pp. 106–110, 1 Jul. 1962. DOI: 10.1042/bj0840106. Available at: https://portlandpress.com/biochemj/article/84/1/106/52792/A-note-on-the-determination-of-the-ester-sulphate.

DOMOZYCH, C. R.; PLANTE, K.; BLAIS, P.; PALIULIS, L.; DOMOZYCH, D. S. Mucilage processing and secretion in the green alga closterium. I. Cytology and biochemistry1. **Journal of Phycology**, vol. 29, no. 5, pp. 650–659, 1 Oct. 1993. DOI: 10.1111/J.0022-3646.1993.00650.X. Available at: https://onlinelibrary.wiley.com/doi/full/10.1111/j.0022-3646.1993.00650.x. Accessed: 12 Sep. 2022.

DONG, W.; MAZZARA, E.; SÁNCHEZ-BACA, A.; MONDAL, K.; VILLAMIEL, M.; BABU, R.; SUN, D.-W.; TIWARI, B. K. A comparative study on heterogeneous deacetylation of chitin to chitosan under various ultrasound irradiation and characterization. **Ultrasonics Sonochemistry**, vol. 128, no. November 2025, p. 107794, May 2026. DOI: 10.1016/j.ultsonch.2026.107794. Available at: https://linkinghub.elsevier.com/retrieve/pii/S1350417726000593.

DUARTE, M. M.; SUPRINOVYCH, A.; VEIGA, A.; LOPES, A. I.; TAVARIA, F. K.; MORAIS, R. C.; OLIVEIRA, A. L. Hydrogel-Forming Ability and Biological Characterization of Exopolysaccharide (EPS) from *Porphyridium cruentum*. **Gels**, vol. 12, no. 5, p. 352, 23 Apr. 2026. DOI: 10.3390/gels12050352. Available at: https://www.mdpi.com/2310-2861/12/5/352.

DUBOIS, M.; GILLES, K. A.; HAMILTON, J. K.; REBERS, P. A.; SMITH, F. Colorimetric Method for Determination of Sugars and Related Substances. **Analytical Chemistry**, vol. 28, no. 3, pp. 350–356, 1 Mar. 1956. DOI: 10.1021/ac60111a017. Available at: https://pubs.acs.org/doi/abs/10.1021/ac60111a017. Accessed: 27 Jan. 2022.

EFREMENKO, E.; SENKO, O.; TEPLOVA, K.; ASLANLI, A. Biomass of Microalgae and Other Phototrophic Microorganisms: Current Trends in Regulation of Its Accumulation and Application of Immobilized Forms. **Applied Sciences**, vol. 15, no. 23, p. 12775, 2 Dec. 2025. DOI: 10.3390/app152312775. Available at: https://www.mdpi.com/2076-3417/15/23/12775.

EGHBALJOO, H.; SANI, I. K.; SANI, M. A.; RAHATI, S.; MANSOURI, E.; MOLAEE-AGHAEE, E.; FATOUREHCHI, N.; KADI, A.; ARAB, A.; SARABANDI, K.; SAMBORSKA, K.; JAFARI, S. M. Advances in plant gum polysaccharides; Sources, techno-functional properties, and applications in the food industry - A review. **International Journal of Biological Macromolecules**, vol. 222, no. PB, pp. 2327–2340, Dec. 2022. DOI: 10.1016/j.ijbiomac.2022.10.020. Available at: https://doi.org/10.1016/j.ijbiomac.2022.10.020.

EL-NAGGAR, N. E.-A.; HUSSEIN, M. H.; SHAABAN-DESSUUKI, S. A.; DALAL, S. R. Production, extraction and characterization of *Chlorella vulgaris* soluble polysaccharides and their applications in AgNPs biosynthesis and biostimulation of plant growth. **Scientific Reports**, vol. 10, no. 1, p. 3011, 20 Feb. 2020. DOI: 10.1038/s41598-020-59945-w. Available at: https://www.nature.com/articles/s41598-020-59945-w. Accessed: 6 Oct. 2022.

EL BAZ KF, H. Induction of Sulfated Polysaccharides in *Spirulina platensis* as Response to Nitrogen Concentration and its Biological Evaluation. **Journal of Aquaculture Research & Development**, vol. 05, no. 01, 2014. DOI: 10.4172/2155-9546.1000206. Available at:

https://www.omicsonline.org/induction-of-sulfated-polysaccharides-in-spirulina-platensis-as-response-to-nitrogen-concentration-and-its-biological-evaluation-2155-9546.1000206.php?aid=21643. Accessed: 5 Oct. 2022.

ESQUEDA, A. B.; GARDARIN, C.; LAROCHE, C. Exploring the Diversity of Red Microalgae for Exopolysaccharide Production. **Marine Drugs**, vol. 20, no. 4, p. 246, 31 Mar. 2022. DOI: 10.3390/md20040246. Available at: https://www.mdpi.com/1660-3397/20/4/246/htm. Accessed: 1 Aug. 2022.

ETESHOLA, E.; KARPASAS, M.; ARAD, S.; GOTTLIEB, M. Red microalga exopolysaccharides: 2. Study of the rheology, morphology and thermal gelation of aqueous preparations. **Acta Polymerica**, vol. 49, nos. 10–11, pp. 549–556, Oct. 1998. DOI: 10.1002/(SICI)1521-4044(199810)49:10/11<549::AID-APOL549>3.0.CO;2-T. Available at: https://onlinelibrary.wiley.com/doi/10.1002/(SICI)1521-4044(199810)49:10/11%3C549::AID-APOL549%3E3.0.CO;2-T.

EVANS, E. W.; DODSON, C. A.; MAEDA, K.; BISKUP, T.; WEDGE, C. J.; TIMME, C. R. Magnetic field effects in flavoproteins and related systems. **Interface Focus**, vol. 3, no. 5, p. 20130037, 6 Oct. 2013. DOI: 10.1098/RSFS.2013.0037. Available at: https://pmc.ncbi.nlm.nih.gov/articles/PMC3915827/. Accessed: 1 Jul. 2026.

FERREIRA, A.; GUERRA, I.; COSTA, M.; SILVA, J.; GOUVEIA, L. Future perspectives of microalgae in the food industry. **Cultured Microalgae for the Food Industry**, pp. 387–433, 1 Jan. 2021. https://doi.org/10.1016/B978-0-12-821080-2.00008-3.

FILALI MOUHIM, R.; CORNET, J. F.; FONTANE, T.; FOURNET, B.; DUBERTRET, G. Production, isolation and preliminary characterization of the exopolysaccharide of the cyanobacterium *Spirulina platensis*. **Biotechnology Letters 1993 15:6**, vol. 15, no. 6, pp. 567–572, 1993. DOI: 10.1007/BF00138541. Available at: https://link.springer.com/article/10.1007/BF00138541. Accessed: 12 Sep. 2022.

FIMBRES-OLIVARRÍA, D.; LÓPEZ-ELÍAS, J. A.; CARVAJAL-MILLÁN, E.; MÁRQUEZ-ESCALANTE, J. A.; MARTÍNEZ-CÓRDOVA, L. R.; MIRANDA-BAEZA, A.; ENRÍQUEZ-OCAÑA, F.; VALDÉZ-HOLGUÍN, J. E.; BROWN-BOJÓRQUEZ, F. *Navicula sp*. Sulfated Polysaccharide Gels Induced by Fe(III): Rheology and Microstructure. **International Journal of Molecular Sciences 2016, Vol. 17, Page 1238**, vol. 17, no. 8, p. 1238, 30 Jul. 2016. DOI: 10.3390/IJMS17081238. Available at: https://www.mdpi.com/1422-0067/17/8/1238/htm. Accessed: 31 Oct. 2022.

FINKEL, Z. V.; FOLLOWS, M. J.; LIEFER, J. D.; BROWN, C. M.; BENNER, I.; IRWIN, A. J. Phylogenetic diversity in the macromolecular composition of microalgae. **PLoS ONE**, vol. 11, no. 5, 2016. https://doi.org/10.1371/journal.pone.0155977.

FONT, Y. S.; DÍAZ, Y. O.; CUYPERS, A.; ALEMÁN, E. I.; VANDAMME, D. The effect of magnetic field treatment on the cultivation of microalgae: An overview of involved mechanisms. **Journal of Applied Phycology**, vol. 35, no. 4, pp. 1525–1536, 1 Aug. 2023. https://doi.org/10.1007/s10811-023-02994-1.

FU, K.; WANG, H.; PAN, T.; CAI, Z.; YANG, Z.; LIU, D.; WANG, W. Gel-forming polysaccharides of traditional gel-like foods: Sources, structure, gelling mechanism, and advanced applications. **Food Research International**, vol. 198, no. July, p. 115329, Dec. 2024. DOI: 10.1016/j.foodres.2024.115329. Available at: https://doi.org/10.1016/j.foodres.2024.115329.

GAIGNARD, C.; LAROCHE, C.; PIERRE, G.; DUBESSAY, P.; DELATTRE, C.; GARDARIN, C.; GOURVIL, P.; PROBERT, I.; DUBUFFET, A.; MICHAUD, P. Screening of marine microalgae: Investigation of new exopolysaccharide producers. **Algal Research**, vol. 44, no. October, p. 101711, 2019. DOI: 10.1016/j.algal.2019.101711. Available at: https://doi.org/10.1016/j.algal.2019.101711.

GARGOUCH, N.; ELLEUCH, F.; KARKOUCH, I.; TABBENE, O.; PICHON, C.; GARDARIN, C.; RIHOUEY, C.; PICTON, L.; ABDELKAFI, S.; FENDRI, I.; LAROCHE, C. Potential of exopolysaccharide from *Porphyridium marinum* to contend with bacterial proliferation, biofilm formation, and breast cancer. **Marine Drugs**, vol. 19, no. 2, 2021. https://doi.org/10.3390/md19020066.

GARGOUCH, N.; KARKOUCH, I.; ELLEUCH, J.; ELKAHOUI, S.; MICHAUD, P.; ABDELKAFI, S.; LAROCHE, C.; FENDRI, I. Enhanced B-phycoerythrin production by the red microalga *Porphyridium marinum*: A powerful agent in industrial applications. **International Journal of Biological Macromolecules**, vol. 120, pp. 2106–2114, 2018. https://doi.org/10.1016/j.ijbiomac.2018.09.037.

GARTZKE, J.; LANGE, K. Cellular target of weak magnetic fields: ionic conduction along actin filaments of microvilli. **American Journal of Physiology-Cell Physiology**, vol. 283, no. 5, pp. C1333–C1346, 1 Nov. 2002. DOI: 10.1152/ajpcell.00167.2002. Available at: https://journals.physiology.org/doi/10.1152/ajpcell.00167.2002.

GARZA-RODRÍGUEZ, Z. B.; HERNÁNDEZ-PÉREZ, J.; SANTACRUZ, A.; JACOBO-VELÁZQUEZ, D. A.; BENAVIDES, J. Prospective on the application of abiotic stresses to enhance the industrial production of exopolysaccharides from microalgae. **Current Research in Biotechnology**, vol. 4, pp. 439–444, 1 Jan. 2022. DOI: 10.1016/j.crbiot.2022.09.007. Available at: https://linkinghub.elsevier.com/retrieve/pii/S2590262822000351. Accessed: 14 Oct. 2022.

GERESH, S.; ARAD, S. (Malis); LEVY-ONTMAN, O.; ZHANG, W.; TEKOAH, Y.; GLASER, R. Isolation and characterization of poly- and oligosaccharides from the red microalga *Porphyridium sp*. **Carbohydrate Research**, vol. 344, no. 3, pp. 343–349, 2009. DOI: 10.1016/j.carres.2008.11.012. Available at: http://dx.doi.org/10.1016/j.carres.2008.11.012.

GHIAT, I.; AL-ANSARI, T. A review of carbon capture and utilisation as a CO_2 abatement opportunity within the EWF nexus. **Journal of CO2 Utilization**, vol. 45, p. 101432, 1 Mar. 2021. DOI: 10.1016/j.jcou.2020.101432. Available at: https://linkinghub.elsevier.com/retrieve/pii/S2212982020310623.

GOHARA-BEIRIGO, A. K.; MATSUDO, M. C.; CEZARE-GOMES, E. A.; CARVALHO, J. C. M. de; DANESI, E. D. G. Microalgae trends toward functional staple food incorporation: Sustainable alternative for human health improvement. **Trends in Food Science and**

Technology, vol. 125, no. May, pp. 185–199, 2022. https://doi.org/10.1016/j.tifs.2022.04.030.

GÓMEZ-ORDÓÑEZ, E.; RUPÉREZ, P. FTIR-ATR spectroscopy as a tool for polysaccharide identification in edible brown and red seaweeds. **Food Hydrocolloids**, vol. 25, no. 6, pp. 1514–1520, Aug. 2011. DOI: 10.1016/j.foodhyd.2011.02.009. Available at: http://dx.doi.org/10.1016/j.foodhyd.2011.02.009.

GOUVÊA, S. P.; VIEIRA, A. A. H.; LOMBARDI, A. T. Copper and cadmium complexation by high molecular weight materials of dominant microalgae and of water from a eutrophic reservoir. **Chemosphere**, vol. 60, no. 9, pp. 1332–1339, 1 Sep. 2005. https://doi.org/10.1016/J.CHEMOSPHERE.2005.01.061.

GUERREIRO, M.; EMMANUEL, C.; DUPUITS, C.; GARDARIN, C.; MOUZEYAR, S.; ROCHE, J.; LAROCHE, C. Transcriptomic Insights into Metabolic Reprogramming and Exopolysaccharide Synthesis in *Porphyridium purpureum* Under Gradual Nitrogen Deprivation. pp. 1–28, 2026.

GUIHÉNEUF, F.; STENGEL, D. B. Towards the biorefinery concept: Interaction of light, temperature and nitrogen for optimizing the co-production of high-value compounds in *Porphyridium purpureum*. **Algal Research**, vol. 10, pp. 152–163, Jul. 2015. DOI: 10.1016/j.algal.2015.04.025. Available at: http://dx.doi.org/10.1016/j.algal.2015.04.025.

HAN, S. Il; HEO, Y. M.; JEON, M. S.; KYUNG, S.; KANG, S.; KWON, S. J.; RYU, J. H.; KIM, J. H.; AHN, J. W. The effect of exopolysaccharides from EMS-induced *Porphyridium cruentum* mutant on human epidermal and dermal layers. **Frontiers in Marine Science**, vol. 11, no. May, pp. 1–12, 2024. https://doi.org/10.3389/fmars.2024.1365311.

HANIFA, M.; AGARWAL, R.; SHARMA, U.; THAPLIYAL, P. C.; SINGH, L. P. A review on CO_2 capture and sequestration in the construction industry: Emerging approaches and commercialised technologies. **Journal of CO_2 Utilization**, vol. 67, p. 102292, 1 Jan. 2023. DOI: 10.1016/j.jcou.2022.102292. Available at: https://linkinghub.elsevier.com/retrieve/pii/S2212982022004115.

HAYASHI, K.; HAYASHI, T.; KOJIMA, I. A natural sulfated polysaccharide, calcium spirulan, isolated from *Spirulina platensis*: In vitro and ex vivo evaluation of anti-herpes simplex virus and anti-human immunodeficiency virus activities. **AIDS Research and Human Retroviruses**, vol. 12, no. 15, pp. 1463–1471, 1996. https://doi.org/10.1089/aid.1996.12.1463.

HIRANO, M.; OHTA, A.; ABE, K. Magnetic Field Effects on Photosynthesis and Growth of the Cyanobacterium *Spirulina platensis*. **Journal of Fermentation and Bioengineering**, vol. 86, no. 3, pp. 313–316, 1998.

HOQUE, M. M.; IANNELLI, V.; PADULA, F.; RADICE, R. P.; SAHA, B. K.; MARTELLI, G.; SCOPA, A.; DROSOS, M. Microalgae: Green Engines for Achieving Carbon Sequestration, Circular Economy, and Environmental Sustainability—A Review Based on Last Ten Years of Research. **Bioengineering**, vol. 12, no. 9, pp. 1–23, 2025. https://doi.org/10.3390/bioengineering12090909.

HORE, P. J.; MOURITSEN, H. The Radical-Pair Mechanism of Magnetoreception. **Annual Review of Biophysics**, vol. 45, no. 1, pp. 299–344, 5 Jul. 2016. DOI: 10.1146/annurev-biophys-032116-094545. Available at: https://www.annualreviews.org/doi/10.1146/annurev-biophys-032116-094545.

HOSSEINI, H.; BOUNNIT, T.; SAADAOUI, I. Trends in *Arthrospira sp* . (Spirulina) Applications : A 15-Year Bibliometric Analysis and Systematic Review. pp. 1–22, 2026.

HU, X.; DAI, S.; LIU, C.; ZHANG, C.; ZHAO, Z.; QIAO, L.; XU, J.; JIN, H.; XU, X.; YANG, Z.; LI, J.; HUANG, L.; MU, Y.; HUANG, H. Exploration into the structural characteristics and functional properties of exopolysaccharide synthesized by *Pseudoduganella armeniaca* ZMN–3. **International Journal of Biological Macromolecules**, vol. 366, no. April, p. 152375, 2026. DOI: 10.1016/j.ijbiomac.2026.152375. Available at: https://doi.org/10.1016/j.ijbiomac.2026.152375.

HUO, S.; CHEN, X.; ZHU, F.; ZHANG, W.; CHEN, D.; JIN, N.; COBB, K.; CHENG, Y.; WANG, L.; RUAN, R. Magnetic field intervention on growth of the filamentous microalgae Tribonema sp. in starch wastewater for algal biomass production and nutrients removal: Influence of ambient temperature and operational strategy. **Bioresource Technology**, vol. 303, no. January, p. 122884, May 2020. DOI: 10.1016/j.biortech.2020.122884. Available at: https://doi.org/10.1016/j.biortech.2020.122884.

INTERNATIONAL ENERGY AGENCY, I. **CO_2 Emissions in 2023**. [*N.d.*]. Available at: www.iea.org. Accessed: 22 Apr. 2024.

JAKHU, S.; SHARMA, Y.; SHARMA, K.; VAID, K.; DHAR, H.; KUMAR, V.; SINGH, R. P.; SHEKH, A.; KUMAR, G. Production and characterization of microalgal exopolysaccharide as a reducing and stabilizing agent for green synthesis of gold-nanoparticle: a case study with a *Chlorella sp*. from Himalayan high-altitude psychrophilic habitat. **Journal of Applied Phycology**, vol. 33, no. 6, pp. 3899–3914, 1 Dec. 2021. DOI: 10.1007/s10811-021-02580-3. Available at: https://link.springer.com/article/10.1007/s10811-021-02580-3. Accessed: 9 Sep. 2022.

JI, L.; ZHAO, C.; HE, Y.; YUAN, Y.; HONG, Z.; SUN, L.; FAN, J. Exploring *Porphyridium purpureum* and *Porphyridium aerugineum* as alternative resources for phycobiliprotein production. **Bioresource Technology**, vol. 416, p. 131800, 1 Jan. 2025. DOI: 10.1016/J.BIORTECH.2024.131800. Available at: https://www.sciencedirect.com/science/article/pii/S0960852424015049. Accessed: 17 Dec. 2025.

JIN, C.; YU, Z.; PENG, S.; FENG, K.; ZHANG, L.; ZHOU, X. The characterization and comparison of exopolysaccharides from two benthic diatoms with different biofilm formation abilities. **Anais da Academia Brasileira de Ciências**, vol. 90, no. 2, pp. 1503–1519, 1 Apr. 2018. DOI: 10.1590/0001-3765201820170721. Available at: http://www.scielo.br/j/aabc/a/KjSqXvLsM8tYVBSjgRwqXtk/?lang=en. Accessed: 12 Sep. 2022.

JU, J.; YANG, J.; ZHANG, W.; WEI, Y.; YUAN, H.; TAN, Y. Seaweed polysaccharide fibers: Solution properties, processing and applications. **Journal of Materials Science & Technology**, vol. 140, pp. 1–18, Mar. 2022. DOI: 10.1016/j.jmst.2022.07.053. Available at:

https://doi.org/10.1016/j.jmst.2022.07.053.

KANEHISA, M.; FURUMICHI, M.; SATO, Y.; MATSUURA, Y.; ISHIGURO-WATANABE, M. KEGG: biological systems database as a model of the real world. **Nucleic Acids Research**, vol. 53, no. D1, pp. D672–D677, 6 Jan. 2025. DOI: 10.1093/nar/gkae909. Available at: https://academic.oup.com/nar/article/53/D1/D672/7824602.

KEIDAN, M.; BROSHY, H.; VAN MOPPES, D.; ARAD, S. Assimilation of sulphur into the cell-wall polysaccharide of the red microalga *Porphyridium* sp. (Rhodophyta). **Phycologia**, vol. 45, no. 5, pp. 505–511, 22 Sep. 2006. DOI: 10.2216/05-57.1. Available at: https://www.tandfonline.com/doi/full/10.2216/05-57.1.

KIM, T. H.; LEE, K.; OH, B. R.; LEE, M. E.; SEO, M.; LI, S.; KIM, J. K.; CHOI, M.; CHANG, Y. K. A novel process for the coproduction of biojet fuel and high-value polyunsaturated fatty acid esters from heterotrophic microalgae *Schizochytrium sp*. ABC101. **Renewable Energy**, vol. 165, pp. 481–490, 2021. DOI: 10.1016/j.renene.2020.09.116. Available at: https://doi.org/10.1016/j.renene.2020.09.116.

KLANCHUI, A.; DULSAWAT, S.; CHALOEMNGAM, K.; CHEEVADHANARAK, S.; PROMMEENATE, P.; MEECHAI, A. An Improved Genome-Scale Metabolic Model of *Arthrospira platensis* C1 (iAK888) and Its Application in Glycogen Overproduction. **Metabolites**, vol. 8, no. 4, p. 84, 26 Nov. 2018. DOI: 10.3390/metabo8040084. Available at: https://www.mdpi.com/2218-1989/8/4/84.

KOÇER, A. T.; İNAN, B.; KAPTAN USUL, S.; ÖZÇIMEN, D.; YILMAZ, M. T.; IŞILDAK, İ. Exopolysaccharides from microalgae: production, characterization, optimization and techno-economic assessment. **Brazilian Journal of Microbiology**, vol. 52, no. 4, pp. 1779–1790, 11 Dec. 2021. DOI: 10.1007/s42770-021-00575-3. Available at: https://link.springer.com/article/10.1007/s42770-021-00575-3. Accessed: 1 Aug. 2022.

LAFARGA, T.; FERNÁNDEZ-SEVILLA, J. M.; GONZÁLEZ-LÓPEZ, C.; ACIÉN-FERNÁNDEZ, F. G. *Spirulina* for the food and functional food industries. **Food Research International**, vol. 137, no. May, p. 109356, 2020. DOI: 10.1016/j.foodres.2020.109356. Available at: https://doi.org/10.1016/j.foodres.2020.109356.

LAFARGA, T.; SÁNCHEZ-ZURANO, A.; VILLARÓ, S.; MORILLAS-ESPAÑA, A.; ACIÉN, G. Industrial production of *Spirulina* as a protein source for bioactive peptide generation. **Trends in Food Science and Technology**, vol. 116, no. June, pp. 176–185, 2021. https://doi.org/10.1016/j.tifs.2021.07.018.

LAROCHE, C. Exopolysaccharides from Microalgae and Cyanobacteria: Diversity of Strains, Production Strategies, and Applications. **Marine Drugs**, vol. 20, no. 5, p. 336, 21 May 2022. DOI: 10.3390/md20050336. Available at: https://doi.org/10.3390/md20050336. Accessed: 29 Jul. 2022.

LEAL, G. B. C.; SANTOS, K. N. dos; SARPAL, A. S.; COSTA, J. A. V. Two-stage cultivation of the microalga *Chlorella fusca* LEB 111 using the phytohormone indole-3-acetic acid and nitrogen reduction for assessment of aviation fuel applications. **Biomass and Bioenergy**, vol.

210, no. December 2025, p. 109046, 2026. DOI: 10.1016/j.biombioe.2026.109046. Available at: https://doi.org/10.1016/j.biombioe.2026.109046.

LEE, M. C.; CHEN, Y. C.; PENG, T. C. Two-stage culture method for optimized polysaccharide production in *Spirulina platensis*. **Journal of the Science of Food and Agriculture**, vol. 92, no. 7, pp. 1562–1569, 2012. https://doi.org/10.1002/jsfa.4743.

LEVASSEUR, W.; PERRÉ, P.; POZZOBON, V. A review of high value-added molecules production by microalgae in light of the classification. **Biotechnology Advances**, vol. 41, no. January, p. 107545, 2020. DOI: 10.1016/j.biotechadv.2020.107545. Available at: https://doi.org/10.1016/j.biotechadv.2020.107545.

LEZCANO, G.; GAUTAM, R.; HITA, I.; YERRAYYA, A.; ALJAZIRI, J.; DE FREITAS, B. B.; SAMARAS, V. G.; LAUERSEN, K. J.; SARATHY, S. M.; CASTAÑO, P. Linking microalgae characteristics with their fast pyrolysis products. **Journal of Analytical and Applied Pyrolysis**, vol. 191, no. May, p. 107170, Oct. 2025. DOI: 10.1016/j.jaap.2025.107170. Available at: https://linkinghub.elsevier.com/retrieve/pii/S0165237025002232.

LI, C.; HU, Z.; GAO, Y.; MA, Y.; PAN, X.; LI, X.; LIU, S.; CHU, B. Bioeffects of static magnetic fields on the growth and metabolites of *C. pyrenoidosa* and *T. obliquus*. **Journal of Biotechnology**, vol. 351, no. November 2021, pp. 1–8, Jun. 2022. DOI: 10.1016/j.jbiotec.2022.04.004. Available at: https://doi.org/10.1016/j.jbiotec.2022.04.004.

LI, P.; LIU, Z.; XU, R. Chemical characterisation of the released polysaccharide from the cyanobacterium *Aphanothece halophytica* GR02. **Journal of Applied Phycology 2001 13:1**, vol. 13, no. 1, pp. 71–77, 2001. DOI: 10.1023/A:1008109501066. Available at: https://link.springer.com/article/10.1023/A:1008109501066. Accessed: 12 Sep. 2022.

LI, T.; XU, J.; WANG, W.; CHEN, Z.; LI, C.; WU, H.; WU, H.; XIANG, W. A Novel Three-Step Extraction Strategy for High-Value Products from Red Algae *Porphyridium purpureum*. **Foods**, vol. 10, no. 9, p. 2164, 13 Sep. 2021. DOI: 10.3390/foods10092164. Available at: https://www.mdpi.com/2304-8158/10/9/2164.

LI, Z.-Y.; GUO, S.-Y.; LI, L.; CAI, M.-Y. Effects of electromagnetic field on the batch cultivation and nutritional composition of *Spirulina platensis* in an air-lift photobioreactor. **Bioresource Technology**, vol. 98, no. 3, pp. 700–705, Feb. 2007. DOI: 10.1016/j.biortech.2006.01.024. Available at: https://linkinghub.elsevier.com/retrieve/pii/S0960852406000678. Accessed: 14 May 2024.

LI, Z.; LIU, Y.; ZHOU, T.; CAO, L.; CAI, Y.; WANG, Y.; CUI, X.; YAN, H.; RUAN, R.; ZHANG, Q. Effects of Culture Conditions on the Performance of *Arthrospira platensis* and Its Production of Exopolysaccharides. **Foods**, vol. 11, no. 14, p. 2020, 8 Jul. 2022. DOI: 10.3390/foods11142020. Available at: https://www.mdpi.com/2304-8158/11/14/2020.

LICHTENTHALER, H. K. [34] Chlorophylls and carotenoids: Pigments of photosynthetic biomembranes. **Methods in Enzymology**. 1987. vol. 148, no. C, pp. 350–382. DOI: 10.1016/0076-6879(87)48036-1. Available at: https://linkinghub.elsevier.com/retrieve/pii/0076687987480361.

LIU, G.; FU, K.; WANG, X.; QIAN, C.; LIU, J.; WANG, D.; WANG, H.; ZHU, L.; ZHAO, Y. One-Dimensional Helical Aggregates Organized from Achiral Imine-Based Polymers. **ACS Materials Letters**, vol. 4, no. 4, pp. 715–723, 4 Apr. 2022. DOI: 10.1021/acsmaterialslett.2c00111. Available at: https://pubs.acs.org/doi/10.1021/acsmaterialslett.2c00111.

LIU, L.; DIAO, J.; BI, Y.; ZENG, L.; WANG, F.; CHEN, L.; ZHANG, W. Rewiring the Metabolic Network to Increase Docosahexaenoic Acid Productivity in *Crypthecodinium cohnii* by Fermentation Supernatant-Based Adaptive Laboratory Evolution. **Frontiers in Microbiology**, vol. 13, 2 Mar. 2022. DOI: 10.3389/fmicb.2022.824189. Available at: https://www.frontiersin.org/articles/10.3389/fmicb.2022.824189/full.

LOKSTEIN, H.; RENGER, G.; GÖTZE, J. P. Photosynthetic Light-Harvesting (Antenna) Complexes—Structures and Functions. **Molecules**, vol. 26, no. 11, p. 3378, 1 Jun. 2021. DOI: 10.3390/molecules26113378. Available at: https://pmc.ncbi.nlm.nih.gov/articles/PMC8199901/. Accessed: 3 Mar. 2026.

LOWRY, O.; ROSEBROUGH, N.; FARR, A. L.; RANDALL, R. PROTEIN MEASUREMENT WITH THE FOLIN PHENOL REAGENT. **Journal of Biological Chemistry**, vol. 193, no. 1, pp. 265–275, Nov. 1951. DOI: 10.1016/S0021-9258(19)52451-6. Available at: https://linkinghub.elsevier.com/retrieve/pii/S0021925819524516. Accessed: 10 Apr. 2023.

LUO, X.; ZHANG, H.; LI, Q.; ZHANG, J. Effects of static magnetic field on *Chlorella vulgaris*: growth and extracellular polysaccharide (EPS) production. **Journal of Applied Phycology**, vol. 32, no. 5, pp. 2819–2828, 19 Oct. 2020. DOI: 10.1007/s10811-020-02164-7. Available at: https://link.springer.com/10.1007/s10811-020-02164-7. Accessed: 14 May 2024.

MA, J.; YOU, X.; SUN, S.; WANG, X.; QIN, S.; SUI, S.-F. Structural basis of energy transfer in *Porphyridium purpureum* phycobilisome. **Nature**, vol. 579, no. 7797, pp. 146–151, 5 Mar. 2020. DOI: 10.1038/s41586-020-2020-7. Available at: http://dx.doi.org/10.1038/s41586-020-2020-7.

MAIZATUL, A. Y.; RADIN, M. S. R.; MOHAMED, A. A.; AMBATI, R. A.; RANGA, R. Influence of nitrogen and phosphorus on microalgal growth, biomass, lipid, and fatty acid production: An overview. **Cells**, vol. 10, no. 393, pp. 10–20, 2021.

MAJDOUB, H.; MANSOUR, M. Ben; CHAUBET, F.; ROUDESLI, M. S.; MAAROUFI, R. M. Anticoagulant activity of a sulfated polysaccharide from the green alga *Arthrospira platensis*. **Biochimica et Biophysica Acta - General Subjects**, vol. 1790, no. 10, pp. 1377–1381, 2009. https://doi.org/10.1016/j.bbagen.2009.07.013.

MAJHI, B. K. Cyanobacteria : Photosynthetic Cell Factories for Biofuel Production. **Journal of Bioresources and Bioproducts**, pp. 0–28, 2024. DOI: 10.1016/j.jobab.2024.10.001. Available at: https://doi.org/10.1016/j.jobab.2024.10.001.

MAO, M.; HAN, G.; ZHAO, Y.; XU, X.; ZHAO, Y. A review of phycocyanin: Production, extraction, stability and food applications. **International Journal of Biological Macromolecules**, vol. 280, no. P3, p. 135860, 2024. DOI: 10.1016/j.ijbiomac.2024.135860. Available at: https://doi.org/10.1016/j.ijbiomac.2024.135860.

MARCATI, A.; URSU, A. V.; LAROCHE, C.; SOANEN, N.; MARCHAL, L.; JUBEAU, S.; DJELVEH, G.; MICHAUD, P. Extraction and fractionation of polysaccharides and B-phycoerythrin from the microalga *Porphyridium cruentum* by membrane technology. **Algal Research**, vol. 5, no. 1, pp. 258–263, Jul. 2014. DOI: 10.1016/j.algal.2014.03.006. Available at: http://dx.doi.org/10.1016/j.algal.2014.03.006.

MARÉCHAL, Y. Interaction configurations of H_2O molecules in a protein (Stratum Corneum) by infrared spectrometry. **Journal of Molecular Structure**, vol. 416, nos. 1–3, pp. 133–143, Oct. 1997. DOI: 10.1016/S0022-2860(97)00032-X. Available at: https://linkinghub.elsevier.com/retrieve/pii/S002228609700032X. Accessed: 11 Apr. 2024.

MARSH, J. B.; WEINSTEIN, D. B. Simple charring method for determination of lipids. **Journal of Lipid Research**, vol. 7, no. 4, pp. 574–576, 1966. https://doi.org/10.1016/s0022-2275(20)39274-9.

MARTIKAINEN, L.; BERTULA, K.; TURUNEN, M.; IKKALA, O. Strain Stiffening and Negative Normal Force of Agarose Hydrogels. **Macromolecules**, vol. 53, no. 22, pp. 9983–9992, 24 Nov. 2020. DOI: 10.1021/acs.macromol.0c00601. Available at: https://pubs.acs.org/doi/10.1021/acs.macromol.0c00601.

MAULINA, D.; MUN'IM, A.; BAYU, A.; SETIAWAN, H.; MOHD HASHIM, N. Sulfated Exopolysaccharides from *Porphyridium purpureum*: A Review of Extraction, Structural Characterization, and Chemical Properties for Advanced Applications. **F1000Research**, vol. 14, p. 1323, 27 Nov. 2025. DOI: 10.12688/f1000research.173006.1. Available at: https://f1000research.com/articles/14-1323/v1.

MEDINA-CABRERA, E. V.; GANSBILLER, M.; RÜHMANN, B.; SCHMID, J.; SIEBER, V. Rheological characterization of *Porphyridium sordidum* and *Porphyridium purpureum* exopolysaccharides. **Carbohydrate Polymers**, vol. 253, no. October 2020, p. 117237, 2021. DOI: 10.1016/j.carbpol.2020.117237. Available at: https://doi.org/10.1016/j.carbpol.2020.117237.

MEDINA-CABRERA, E. V.; RÜHMANN, B.; SCHMID, J.; SIEBER, V. Characterization and comparison of Porphyridium sordidum and *Porphyridium purpureum* concerning growth characteristics and polysaccharide production. **Algal Research**, vol. 49, no. October 2019, p. 101931, Aug. 2020. DOI: 10.1016/j.algal.2020.101931. Available at: https://doi.org/10.1016/j.algal.2020.101931.

MENESTRINO, B. da C.; PINTOS, T. H. C.; SALA, L.; COSTA, J. A. V.; SANTOS, L. O. Application of Static Magnetic Fields on the Mixotrophic Culture of *Chlorella minutissima* for Carbohydrate Production. **Applied Biochemistry and Biotechnology**, vol. 192, no. 3, pp. 822–830, 29 Nov. 2020. DOI: 10.1007/s12010-020-03364-0. Available at: https://link.springer.com/10.1007/s12010-020-03364-0.

MENESTRINO, B. da C.; SALA, L.; COSTA, J. A. V.; BUFFON, J. G.; SANTOS, L. O. Magnetic fields exhibit a positive impact on lipid and biomass yield during phototrophic cultivation of Spirulina sp. **Bioprocess and Biosystems Engineering**, vol. 44, no. 10, pp. 2087–2097, 2021. DOI: 10.1007/s00449-021-02585-9. Available at: https://doi.org/10.1007/s00449-

021-02585-9.

MOLAEI, H.; JAHANBIN, K. Structural features of a new water-soluble polysaccharide from the gum exudates of *Amygdalus scoparia* Spach (Zedo gum). 2017. DOI: 10.1016/j.carbpol.2017.10.099. Available at: www.elsevier.com/locate/carbpol. Accessed: 21 May 2024.

MONSIGNY, M.; PETIT, C.; ROCHE, A.-C. Colorimetric determination of neutral sugars by a resorcinol sulfuric acid micromethod. **Analytical Biochemistry**, vol. 175, no. 2, pp. 525–530, Dec. 1988. https://doi.org/10.1016/0003-2697(88)90578-7.

MONTEIL, C. L.; LEFEVRE, C. T. Magnetoreception in Microorganisms. **Trends in microbiology**, vol. 28, no. 4, pp. 266–275, Apr. 2020. DOI: 10.1016/j.tim.2019.10.012. Available at: https://doi.org/10.1016/j.tim.2019.10.012.

MONTREUIL, J.; SPIK, G.; CHOSSON, A.; SEGARD, E.; SCHEPPLER, N. Methods of study of the structure of glycoproteins. **Journal de pharmacie de Belgique**, vol. 18, pp. 529–46, 1963. Available at: http://www.ncbi.nlm.nih.gov/pubmed/14096752.

MORENO, J.; VARGAS, M. A.; OLIVARES, H.; RIVAS, J.; GUERRERO, M. G. Exopolysaccharide production by the cyanobacterium *Anabaena sp*. ATCC 33047 in batch and continuous culture. **Journal of Biotechnology**, vol. 60, no. 3, pp. 175–182, 1998. https://doi.org/10.1016/S0168-1656(98)00003-0.

MOTHÉ, C. G.; FREITAS, J. S. de. Lifetime prediction and kinetic parameters of thermal decomposition of cashew gum by thermal analysis. **Journal of Thermal Analysis and Calorimetry**, vol. 131, no. 1, pp. 397–404, 28 Jan. 2018. DOI: 10.1007/s10973-017-6844-9. Available at: https://doi.org/10.1007/s10973-017-6844-9.

MÜLLER, P.; AHMAD, M. Light-activated cryptochrome reacts with molecular oxygen to form a flavin-superoxide radical pair consistent with magnetoreception. **Journal of Biological Chemistry**, vol. 286, no. 24, pp. 21033–21040, 17 Jun. 2011. DOI: 10.1074/jbc.M111.228940. Available at: https://pubmed.ncbi.nlm.nih.gov/21467031/. Accessed: 1 Jul. 2026.

MÜNSTEDT, H. Rheological Measurements and Structural Analysis of Polymeric Materials. **Polymers**, vol. 13, no. 7, p. 1123, 1 Apr. 2021. DOI: 10.3390/polym13071123. Available at: https://www.mdpi.com/2073-4360/13/7/1123.

MURO-PASTOR, M. I.; REYES, J. C.; FLORENCIO, F. J. Ammonium assimilation in cyanobacteria. **Photosynthesis Research**, vol. 83, no. 2, pp. 135–150, Feb. 2005. DOI: 10.1007/s11120-004-2082-7. Available at: http://link.springer.com/10.1007/s11120-004-2082-7.

NAVALHO, S.; FERRER-LEDO, N.; BARBOSA, M. J.; VARELA, J. Nannochloropsis Lipids and Polyunsaturated Fatty Acids: Potential Applications and Strain Improvement. **Marine Drugs**, vol. 23, no. 3, pp. 1–34, 2025. https://doi.org/10.3390/md23030128.

NAVEED, S.; LI, C.; LU, X.; CHEN, S.; YIN, B.; ZHANG, C.; GE, Y. Microalgal extracellular polymeric substances and their interactions with metal(loid)s: A review. **Critical Reviews in**

Environmental Science and Technology, vol. 49, no. 19, pp. 1769–1802, 2019. DOI: 10.1080/10643389.2019.1583052. Available at: https://doi.org/10.1080/10643389.2019.1583052.

NGUYEN, A. Q.; MOHAMMADI, M.; ALIAN, M.; MURALITHARAN, G.; CHAUHAN, V. S.; BALAN, V. Exploring the versatility of *Porphyridium sp*.: A comprehensive review of cultivation, bio-product extraction, purification, and characterization techniques. **Biotechnology Advances**, vol. 77, no. October, p. 108471, 2024. DOI: 10.1016/j.biotechadv.2024.108471. Available at: https://doi.org/10.1016/j.biotechadv.2024.108471.

NIE, J.; PEI, B.; WANG, Z.; HU, Q. Construction of ordered structure in polysaccharide hydrogel: A review. **Carbohydrate Polymers**, vol. 205, no. October 2018, pp. 225–235, Feb. 2019. DOI: 10.1016/j.carbpol.2018.10.033. Available at: https://doi.org/10.1016/j.carbpol.2018.10.033.

NOWICKA-KRAWCZYK, P.; MÜHLSTEINOVÁ, R.; HAUER, T. Detailed characterization of the *Arthrospira* type species separating commercially grown taxa into the new genus *Limnospira* (Cyanobacteria). **Scientific Reports**, vol. 9, no. 1, p. 694, 24 Jan. 2019. DOI: 10.1038/s41598-018-36831-0. Available at: https://www.nature.com/articles/s41598-018-36831-0.

NUR, S.; OSLAN, H.; SHOPARWE, N. F.; YUSOFF, A. H.; RAHIM, A. A.; CHANG, C. S.; TAN, J. S.; OSLAN, S. N.; ARUMUGAM, K.; ARIFF, A. Bin; SULAIMAN, A. Z.; MOHAMED, M. S. A Review on *Haematococcus pluvialis* Bioprocess Optimization of Green and Red Stage Culture Conditions for the Production of Natural Astaxanthin. **Biomolecules**, vol. 11, no. 256, pp. 1–15, 2021.

NURAZZI, N. M.; ASYRAF, M. R. M.; RAYUNG, M.; NORRRAHIM, M. N. F.; SHAZLEEN, S. S.; RANI, M. S. A.; SHAFI, A. R.; AISYAH, H. A.; RADZI, M. H. M.; SABARUDDIN, F. A.; ILYAS, R. A.; ZAINUDIN, E. S.; ABDAN, K. Thermogravimetric Analysis Properties of Cellulosic Natural Fiber Polymer Composites: A Review on Influence of Chemical Treatments. **Polymers**, vol. 13, no. 16, p. 2710, 13 Aug. 2021. DOI: 10.3390/polym13162710. Available at: https://www.mdpi.com/2073-4360/13/16/2710.

OLIVEIRA, C. Y. B.; JACOB, A.; NADER, C.; OLIVEIRA, C. D. L.; MATOS, Â. P.; ARAÚJO, E. S.; SHABNAM, N.; ASHOK, B.; GÁLVEZ, A. O. An overview on microalgae as renewable resources for meeting sustainable development goals. **Journal of Environmental Management**, vol. 320, no. May, 2022. https://doi.org/10.1016/j.jenvman.2022.115897.

ONG, Y. X. J.; LEE, L. Y.; DAVOODI, P.; WANG, C. H. Production of drug-releasing biodegradable microporous scaffold using a two-step micro-encapsulation/supercritical foaming process. **Journal of Supercritical Fluids**, vol. 133, no. July 2017, pp. 263–269, 2018. DOI: 10.1016/j.supflu.2017.10.018. Available at: https://doi.org/10.1016/j.supflu.2017.10.018.

PANYAKAMPOL, J.; CHEEVADHANARAK, S.; SENACHAK, J.; DULSAWAT, S.; SIANGDUNG, W.; TANTICHAROEN, M.; PAITHOONRANGSARID, K. Different effects of the combined stress of nitrogen depletion and high temperature than an individual stress on the synthesis of biochemical compounds in Arthrospira platensis C1 (PCC 9438). **Journal of Applied Phycology**, vol. 28, no. 4, pp. 2177–2186, 1 Aug. 2016. DOI: 10.1007/S10811-015-0765-4/TABLES/3. Available at: https://link.springer.com/article/10.1007/s10811-015-0765-4.

Accessed: 5 Oct. 2022.

PAZUR, A.; WINKLHOFER, M. Magnetic effect on CO_2 solubility in seawater: A possible link between geomagnetic field variations and climate. **Geophysical Research Letters**, vol. 35, no. 16, 30 Aug. 2008. DOI: 10.1029/2008GL034288. Available at: https://agupubs.onlinelibrary.wiley.com/doi/10.1029/2008GL034288.

PESSÔA, L. C.; DEAMICI, K. M.; PONTES, L. A. M.; DRUZIAN, J. I.; ASSIS, D. de J. Technological prospection of microalgae-based biorefinery approach for effluent treatment. **Algal Research**, vol. 60, no. September, 2021. https://doi.org/10.1016/j.algal.2021.102504.

PHÉLIPPÉ, M.; GONÇALVES, O.; THOUAND, G.; COGNE, G.; LAROCHE, C. Characterization of the polysaccharides chemical diversity of the cyanobacteria *Arthrospira platensis*. **Algal Research**, vol. 38, no. December 2018, p. 101426, 2019. DOI: 10.1016/j.algal.2019.101426. Available at: https://doi.org/10.1016/j.algal.2019.101426.

PIERRE, G.; DELATTRE, C.; DUBESSAY, P.; JUBEAU, S.; VIALLEIX, C.; CADORET, J. P.; PROBERT, I.; MICHAUD, P. What is in store for EPS microalgae in the next decade? **Multidisciplinary Digital Publishing Institute**, vol. 24, no. 23, p. 4296, 25 Nov. 2019. DOI: 10.3390/molecules24234296. Available at: https://www.mdpi.com/1420-3049/24/23/4296/htm. Accessed: 13 Oct. 2022.

PLETIKAPIĆ, G.; LANNON, H.; MURVAI, Ü.; KELLERMAYER, M. S. Z.; SVETLIČIĆ, V.; BRUJIC, J. Self-Assembly of Polysaccharides Gives Rise to Distinct Mechanical Signatures in Marine Gels. **Biophysical Journal**, vol. 107, no. 2, pp. 355–364, Jul. 2014. DOI: 10.1016/j.bpj.2014.04.065. Available at: https://linkinghub.elsevier.com/retrieve/pii/S0006349514006043.

POLUEKTOV, O. G.; UTSCHIG, L. M. Quantum Sensing of Electron Transfer Pathways in Natural Photosynthesis Using Time-Resolved High-Field Electron Paramagnetic Resonance/Electron–Nuclear Double Resonance Spectroscopy. **The Journal of Physical Chemistry B**, vol. 125, no. 16, pp. 4025–4030, 29 Apr. 2021. DOI: 10.1021/acs.jpcb.1c00946. Available at: /doi/pdf/10.1021/acs.jpcb.1c00946?ref=article_openPDF. Accessed: 3 Mar. 2026.

PORRA, R. J. The chequered history of the development and use of simultaneous equations for the accurate determination of chlorophylls a and b. **Photosynthesis research**, vol. 73, nos. 1–3, pp. 149–56, 2002. DOI: 10.1023/A:1020470224740. Available at: http://www.ncbi.nlm.nih.gov/pubmed/16245116.

PRIORETTI, L.; GONTERO, B.; HELL, R.; GIORDANO, M. Diversity and regulation of ATP sulfurylase in photosynthetic organisms. **Frontiers in Plant Science**, vol. 5, no. November, pp. 1–12, 5 Nov. 2014. DOI: 10.3389/fpls.2014.00597. Available at: http://journal.frontiersin.org/article/10.3389/fpls.2014.00597/abstract.

RAHMAN, P. K. S. M.; MAYAT, A.; HARVEY, J. G. H.; RANDHAWA, K. S.; RELPH, L. E.; ARMSTRONG, M. C. Biosurfactants and Bioemulsifiers from Marine Algae. **The Role of Microalgae in Wastewater Treatment**, pp. 169–188, 2019. DOI: 10.1007/978-981-13-1586-2_13. Available at: https://link.springer.com/chapter/10.1007/978-3-319-24945-2_21.

RAWAT, E.; SHARMA, S.; VYAS, S.; ALSAIDAN, O. A.; KAPOOR, D. U.; PRAJAPATI, B. G. Advances in alginate-based nanoformulations: Innovative and effective strategies for targeting and treating brain disorders. **International Journal of Pharmaceutics**, vol. 681, no. May, p. 125851, Aug. 2025. DOI: 10.1016/j.ijpharm.2025.125851. Available at: https://doi.org/10.1016/j.ijpharm.2025.125851.

RICHMOND, A. **Handbook of Microalgal Culture**. Oxford, UK: Wiley, 25 Nov. 2003. DOI: 10.1002/9780470995280. Available at: https://onlinelibrary.wiley.com/doi/book/10.1002/9780470995280.

ROSA, G. M. da; MORAES, L.; CARDIAS, B. B.; SOUZA, M. da R. A. Z. de; COSTA, J. A. V. Chemical absorption and CO_2 biofixation via the cultivation of *Spirulina* in semicontinuous mode with nutrient recycle. **Bioresource Technology**, vol. 192, pp. 321–327, Sep. 2015. https://doi.org/10.1016/j.biortech.2015.05.020.

ROSA, G. M. da; MORAIS, M. G. de; COSTA, J. A. V. Green alga cultivation with monoethanolamine: Evaluation of CO_2 fixation and macromolecule production. **Bioresource Technology**, vol. 261, no. April, pp. 206–212, 2018. https://doi.org/10.1016/j.biortech.2018.04.007.

ROSA, G. M.; MORAES, L.; DE SOUZA, M. da R. A. Z.; COSTA, J. A. V. *Spirulina* cultivation with a CO_2 absorbent: Influence on growth parameters and macromolecule production. **Bioresource Technology**, vol. 200, pp. 528–534, 1 Jan. 2016. https://doi.org/10.1016/J.BIORTECH.2015.10.025.

ROSSI, F.; PHILIPPIS, R. De. **The Physiology of Microalgae**. Cham: Springer International Publishing, 2016. DOI: 10.1007/978-3-319-24945-2. Available at: http://link.springer.com/10.1007/978-3-319-24945-2.

SAFI, C.; ZEBIB, B.; MERAH, O.; PONTALIER, P. Y.; VACA-GARCIA, C. Morphology, composition, production, processing and applications of *Chlorella vulgaris*: A review. **Renewable and Sustainable Energy Reviews**, vol. 35, pp. 265–278, 2014. https://doi.org/10.1016/j.rser.2014.04.007.

SAHA, D.; BHATTACHARYA, S. Hydrocolloids as thickening and gelling agents in food: a critical review. **Journal of Food Science and Technology**, vol. 47, no. 6, pp. 587–597, 6 Dec. 2010. DOI: 10.1007/s13197-010-0162-6. Available at: http://link.springer.com/10.1007/s13197-010-0162-6.

SAID, R. Ben; KOLLE, J. M.; ESSALAH, K.; TANGOUR, B.; SAYARI, A. A Unified Approach to CO_2 –Amine Reaction Mechanisms. **ACS Omega**, vol. 5, no. 40, pp. 26125–26133, 13 Oct. 2020. DOI: 10.1021/acsomega.0c03727. Available at: https://pubs.acs.org/doi/10.1021/acsomega.0c03727.

SAIEV, S.; BELJONNE, D.; LAZZARONI, R.; ROOSE, P. Decoding Elasticity Build-Up and Network Topology in Free-Radical Cross-Linking Polymerization: A Combined Experimental and Atomistic Approach. **Macromolecules**, vol. 56, no. 18, pp. 7396–7405, 26 Sep. 2023. DOI: 10.1021/acs.macromol.3c00644. Available at:

https://pubs.acs.org/doi/10.1021/acs.macromol.3c00644.

SANTOS, L. O.; SILVA, P. G. P.; MACHADO, B. R.; SALA, L.; DEAMICI, K. M. Update on the application of magnetic fields to microalgal cultures. **World Journal of Microbiology and Biotechnology**, vol. 38, no. 11, pp. 1–10, 2 Nov. 2022. DOI: 10.1007/s11274-022-03398-y. Available at: https://link.springer.com/article/10.1007/s11274-022-03398-y. Accessed: 3 Oct. 2022.

SAYKO, R.; JACOBS, M.; DOBRYNIN, A. V. Quantifying Properties of Polysaccharide Solutions. **ACS Polymers Au**, vol. 1, no. 3, pp. 196–205, 8 Dec. 2021. DOI: 10.1021/acspolymersau.1c00028. Available at: https://pubs.acs.org/doi/10.1021/acspolymersau.1c00028.

SCHOETERS, F.; SPIT, J.; SWINNEN, E.; DE CUYPER, A.; VLEUGELS, R.; NOYENS, I.; VAN MIERT, S. Pilot-scale cultivation of the red alga *Porphyridium purpureum* over a two-year period in a greenhouse. **Journal of Applied Phycology**, vol. 35, no. 5, pp. 2095–2109, 2 Oct. 2023. DOI: 10.1007/s10811-023-03045-5. Available at: https://link.springer.com/10.1007/s10811-023-03045-5.

SCHUBERT, N.; GARCÍA-MENDOZA, E.; PACHECO-RUIZ, I. CAROTENOID COMPOSITION OF MARINE RED ALGAE. **Journal of Phycology**, vol. 42, no. 6, pp. 1208–1216, 16 Dec. 2006. DOI: 10.1111/j.1529-8817.2006.00274.x. Available at: https://onlinelibrary.wiley.com/doi/10.1111/j.1529-8817.2006.00274.x.

SERRANO, G.; MIRANDA-OSTOJIC, C.; FERRADA, P.; WULFF-ZOTELLE, C.; MAUREIRA, A.; FUENTEALBA, E.; GALLARDO, K.; ZAPATA, M.; RIVAS, M. Response to static magnetic field-induced stress in *Scenedesmus* obliquus and *Nannochloropsis* gaditana. **Marine Drugs**, vol. 19, no. 9, 2021. https://doi.org/10.3390/md19090527.

SHAO, W.; EBAID, R.; ABOMOHRA, A. E.-F.; SHAHEN, M. Enhancement of *Spirulina* biomass production and cadmium biosorption using combined static magnetic field. **Bioresource Technology**, vol. 265, pp. 163–169, Oct. 2018. DOI: 10.1016/j.biortech.2018.06.009. Available at: https://linkinghub.elsevier.com/retrieve/pii/S0960852418307880. Accessed: 14 May 2024.

SIMON-BERCOVITCH, B.; BAR-ZVI, D.; ARAD, S. (Malis). Cell-wall formation during the cell cycle of porphyridium sp. (Rhodophyta). **Journal of Phycology**, vol. 35, no. 1, pp. 78–83, Feb. 1999. DOI: 10.1046/j.1529-8817.1999.3510078.x. Available at: http://doi.wiley.com/10.1046/j.1529-8817.1999.3510078.x.

SOANEN, N.; DA SILVA, E.; GARDARIN, C.; MICHAUD, P.; LAROCHE, C. Improvement of exopolysaccharide production by *Porphyridium marinum*. **Bioresource Technology**, vol. 213, pp. 231–238, 2016. DOI: 10.1016/j.biortech.2016.02.075. Available at: http://dx.doi.org/10.1016/j.biortech.2016.02.075.

SORICHETTI, V.; NINARELLO, A.; RUIZ-FRANCO, J.; HUGOUVIEUX, V.; ZACCARELLI, E.; MICHELETTI, C.; KOB, W.; ROVIGATTI, L. Structure and elasticity of model disordered, polydisperse, and defect-free polymer networks. **Journal of Chemical Physics**, vol. 158, no. 7, 2023. DOI: 10.1063/5.0134271. Available at: https://doi.org/10.1063/5.0134271.

STOJKOV, G.; NIYAZOV, Z.; PICCHIONI, F.; BOSE, R. K. Relationship between Structure and Rheology of Hydrogels for Various Applications. **Gels**, vol. 7, no. 4, p. 255, 9 Dec. 2021. DOI: 10.3390/gels7040255. Available at: https://www.mdpi.com/2310-2861/7/4/255.

SUN, L.; WANG, C.; SHI, Q.; MA, C. Preparation of different molecular weight polysaccharides from *Porphyridium cruentum* and their antioxidant activities. **International Journal of Biological Macromolecules**, vol. 45, no. 1, pp. 42–47, 2009. https://doi.org/10.1016/j.ijbiomac.2009.03.013.

SUN, L.; WANG, L.; ZHOU, Y. Immunomodulation and antitumor activities of different-molecular-weight polysaccharides from *Porphyridium cruentum*. **Carbohydrate Polymers**, vol. 87, no. 2, pp. 1206–1210, 2012. DOI: 10.1016/j.carbpol.2011.08.097. Available at: http://dx.doi.org/10.1016/j.carbpol.2011.08.097.

TAMIAKI, H.; KICHISHIMA, S. Chlorophyll Pigments and Their Synthetic Analogs. **Plant and Cell Physiology**, vol. 66, no. 2, p. 153, 28 Feb. 2024. DOI: 10.1093/pcp/pcae094. Available at: https://pmc.ncbi.nlm.nih.gov/articles/PMC11879082/. Accessed: 3 Mar. 2026.

TAN, T.; HOU, Y.; SHI, J.; WANG, B.; ZHANG, Y. Materials Today Bio Biostable hydrogels consisting of hybrid β -sheet fibrils assembled by a pair of enantiomeric peptides. **Materials Today Bio**, vol. 25, no. January, p. 100961, 2024. DOI: 10.1016/j.mtbio.2024.100961. Available at: https://doi.org/10.1016/j.mtbio.2024.100961.

USOV, A. I.; ZELINSKY, N. D. Chemical structures of algal polysaccharides. **Functional Ingredients from Algae for Foods and Nutraceuticals**. Elsevier, 2013. no. 2011, pp. 23–86. DOI: 10.1533/9780857098689.1.23. Available at: http://dx.doi.org/10.1533/9780857098689.1.23.

VAN CAMP, C.; FRAIKIN, C.; CLAVERIE, E.; ONDERWATER, R.; WATTIEZ, R. Capsular polysaccharides and exopolysaccharides from *Gloeothece verrucosa* under various nitrogen regimes and their potential plant defence stimulation activity. **Algal Research**, vol. 64, p. 102680, 1 May 2022. DOI: 10.1016/j.algal.2022.102680. Available at: https://linkinghub.elsevier.com/retrieve/pii/S2211926422000510.

VAZ, B. da S.; COSTA, A. V.; MORAIS, M. G. de. Physical and biological fixation of CO_2 with polymeric nanofibers in outdoor cultivations of *Chlorella fusca* LEB 111. **International Journal of Biological Macromolecules**, vol. 151, pp. 1332–1339, May 2020. DOI: 10.1016/j.ijbiomac.2019.10.179. Available at: https://linkinghub.elsevier.com/retrieve/pii/S0141813019357472.

VAZ, B. da S.; COSTA, J. A. V.; MORAIS, M. G. de; VIEIRA COSTA, J. A.; GREQUE DE MORAIS, M. Innovative nanofiber technology to improve carbon dioxide biofixation in microalgae cultivation. **Bioresource Technology**, vol. 273, pp. 592–598, Feb. 2019. DOI: 10.1016/j.biortech.2018.11.054. Available at: https://doi.org/10.1016/j.biortech.2018.11.054. Accessed: 15 May 2024.

VAZ, B. da S.; MASTRANTONIO, D. J. da S.; COSTA, J. A. V.; MORAIS, M. G. de. Green alga cultivation with nanofibers as physical adsorbents of carbon dioxide: Evaluation of gas

biofixation and macromolecule production. **Bioresource Technology**, vol. 287, no. May, p. 121406, Sep. 2019. DOI: 10.1016/j.biortech.2019.121406. Available at: https://linkinghub.elsevier.com/retrieve/pii/S0960852419306364.

VAZ, B. da S.; VIEIRA COSTA, J. A.; GREQUE DE MORAIS, M. Innovative nanofiber technology to improve carbon dioxide biofixation in microalgae cultivation. 2018. DOI: 10.1016/j.biortech.2018.11.054. Available at: https://doi.org/10.1016/j.biortech.2018.11.054. Accessed: 15 May 2024.

VEIGA, M. C.; FONTOURA, M. M.; DE OLIVEIRA, M. G.; COSTA, J. A. V.; SANTOS, L. O. Magnetic fields: biomass potential of *Spirulina sp*. for food supplement. **Bioprocess and Biosystems Engineering**, vol. 43, no. 7, pp. 1231–1240, 2020. DOI: 10.1007/s00449-020-02318-4. Available at: https://doi.org/10.1007/s00449-020-02318-4.

VILLAY, A.; LAROCHE, C.; RORIZ, D.; EL ALAOUI, H.; DELBAC, F.; MICHAUD, P. Optimisation of culture parameters for exopolysaccharides production by the microalga *Rhodella violacea*. **Bioresource Technology**, vol. 146, pp. 732–735, 2013. https://doi.org/10.1016/j.biortech.2013.07.030.

VINCENZINI, M.; DE PHILIPPIS, R.; SILI, C.; MATERASSI, R. Stability of molecular and rheological properties of the exopolysaccharide produced by *Cyanospira capsulata* cultivated under different growth conditions. **Journal of Applied Phycology 1993 5:5**, vol. 5, no. 5, pp. 539–541, Oct. 1993. DOI: 10.1007/BF02182513. Available at: https://link.springer.com/article/10.1007/BF02182513. Accessed: 12 Sep. 2022.

WAN, D.; WU, Q.; KUČA, K. *Spirulina*. **Nutraceuticals: Efficacy, Safety and Toxicity**, pp. 569–583, 2016. https://doi.org/10.1016/B978-0-12-802147-7.00042-5.

WANG, M.; YIN, Z.; ZENG, M. Microalgae as a promising structure ingredient in food: Obtained by simple thermal and high-speed shearing homogenization. **Food Hydrocolloids**, vol. 131, no. April, p. 107743, Oct. 2022. DOI: 10.1016/j.foodhyd.2022.107743. Available at: https://doi.org/10.1016/j.foodhyd.2022.107743.

WANG, S. C.; BLIGH, S. W. A.; SHI, S. S.; WANG, Z. T.; HU, Z. B.; CROWDER, J.; BRANFORD-WHITE, C.; VELLA, C. Structural features and anti-HIV-1 activity of novel polysaccharides from red algae *Grateloupia longifolia* and *Grateloupia filicina*. **International Journal of Biological Macromolecules**, vol. 41, no. 4, pp. 369–375, Oct. 2007. DOI: 10.1016/j.ijbiomac.2007.05.008. Available at: https://doi.org/10.1016/j.ijbiomac.2007.05.008.

WANG, W. N.; LI, Y.; ZHANG, Y.; XIANG, W. Z.; LI, A. F.; LI, T. Comparison on characterization and antioxidant activity of exopolysaccharides from two *Porphyridium* strains. **Journal of Applied Phycology**, vol. 33, no. 5, pp. 2983–2994, 1 Oct. 2021. DOI: 10.1007/s10811-021-02518-9. Available at: https://link.springer.com/article/10.1007/s10811-021-02518-9. Accessed: 26 Aug. 2022.

WANG, X.; ZHANG, Z.; YAO, Q.; ZHAO, M.; QI, H. Phosphorylation of low-molecular-weight polysaccharide from Enteromorpha linza with antioxidant activity. **Carbohydrate Polymers**, vol. 96, no. 2, pp. 371–375, Jul. 2013. DOI: 10.1016/j.carbpol.2013.04.029. Available at:

http://dx.doi.org/10.1016/j.carbpol.2013.04.029.

WIERCIGROCH, E.; SZAFRANIEC, E.; CZAMARA, K.; PACIA, M. Z.; MAJZNER, K.; KOCHAN, K.; KACZOR, A.; BARANSKA, M.; MALEK, K. Raman and infrared spectroscopy of carbohydrates: A review. **Spectrochimica Acta - Part A: Molecular and Biomolecular Spectroscopy**, vol. 185, pp. 317–335, 2017. DOI: 10.1016/j.saa.2017.05.045. Available at: http://dx.doi.org/10.1016/j.saa.2017.05.045.

WÓJCIK-AUGUSTYN, A.; JOHANSSON, A. J.; BOROWSKI, T. Mechanism of Sulfate Activation Catalyzed by ATP Sulfurylase - Magnesium Inhibits the Activity. **Computational and Structural Biotechnology Journal**, vol. 17, pp. 770–784, 2019. DOI: 10.1016/j.csbj.2019.06.016. Available at: https://linkinghub.elsevier.com/retrieve/pii/S2001037018303118.

WU, N.; LI, Y.; LAN, C. Q. Production and Rheological Studies of Microalgal Extracellular Biopolymer from Lactose Using the Green Alga Neochloris oleoabundans. **Journal of Polymers and the Environment**, vol. 19, no. 4, pp. 935–942, 6 Dec. 2011. DOI: 10.1007/s10924-011-0351-z. Available at: http://link.springer.com/10.1007/s10924-011-0351-z.

WU, X.; LIU, Z.; LIU, Y.; YANG, Y.; SHI, F.; CHEONG, K.-L.; TENG, B. Immunostimulatory Effects of Polysaccharides from *Spirulina platensis* In Vivo and Vitro and Their Activation Mechanism on RAW246.7 Macrophages. **Marine Drugs**, vol. 18, no. 11, p. 538, 28 Oct. 2020. DOI: 10.3390/md18110538. Available at: https://www.mdpi.com/1660-3397/18/11/538.

XIA, P.; ZHANG, W.; PENG, C.; YIN, H.; WANG, D. M.; YANG, J.; TUAN, R. S.; JIANG, L.; WANG, J. A High-Order Double Network Hydrogel. **Macromolecules**, vol. 57, no. 23, pp. 11251–11265, 2024. https://doi.org/10.1021/acs.macromol.4c01880.

XIAO, R.; ZHENG, Y. Overview of microalgal extracellular polymeric substances (EPS) and their applications. **Biotechnology Advances**, vol. 34, no. 7, pp. 1225–1244, 2016. DOI: 10.1016/j.biotechadv.2016.08.004. Available at: http://dx.doi.org/10.1016/j.biotechadv.2016.08.004.

XIE, L.; SHEN, M.; WANG, Z.; XIE, J. Structure, function and food applications of carboxymethylated polysaccharides: A comprehensive review. **Trends in Food Science and Technology**, vol. 118, no. PA, pp. 539–557, 2021. DOI: 10.1016/j.tifs.2021.09.016. Available at: https://doi.org/10.1016/j.tifs.2021.09.016.

XIONG, W.; CANO, M.; WANG, B.; DOUCHI, D.; YU, J. The plasticity of cyanobacterial carbon metabolism. **Current Opinion in Chemical Biology**, vol. 41, pp. 12–19, 2017. DOI: 10.1016/j.cbpa.2017.09.004. Available at: http://dx.doi.org/10.1016/j.cbpa.2017.09.004.

XU, H.; LI, Y.; SONG, J.; ZHOU, L.; WU, K.; LU, X.; ZHAI, X.; WAN, Z.; GAO, J. Highly active probiotic hydrogels matrixed on bacterial EPS accelerate wound healing via maintaining stable skin microbiota and reducing inflammation. **Bioactive Materials**, vol. 35, no. January, pp. 31–44, May 2024. DOI: 10.1016/j.bioactmat.2024.01.011. Available at: https://doi.org/10.1016/j.bioactmat.2024.01.011.

XU, P.; LI, J.; QIAN, J.; WANG, B.; LIU, J.; XU, R.; CHEN, P.; ZHOU, W. Recent advances in CO_2 fixation by microalgae and its potential contribution to carbon neutrality. **Chemosphere**, vol. 319, p. 137987, Apr. 2023. DOI: 10.1016/j.chemosphere.2023.137987. Available at: https://linkinghub.elsevier.com/retrieve/pii/S0045653523002540.

XU, S.; JIANG, Y.; LIU, Y.; ESAKKIMUTHU, S.; CHEN, H.; WANG, S. Impact of constant magnetic field on enhancing the microalgal biomass and biomolecules accumulations and life cycle assessment of the approach. **Algal Research**, vol. 80, p. 103563, Jun. 2024. DOI: https://doi.org/10.1016/j.algal.2024.103563. Available at: https://www.sciencedirect.com/science/article/pii/S2211926424001759.

XUE, J.-T.; BAI, Y.; PENG, L.; HUANG, X.-B.; SUN, Z.-Y. Exploring the Interplay between Local Chain Structure and Stress Distribution in Polymer Networks. **Chinese Journal of Polymer Science**, vol. 42, no. 6, pp. 874–885, 7 Jun. 2024. DOI: 10.1007/s10118-024-3099-3. Available at: https://link.springer.com/10.1007/s10118-024-3099-3.

YI, S.; ZHANG, A. H.; HUANG, J.; YAO, T.; FENG, B.; ZHOU, X.; HU, Y.; PAN, M. Maximizing Polysaccharides and Phycoerythrin in *Porphyridium purpureum* via the Addition of Exogenous Compounds: A Response-Surface-Methodology Approach. **Marine Drugs**, vol. 22, no. 3, 2024. https://doi.org/10.3390/md22030138.

YOON, S.; CHANG, S. C.; PAYNE, G. F.; LEE, S.; KYHM, K.; PARK, S. G.; KANG, M. Effect of a magnetic field on the activity of superoxide dismutase studied at the enzyme level. **RSC Advances**, vol. 16, no. 28, pp. 25395–25401, 15 May 2026. DOI: 10.1039/D5RA10059C. Available at: https://dx.doi.org/10.1039/d5ra10059c. Accessed: 1 Jul. 2026.

YU, Y.; JIA, X.; WANG, W.; JIN, Y.; LIU, W.; WANG, D.; MAO, Y.; XIE, C.; LIU, T. Floridean Starch and Floridoside Metabolic Pathways of Neoporphyra haitanensis and Their Regulatory Mechanism under Continuous Darkness. **Marine Drugs**, vol. 19, no. 12, p. 664, 26 Nov. 2021. DOI: 10.3390/md19120664. Available at: https://www.mdpi.com/1660-3397/19/12/664.

YU, Z.; ZHAO, W.; SUN, H.; MOU, H.; LIU, J.; YU, H.; DAI, L.; KONG, Q.; YANG, S. Phycocyanin from microalgae: A comprehensive review covering microalgal culture, phycocyanin sources and stability. **Food Research International**, vol. 186, no. December 2023, p. 114362, Jun. 2024. DOI: 10.1016/j.foodres.2024.114362. Available at: https://doi.org/10.1016/j.foodres.2024.114362.

YUNUS, R. A. M.; PARISI, D. Scaling Laws in Polysaccharide Rheology: Comparative Analysis of Water and Ionic Liquid Systems. **Biomacromolecules**, vol. 25, no. 10, pp. 6883–6898, 14 Oct. 2024. DOI: 10.1021/acs.biomac.4c01125. Available at: https://pubs.acs.org/doi/10.1021/acs.biomac.4c01125.

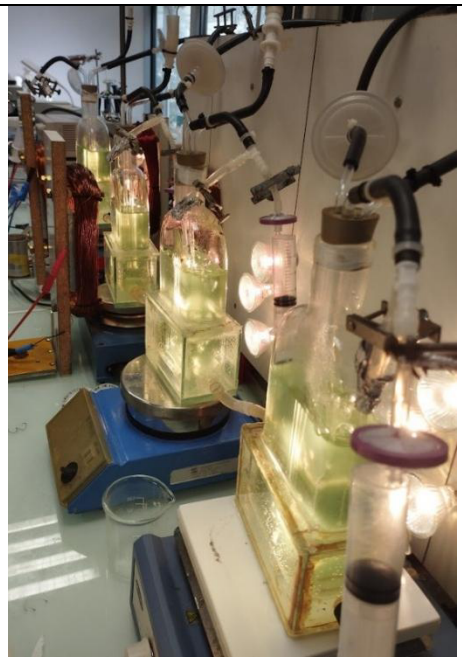
ZHANG, A. H.; FENG, B.; ZHANG, H.; JIANG, J.; ZHANG, D.; DU, Y.; CHENG, Z.; HUANG, J. Efficient cultivation of *Porphyridium purpureum* integrated with swine wastewater treatment to produce phycoerythrin and polysaccharide. **Journal of Applied Phycology**, vol. 34, no. 5, pp. 2315–2326, 2022. https://doi.org/10.1007/s10811-022-02785-0.

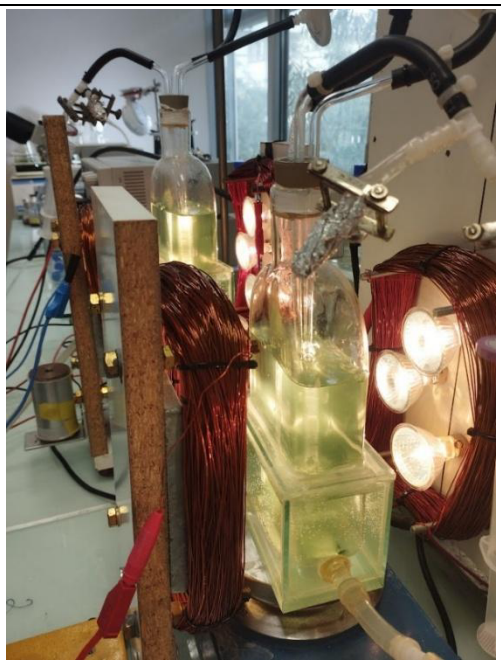
ZHANG, J.; LIU, L.; REN, Y.; CHEN, F. Characterization of exopolysaccharides produced by microalgae with antitumor activity on human colon cancer cells. **International Journal of Biological Macromolecules**, vol. 128, pp. 761–767, 2019. DOI: 10.1016/j.ijbiomac.2019.02.009. Available at: https://doi.org/10.1016/j.ijbiomac.2019.02.009.

ZHANG, S.; LIU, Z. Advances in the biological fixation of carbon dioxide by microalgae. **John Wiley and Sons Ltd**, vol. 96, no. 6, pp. 1475–1495, 1 Jun. 2021. https://doi.org/10.1002/jctb.6714.

APPENDIX

APPENDIX A – SUPPORT MATERIALS PAPER I



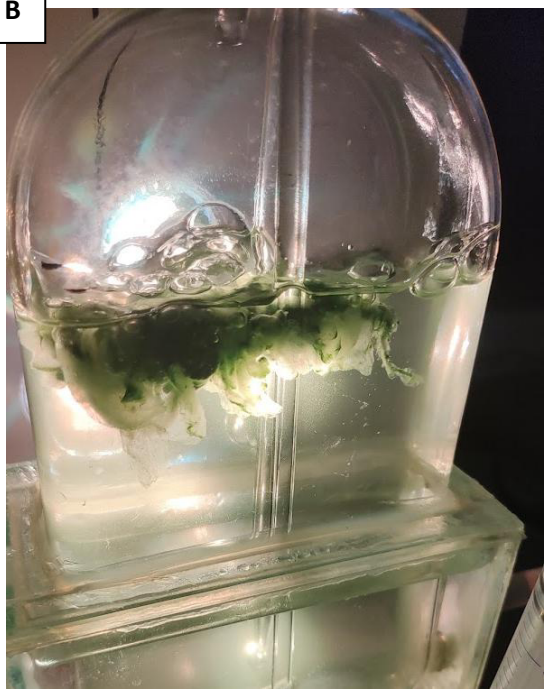


Bioreactors and magnetic field apparatus

A



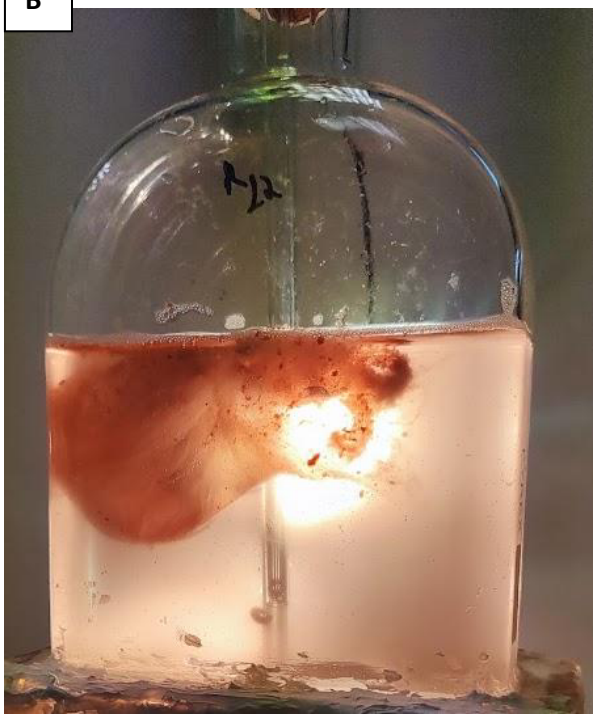
B



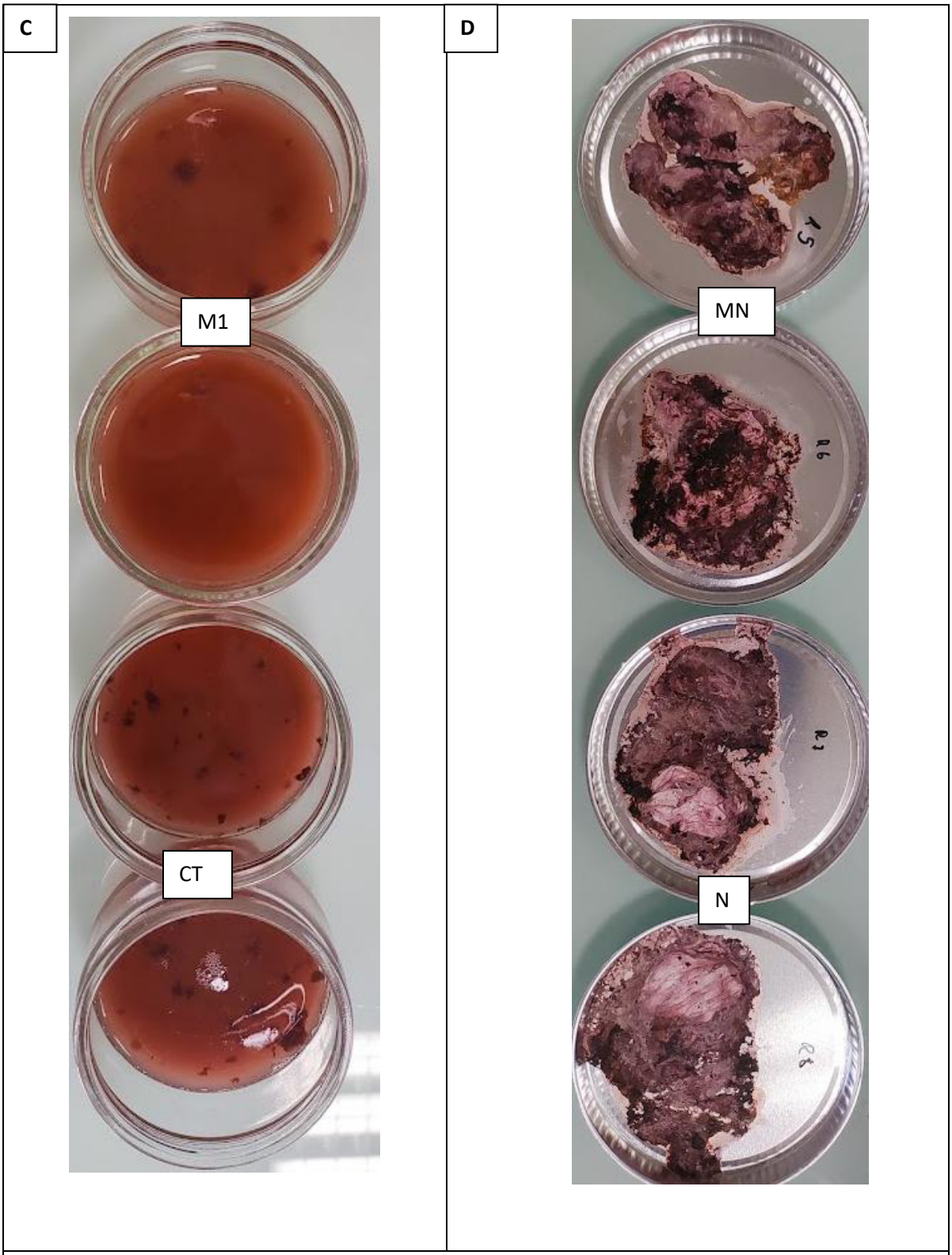
Polymeric nanofibers at T_0 (A) and T_1 (B)– The images show the *L. indica* biomass attached to the nanofiber after some time; using optical density as a tool to measure growth at the beginning of the cultivation is not accurate.

APPENDIX B – SUPPORT MATERIALS PAPER II





Bioreactors and magnetic field apparatus **A**, nanofibers **B** in *P. purpureum* cultivation



C - *P. purpureum* Cultivation with magnetic field (M1) seems to be more homogeneous than CT.

D - Dried polymeric nanofibres.